Cataloged

FAA WJH Technical Center
00026701

Report No. FAA-RD-74-127

SQUARE WAVE VOR

R.W. Redlich

July 1974

Final Report

Document is available to the public through the
National Technical Information Service,
Springfield, Virginia 22151

Prepared for

U.S. DEPARTMENT OF TRANSPORTATION
FEDERAL AVIATION ADMINISTRATION
Systems Research & Development Service
Washington, D.C. 20590

NOTICE

This document is disseminated under the sponsorship of the Department of Transportation in the interest of information exchange. The United States Government assumes no liability for its contents or use thereof.

TECHNICAL REPORT STANDARD TITLE PAGE

1. Report No. FAA-RD-74-127	2. Government Accession No.	3. Recipient's Catalog No.
4. Title and Subtitle SQUARE WAVE VOR		5. Report Date July 1974
		6. Performing Organization Code
7. Author(s) R. W. Redlich		8. Performing Organization Report No.
9. Performing Organization Name and Address Electrical Engineering Department, Ohio University, Athens, Ohio 45701		10. Work Unit No.
		11. Contract or Grant No. DOT FA71WA-2664
12. Sponsoring Agency Name and Address Department of Transportation, Federal Aviation Administration, Systems Research and Development Service, Washington, D. C. 20590		13. Type of Report and Period Covered Final, July 1971 - October 1972
		14. Sponsoring Agency Code

15. Supplementary Notes

16. Abstract

This report presents results of theoretical and experimental study of a new type of VOR, which has been named "Square Wave" VOR (SVOR) because its variable phase waveshape is roughly square. Two experimental SVORs have been built and tested. The second one was built under FAA contract and was extensively ground and flight tested at both NAFEC and Ohio University. Results of these tests are reported. Tests of a number of receivers for compatibility with SVOR signals were made, and the results are presented. A theoretical and experimental investigation of VOR and SVOR errors caused by Doppler shift in a multipath carrier is included. A feasibility study of a wide aperture SVOR designed for a 13 times reduction in multipath is presented.

17. Key Words: VOR, DVOR, Square Wave VOR	18. Distribution Statement: Document is available to the public through the National Technical Information Service, Springfield, Virginia 22151

19. Security Classif. (of this report)	20. Security Classif. (of this page)	21. No. of Pages	22. Price
Unclassified	Unclassified	154	

Form DOT F 1700.7 (8-69)

TABLE OF CONTENTS

I	SUMMARY	1
II	GENERAL DESCRIPTION AND PRINCIPLE OF SQUARE WAVE VOR	2
	A. General Description	2
	B. Principle of SVOR	3
III	CONVENTIONAL AND DVOR MULTIPATH ERRORS. REDUCTION OF MULTIPATH AND STATION ERRORS BY SVOR	6
	A. Static Multipath Error	6
	B. Cross Modulation Error	8
	C. Dynamic Multipath Error	8
	D. Reduction of Conventional VOR Station Error by SVOR	13
IV	DESIGN OF SVOR RING ARRAY. SVOR STATION ERROR DUE TO FINITE NUMBER OF ANTENNAS	16
	A. General Theory	16
	B. SVOR Station Error Due to Finite Number of Antennas	16 20
V	SVOR STATION ERROR DUE TO PRACTICAL TOLERANCES ON ANTENNA CURRENTS	24
	A. General	24
	B. Statistical Station Errors of 5X SVOR Tested at NAFEC and of 13X SVOR	25
	C. Statistical Station Error of Single Ring 5X SVOR Used With a Conventional Receiver	26
VI	SVOR RECEPTION AND COMPATIBILITY	28
	A. General Considerations	28
	B. Modification of Conventional Receiver for Zero Crossing Phase Detection	28
	C. Performance of Modified Receiver With Conventional Signals	29
	D. Noise Performance of Zero Crossing Receiver	29
	E. Performance of Conventional Receivers With SVOR Signals	31

	F. Vertically Polarized Signals	33
VII	SVOR DRUM MODULATOR	37
	A. General	37
	B. Principle	37
	C. Suppression of Parasitics	40
	D. Drum Modulator for Single Ring 5X SVOR	41
	E. Drum Modulator for 5X SVOR Tested at NAFEC	42
	F. Drum Modulator for 13X SVOR	42
	G. Drum Modulator Input Power	46
VIII	TESTS OF SINGLE RING 5X SVOR	47
	A. General Comments	47
	B. Ground Tests	48
	C. Flight Tests	49
IX	TESTS OF 5X SVOR WITH NO CONE OF CONFUSION	50
	A. General Comments	50
	B. Ground Tests (Ohio University)	51
	C. Ground Tests (NAFEC)	51
	D. Flight Tests (Ohio University)	52
	E. Flight Tests (NAFEC)	52
X	DESIGN AND FEASIBILITY STUDY OF 13X SVOR	55
	A. Design of Ring Array	55
	B. Feasibility of Drum Modulator	56
	C. Reducing Cone of Confusion	56
XI	FEASIBILITY OF VERY LARGE APERTURE SVOR	59
XII	FEASIBILITY OF ELECTRONIC SVOR MODULATOR	60
XIII	ALTERNATIVE PROCESSING OF SVOR SIGNALS	61
	REFERENCES	63
	FIGURES	66

I SUMMARY

This report presents results of theoretical and experimental study of a new type of VOR*, which has been named "Square Wave" VOR (SVOR) because its variable phase waveshape is roughly square. Two experimental SVORs have been built and tested. The second one was built under FAA contract and was extensively ground and flight tested at both NAFEC and Ohio University. Results of these tests are reported. Tests of a number of receivers for compatibility with SVOR signals were made, and the results are presented. A theoretical and experimental investigation of VOR and SVOR errors caused by Doppler shift in a multipath carrier is included. A feasibility study of a wide aperture SVOR designed for a 13 times reduction in multipath is presented.

* U.S. Patent 3,754,259

II GENERAL DESCRIPTION AND PRINCIPLE OF SQUARE WAVE VOR

A. GENERAL DESCRIPTION.

The purpose of square wave VOR (SVOR) is to reduce, without bearing ambiguities, multipath errors to which both conventional and DVOR are subject. The fundamental reason for vulnerability of conventional VOR to multipath error is insufficient aperture of the variable phase transmitting array (four loop, cage, or slot array) (Ref. 1), and it is this fundamental deficiency that is corrected by SVOR, with the result that all sources of multipath error are reduced at one stroke. SVOR employs exactly the same reference signal as conventional VOR. SVOR variable phase, however, consists of the conventional rotating figure of eight pattern plus an additional multiplexed variable phase signal which rotates at 30 hz. in synchronism with the figure of eight. The additional variable phase signal consists of one or more odd order harmonics of 30 hz., i.e., 90 hz., 150 hz., etc. An equivalent statement is that multiplexed pattern at a fixed instant of time contains one or more odd order spatial harmonics. The zero crossings of the additional harmonics coincide with the zero crossings of the conventional figure of eight pattern, and the amplitudes of these harmonics are such that the slope of the resultant variable phase pattern at zero crossing is greater than the slope of the conventional figure of eight at zero crossing. The increase in slope turns out to be proportional to the highest order harmonic in the multiplexed signal. When an SVOR signal is processed by a receiver employing zero crossing phase detection (that is, a receiver which essentially measures the difference in phase between the reference and variable signals by measuring the time between their zero crossings), the error caused by multipath will be equal to the shift in zero crossing time of the variable phase, regardless of the nature of the multipath signal. Because of the increased slope of the SVOR signal at zero crossing, the shift in zero crossing time, and the multipath error, will be reduced. Error reduction is proportional to the factor by which zero crossing slope is increased, which is proportional to the order of the highest order multiplexed harmonic, which in turn is proportional to the aperture (diameter) of the ring array that is used to radiate the multiplexed variable phase harmonics (Ref. 2 and Section IV of this report). Thus, any degree of error reduction is possible in principle, the price for more reduction being a larger diameter transmitting array. The siting situation for SVOR would resemble that of the ILS localizer in that the size of the array can be made to suit the site requirements. This is possible because a zero crossing phase detector will correctly process SVOR signals containing any number of harmonics (including no additional harmonics, i.e., conventional VOR or DVOR signals).

Receiver tests (Section VI) have shown that conventional receivers do not respond significantly to the multiplexed SVOR harmonics, and that receivers modified for zero crossing phase detection will respond to conventional signals without deterioration of performance. Thus, the possibility of gradual introduction of SVOR without depriving any users

of service exists. Those wishing to take advantage of the increased accuracy of SVOR can modify their receivers to do so (very simple circuits, e.g., Fig. 14, accomplish the modification) and continue to receive conventional or DVOR normally. Those using conventional receivers will obtain service from an SVOR equivalent to conventional VOR.

SVOR is particularly well suited for digital bearing measurement, since if such a measurement takes the obvious form of counting clock pulses between a reference marker and a variable phase zero crossing, the receiver automatically becomes a zero crossing detector and all the multipath reduction benefits of SVOR will apply without receiver modification. Digital phase measurement would virtually eliminate receiver error, so that its use in conjunction with SVOR should result in a flexible system that is greatly superior to contemporary VOR. Digital bearing measurement, either with transmitted clock signals or an on board clock, is feasible and is probably an inevitable step in modernizing VOR (Ref. 12).

Conversion of a conventional station to SVOR would be relatively inexpensive, as all parts of the existing station can be used without modification (transmitter, goniometer, tone wheel, and antennas). Conversion would consist of adding a ring array concentric with the four loop or slot array, and a power divider and modulator to drive the ring array. Smaller aperture SVOR (third or fifth order highest multiplexed harmonic) could use the existing counterpoise.

B. PRINCIPLE OF SVOR.

The principle of an idealized square wave VOR is illustrated by Figure 1. If the normal rotating figure eight pattern of a conventional VOR was replaced by a rotating square wave pattern, as illustrated, then an interfering signal arriving via multipath from a reflector at a different bearing than the receiver would not cause any change in the zero crossing time of the variable phase signal. Hence, a receiver which used zero crossing phase detection would not indicate an erroneous bearing as a result of simultaneous reception of direct and multipath signals. Coherent 30 hz. signals arising from Doppler shifts in the multipath carrier similarly would not cause any error in indicated bearing.

Figure 2 shows the polar pattern of an ideal square wave VOR. It will be noted that the pattern is constant amplitude and has a phase transition on a vertical plane that passes through the center of the VOR and rotates at 30 hz. The ideal pattern contains an infinite number of spatial harmonics, and thus cannot be radiated by a finite sized array, since radiation of harmonic order N by a non-supergain ring array can be shown to require an array not much smaller than N wavelengths in circumference (Ref. 2 or Section IV).

Basically, the ideal SVOR is immune to multipath error because the slope of the variable phase pattern at zero crossing is infinite. By Newton's rule* of elementary calculus, the displacement of the zero crossing by a small disturbing signal is inversely proportional to the

*Thomas, G. B., "Calculus and Anlytic Geometry," pg. 451.

slope at zero crossing so that infinite slope means no displacement. A practical form of SVOR having high but not infinite variable phase pattern slope at zero crossing thus suggests itself. For example, consider a variable phase pattern $P(\omega t-\phi)$ consisting of the first three harmonics of a square wave, as follows

$$P(\omega t-\phi) = \sin(\omega t-\phi) + \frac{1}{3}\sin[3(\omega t-\phi)] + \frac{1}{5}\sin[5(\omega t-\phi)] \qquad (1)$$

$$\phi = \text{azimuth}$$

$$\omega = 2\pi \times 30 \text{ rad/sec}$$

It will be noted that the first term in Equation (1) is the variable phase pattern of a conventional VOR. The slope of P at zero crossing (that is, at $\omega t = \phi$) is readily shown to be 3.0, each term contributing one unit of slope. Higher slope at zero crossing can be realized by increasing the amplitude of the third or fifth harmonics, subject to the limitation that no false zero crossings be generated. For a given amplitude increase the fifth harmonic produces the greatest increase in slope. The amount that the fifth harmonic may be increased can be calculated by noting that Equation (1) represents the first three terms in the Fourier expansion of a square wave whose amplitude is $\pi/4$ (Ref. 3). If the fifth harmonic is increased by an amount ε, ripples will be introduced into the variable phase waveshape. Maximum and minimum amplitudes will be given approximately by

$$\text{MAX. AMPLITUDE} = \pi/4 + \varepsilon$$

$$\text{MIN. AMPLITUDE} = \pi/4 - \varepsilon$$

Under multipath conditions, the maximum amplitude of the multipath signal could coincide with the minimum of the direct signal and produce a worst case as regards generation of a false zero crossing. Assuming that the worst multipath encountered in practice is less than 20% of the direct signal (corresponding to 23° peak to peak scalloping of a conventional VOR), ε can be calculated from the condition that 20% reflection and coincidence of a reflected maximum with a direct minimum just produces a false zero crossing. This condition is:

$$.20(\pi/4 + \varepsilon) = \pi/4 - \varepsilon \qquad (2)$$

Solving for ε gives $\varepsilon = .52$. In the experimental SVOR described later in this report, a more conservative value of ε, namely, $\varepsilon = 0.4$, was used. The variable phase pattern of the experimental SVOR was thus;

$$\sin(\omega t-\phi) + \frac{1}{3}\sin[3(\omega t-\phi)] + \frac{3}{5}\sin[5(\omega t-\phi)] \qquad (3)$$

The slope of Equation (3) at zero crossing is readily shown to be 5.0, of which the first two terms contribute one unit each and the last term contributes three units. Thus, the SVOR with variable phase pattern Equation (3) has five times higher slope at zero crossing than a conventional VOR (the conventional VOR signal is the first term in Equation (3)). Therefore, the nomenclature 5X SVOR was adopted. Figures 3 and 4 show the variable phase pattern of the 5X SVOR, with the conventional pattern plotted for comparison. Figure 5 illustrates how the ring array and the four loop patterns combine to produce the SVOR variable phase. It will be noted that, for 30% modulation by 30 hz., the total SVOR percentage modulation is approximately 37%.

Clearly, SVORs with still higher slope at zero crossing can be realized by taking more terms of the Fourier expansion of a square wave and adding approximately 0.5 to the highest harmonic amplitude (since the condition, Equation (2), applies regardless of the number of terms taken*). If n terms are taken, the slope of the pattern at zero crossing has (n-1) contributions of 1 unit each, plus a contribution

$$1 + .5\ (2\ n-1).$$

from the last term. Thus, the total slope is

$$2\ n - \frac{1}{2}$$

which is approximately the order of the highest harmonic. Thus, a 13X SVOR would employ seven Fourier terms, the highest of which was a 13th harmonic. Its variable phase pattern would be

$$\sum_{n=0}^{5} \frac{1}{2n+1} \sin\left[(2n+1)(\omega t-\phi)\right]$$

$$+ \left(.5 + \frac{1}{13}\right) \sin\left[13(\omega t-\phi)\right] \qquad (4)$$

and it would have a slope of approximately 13 at zero crossing.

*See also Section IV B.

III CONVENTIONAL AND DVOR MULTIPATH ERRORS, REDUCTION OF MULTIPATH AND STATION ERRORS BY SVOR

A. STATIC MULTIPATH ERROR.

The term "static" multipath error will be used here to refer to the error experienced by a stationary receiver when it simultaneously receives a direct signal and a signal reflected from a single obstacle. Although static error of conventional and DVOR is well understood and is treated in many references (e.g., Refs. 4 and 5), the formula for static error of conventional VOR will be rederived here from a standard viewpoint (phase shift of resultant signal) and from the viewpoint of a zero crossing shift. The fact that the two viewpoints give identical results shows that a zero crossing receiver will perform identically with a standard receiver in the presence of static multipath. The second derivation will also serve to introduce the technique used to analyze multipath error of SVOR.

Let the receiver bearing from the VOR be ϕ, the reflector bearing be ψ, and let the direct variable phase signal $P_c(t)$ be normalized to unit amplitude, i.e.,

$$P_c(t) = \sin(\omega t - \phi) \text{ (modulation only)}$$

where $\omega = 2\pi \times 30$ rad/sec.

If the reflected signal amplitude is δ, and the reflected signal is in RF phase with the direct signal (worst case condition) then the resultant signal is

$$\sin(\omega t - \phi) + \delta \sin(\omega t - \psi) \tag{5}$$

By using trigonometric identities and assuming $\delta \ll 1$ Equation (5) can be reduced to

$$\sin[(\omega t - \phi) + \delta \sin(\phi - \psi)] \tag{6}$$

The last phase term in Equation (6) represents an error. Therefore,

$$\text{Static Multipath Error} = \delta \sin(\phi - \psi) \tag{7}$$

Equation (7) can also be derived by computing the shift in the zero crossing due to the multipath signal. The derivative of the direct

signal with respect to phase is, in general,

$$\frac{dP_c}{d(\omega t)} = \cos\ (\omega t-\phi).$$

Zero crossing occurs at $\omega t-\phi = 0$, hence, the derivative at zero crossing is simply 1.0. The shift in zero crossing phase due to multipath can be evaluated by dividing the multipath amplitude at zero crossing by the slope at zero crossing (Newton's rule of elementary calculus). Since zero crossing occurs at $\omega t = \phi$, the multipath signal at zero crossing is

$$\delta \sin\ (\phi-\psi)$$

and, with unit direct signal slope at zero crossing,

$$\text{shift in zero crossing phase} = \delta \sin\ (\phi-\psi) \tag{8}$$

The fact that the right hand sides of Equation (7) and (8) are identical shows that phase detection and zero crossing detection give identical results with standard VOR signals contaminated by multipath. The implication of this for SVOR is that receivers modified for zero crossing detection in order to take advantage of SVOR would receive standard VOR without change in performance (they would also receive DVOR without change in performance, since there would be no modification of the reference channel).

Static multipath error of SVOR can readily be computed by dividing the multipath signal at zero crossing by the slope at zero crossing. If the SVOR variable phase pattern is denoted by P_s, then given the same reflector as was used to compute the standard VOR error (that is, δ unchanged and ψ unchanged), the static error of an NX SVOR is given by

$$\frac{\delta\ P_s(\phi-\psi)}{N}, \tag{9}$$

since the zero crossing slope of an NX SVOR is N.

The improvement over conventional VOR, that is, the factor by which course scalloping is reduced, is simply the ratio of Equation (9) to the right hand side of Equation (7) or (8). Therefore,

$$\text{Reduction factor of NX SVOR} = \frac{P_s(\phi-\psi)}{N \sin\ (\phi-\psi)} \tag{10}$$

Equation (10) is plotted in Figure 6 for a 5X SVOR and a 13X SVOR, using P_c as given by Equation (3) and (4) respectively.

Two general features of Equation (10) are of considerable practical significance. First, there is an angular region around $\phi-\psi = 0$ where SVOR gives no improvement over conventional VOR. This can be seen from the fact that in the neighborhood of $\phi-\psi = 0$,

$$P_s(\phi-\psi) \approx N\ (\phi-\psi)$$
$$\sin\ (\phi-\psi) \approx (\phi-\psi) \qquad (11)$$

Substitution of Equation (11) into (10) given a reduction factor of 1.0; in other words, no improvement. Examination of Figure 6 shows that the range of little improvement diminishes roughly in proportion to N. Figure 7 shows the scalloping of conventional VOR, 5X SVOR, and 13X SVOR on a scale for which the peak scalloping of the conventional VOR is 1.0. This figure illustrates a second significant feature of Equation (10), namely, that the scalloping reduction factor of an NX SVOR averages about 1/N well outside the no improvement region, as a consequence of the fact that P_s averages about $\pi/4$ (see page 3), which is roughly comparable to sin $(\phi-\psi)$ over a considerable range of $\phi-\psi$.

It should be noted that the property of no scalloping improvement in the neighborhood of $(\phi-\psi) = 0$ is shared by DVOR (Ref. 5) and multilobe VOR.

B. CROSS MODULATION ERROR.

Cross modulation error is peculiar to the Single Sideband DVOR. It occurs when the DVOR, reflector, and receiver are nearly in line, and in this condition generates scalloping that is worse than a conventional VOR. A detailed analysis of cross modulation error is presented in Ref. 1. Cross modulation error is eliminated by adding the second DVOR sideband or by adding an FM reference signal.

SVOR is not subject to cross modulation error.

C. DYNAMIC MULTIPATH ERROR.

There is very strong theoretical evidence, and some experimental evidence, that large amplitude VOR or DVOR errors can occur when a multipath carrier is Doppler shifted in frequency by about 30 hz. relative to the direct signal. VOR and DVOR aberrations observed at low altitudes in mountainous terrain or near large cities may well be due to this phenomenom. For brevity, this error source will be referred to here as "dynamic" error.

If, during reception of a direct signal at carrier frequency ω_c rad/sec, a multipath signal whose carrier was Doppler shifted to a frequency $\omega_c + \omega_D$ was simultaneously received, the net RF signal S(t) at $\phi = 0$ (north) would be;

$$S(t) = e^{j\omega_c t}[1+V(\omega t) + R(t)] + \delta e^{j(\omega_c+\omega_D)t}[1+V(\omega t-\psi)+R(t)] \qquad (10)$$

In Equation (10), ψ is the bearing of the reflector, δ is the ratio of the amplitude of the multipath signal to the direct signal, V is the variable phase signal (either conventional or square wave), and R is the omnidirectional FM reference signal. The scale of Equation (10) is such that carrier amplitude is 1.0.

Equation (10) can be rearranged into the following form, from which the response of an envelope detector to S(t) can be readily deduced;

$$S(t) = e^{j\omega_c t}\{1+V(\omega t)+R(t)+\delta e^{j\omega_D t}[1+V(\omega t-\psi)+R(t)]\} \qquad (11)$$

The output of an envelope detector supplied with S(t) will simply be the magnitude of the bracketed term in Equation (11), which, if $\delta << 1$, is approximately

$$1 + V(\omega t) + R(t) + \delta\cos\omega_D t\ [1+V(\omega t-\psi) + R(t)] \qquad (12)$$

As ω_D approaches zero, Equation (12) approaches the static case. However, if ω_D is near 30 hz., the detected multipath carrier term in Equation (12), $\delta \cos \omega_D t$, will be amplified in the variable phase channel (or the reference phase channel of DVOR) and cause CDI disturbance. To analyze this situation, let

$$\omega_D = 2\pi\ (30 + \Omega) \qquad (13)$$

where Ω represents a frequency that is small compared to 30 hz. The only multipath term in Equation (12) whose frequency is within the passband of the variable phase channel is then the carrier term. Thus, the variable phase signal is

$$V(\omega t) + \delta \cos\ [2\pi(30 + \Omega)]t \qquad (14)$$

For conventional VOR,

$$V(\omega t) = .3 \sin (\omega t) \tag{15}$$

If δ is small, Equation (14) reduces approximately to the following for conventional VOR (or DVOR, for which $R(t) = .3 \sin \omega t$)

$$.3 \sin (\omega t + \frac{\delta}{.3} \cos 2\pi\Omega t) \tag{16}$$

The second bracketed term in Equation (16) represents a time varying phase error. Therefore

$$\begin{array}{l}\text{Dynamic Error;}\\ \text{Conventional VOR}\\ \text{ or DVOR}\end{array} = \frac{\delta}{.3} \cos (2\pi\Omega t) \tag{17}$$

Equation (17) shows that the peak dynamic error is larger than the max. static error that the same multipath signal could produce by a factor of 3.33 (compare Equation (7)). CDI fluctuation will be at a frequency Ω, and thus will be attenuated by CDI damping as Ω increases. Assuming that typical VOR receivers respond from $\Omega = 0$ to about $\Omega = 1$ hz., multipath Doppler shifts in the range 30 ± 1 hz. can be expected to cause large amplitude CDI fluctuations.

To demonstrate how SVOR attenuates dynamic error in comparison to conventional or DVOR, the SVOR variable phase pattern, which is

$$.3 \left[\sin \omega t + \frac{1}{3} \sin 3\omega t + \ldots\ldots + (\frac{1}{N} + \varepsilon)\sin(N\omega t)\right] \tag{18}$$

for an NX SVOR on a scale for which carrier equals 1.0, may be substituted in Equation (14) and the shift in zero crossing time calculated. Zero crossing time is

$$\omega t = p \times 2\pi, \; p = 0,1,2,3 \text{ ----}$$

At the above times, the multipath signal in Equation (14) is equal to

$$\delta \cos (2\pi\Omega t)$$

The slope of Equation (18) at zero crossing is .3N, hence the

multipath error is given by;

$$\text{Dynamic Error (SVOR)} = \frac{\delta \cos (2\pi\Omega t)}{.3N} \tag{17a}$$

Comparing Equation (17) and (17a) shows that SVOR attenuates dynamic error by a factor of N compared to conventional or DVOR.

To show that Doppler shifts in a frequency range around 30 hz. can readily occur at normal aircraft speeds, and that they can persist for many seconds, consider the situation depicted below, in which an aircraft is flying a radially outbound track that takes it within a distance D (not necessarily horizontal) of closest approach to a reflector. It will be assumed that the aircraft is equipped with a receiver having bandwidth ±B in the variable phase channel, that is, signals applied to the variable phase amplifier in the frequency range (30 ± B) hz. will produce a CDI oscillation whose peak amplitude is within 3 db. of the CDI response at 30 hz.

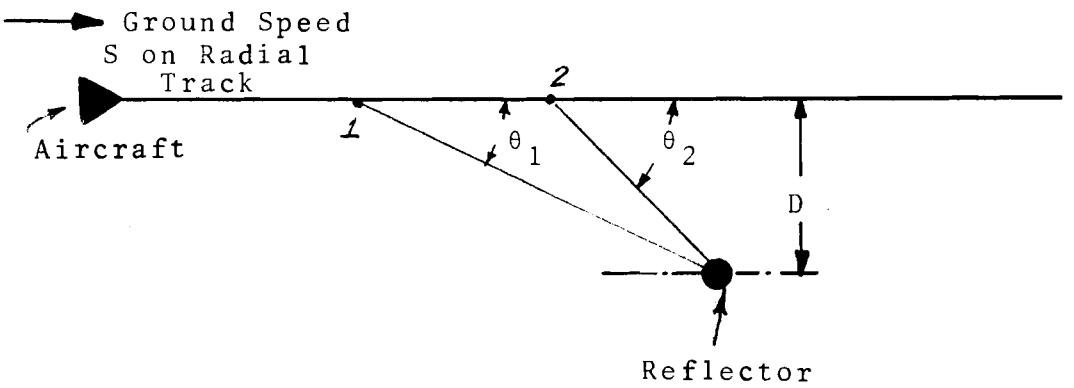

The direct carrier is Doppler shifted down by a frequency $f = S/\lambda$ (Ref. 6). The multipath carrier at point 1 is shifted up in frequency by $f \cos \theta_1$. Thus, the Doppler beat between the direct and multipath carriers at point 1 is

$$f + f \cos \theta_1$$

if points 1 and 2 are located so that

$$f + f \cos \theta_1 = 30 + B$$

$$f + f \cos \theta_2 = 30 - B$$

Then, between points 1 and 2, the detected Doppler beat will pass through the 30 hz. amplifier and cause a CDI fluctuation at a frequency equal to (30 - beat frequency). The duration t of the disturbance is given by

$$t = D/S\ (\cot \theta_2 - \cot \theta_1)$$

or

$$t/D = 1/S\ (\cot \theta_2 - \cot \theta_1). \qquad (19)$$

Figure 8 is a graph of t/D versus S. The value of B used in the computations from which the graph was plotted was 1.0 hz., which is representative of VOR receivers. It is apparent from the graph that disturbances of considerable duration can occur at normal aircraft speeds and normal distances of closest approach to a reflecting obstacle such as a mountain or tall building.

A special case occurs for an aircraft speed of 80 knots, which corresponds to f = 15 hz. At this speed, the direct carrier is shifted by 15 hz., and the reflected carrier is continuously shifted by 15 hz. in the other direction if D = 0. Thus, if the aircraft flies directly over the reflecting obstacle at 80 knots ground speed, a long duration beat at 30 hz. is to be expected. To test this hypothesis, a radial flight between the experimental VOR and a cylindrical water tower was made at 80 knots with only reference phase being radiated from the VOR. The absence of 30 hz. variable phase insured that any observed CDI current was a consequence of 30 hz. components of a beat between direct and reflected carriers. Figure 9 shows the flight record. A disturbance lasting about one minute was observed, with a peak-to-peak amplitude of 2.5° occuring just before passage over the water tower. The flight was continued past the water tower, and records for this portion showed negligible disturbance.

Additional tests simulating the effect of Doppler shifted multipath carrier were performed by sine wave modulating the RF output of a signal generator by means of the circuit shown below;

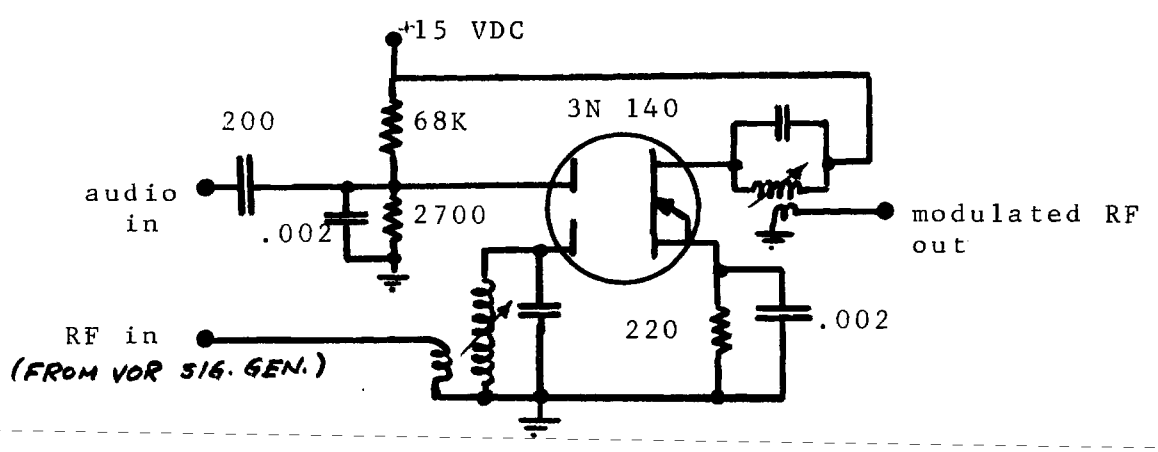

Linear modulation up to 50% with negligible distortion was achieved by the above circuit. Percentage modulation was independent of RF input level.

Ten percent modulation of a VOR signal generator output was used in the tests, which corresponds to $\delta = .1$ in Equation (18) and should thus cause maximum CDI error of 19.1° at a simulated Doppler frequency close to 30 hz. (Equation (17)). Test results are shown in Table I. Both of the receivers tested showed peak CDI errors of 16° near 30 hz., which agrees with the predicted value within the accuracy to which modulation percentages could be measured. Both receivers showed appreciable error near 60 hz., probably as a result of nonlinearity in the second detector, which would cause detection of a 30 hz. beat between 60 hz. and 30 hz. variable modulation. The Collins receiver showed a large, unexplained CDI error which peaked at a value of eight degrees, at a frequency of six hz. This phenomenom did not occur in the Bendix receiver.

It seems evident from these tests and on theoretical grounds that Doppler shift in multipath carrier can be a serious source of VOR error when the Doppler shift approaches 30 hz., as it may readily do at normal aircraft speeds. Detected beats at 30 hz. will affect any VOR receiver, and clearly cannot be eliminated if the receiver is to process normal 30 hz. modulations. Receiver vagaries may result in responses to Doppler beats at frequencies other than 30 hz., but these would seem to be considerably less significant than the ineradicable response to 30 hz.

Additional evidence (believed unpublished) as to the existence of Doppler shifted carrier error is observed improvement in performance of Double Sideband DVOR upon addition of an FM reference. Improvement of SSB DVOR when an FM reference is added can be attributed to elimination of cross-modulation and counterpoise error, but DSB DVOR is not affected by cross modulation error and not significantly by counterpoise error. The observations referred to were made in Europe on an Alternating Sideband DVOR.

D. REDUCTION OF CONVENTIONAL VOR STATION ERROR BY SVOR.

Both the 5X SVOR that was tested at NAFEC and the 13X SVOR whose feasibility is studied in this report consist of a conventional VOR which radiates the 30 hz. component of the SVOR variable phase, plus a ring array to radiate the remaining harmonic components. Assuming a perfect ring array radiation pattern, an NX SVOR of this type (ring array plus conventional array) will have a lower station error than the conventional station alone by a factor of N, if a receiver using zero crossing phase detection is used for measurement of the SVOR station error. To show this, let the angular error of the conventional station be $\psi(\phi)$, so that the 30 hz. component of the SVOR variable phase signal is $\sin[(\omega t-\phi) + \psi(\phi)]$, where ψ is assumed to be a small angle. The signal amplitude at nominal zero crossing ($\omega t = \phi$) is $\sin[\psi(\phi)]$. By Newton's rule, the displacement of the NX SVOR zero crossing time because of the

TABLE I

Receiver Response to Simulated Doppler Shifted Multipath Carrier (Amplitude 10% of Direct Carrier)

Doppler Shift (hz.)	(CDI Error (Degrees) 51R3	RA21
5.0	± 4.7	± 0.4
6.0	± 8.0	± 0.7
6.5		± 1.3
7.0	± 5.7	± 1.3
7.5	± 5.1	± 1.3
8.0	± 4.6	± 1.3
9.0	± 3.3	± 1.3
10.0	± 2.6	± 0.7
12.0	± 1.7	± 0.7
14.0	± 1.3	± 0.5
15.0	± 1.0	± 1.0
16.0	± 1.3	± 0.3
17.0	± 1.0	± 0.4
20.0	± 1.0	± 0.4
25.0	± 2.7	± 0.4
27.5	± 1.4	± 0.7
29.0	± 1.6	± 2.4
30.0	± 16.0	± 16.0
31.0	± 3.9	± 2.7
32.0	± 2.7	± 1.0
45.0	± 0.0	± 0.0
60.0	± 1.9	± 2.5
90.0		
120.0 - - - - -	± 0.0	± 0.0
150.0		

conventional VOR error signal is

$$\frac{\sin\,[\psi(\phi)]}{N} \approx \frac{\psi(\phi)}{N}$$

Thus, conventional station error is reduced by a factor of N by the additional SVOR harmonics and the use of a zero crossing phase detector.

In practice, the assumption of a perfect ring array will not be realized, because of the inherent station error of the ring array itself (Section IV) and because of statistical errors arising from discrepancies in construction and drive of the ring array (Section V). For these reasons, an N fold reduction of the conventional station error will not be achieved. The statistical analysis of Section V shows that in the case of 5X SVOR, a reduction of station error should be realized for any conventional error spread exceeding about .8°. For 13X SVOR, error spread reduction should be achieved for any conventional error spread exceeding .5°.

Experimental data taken at NAFEC confirm the expected reduction in station error. Figure 10 shows the results of two six mile radius orbital flights with radar reference. In one flight the radiated signal was generated by a conventional four-loop VOR and reception was with a conventional receiver. In the second flight, a 5X SVOR signal was radiated whose 30 hz. component was generated by the same four-loop VOR used in the first flight, and reception was with a receiver modified for zero crossing phase detection. Error spreads were 2.8° and 1.4° respectively.

Further confirmation of the expected reduction in error spread is shown in the ground check data (Figure 11) taken at NAFEC with a monitor modified for zero crossing detection. One ground check was made with the SVOR ring array energized, and the second with the ring array present but not energized (four-loop radiation only). Error spreads were .8° and 2.0° respectively.

Statistical analysis (Section V) of 13X SVOR station error shows that a four-loop error spread of 2° will be reduced to 0.5° by addition of the 13X SVOR harmonics.

IV. DESIGN OF SVOR RING ARRAY. SVOR STATION ERROR DUE TO FINITE NUMBER OF ANTENNAS

A. GENERAL THEORY.

The most difficult theoretical problem in development of SVOR was devising a technique for designing a ring array that would radiate all of the required SVOR harmonics. Ring arrays used in DVOR or precision multilobe VOR are special cases, the latter radiating only a single spatial harmonic from an array the number of whose elements is four times the harmonic order, the former being designed to simulate rotation of a single antenna. No suitable general theory was found in the literature, so the theory described in Ref. 1 was developed in order to answer the questions; a) what should the ring diameter be?, b) how many antennas are necessary?, c) what are the required antenna currents?, d) what is the station error?

The theory of Ref. 1 treats only the radiation pattern in the plane of the ring (horizontal plane) and only stationary patterns. A more general treatment that accounts for pattern rotation and pattern change with elevation follows. The coordinates and the geometry of the ring are shown in the drawing below.

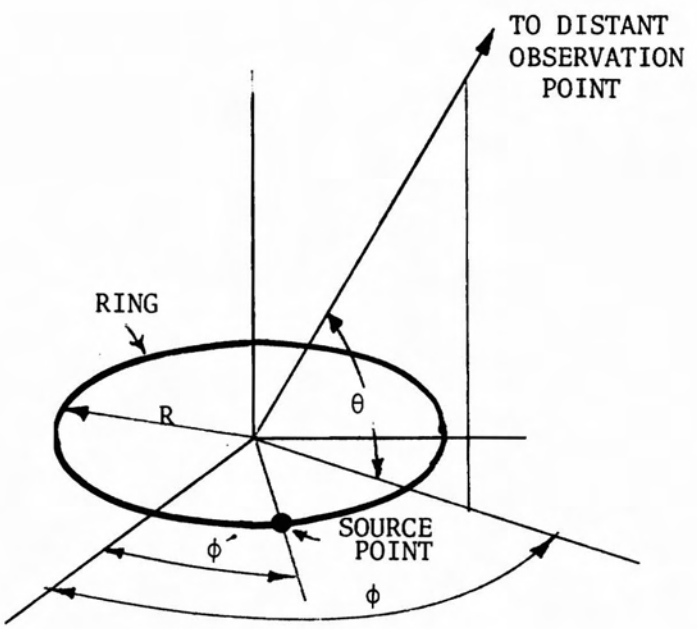

The theory is based on sampling of a continuous distribution of sources on the ring of radius R; the sampling process yielding a discrete array (Ref. 7). Suppose, then, that a continuous distribution of omnidirectional sources exists on the ring, and that this source distribution rotates bodily around the ring at frequency ω. In terms of source coordinate ϕ' and time t, the rotating distribution $I(\phi',t)$ can be written

$$I(\phi',t) = \sum_{n=1}^{N} a_n \sin\,[n(\omega t-\phi')] \tag{20}$$

Equation (20) is a truncated Fourier series containing only odd order sine terms, as is appropriate for SVOR analysis. N in Equation (20) has the same meaning as in previous sections. It is the order of the highest harmonic and, approximately, the average scalloping improvement factor. The array factor (Ref. 7) of the distribution Equation (20) will be designated $P(\phi,\theta,t)$ and from the definition of array factor is given by

$$P(\phi,\theta,t) = \sum_{n=1}^{N} \int_0^{2\pi} a_n \sin\,[n(\omega t-\phi')]\; e^{jKR\cos\theta\cos(\phi-\phi')} R d\phi' \tag{21}$$

where $K = 2\pi/\text{wavelength}$. Equation (21) can be integrated using standard Bessel function identities (Ref. 8) to give

$$P(\phi,\theta,t) = \sum_{n=1}^{N} 2\pi R\; j^n a_n J_n(KR\cos\theta)\sin\,[n(\omega t-\phi)] \tag{22}$$

where J_n is a Bessel function of order n.

Comparing Equation (20) and (22) shows that each harmonic of the source distribution radiates a harmonic in Equation (22) whose nulls align with the nulls of the source harmonic. Since Bessel functions have the general property that they are small if their argument is appreciably less than their order (see Figures 12 and 13) the ring radius should satisfy

$$KR \approx N \tag{23}$$

for efficient radiation of Nth harmonic. Also, Bessel functions are oscillatory so that even if Equation (23) is satisfied, one of the lower order harmonics may be very inefficiently radiated if KR is close to a zero of one of the lower order Bessel functions, so that R must be selected to avoid this condition.

If an array factor in the horizontal plane is specified, Equation (22) can be used to work backwards and find the coefficients of the distribution that will radiate as specified. Let an array factor $AF(\phi,0,t)$ be given as

$$AF(\phi,0,t) = \sum_{n=1}^{N} b_n \sin n(\omega t-\phi) \tag{24}$$

Then, setting AF = P and equating coefficients of like harmonics gives

$$a_n = \frac{b_n}{2\pi R\ j^n J_n(KR)} \tag{25}$$

Thus, designing a continuous array that will radiate a prescribed pattern in the plane of the ring is a straightforward job, and the synthesis gives an exact answer, that is, the continuous array radiates exactly the given pattern.

A practical array must be a finite number of discrete sources on the ring R. The radiation from such an array can be investigated by multiplying the continuous distribution Equation (20) by a sampling function (Ref. 9) consisting of M impulse functions spaced uniformly around the ring. The location of the impulse functions will be the eventual location of M antennas. The sampling function can be written as

$$S(\phi') = \frac{2\pi}{M} \sum_{p=0}^{M-1} \delta(\phi' - \frac{2\pi p}{M}) \tag{26}$$

In Equation (26), $\delta(\phi' - \frac{2\pi p}{M})$ is an impulse function located at $\phi' = \frac{2\pi p}{M}$. The factor $2\pi/M$ in Equation (26) gives S the property

$$\int S(\phi')\ d\phi' = 2\pi \tag{27}$$

The property Equation (27) simplifies later results. To use S in a calculation of array factor, it is easier to use its Fourier expansion than the form Equation (26). S is an even periodic function of ϕ', and has the cosine expansion

$$S(\phi') = 1 + 2 \sum_{\ell=1}^{\infty} \cos \ell M \phi' \tag{28}$$

A sampled current distribution $I_s(\phi',t)$ is now defined as the product of the original continuous distribution (Equation (20)) and the sampling function $S(\phi')$. After carrying out the multiplication and

applying the trigonometric identity

$$\text{Sin}\ (A)\ \cos\ (B) = \frac{1}{2}\ [\sin(A-B) + \text{Sin}(A+B)], \tag{29}$$

the following result is obtained for $I_s(\phi',t)$;

$$I_s(\phi',t) = I(\phi',t) + \sum_{\ell=1}^{\infty} \sum_{n=1}^{N} a_n\{\text{Sin}[n\omega t-\phi'(n+\ell M)+\text{Sin}[n\omega t+\phi'(\ell M-n)]\} \tag{30}$$

The array factor $P_s(\phi,\theta,t)$ of the sampled current distribution (Equation (30) can be found in the same manner as that of the continuous distribution. The result is

$$P_s(\phi,\theta,t) = P(\phi,\theta,t) + \sum_{\ell=1}^{\infty} \sum_{n=1}^{N} 2\pi R a_n\{ j^{\ell M+n} J_{\ell M+n}(KR\cos\theta)\text{Sin}[n\omega t-\phi(\ell M+n)]$$

$$+ j^{\ell M-n} J_{\ell M-n}(KR\cos\theta)\ \text{Sin}[n\omega t+\phi(\ell M-n)]\} \tag{31}$$

if the number of sample points M is chosen so as to satisfy

$$M > 2N \tag{32}$$

then the lowest Bessel function order under the double sum in Equation (31), which occurs for $\ell = 1$, $n = N$, satisfies

Lowest Bessel Function Order > N

From the property that Bessel functions decrease rapidly if their argument is less than their order, it may be seen that the terms under the double sum can then be suppressed by choosing the ring radius R according to Equation (23). Assuming that the design choices Equations (32) and (23) are made, P_s will approximate P. The required antenna currents for radiation of a specified horizontal plane array factor Equation (24) may then be found by:

a) Computing the coefficients a_n of the continuous distribution from Equation (25), and the continuous distribution from Equation (20).

b) Computing the current I_p in the antenna at $\phi' = \frac{2\pi p}{M}$ from

$$I_p(t) = \frac{2\pi R}{M} \; I\left(\frac{2\pi p}{M}, t\right) \tag{33}$$

Equation (33) follows from general properties of impulse functions and the fact that

$$I_p = \lim_{\varepsilon \to 0} \int_{\phi' = \frac{2\pi p}{M} - \varepsilon}^{\frac{2\pi p}{M} + \varepsilon} S(\phi') \; I(\phi', t) \; R \; d\phi' \tag{34}$$

A ring array designed by the foregoing procedure will radiate the specified horizontal plane array factor plus error terms represented by the double sum in Equation (31). The dominant error term is the one of order M-N, since the Bessel function multipliers of the error terms decrease rapidly with order. If only the dominant error term is retained, then combining Equation (22), (25), and (31) gives the radiated pattern of the discrete array as follows;

$$P_s(\phi,\theta,t) = \left\{ \sum_{n=1}^{N} b_n \frac{J_n(KR\cos\theta)}{J_n(KR)} \operatorname{Sin} n(\omega t - \phi) \right\}$$

$$+ b_N \, j^{M-2N} \frac{J_{M-N}(KR\cos\theta)}{J_N(KR)} \operatorname{Sin} [N\omega t + (M-N)\phi] \tag{35}$$

The summation in Equation (35) reduces to the prescribed horizontal plane array factor Equation (24) when $\theta = 0$. Equation (35) is the basic equation from which SVOR station error and variation of SVOR radiation pattern with elevation can be analyzed. It will be noted that if M is an even number, the error term is in phase with the other terms.

B. SVOR STATION ERROR DUE TO FINITE NUMBER OF ANTENNAS.

SVOR station error will arise from two causes. First, from the difference between the ideal rotating field and the actual field of the discrete ring array, which difference is embodied in the last term of Equation (35). Second, as a result of imperfections in construction and inaccuracies in drive currents. Only the first cause is treated here, the second being covered in Section V.

For an NX SVOR, station error will be the last term of Equation (35), evaluated at

$$\theta = 0 \quad \text{(horizon)}$$

$$\omega t = \phi \quad \text{(nominal zero crossing)}$$

and divided by N (slope at zero crossing) to give the shift in zero crossing. Thus

$$\text{Station Error Due To Finite Number of Antennas} = \frac{b_N}{N} \frac{J_{M-N}(KR)}{J_N(KR)} \text{ Sin } M\phi \qquad (36)$$

Equation (36) shows that the station error is periodic with angular period equal to the angular spacing between antennas, as would be expected.

Equation (36) can be used to decide on a value for M, the number of antennas, on the basis of an allowable station error. The station error will decrease as M is increased, because the ratio of Bessel functions that appears in Equation (36) will decrease rapidly with increasing M if KR is in the neighborhood of N (design choice Equation (23)). For example, consider a 5X SVOR with KR = 5 (as in the NAFEC SVOR).

In this case,

$N = 5$

$b_1 = 1.0$

$b_3 = 1/3$ (See Equation (3))

$b_5 = 3/5$

If M = 14 (same number of antennas as SVOR tested at NAFEC);

$$\text{Station Error Due to Finite Number of Antennas, in Degrees} = \frac{(3/5)}{5} \frac{J_9(5)}{J_5(5)} \text{ Sin } (14\phi) \times 57.3$$

$$\text{Station Error Due to Finite Number of Antennas, in Degrees} = .14 \text{ Sin } (14\phi)$$

The irreducible station error spread of the 14 element 5X SVOR that was tested at NAFEC was therefore .28°, which was considered acceptable. If the number of antennas had been reduced to 12, the irreducible station error would have increased by a factor of more than 10, which would clearly have been unacceptable.

An approximate formula for the station error of an NX SVOR due to the finite number of antennas can be derived from Equation (36) and the following approximation for $J_n(x)$, which holds well for values of x less

than n (Ref. 11).

$$J_n(x) \approx \frac{x^n}{2^n n!} \tag{37}$$

Substitution in Equation (36) gives;

$$\text{Peak Station Error Due to Finite Number of Antennas} = \frac{b_N}{N} \frac{(KR)^{M-2N} N!}{2^{M-2N} (M-N)!} \tag{38}$$

b_N in Equation (38) is the coefficient of the highest order harmonic in the variable phase pattern of the NX SVOR. A general formula for b_n can be obtained by noting that an NX SVOR employs (N+1)/2 harmonics, each of which contributes one unit of slope at zero crossing except the Nth, whose amplitude must be augmented by an amount Δb_N in order to increase the slope at zero crossing to N units. Noting that the unaugmented amplitude of b_N, that is, the amplitude of the Nth Fourier coefficient of a square wave, is 1/N, and that the increase in slope due to augmentation of b_N is $N\Delta b_N$, there follows

$$b_n = \frac{1}{N} + \Delta b_N \tag{39}$$

$$N\Delta b_N = N - \left(\frac{N+1}{2}\right) \tag{40}$$

Simultaneous solution of Equation (39) and (40) gives

$$b_N = \frac{(N+1)}{2N} \tag{41}$$

Substitution of Equation (41) in Equation (38), use of Equation (23), and the assumption that N is large lead to

$$\text{Peak Station Error Due to Finite Number of Antennas} \approx \frac{N^{M-2N-1} N!}{2^{M-2N+1} (M-N)!} \tag{42}$$

For very large N, Equation (42) can be further reduced. In terms of the excess number of antennas E, where E = M-2N the station error becomes

$$\text{Station Error Due to Finite Number of Antennas} = \frac{1}{2^{E+1} N} \tag{43}$$

Equation (43) immediately shows that station error will decrease with increasing N and with increasing E. The same conclusions follows from the more accurate formula Equation (42), but are less apparent.

To illustrate reduction in station error as N is increased, Equation (36) or (42) can be applied to a 13X SVOR (Section X) consisting of 30 antennas on a ring 11.6 electrical radians in radius. Substitution of

$$J_{17}\ (11.6) = .0037$$

$$J_{13}\ (11.6) = .0955$$

into Equation (36) gives

$$\text{Peak Station Error} = .092^\circ$$

in comparison with the peak error of .14° for the 5X SVOR.

V SVOR STATION ERROR DUE TO PRACTICAL TOLERANCES ON ANTENNA CURRENTS

A. GENERAL

The design radiation pattern of an SVOR can only be realized within a tolerance determined by the accuracy of the antenna currents in amplitude and phase. Practical variations in length and impedance of coaxial line, in antenna impedance, and in modulator output all contribute to errors in antenna current. The resulting departure from the design radiation pattern can be analyzed statistically with reasonable assumptions as to the statistics of individual antenna currents, and the assumption that the statistics of the error curve of a given array are the same as the error statistics of a large collection of arrays. Each antenna generally has an error current in addition to its nominal current. The amplitude of the contribution of the error current to the array factor is equal to the amplitude of the error current (since array factor computation involves only multiplication by a phase factor). The phase of the contribution of the error current to the array factor is random; all phases being equally probable. Only the contribution that is in phase with the nominal array factor will cause an error at the output of an envelope detector. It will be assumed that the in-phase error contribution of an individual antenna to the array factor has a Gaussian statistical distribution whose standard deviation is a constant, σ, times the nominal antenna current. The standard deviation (S.D.) of the total error signal is then, by a theorem of statistics (Ref. 9) equal to the RMS value of the individual standard deviations. Thus, in terms of individual nominal antenna currents I_n, S.D. is given by

$$\text{S.D.} = \sigma(\Sigma\ I_n^{\ 2})^{1/2} \tag{44}$$

Equation (44) gives the standard deviation of the error signal at any value of bearing or time, hence it applies to the error signal at nominal zero crossing. Application of Newton's rule for the displacement of the zero crossing gives the standard deviation of the statistical station error of an NX SVOR as

$$\text{S.D. of Station Error (Radians)} = \frac{\sigma}{N}\ (\Sigma\ I_n^{\ 2})^{1/2} \tag{45}$$

If the SVOR consists of a conventional four-loop or cage array surrounded by a ring array, then Equation (45) must be modified to account for the error contribution of the conventional array. This can be done by assuming that the station error statistics of a large number of conventional arrays is Gaussian, with a standard deviation equal to a reasonable practical value based on experience, such as 1° (2° standard deviation of error spread). The modified form of Equation (45) is then

the following

$$\text{S.D. of Station Error (Degrees)} = \frac{1}{N}\left(1^2+57.3^2 x\sigma^2 \Sigma\, I_n^{\,2}\right)^{1/2} \qquad (46)$$

Addition of an SVOR ring array to a four-loop VOR will have two counteracting effects on error spread when a zero crossing receiver is used; it will tend to reduce error spread because of the 1/N multiplier in Equation (46), but it contributes its own errors in the form of the summation term in Equation (46). If the four-loop error spread is low enough, the SVOR ring array could conceivably increase rather than reduce error spread. The value of four-loop error spread at which the effect of an SVOR changes from an increase in error spread to a decrease may be found by treating the assumed 1° S.D. of four-loop error spread in Equation (46) as an unknown (x) and solving for the value of x at which the SVOR station error equals the four-loop station error, i.e., solving the equation

$$x = \frac{1}{N}\left(x^2+57.3^3 x\sigma^2\, \Sigma\, I_n^{\,2}\right)^{1/2} \qquad (47)$$

For the 5X SVOR, x = .39 (with σ = .07). Thus, if the four-loop error spread exceeds approximately .78°, it may be expected that addition of a 5X SVOR ring array will reduce the station error. Since practical conventional VOR error spreads are in the range 1° - 3°, 5X SVOR should reduce station error in almost all cases.

A solution of Equation (47) for a 13X SVOR (Section X), gives x = .24, so that 13X SVOR should reduce station error in all practical cases.

B. STATISTICAL STATION ERROR OF 5X SVOR TESTED AT NAFEC, AND OF 13X SVOR.

The ring array of the 5X SVOR tested at NAFEC radiated only third and fifth harmonics, so that

$$b_1 = 0$$

$$b_3 = 1/3 \quad \text{(See Equation (3))}$$

$$b_5 = 3/5$$

The antenna current I_n to be substituted in Equation (46) for determination of statistical station error can be found from Equation (33) and the design procedure described in Section IV. If the antennas are numbered clockwise and the #1 antenna is at $\phi' = 0$, the currents

at t = 0 are

$$|I_1| = |I_8| = 0$$

$$|I_2| = |I_7| = |I_9| = |I_{14}| = .0661$$

$$|I_3| = |I_6| = |I_{10}| = |I_{13}| = .180$$

$$|I_4| = |I_5| = |I_{11}| = |I_{12}| = .123$$

Equation (46) requires that a reasonable value for percentage error in antenna current be assumed. Based on experience with Alford loops and the SVOR modulator, a realistic figure is $\sigma = .07$, which corresponds approximately to observed errors in phase and amplitude. Substitution into Equation (46) then gives

$$\text{S.D. of Station Error (Degrees)} = .43 \quad \text{(5X SVOR)} \tag{48}$$

The S.D. of the error spread is twice the value given by Equation (48), i.e., .86°, which checks well with error spreads observed at NAFEC (Figure 11).

Substitution of the I_n values for a 13X SVOR (Section X) in Equation (46) gives

$$\text{S.D. of Station Error (Degrees)} = .25 \quad \text{(13X SVOR)} \tag{49}$$

Comparison of Equation (49) and (48) illustrates a reduction of statistical station error with increasing N which can be expected because of the 1/N factor in Equation (46).

C. STATISTICAL STATION ERROR OF SINGLE RING 5X SVOR WHEN USED WITH A CONVENTIONAL RECEIVER.

The first SVOR to be built and tested (at Ohio University) was a single ring 5X SVOR which radiated 30 hz., 90 hz., and 150 hz., from a single ring array comprising 14 antennas on a 14 foot diameter circle. A basic difference between this array and the 5X SVOR tested at NAFEC was the method of radiation of 30 hz., which was radiated separately by a conventional four-loop array in the NAFEC SVOR. With the NAFEC SVOR, it was thus possible to adjust the four-loop error spread using standard VOR adjustment procedures, so that the NAFEC SVOR, when used with a conventional receiver, could be expected to have error spreads equal to a conventional four-loop VOR. This was not possible with the single

ring prototype, as all fourteen antennas contributed to radiation of 30 hz., and to the 30 hz., error spread. The complex nature of the contribution of a single antenna to the 30 hz. error made it practically impossible to achieve reduction of 30 hz. error spreads independent of the SVOR error spread, in contrast with the four-loop VOR, where the effects of a single antenna error (or goniometer errors) are relatively simple and can be eliminated or compensated for.

In flight tests of the prototype large error spreads (up to 4°) were observed when a conventional receiver was used, and an impasse was reached because no adjustment procedure was available.

The following statistical analysis of 30 hz. error spread of the single ring 5X SVOR shows that, even if close tolerances are maintained on antenna currents, the statistical error spread will be so large as to probably disqualify the single ring SVOR from practical application.

Consider the 30 hz. error signal of a single ring 5X SVOR as observed at zero degrees azimuth. The nominal 30 hz. signal has a 30 hz. phase of zero degrees. The received error signal of an antenna located at azimuth ϕ_n has 30 hz. phase of ϕ_n. Only the 30 hz. error component in quadrature with the nominal signal, i.e., proportional to sin (ϕ_n) produces a 30 hz. phase error. Suppose the 30 hz. error current components that radiate an error signal in RF phase with the nominal signal have a Gauss distribution with magnitude,

$$\sigma \times I_{p30}$$

where I_{p30} represents the peak 30 hz. current component in a given antenna. For the 5X SVOR, I_{p30} = .218 for a nominal 30 hz. array factor of 1.0 peak. The resultant 30 hz. error signal in 30 hz. quadrature with the nominal signal then has a Gaussian distribution with standard deviation Δ given by

$$\Delta = \sigma \times .218 \times \sqrt{\sum_n \sin^2 \phi_n}$$

Again, taking σ = .07, and substituting $\phi_n = \frac{2\pi n}{14}$ gives

$$\Delta = .040 \text{ radians}$$

The S.D. of the statistical station error is two times Δ. Therefore;

Statistical Station Error Spread of Single Ring 5X SVOR With Conventional Receiver = 4.6°

which checks well with observations and, as previously noted, is probably too large for practical use.

VI SVOR RECEPTION AND COMPATIBILITY

A. GENERAL CONSIDERATION.

The SVOR signal includes the conventional reference and variable phase signals, but contains additional multiplexed odd-order harmonics of 30 hz. that will reduce scalloping if the receiver performs phase comparison based on the zero crossing time of the variable phase signal. Although proposed digital receivers would measure phase in this way, current receivers would require modification to benefit from SVOR, as they would to benefit from any contemplated change in VOR signal format other than DVOR.

A receiver modified for reception of SVOR would have to be capable of receiving conventional and DVOR without deterioration of performance. Also, the multiplexed SVOR signals cannot degrade performance of a conventional receiver. If both these conditions are met, conventional and SVOR could be used concurrently, with either standard receivers or zero crossing receivers.

B. MODIFICATION OF CONVENTIONAL RECEIVER FOR ZERO CROSSING PHASE DETECTION.

Figure 14 shows a simple, compact (1 1/4 inch square) circuit that operates from 28 V. DC and will convert a conventional receiver to zero crossing phase detection. This circuit, like other zero-crossing detectors, has the practical side benefit that course width is independent of percent modulation. The circuit is inserted between the second detector and the variable phase amplifier of a conventional receiver. It consists of a Twin-Tee reference rejection filter, followed by a high gain integrated circuit amplifier that serves as a hard limiter. The amplifier saturates at an input level of about 10 millivolts. Since the normal variable phase level at the second detector is much higher than the saturation level of the I.C. amplifier, the amplifier output is essentially a square wave whose zero crossings coincide very nearly with the zero crossings of the variable phase, regardless of the variable phase waveform. The square wave output is amplified and filtered in the conventional variable phase amplifier, whose output is applied to the conventional phase detector. Thus, the phase detector output depends only on the time of variable phase zero crossing, regardless of the details of the variable phase amplifier and phase detector. Figure 14 illustrates how the circuit would operate with conventional and SVOR signals having identical zero crossing times. The square wave input to the variable phase amplifier would be identical in both cases, hence the phase detector null would occur at the same OBS setting for any type of amplifier or phase comparator. The SVOR signal illustrated in Figure 14 is 5X, but an NX signal would be treated identically.

Use of the modification circuit requires recalibration of the receiver because of small phase shifts in the reference filter (6° in the prototype). Recalibration would use standard VOR signals.

Two Collins 51R3 receivers were modified with the circuit illustrated in Figure 14 and used in SVOR tests at NAFEC. Two different 51R3 receivers were used for SVOR tests at NAFEC.

C. PERFORMANCE OF MODIFIED RECEIVER WITH CONVENTIONAL SIGNALS.

There is now abundant experimental evidence, from tests made at Ohio University and NAFEC, that a receiver modified for zero crossing detection as shown in Figure 14 will perform almost identically to a conventional receiver with conventional signals, under flight conditions, in laboratory simulation, and in ground checks.

Figure 15 shows error curves obtained at NAFEC for two different 51R3 receivers, one modified, the other unmodified. Both were checked with standard signals. Error spreads were .6 and .25 degrees respectively; both figures being within normal receiver tolerance.

Figure 16 shows four-loop VOR station error curves obtained at NAFEC in a six NM orbit using modified and unmodified receivers simultaneously. The curves are identical within tolerances of receivers and tracking.

Figure 17 shows four-loop VOR roughness and scalloping curves obtained at NAFEC in a 20 NM orbit using modified and unmodified receivers simultaneously. Again, the curves are identical within measurement tolerance.

Figure 18 shows nearly identical polariscope flight measurements made on a four-loop VOR at NAFEC using modified and unmodified receivers simultaneously.

Figures 19 through 29 are simultaneous recordings of CDI indication of modified and unmodified 51R3 receivers, as obtained in orbital flight around a four-loop VOR (part of the experimental 5X SVOR) at Albany, Ohio. The traces match to within small details of scalloping and roughness. Displacement between the traces can be accounted for by differences in receiver calibration and by displacement between the two pens.

D. NOISE PERFORMANCE OF ZERO-CROSSING RECEIVER.

It has been suggested that zero crossing phase measurement, which uses only one or two points on the variable phase waveform, may be less accurate and more susceptible to noise than conventional analog phase measurement, which uses the entire waveform. However, the practical VOR signal environment is one of high signal to noise ratio, narrow band signals, and narrow detection bandwidth. Under such conditions, a limiter type zero crossing detector and an analog phase detector should perform identically, and are indeed found to do so in practice (Figures 16-29).

Data taken at NAFEC shows that flag will appear on the CDI of a modified receiver before the signal to noise ratio drops sufficiently to cause deterioration of performance. This is illustrated by Figure 30,

which shows data on roughness of a 5X SVOR during outbound radial flight to maximum usable distance. The modified receiver showed substantial reduction in roughness compared to the unmodified receiver out to 62 miles when it became rougher than the unmodified receiver. However, unmodified receiver flag appeared at 58 miles and modified receiver flag appeared at 61.6 miles.

The noise performance of the zero crossing phase detector shown in Figure 14 can be analyzed mathematically. Some of the results of the analysis can, however, be anticipated without calculation. The limiter circuit is insensitive to the input voltage during the interval between zero crossings, since it is saturated during that interval. Thus, all noise frequency components that behave identically at the zero crossing times of the nominal input will cause identical changes in the limiter output. Any odd-order harmonic of 30 hz. will therefore have the same effect as 30 hz. itself, namely a shift in phase of the 30 hz. component of limiter output and a consequent CDI error.

Suppose a noise signal N(t) is superimposed on a variable phase signal V(t), and V + N is hard limited and supplied to a 30 hz. bandpass amplifier. In units of 30 hz. phase, the nominal zero crossings of V are at $m\pi$, where m is an integer. The effect of N is to displace the mth zero crossing by an amount

$$\frac{N(m\pi)}{\alpha} \tag{50}$$

where:

$$\alpha = \left|\frac{dV}{d(\omega t)}\right|_{\omega t = m\pi}$$

$$\omega = 2\pi \times 30 \text{ hz.}$$

Equation (50) applies if N is small compared to V. The effect of the zero crossing displacement given by Equation (50) is to change the limiter output from its nominal square shape with equal positive and negative intervals to a square wave with generally unequal positive and negative intervals. The "error" in limiter output is a train of narrow rectangular pulses of width Equation (50), which may be expressed approximately as a train of impulses modulated by N, as follows

$$\text{Error} \approx \frac{N(t)}{\alpha} \sum_{m=-\infty}^{\infty} \delta(\omega t - m\pi) \tag{51}$$

Only the Fourier components of Equation (51) which lie within the passband of the 30 hz. variable phase amplifier will actually reach the phase detector to generate a CDI error. These components may be determined from an examination of the Fourier expansion of Equation (51).

If

$$N(t) = \int N(\Omega)\ e^{j\omega t} d\Omega$$

Then, using the Fourier expansion of an impulse train, the Fourier expansion of Equation (51) is;

$$\text{Error} = \frac{1}{2\pi\alpha} \sum_{m=-\infty}^{\infty} \int N(\Omega)\ e^{j(\Omega+2m\omega)t}\ d\Omega \qquad (52)$$

Equation (52) states that the spectrum of N is repeated at intervals of 60 hz. Letting $F = \Omega/2\pi$ and $f = 30$ hz.; the condition for CDI error is;

$$|F \pm 2mf| = f \pm B,\ m = 1,2,3 \text{ -----}$$

where B = bandwidth of 30 hz. amplifier

If $m = 0$

$F = 30 \pm B$

If $m = 1$

$$F = \begin{matrix} 30 \pm B \\ 90 \pm B \end{matrix}$$

If $m = 2$

$$\begin{matrix} 90 \pm B \\ 150 \pm B \end{matrix}$$

The above shows that only noise components that lie within ±B of an odd harmonic of 30 hz. will cause CDI error. Additional noise error, over and above 30 hz. errors which would be experienced with the same magnitude by an unmodified receiver (assuming reception of a standard VOR signal), is due to 90 hz., 150 hz., etc., noise. Because of limitations on propeller speed and aircraft speed, the only such noise components which are likely to be encountered in practice as a result of either propeller modulation or Doppler shift in carrier frequency are 90 and 150 hz., and for either component the noise frequency must be within ± about one hz. of nominal.

E. PERFORMANCE OF CONVENTIONAL RECEIVERS WITH SVOR SIGNALS.

One expectation underlying SVOR development was that any reasonably well designed VOR receiver would not show significant response to the multiplexed SVOR variable phase harmonics (90 hz., 150 hz., etc.). A

general principle in communications is to have no more receiver bandwidth than is required to handle any anticipated signals, as additional bandwidth can only contribute noise. In the VOR case, the variable phase amplifier should then have a bandpass of about one or two hz. centered around 30 hz. Because of the significance of 30 hz. phase in VOR, a somewhat larger bandwidth might be expected, say five hz., for phase stability reasons, but even such a wideband amplifier would be down by a factor of about 25:1 at the lowest SVOR harmonic frequency. Even with the assumption that the phase detector will respond to odd harmonics of 30 hz. with the same amplitude that it would to 30 hz., the fact that the 90 hz. SVOR amplitude is down relative to 30 hz. by a factor of 1/3 should lead to an indicated phase error no worse than .7°.

Extensive simulation tests were done at Ohio University and NAFEC to test the effects of 5X SVOR harmonics on conventional receivers. The test setup is illustrated in Figure 31. A harmonic synthesizer was built to obtain 90 and 150 hz. from the 30 hz. audio output of a VOR signal generator. Reference phase plus synthesized variable phase was then used to modulate an RF generator which supplied the receiver signal. The synthesizer was arranged so that the additional SVOR harmonics could be switched out, leaving only conventional 30 hz. variable phase. The test procedure consisted of setting the OBS in increments of 10°, and for each setting nulling the CDI by means of the phase control of the VOR signal generator. The CDI was first nulled with 30 hz. only, and then with 30, 90, and 150 hz. The effect of the multiplexed harmonics was then taken as the difference between the two readings of the VOR generator's phase dial.

The results of simulation tests of eleven conventional receivers and one modified 51R3 receiver are shown in Figure 32. Of the eleven conventional receivers tested, seven showed a maximum difference less than 0.9°, three showed maximum differences between one and two degrees, and one showed a maximum difference of 3.65°. In most cases the receiver error curves are nearly straight, indicating a fixed difference between conventional and SVOR response.

SVOR compatibility as indicated by Figure 32 appears as good or better than the compatibility of a similar selection of receivers with SSB DVOR, as shown by the curves of Figures 33 and 34, which are taken from Ref. 13. The one receiver that showed poor compatibility with SVOR (the DR 560) showed even worse compatibility with SSB DVOR.

Further evidence of compatibility of SVOR with conventional receivers is presented in Figure 35, which shows two station error curves of a 5X SVOR, one with the ring array energized, the other with the ring array deenergized so that only the conventional four-loop array signal was received. The curves were obtained at NAFEC in six NM orbital flight with radar reference. The curves are generally parallel but displaced from each other by about .8°. The fact that simulation tests showed that SVOR signals produced a nearly constant error at all bearings with most receivers can account for the displacement between the two station error curves.

Another possible cause is a small 30 hz. component of ring array signal, which would be compensated for in practice by course alignment. It should be noted that each of the two curves shown is the average of data from two orbits, which data showed discrepancies of up to 1° at some bearings.

A somewhat academic question regarding compatibility of SVOR with conventional receivers is the effect of the presence of a deenergized SVOR ring array on the signals radiated from the concentric four loop array that would furnish the 30 hz. SVOR component. The question is considered academic because in practice, standard adjustment procedures for reduction of four loop error spread would be carried out with the ring array in place and energized. Nevertheless, a test was carried out at NAFEC to determine whether the presence of the deenergized ring had any effect on the station error of a four loop VOR. Two sets of station error data were taken in six NM orbital flight, with radar reference, one set with a 5X SVOR ring array in place but not energized, the second with the ring array removed. The first set of data was taken with all ring array feeders connected to the SVOR modulator. Expectations were that the ring array should have little effect, because of the design of the SVOR modulator (Section VII), which rendered the ring array antennas antiresonant under the test conditions. It was further expected that whatever effect was observed should be the same at all bearings, since the modulator rotated in synchronism with the goniometer and any parasitic effects should therefore also have been synchronous. Figure 36 shows the test results. The two station error curves coincided within measurement accuracy for most of the orbit, but an unexplained discrepancy of 3° occurred around 100° azimuth.

F. VERTICALLY POLARIZED SIGNALS.

It was not anticipated that the SVOR ring array of the 5X SVOR tested at NAFEC would add appreciably to the vertical polarization error of the four loop VOR that radiated the 30 hz. component of the SVOR signal. Possible causes of additional V.P. would be parasitic currents induced in the ring array loops or pedestals by the four loop field, and direct radiation of V.P. by the design currents in the ring loops. Since the current distribution on the four sides of the ring loops had been measured and found to be very nearly uniform, little V.P. was expected from the design currents because a loop with uniform current distribution radiates only a horizontally polarized signal (Ref. 14). Anticipated parasitic currents in the ring array loops were small because the design of the ring feed system and modulator renders the loops antiresonant for parasitic excitation (see Section VII). Since the ring array loop pedestals were located seven feet from the four loop array and were themselves antiresonant (half wavelength long with one shorted and one nearly open end), little parasitic reradiation from them was expected. Polariscope runs made at NAFEC confirmed expectations by showing nearly equal V.P. for the four loop array and the complete SVOR. Figure 37 shows the data from these runs. Modified and unmodified receivers gave practically identical V.P. indications for the four loop VOR. With the complete SVOR radiating, however, a modified receiver showed a three to

fourfold reduction in V.P., as could be expected on the basis of the theory of Section III. Modified receiver polariscope data is plotted on Figure 37 for the complete SVOR configuration.

Installation of a TACAN antenna will, on theoretical grounds, increase the vertically polarized radiation of an SVOR. This may be understood by considering the SVOR field at the TACAN antenna and the reradiation from resulting induced currents in the TACAN antenna. For illustrative purposes, consider an SVOR consisting of eight antennas. At some instant of time, the current distribution among the eight antennas will be as in the sketch below

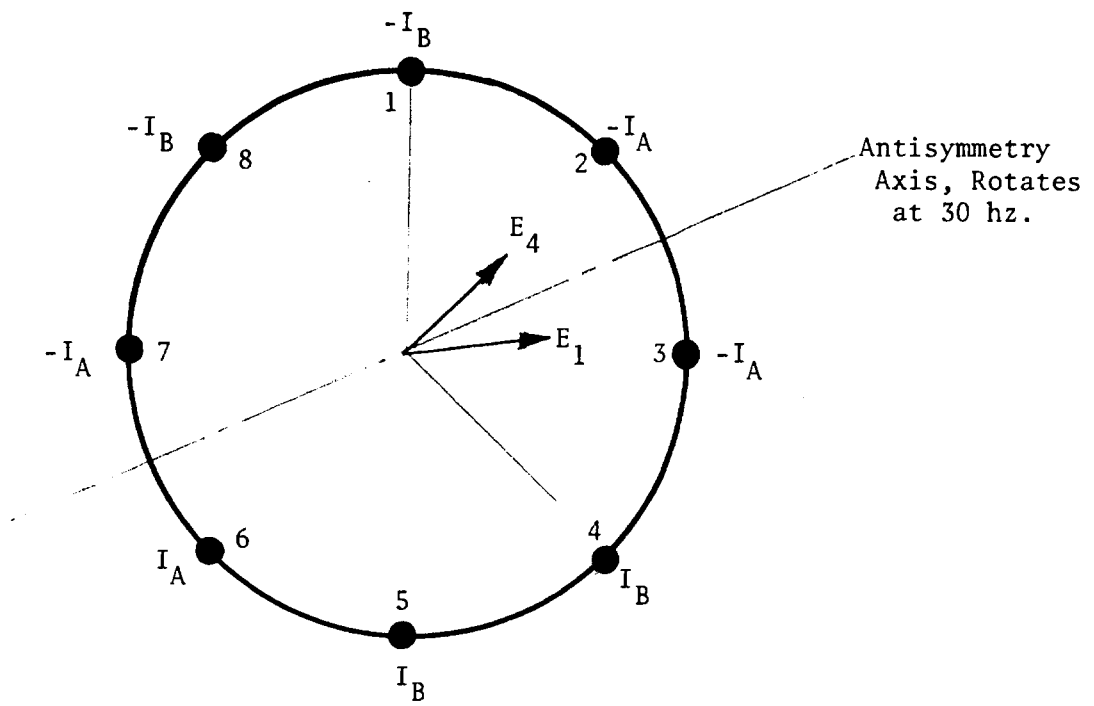

Because an SVOR current distribution contains only odd order harmonics (Equation (20)) with coincident zero crossings, each antenna of a continuous distribution of antennas could be paired with an oppositely excited mirror image in the antisymmetry axis ((1,4), (2,3), etc.) The pairing is approximately true for the discrete array (it is exact only when the antisymmetry axis passes through an antenna or passes halfway between antennas). The E field generated by each member of the mirror image pair (1,4) at the center of the array is shown in the sketch. The resultant field of this pair lies along the antisymmetry axis, as does the resultant field of every other pair. Clearly, then, the SVOR field at the center of the array lies on the antisymmetry axis. Therefore, if a TACAN antenna is installed, it will be immersed in a rotating horizontal E field of amplitude E_o. The component of this field tangential

to the TACAN antenna, in terms of an angular coordinate ϕ' is

$$E_{tang.} = E_o \text{ Sin } (\omega t - \phi') \tag{53}$$

Since the TACAN antenna is a conductor, E_{tang} must be canceled by the field of currents induced in the ring. It can be shown (Ref. 15) that the induced currents in a cylinder of radius a immersed in a uniform E field are

$$I_\phi = \frac{E_o}{K} \frac{H_1^{(2)}(Ka)}{H_1^{(2)\prime}(Ka)} \text{ Sin } (\omega t - \phi) \tag{54}$$

In other words, the induced currents are horizontal, sinusoidally distributed around the cylinder, and rotate in synchronism with the SVOR field. The terms preceding sin $(\omega t-\phi)$ in Equation (54) are simply a constant multiplier. The current distribution is illustrated by the following sketch

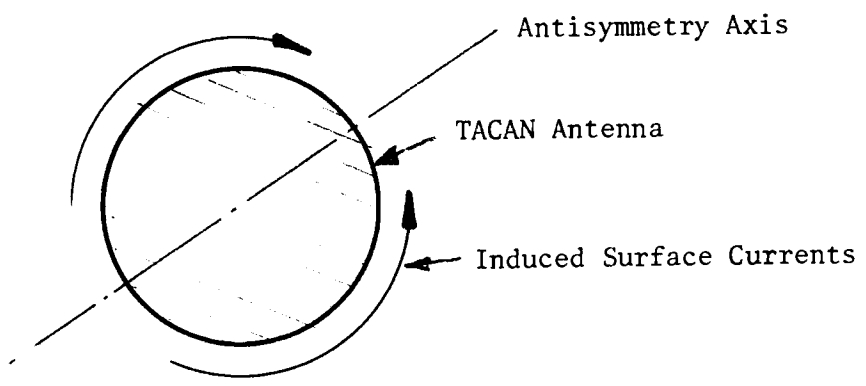

It can further be shown (Ref. 16) that the induced currents will reradiate a horizontally polarized field with azimuth distribution sin $(\omega t-\phi)$, and a vertically polarized field with azimuth distribution cos $(\omega t-\phi)$. The horizontally polarized field is in audio phase with the 30 hz. VOR signal, but the vertically polarized field is in audio quadrature and thus can cause a bearing error.

NAFEC test results confirm increase in V.P. upon installation of a TACAN antenna. Figure 38 shows polariscope runs, made with a conventional receiver, on a 5X SVOR before and after installation of a TACAN antenna. Observed V.P. approximately doubled.

Increased V.P. as a result of induced currents in a TACAN antenna should not be as severe for SVORs larger than 5X, since the SVOR antennas will be farther from the TACAN antennas.

VII SVOR DRUM MODULATOR

A. GENERAL.

The SVOR modulator must supply each antenna of the ring array with the required current, namely the continuous distribution (Equation (20)) evaluated at the angular position of the antenna. The principle underlying the two SVOR drum modulators that have been designed and built was selected from among other possibilities because it made feasible almost complete suppression of parasitics in the Alford loops that comprise the SVOR ring array. The spacing of these antennas is low enough* so that the measured mutual impedance of two adjacent antennas is almost 45% of the self impedance, so that some means had to be devised to suppress parasitics if there was to be any hope of achieving precise radiation patterns.

B. PRINCIPLE.

The principle of the SVOR drum modulator is based on a property of quarter wavelength transmission lines having characteristic admittance (reciprocal of characteristic impedance) Y_o. If the voltage at one end of the line is V, then the quarter wavelength line has the remarkable property that, regardless of the impedance at the other end of the line, the current in that impedance is $-jVY_o$. This property is readily proved from the fundamental transmission line equations for voltage and current (Ref. 3), which are

$$V(z) = C_1 e^{-jKz} + C_2 e^{+jKz} \tag{55}$$

$$I(z) = Y_o(C_1 e^{-jKz} - C_2 e^{-jKz}) \tag{56}$$

where z is a coordinate along the line. If the input end of the line, where the voltage V exists, is taken as z = 0, then, from Equation (55),

$$C_1 + C_2 = V \tag{57}$$

Evaluating I at $z = \lambda/4$ gives

$$I(\lambda/4) = -jY_o\ (C_1 + C_2) \tag{58}$$

from which the stated property follows. Although the current at $\lambda/4$

*From Equations (23) and (32), it may readily be deduced that, for any size SVOR, spacing between adjacent antennas $< \lambda/2$.

from the input end is independent of V, the input impedance is not. From the well known transformation property of quarter wave sections (or directly from Equation (55) and (56)). the normalized input impedance is equal to the normalized terminating admittance.

Figure 39 illustrates the 5X SVOR drum modulator. It consists of a rotating cylindrical metal drum, $\lambda/4$ long and of variable radius, surrounded by 14 stationary axial metal rods, equispaced on a circular cylindrical surface concentric with the axis of drum rotation. Each rod and the surface of the drum form a quarter wave section of transmission line, the characteristic impedance of which varies as the drum rotates. The drum is shaped so that the characteristic admittance Y_o of the line formed by the drum and a rod at angular coordinate γ is

$$Y_o\ (\gamma,t) = y(1 + \frac{1}{2}\ \Sigma\ A_n\ \text{Sin}\ n\ (\omega t-\gamma) \tag{59}$$

where

$$A_n = \zeta\ a_n \quad , \quad \zeta = \text{const.} \tag{60}$$

The a_n in Equation (60) are the Fourier coefficients of the required continuous current distribution Equation (20), as computed from Equation (25), and ζ is a normalizing constant chosen so that the peak value of the summation in Equation (59) is 1.0. y is a constant with dimensions of admittance, that is selected to give a practical ratio of maximum to minimum drum radius, and a practical modulator input impedance.

Therefore, if the rod at γ is supplied with a constant voltage V at one end, the current at its other end will be;

$$I(\gamma,t) = -jVy\ (1 + \frac{1}{2}\ \Sigma\ A_n\ \text{Sin}\ n\ (\omega t - \gamma) \tag{61}$$

Equation (61) contains a carrier term plus 50% modulation having a waveshape that is a correct sampling of the required continuous distribution for an antenna at $\phi = \gamma$. The 50% figure for modulation percentage was chosen to give a practical ratio of maximum to minimum drum radius.

By taking advantage of the facts that Equation (61) contains only odd order harmonics and

$$\text{Sin}\ n\ (\omega t-\gamma-180^\circ) = -\ \text{Sin}\ n\ (\omega t-\gamma),\ n\ \text{odd}$$

the undesired carrier term in Equation (61) can be eliminated by exciting the rod at $(\gamma+180^\circ)$ with voltage -V, and adding the current output of that rod to the current output of the rod at γ by connecting the two

outputs through $\lambda/2$ transmission lines. Thus;

$$\text{Combined Current Output of Rod at } \gamma \text{ and Rod at } (\gamma+180^\circ) = -jVy\zeta \; \Sigma \; a_n \; \mathrm{Sin}(\omega t-\gamma) \qquad (62)$$

From the foregoing, it is apparent that a drum modulator with M rods has only M/2 outputs. However, as a consequence of the fact that the required current distribution contains only odd harmonics, the members of a diametrically opposite pair of antennas are always excited with equal amplitude and opposite phase, so that for an M element ring, only M/2 independent modulator outputs are necessary, each output feeding both members of a diametrically opposite pair, with the current in one member being shifted 180° relative to the other by means of an extra 180° of feeder line or by a reversal in antenna polarization (the latter alternative was used in the experimental arrays). Figure 40 shows the connection scheme, embodying the above principles, that was used in the NAFEC SVOR.

Design of the modulator drum shape is straightforward if coupling between the rods is neglected, and if, for design purposes, the separation between rod and drum is calculated as if the drum surface was planar instead of irregularly cylindrical. The second approximation is good if the rod-drum spacing and the rod diameter are small compared to the local radius of drum curvature. The first is good if the rod to rod spacing is large compared to the rod-drum spacing. If the approximations are made, then the required separation between rod and drum can be calculated from the following standard formula for characteristic impedance of a circular rod above a ground plane (Ref. 17)

$$Z_o = 60 \cosh^{-1} \frac{D}{R} \qquad \begin{array}{ll} R = \text{rod radius} & (63) \\ D = \text{distance from center of rod to ground plane} & (63) \end{array}$$

Combining Equation (63) and (59), and setting t = 0 gives

$$D = R \cosh \left[\frac{1}{60y(1+\frac{1}{2} \Sigma A_n \mathrm{Sin}n\gamma)}\right] \qquad (64)$$

Equation (64) determines the drum shape.

The drum shape determined by Equation (64) will contain inaccuracies because of the approximations involved. Further inaccuracies will result from fabrication tolerances. It is essential that these inaccuracies not have a serious effect on SVOR performance. Two factors allow considerable latitude in drum shape without serious SVOR deterioration;

a) the harmonic coefficients of the array factor, b_n

(Equation (24)) need be maintained only within a fairly wide tolerance. For example, nominal b_n for a 5X SVOR are 1.0, 1/3, and 3/5, but performance would be virtually unaffected if they were 1.0, .37, and .55. A limit on tolerance is imposed only by generation of false zero crossings or by serious reduction in zero crossing slope.

b) the method of modulator connection, which adds currents from diametrically opposite rods, eliminates any even order harmonics from the modulator output.

C. SUPPRESSION OF PARASITICS.

The drum modulator has the important property that it makes possible almost complete suppression of parasitics. The explanation of parasitic suppression requires little mathematics, but is fairly subtle. It depends on the fact that an Alford Loop is antiresonant when it is short circuited at its balanced drive terminals. When antiresonant, little current will flow in the antenna even if it is placed in a strong external field. The theoretical basis for demonstration of parasitic suppression is the superposition theorem (Refs. 3, 15). In general electromagnetic theory terms, the SVOR array and its feeders have M input "ports", which are the input ends of the feeders. If only one of these ports was driven with a current, while the others were open circuited, there would, in general, be currents in all of the M Alford loops; a driven current in the loop connected to the driven feeder, and parasitics in the other loops. Let the current in the nth antenna when the qth input port is driven with unit current and all other ports are open circuited be C_{nq}. The superposition theorem states that I_n, the current in the nth antenna in general, is given by

$$I_n = \Sigma\, C_{nq}\, i_q \tag{65}$$

where i_q = current in qth input port.

For $n \neq q$, C_{nq} represents a parasitic current in the nth antenna under conditions where the input port to the nth antenna is open circuited. With proper feeder length, the open input port can reflect back to the drive terminals of the Alford Loop as a short circuit, thus rendering the loop antiresonant, so that the induced current, and consequently C_{nq}, $n \neq q$, becomes very small. With the antiresonant feeder length

$$I_n = C_{nn}\, i_n \tag{66}$$

In Equation (66), C_{nn} is the current in the nth antenna when the nth port is driven with unit current, all other ports being open circuited. Because of the symmetry of the SVOR array, C_{nn} is the same

for all n, and thus can be denoted simply as C. Equation (66) then becomes

$$I_n = C\, i_n \tag{67}$$

Equation (67) asserts simply that the current in the nth antenna depends only on the current in the nth input port. As previously described, the drum modulator provides correct i_n for any terminating impedance, so that, with correct feeder line length, I_n is determined solely by the shape of the modulator drum.

Experimentally, feeders were cut by placing two loops side by side with about an 18 inch separation, exciting one at the operating frequency, and measuring the parasitic current induced in the other while it was terminated in a variable length open circuited feeder whose length could be trimmed to minimize the induced current.

It was found that the coupling between Alford loops spaced as they would be in an SVOR (or DVOR) array is very high. With a feeder cut to maximize parasitics, an induced current 45 percent of the driven current was observed in the experimental arrangement. Clearly suppression of parasitics is absolutely essential for achievement of controlled radiation patterns.

D. DRUM MODULATOR FOR SINGLE RING 5X SVOR.

The prototype single ring 5X SVOR built at Ohio University in 1969-70 radiated 30 hz., 90 hz., and 150 hz. from a single ring. KR was taken as 5.0 for a ring diameter of 14 feet at 110.5 mhz. Application of Equation (25) to the Fourier coefficients of the array factor,

$$b_1 = 1.0$$

$$b_3 = 1/3$$

$$b_5 = 3/5$$

gives

$$\begin{aligned} a_1 &= -j\ (.487) \\ a_3 &= -j\ (.146) \\ a_5 &= \ \ j\ (.366) \end{aligned} \tag{68}$$

Hence, the unnormalized continuous current distribution at t = 0, omitting the irrelevant phase factors in Equation (68), is

$$.487 \operatorname{Sin} \gamma + .146 \operatorname{Sin}(3\gamma) - .366 \operatorname{Sin}(5\gamma) \tag{69}$$

The factor ζ that normalizes Equation (69) to unit peak amplitude is

1.23, and the normalized distribution is

$$.598 \text{ Sin } \gamma + .179 \text{ Sin } 3\gamma - .450 \text{ Sin } 5\gamma \qquad (70)$$

(70) was used in Equation (64) to design the drum shape. Mean drum diameter was about 12". The quarter wave rods were placed on a cylindrical surface 14" in diameter, so that rod spacing was just over 3". Rod diameter was 3/8" and minimum rod to drum spacing was .100". A standard VOR tone wheel was driven by the drum shaft to provide reference modulation. The modulator was powered by a 1/3 HP synchronous motor.

The completed modulator was tested working into dummy loads. Figure 41 is a photograph of the modulator undergoing bench tests. Figure 42 shows measured output of one pair of rods, with the design amplitude Equation (69) plotted for comparison. Figure 43 shows measured and design phase.

E. DRUM MODULATOR FOR 5X SVOR TESTED AT NAFEC.

The design procedure for this modulator was exactly the same as for the prototype single ring SVOR, except that $b_1 = 0$. The normalized current distribution in this case was

$$.28 \text{ Sin } (3\gamma) + .72 \text{ Sin } (5\gamma) \qquad (71)$$

Figure 44 and 45 show measured and design amplitude and phase. Figure.46 is a photograph of the modulator viewed from the drive motor end. A standard goniometer-tone wheel assembly is just visible at the other end for provision of 30 hz. and reference. Figure 47 is an oscilloscope photograph of the RF output of one pair of rods.

F. DRUM MODULATOR FOR 13X SVOR.

Section X describes a 13X SVOR design that consists of a 30 element ring array concentric with a four-loop array. A drum modulator for this design would require 30 rods, so that if the same spacing between rods as was used in the 5X SVOR, which had 14 rods, was retained, over twice the drum diameter would be necessary. The weight, volume, and requirement for a large, heavy motor in order to reach synchronous rotation speed probably make such a large drum impractical. The largest practical size for a drum modulator is probably about that of the 5X SVOR unit.

If the spacing between rods were reduced by a factor of 14/30 in order to fit 30 rods into the space formerly occupied by 14, coupling between the rods could not be neglected as it was in the 5X modulator design. Equation (63), which gives the characteristic impedance of a transmission line formed by a single isolated rod and a ground plane,

would become very inaccurate, and if used in design would lead to serious errors in the modulator output waveshape.

A drum modulator with closely spaced rods must be analyzed by general multiconductor transmission line theory (Ref. 18). Thirty rods and the drum plane form a multiconductor transmission line that can be characterized by 30 independent TEM "modes". For the nth mode, the electric and magnetic fields are determined by a solution of Laplace's equation in two dimensions, with the pth rod at a voltage V_{np} above the ground plane. The 30 sets of 30 voltages must be linearly independent so that any arbitrary set of voltages can be expressed as a linear combination of them. Associated with each set of mode voltages is a set of mode currents I_{np}. The most general distribution of voltages and currents can be written as

$$V_p = \sum_{n=1}^{30} [a_n e^{-jKZ} + b_n e^{+jKZ}] V_{np}$$

$$I_p = \sum_{n=1}^{30} [a_n e^{-jKZ} - b_n e^{+jKZ}] I_{np} \tag{72}$$

Equation (72) represents a sum of 30 waves towards + z, and 30 waves towards -z, with general amplitude coefficients for the nth mode of a_n and b_n respectively.

The mode voltages v_{np} can always be chosen to be orthogonal, that is, to satisfy

$$V_{np} V_{qp} = 0 \ , \quad n \neq q \tag{73}$$

Also, without losing generality, the n = 1 mode can be chosen so that

$$V_{1p} = 1, \quad \text{all } p \tag{74}$$

Assuming Equations (73) and (74) to be satisfied, a drum modulator with a common input voltage V_o at z = 0 can be readily analyzed*. Substituting z = 0 into the first of equations (72) and using the orthogonality condition Equation (73) leads to

$$a_1 + b_1 = V_o \tag{75}$$

$$a_n + b_n = 0, \ n \neq 1$$

*The 180° phase difference between the outputs of opposite halves of such a modulator would be obtained by half wavelength lines at the output end of the modulator.

Substituting $z = \lambda/4$ and Equation (75) into the second of Equations (72) gives the output currents

$$I_p = -j\, V_o\, I_{1p} \tag{76}$$

For the n = 1 mode, I_{1p} can be expressed in terms of a characteristic impedance as follows

$$I_{ip} = \frac{1}{Z_{1p}} \tag{77}$$

So that Equation (76) becomes

$$I_p = -j\, \frac{V_o}{Z_{ip}} \tag{78}$$

The quantities I_{1p} or Z_{1p} are determined from a potential Φ that is a solution of Laplace's equation

$$\nabla^2 \Phi = 0 \tag{79}$$

with the boundary condition $\Phi_{rods} - \Phi_{drum} = 1.0$. The exact solution of Equation (79) depends on the shape of the entire drum. However, Φ in the vicinity of a particular rod is determined almost entirely by the spacing between that rod and the drum, and by the coupling to the two adjacent rods. Therefore, Equation (79) was solved for the configuration shown below

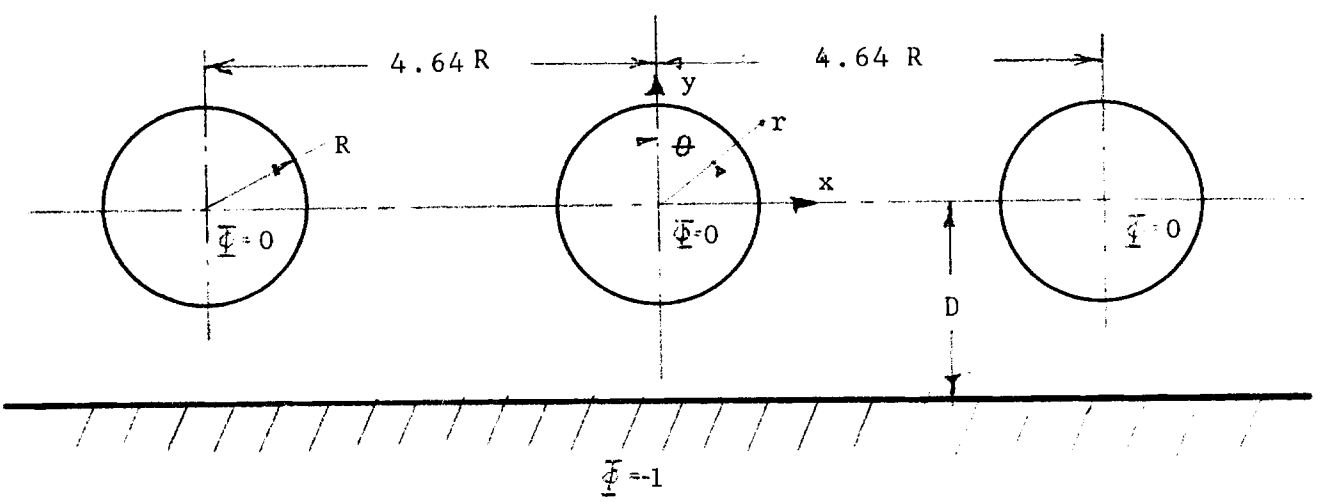

The rod separation shown in the sketch corresponds to the contemplated separation in a 13X drum modulator having the same diameter as the 5X modulator. Assuming the pattern of rods shown in the sketch to continue indefinitely, the additional boundary condition

$$\frac{\partial \Phi}{\partial x} = 0 \quad \text{at } x = 2.32\ R$$

can be imposed by symmetry and a solution of Equation (79) sought only between $x = \pm 2.32R$. Clearly, Φ is an even function of θ. For the problem at hand, then, a suitable solution of Equation (79) in polar coordinates is (Ref. 3).

$$\Phi = C_o \ln r + \sum^{\infty} C_n (r^n - r^{-n}) \cos n\theta \tag{80}$$

Equation (80) was solved by machine computation, subject to the boundary conditions, for values of D ranging from R to 3R. The characteristic impedance z_c was found for each D from

$$Z_o(D) = \frac{120\pi}{\int_{rod} \bar{n}\cdot\bar{\nabla}\Phi d\ell} = \frac{60}{C_o(h)} \tag{81}$$

Equation (81) is plotted in Figure 48. For comparison the characteristic impedance of an uncoupled rod, which is given by $60 \cosh^{-1} (\frac{D}{R})$ is plotted. It is clear from the figure that the shielding effect of adjacent rods, which tends to reduce the rod-ground capacitance and increase Z, cannot be neglected in drum design.

For design purposes, an equation giving $D(Z_o)$ is more convenient than $Z_o(D)$, since Z_o as a function of drum angle is known from Equation (59), and D is required to determine the drum shape. Therefore, the results of Equation (81) were least squares fitted to the following form, which is the inversion of $Z_o(D)$ for an isolated rod, plus a correction series,

$$D/R = \cosh \left(\frac{Z_o}{60}\right) + \sum_1^3 C_n Z_o^n \tag{82}$$

C_n in Equation (82), for (S/R) = 4.64, were found to be

$$\begin{aligned} C_1 &= -.981 \times 10^{-3} \\ C_2 &= .497 \times 10^{-4} \\ C_3 &= -.131 \times 10^{-5} \end{aligned} \tag{83}$$

Using Equation (82) and (83), a 13X drum modulator, no larger than the 5X modulator, can be readily designed.

G. DRUM MODULATOR INPUT POWER.

The multiplexed SVOR variable phase harmonics represent radiated energy that must be supplied to the drum modulator. The additional variable phase power, as a fraction of the 30 hz. variable phase power, can be computed from the variable phase array factor (Equation (24)). If the first term (30 hz.) of Equation (24) is deleted, and the remainder of the array factor squared and integrated from $\phi = 0$ to $\phi = 2\pi$, the result, when divided by 2π, is the average additional variable phase power. Since the average power in the 30 hz. component of Equation (24) is 1/2 (since $b_1 = 1$), there follows

$$\frac{\text{Drum Power}}{\text{30 hz. Goniometer Power}} = \sum_{n=2}^{N} b_n^{\,2} \tag{83}$$

For N = 5 and N = 13, the ratios of drum to goniometer power are .472 and .481 respectively. The nearly identical values of the latter numbers suggest that they represent the drum to goniometer power generally. To show that this is indeed true, the fact that the SVOR signal is nearly a square wave of amplitude $\pi/4$ with a superimposed ripple $\Delta b_N \operatorname{Sin} N(\omega t-\phi)$ (see Equations (39), (40), (41)) may be used. The average drum power is then approximately, in terms of a unit square wave $S(\theta)$

$$\text{Drum Power} = \left[\frac{1}{2\pi}\int_0^{2\pi} \left(\frac{\pi}{4}\right) S(\theta) + \Delta b_n \operatorname{Sin} N\phi - \operatorname{Sin}\phi\right]^2 d\phi \tag{84}$$

Substituting $\Delta b_N = (N-1)/2N$ in Equation (84) and performing the integration gives

$$\frac{\text{Drum Power}}{\text{Goniometer Power}} = \frac{\pi^2}{8} + \frac{1}{4}\left(\frac{N-1}{N}\right)^2 + \frac{(N-1)}{N^2} - 1 \tag{85}$$

The limit of Equation (85) for large N is

$$\frac{\text{Drum Power}}{\text{Goniometer Power}} = .49 \tag{86}$$

From Equation (83) or (86), it may be seen that the drum modulator must be supplied by the modulation eliminator with approximately 50% of the power required by the 30 hz. goniometer. In both experimental SVORs, the additional power has been within the capability of a standard modulation eliminator.

VIII TESTS OF SINGLE RING 5X SVOR

A. GENERAL COMMENTS.

The first SVOR to be built and tested was a single ring 5X SVOR, which was constructed at Ohio University during 1969-70. Figure 49 is a photograph of the prototype SVOR array. A central Alford loop radiated reference modulated carrier, and a 14 foot D. (KR = 5), 14 element ring array radiated 30 hz., 90 hz., and 150 hz. simultaneously.

The prototype array achieved the predicted reduction in course scalloping, but proved to have several properties that would be disadvantageous in practice. These were

1) Low cone of confusion. From Equations (3) and (35), the pattern of the single ring 5X SVOR (neglecting the station error term in Equation (35) is

$$P_s(\theta,\phi,t) = \frac{J_1(KR\cos\theta)}{J_1(KR)} \operatorname{Sin}(\omega t-\phi)+\frac{1}{3}\frac{J_3(KR\cos\theta)}{J_3(KR)} \operatorname{Sin}[3(\omega t-\phi)]$$

$$+ \frac{3}{5}\frac{J_5(KR\cos\theta)}{J_5(KR)} \operatorname{Sin}[5(\omega t-\phi)] \qquad (87)$$

The ratios of Bessel functions appearing in Equation (87) range in value from 1.0 at the horizon to zero at the zenith, so that the Fourier coefficients of P_s vary with elevation. Figure 50, which is a graph of P_s for several elevation angles, illustrates the changing shape of P_s with elevation. It will be noted that a false zero crossing of P_s occurs between 30° and 40° elevation. Since a zero crossing phase detector gives erroneous readings if a false zero crossing occurs, the cone of confusion for the single ring 5X SVOR has an elevation angle of only 35°.

2) High Error spread when used with a conventional receiver. This point is covered in Section V-C.

3) Inflexibility, in that the relative amplitudes of all three harmonics, and their zero crossing times, are built into the drum.

All three of the above defects were corrected in the second 5X SVOR to be built. Prototype tests will therefore not be presented at great length.

B. GROUND TESTS.

After building the drum modulator according to the principles of Section VII-B and cutting feeders according to VII-C, currents in the ring array were measured and compared with design values. Results of these measurements are shown in Figure 51. Agreement was considered good except at the low values of current, where two large current vectors from opposite halves of the modulator nearly cancel, so that a large percentage inaccuracy is to be expected. The observed good agreement also confirmed that parasitic suppression was being achieved.

A variable phase radiation pattern was measured using a fixed receiving Yagi stationed 300 feet from the VOR. The output voltage of the Yagi was measured by a "Vector Voltmeter". Design pattern amplitude and measured amplitudes for every 10° of drum rotation are shown in Figure 52. Agreement was within a tolerance that correlated with observed antenna current tolerances.

A station error curve (Figure 53) was determined by moving a pickup Yagi successively to each of 36 surveyed positions on a 150 foot D circle and observing the drum rotation angle that produced a pattern null at each position. For each position, two nulls nominally 180 degrees apart are observed. If E_1 and E_2 were the observed deviations in bearing of the two nulls associated with a given pickup antenna position, then the station error for that bearing was taken as

$$\text{Station Error} = \left(\frac{E_1+E_2}{2}\right) \tag{88}$$

Equation (88) is based on the assumption that the SVOR receiver has a zero crossing phase detector of the type described in Section VI-B, which processes the variable phase signal by hard limiting it and supplying the resulting limited waveform to a conventional amplifier and phase detector. The nominal limiter output has equal positive and negative duration. If its nominal amplitude is 1.0, the amplitude of its 30 hz. Fourier component is $4/\pi$ (Ref. 3). The effect of E_1 and E_2 is the generation of unequal positive and negative duration of limiter output, or, in other words, the generation of error pulses, 2.0 units in amplitude (since the zero crossing displacement errors reverse the sign of the limiter output from its nominal value), of duration E_1 and E_2, and located at the nominal zero crossings. By standard Fourier analysis, it is readily shown that these error pulses, if narrow in duration, produce a 30 hz. Fourier component, in quadrature with the nominal 30 hz. component, and of amplitude

$$\frac{2}{\pi}(E_1 + E_2)$$

The resulting phase shift in the 30 hz. Fourier component is given by Equation (88).

Observed station error spread was 1.2°, which agrees well with statistical analysis by the methods of Section V.

C. FLIGHT TESTS.

CDI recordings were made in orbital flight at approximately 10 miles radius, using a conventional 51R3 receiver and a 51R3 modified as described in Section VI-B. The main source of scalloping was a grove of trees located 300 feet from the VOR at bearings between 270° and 350°. Typical orbital records are shown in Figures 54, 55, and 56. Figures 54 and 55 were taken in sectors nearly at right angles to the scalloping source, and the modified receiver therefore showed a large reduction in scalloping compared to the unmodified receiver (see Figure 6). Figure 56 was taken in a sector nearly in line with the scalloping source, and little reduction in scalloping was observed.

Figure 55 shows a difference of nearly 4° in the courses indicated by the modified and unmodified receivers. This condition is to be expected because the 30 hz. signal and the complete SVOR signal are built into the same drum, and thus will in general give different courses if the drum construction is imperfect. This is a major and probably disqualifying disadvantage of the Single Ring SVOR, since there is no practical way of separately adjusting the conventional and SVOR courses.

Figure 57 is a polar plot of scalloping observed with conventional and modified receivers.

IX TESTS OF 5X SVOR WITH NO CONE OF CONFUSION

A. GENERAL COMMENTS.

The reason for the low elevation angle of the cone of confusion associated with the single ring 5X SVOR is revealed by examination of Equation (87) and Figure 12. For the VOR, KR was equal to 5.0. Study of the curve of $J_1(x)$ between x = 0 and x = 5.0 shows that the Bessel function ration that multiplies the 30 hz. term in Equation (87) becomes zero at an elevation angle of 40° and reverses sign at higher elevations. Thus 40° would mark the onset of the cone of confusion for a conventional receiver. Because of the severe amplitude change of the 30 hz. component with increasing elevation, the complete SVOR signal becomes distorted and generates a false zero crossing between 30° and 40° (Figure 50).

Separate generation of the 30 hz. signal by a conventional four-loop array would eliminate the phenomena described in the preceding paragraph, and also have the important operational advantage of permitting separate adjustment of the courses as seen by conventional and modified receivers. With separate 30 hz. generation, the 30 hz. component in Equation (87) must be replaced by

$$\cos\theta \sin(\omega t-\phi) \tag{89}$$

which is the azimuth and elevation pattern of the rotating 30 hz. field of a perfect four-loop VOR in free space. (Image patterns have been neglected here as they are assumed to be the same for all components of the array, so that they contribute only an irrelevant factor of 2j sin (Kh sinθ), where h is the common height of all loops in the SVOR). The modified form of Equation (87) is plotted in Figure 58, which indicates no false zero crossings at any elevation, hence no theoretical cone of confusion.

Since separate radiation of the 30 hz. signal by a four-loop array appeared to eliminate the undesirable features of the single ring array, an SVOR was designed according to the principles of preceding sections to incorporate this feature. A photograph of the array is shown in Figure 59. The four loop array was concentric with a 14 element ring array having KR = 5.0. The difference in height of the four loop and ring arrays that is visible in the photograph was a matter of practical convenience in the Albany, Ohio, tests and was not used for the NAFEC tests. Also visible in the photograph are the modulator, goniometer, and drive motor, which were normally housed in a pit under the four loop array. Figures 40 and 60 show the array layout and schematic diagrams of the modulator connections and layout. Figure 60 shows division of modulation eliminator power between the goniometer and the drum modulator.

B. GROUND TESTS (OHIO UNIVERSITY).

Bench tests of the drum modulator were conducted first. These have previously been covered in Section VII-E, and in Figures 44, 45, 46, and 47.

After aligning the four loop course with the SVOR course by setting the angular position of the goniometer relative to the drum modulator until zero crossings of the 30 hz. and of the composite 90 and 150 hz. signals coincided at a particular azimuth, the radiation patterns shown in Figure 61 were observed. The figure shows oscilloscope photographs of the RF picked up by a Yagi 300 feet from the VOR, with reference modulation turned off. The figure also clearly shows the process of multiplexing the ring array signal with the four loop signal to generate the resultant SVOR signal.

After aligning the SVOR course with North by setting the reference tone wheel position relative to the goniometer-drum modulator assembly, station error curves were taken under each of the following four conditions:

a) Four loop array only, conventional VOR receiver (RA-21).

b) Four loop array only, VOR receiver modified for zero crossing phase measurement (Collins 51R3).

c) Complete array, conventional receiver.

d) Complete array, zero crossing receiver.

A substitution technique as follows was used to eliminate receiver OBS error. A receiving Yagi was moved successively to each of 18 surveyed angles. For each position, the CDI was nulled, and a signal from a VOR test generator was substituted for the radiated signal. The CDI was again nulled and the reading of the angle dial of the test generator recorded.

From the considerations of Section VI, it was expected that the station error curves taken under conditions a), b), and c) would be nearly identical, while the error spread under condition d) should be less than that of the other three cases. This was in fact the case, as is shown in Figure 62. Error spread under conditions a), b), c) averaged 4.2°, while error spread under condition d) was 1.8°. The curves for a), b), and c) were clearly similar in appearance although local differences of up to 2° between the curves existed. These may have been due to the fact that one of the receivers was an RA-21, which showed CDI response to the 90 and 150 hz. tones of 1°-1.5° (Figure 32).

C. GROUND TESTS (NAFEC).

Three station error curves taken at NAFEC under various conditions are illustrated in Figures 11, 63, and 64. As noted in Section III-D, Figure 11 illustrates the reduction in station error indicated by a

modified receiver when SVOR harmonics are added to the normal 30 hz. signal. Figure 63 shows similar four loop VOR ground check curves with a modified and an unmodified receiver. Figure 64 illustrates reduction in SVOR station error of a modified receiver in comparison with conventional receiver.

D. FLIGHT TESTS (OHIO UNIVERSITY).

Figures 65-75 show simultaneous eight mile orbital flight recordings of the CDI indications of modified and unmodified 51R3 receivers, with the complete 5X SVOR transmitting. The records show scalloping reduction factors ranging from a low of approximately two in the vicinity of 320°, which was nearly in line with the grove of trees that provided the main source of reflections, to high values of eight or more around 50° and 280°. Displacements between the average values of the two simultaneous recordings can be accounted for by the different error curves of the four loop VOR and the complete SVOR (Figure 62).

Comparison of the unmodified receiver records of Figures 19-29 (four loop only) with the unmodified receiver records of Figures 65-75 (complete SVOR) shows nearly identical roughness at each OBS setting, as would be expected on the basis of the results of Section VI, which show that the unmodified receiver does not respond significantly to the additional SVOR harmonics. It should be noted that the two sets of records (complete SVOR and four loop array only) were made on the same day, so that the reflecting environment did not change between runs.

Figures 76 and 77 show recordings of a modified receiver's CDI current made during radial flight outbound from the VOR. For each radial, two records are shown, one with the complete SVOR transmitting, one with the four loop array alone transmitting. The improvement in flyability effected by the SVOR is evident from the figures.

E. FLIGHT TESTS (NAFEC).

The same 5X SVOR that was flight tested at Ohio University was shipped to NAFEC and extensively flight tested there. One possibly significant difference between the NAFEC and Ohio University installations was ground mounting of the entire array at Ohio University as compared to mounting on a standard VOR counterpoise at NAFEC.

Some of the extensive NAFEC flight test data will be presented here according to the following breakdown based on general conclusions that can be drawn from the data.

1. Effect of SVOR on Four Loop Station Error. This has already been commented on in Section III-D. Figure 10, which is taken from the NAFEC data, shows a reduction in station error spread from 2.8° to 1.4° when SVOR harmonics were added to the four loop signal and a modified receiver was used.

2. Effect of Receiver Modification on Performance with Conventional Signals. This point has been covered in Section VI-C. Figures 15-18, from NAFEC data, show convincingly that receiver modification has no effect on receiver performance with standard signals.

3. Effect of SVOR Signals on Conventional Receiver. This point has been discussed in Section VI-E. Theory, simulation tests, and Ohio University flight test data (compare unmodified receiver data of Figures 19-29 with unmodified receiver data of Figures 65-75) all indicate that addition of SVOR signals should have little effect (.2 or .3° at most) on an unmodified 51R3 receiver. Initial data from NAFEC indicated otherwise. Figures 78 and 79 show NAFEC station error data for the four loop VOR and the 5X SVOR. Examination of the error curves for the unmodified receiver shows 1.6° error spread for the four loop and 3.7° for the SVOR, with dissimilar error curve shapes. Two months elapsed between the two tests. The tests were later repeated, both on the same day, to resolve the apparently anomalous initial results which might have been due to a change in the reflecting environment or a change in the four loop VOR during the two month interval between the first tests. Figures 35 and 36 show the results. With the complete SVOR radiating error spread was 4.05° (average of two runs). With the ring array present but not radiating, error spread was 3.7°. With the ring array removed, error spread was 3.1°. Error curve shapes in the first two cases were the same within experimental error. Shapes of the second and third case error curves were generally the same except for one unexplained discrepancy near 100° bearing. These results clearly contradict the initial results and agree with simulation, Ohio University flight test, and theory in confirming that SVOR signals have little effect on station error seen by a conventional receiver.

   Initial NAFEC test results, shown in Figures 80 and 81, seemed to show that addition of SVOR to four loop signal caused the roughness seen by a conventional receiver to increase, in contradiction to theory, simulation, and Ohio University flight tests. Comparison of Figures 80 and 81 shows that the unmodified receiver roughness increased by a factor of about two upon addition of the SVOR signal. Again, two months had elapsed between the two tests. Upon repetition of the tests, both taking place on the same day, the recordings disclosed no change in roughness upon addition of SVOR to four loop signal. Figures 82 and 83 show two of the later orbital records taken at NAFEC with a conventional receiver. The detailed agreement between the two traces (which were made on two different orbits) clearly indicates no measurable effect of SVOR on roughness seen by a conventional receiver.

4. Scalloping Reduction by SVOR. Figure 81 (NAFEC data) shows SVOR roughness and scalloping in 20 NM orbit, as seen by modified and unmodified receivers. Assuming the unmodified receiver roughness to be that of the four loop VOR alone (see 3, above), the curves show the reduction in scalloping effected by SVOR. Figure 84 is a graph of the numerical reduction factor. The main source of scalloping was a tower at 220°, so that the low improvement factor observed near 220° and 40° agrees with Equation (10) and Figure 6. However, the scalloping improvement factors shown in Figure 84 and in other NAFEC data are not as high as were observed at Ohio University (Figures 65-75), nor as high as theory would predict. This was almost certainly caused by incorrect phasing and amplitude of the ring array signal in the far field, as a consequence of the ring array being mounted on a standard counterpoise and adjustments being performed using a near field signal (500 feet). Counterpoise effect in the near field would tend to make the ring array signal larger relative to the four loop signal than it would be in the far field near the horizon. This problem did not arise at Ohio University because the entire array was ground mounted.

5. SVOR Effects on Vertical Polarization. V.P. effects are discussed at length in Section VI-F. The following conclusions follow from the NAFEC data shown in Figures 36, 37, and 38: a) addition of SVOR to a four loop array causes little additional V.P., provided no TACAN antenna is present. Installing of a TACAN antenna causes a twofold increase in V.P., b) a modified receiver in conjunction with SVOR will reduce V.P. by an observed factor of three to four.

X DESIGN AND FEASIBILITY STUDY OF 13X SVOR

A. DESIGN OF RING ARRAY.

A 13X SVOR variable phase will contain 30 hz. plus its 3rd, 5th, 7th, 9th, 11th, and 13th harmonics. The Fourier coefficients of a square wave will be the relative amplitudes of all but the 13th harmonic, which will be augmented by an amount ε to increase slope at zero crossing (see Section II-B). If ε is taken as 6/13, slope at zero crossing is exactly 13 and falze zero crossings will not occur unless multipath exceeds 26% of the direct signal (Section II-B). Therefore, a suitable 13X SVOR variable phase radiation pattern P_s is

$$P_s = \frac{7}{13} \text{Sin } [13(\omega t-\phi)] + \sum_{n=1}^{5} \frac{1}{(2n+1)} \text{Sin } [(2n+1)(\omega t-\phi)] \qquad (90)$$

The radius of the ring array can be determined from Equation (25) and the requirement that Bessel function in the denominator of that equation be reasonably large for all n to avoid excessively large currents in the ring array. Examination of the Bessel function curves of Figures 12 and 13 shows that a good value of KR is 11.6, for which the values of the Bessel functions in Equation (25) will be

$$J_{1,3,5,7,9,11,13}(11.6) = -.232,\ .234,\ -.153,\ -.104,\ .274,\ .246,\ .096.$$

With KR = 11.6, ring diameter at 110 mhz is 33 feet.

The number of antennas required can be decided by calculation of the station error due to the finite number of antennas from Equation (36). For a first trial, let the number of antennas be 28, which is one more than the theoretical absolute minimum. Then, Equation (36) predicts

$$\text{Station Error Due to Finite Number of Antennas} = \frac{7/13}{13} \frac{J_{15}(11.6)}{J_{13}(11.6)} \times 57.3 \text{ deg.}$$

$$= .561° \text{ peak}$$

Since .561° peak is unacceptably high, more antennas are required. An even number is necessary so that the antennas can be fed in pairs, so the next highest candidate is M = 30. Equation (36) then gives

$$\text{Station Error Due to Finite Number of Antennas} = .092° \text{ peak} \qquad \text{(30 antennas)}$$

.092° is well below the .25° standard deviation statistical station error (Equation (49)), and is thus acceptable.

A suitable 13X SVOR ring array therefore comprises 30 antennas on a circle 11.6 wavelengths in circumference (33 feet diameter at 110 mhz.).

B. FEASIBILITY OF DRUM MODULATOR.

The difficulty with a 13X drum modulator is keeping its dimensions no larger than those of the 5X modulator, which are probably as large as is practical. This problem has been discussed at length in Section VII-F. The conclusion reached there was that a 13X modulator no larger than the 5X modulator could be designed and built with the aid of theoretical formulas that account for coupling between the modulator rods.

C. REDUCING CONE OF CONFUSION.

It can be seen without extensive calculation that a single ring 13X SVOR will have an impractically large cone of confusion. Equation (35) is the general formula for SVOR variable phase radiation pattern. Omitting the small station error term from Equation (35), it is apparent from the remaining summation that the amplitude of the nth harmonic changes with elevation in proportion to the factor

$$\frac{J_n(KR \cos\theta)}{J_n(KR)} \tag{91}$$

Examination of Bessel function tables shows that zeros of the fundamental (30 hz.) and 3rd harmonic occur at 10.2 and 9.8 respectively. Therefore, if KR = 11.6, the numerator of the factor (91) disappears at approximately $\theta = 30°$ for both n = 1 and n = 3. Thirty degrees elevation would then be the boundary of the cone of confusion with a conventional receiver, since 30 hz. would reverse phase at that elevation. A false zero crossing would occur well below 30° elevation because of decreased amplitude of the two harmonics that have largest magnitude on the horizon.

A single ring 13X SVOR is thus impractical because of its large cone of confusion. The following means of reducing the cone of confusion were therefore devised, and calculations made to test their feasibility.

1. Radiation of 30 hz. from a concentric four loop array, with ring and four loop elements at the same height.

   This is the same scheme used successfully with the 5X SVOR. Its chances for success in this case are reduced, however, because of the larger array diameter. The variable phase radiation pattern will be Equation (35) with the 30 hz. term deleted from the summation and replaced by Equation (89) (see Section IX-A).

Computed variable phase patterns of this configuration are presented in Figure 85 for several elevation angles. A false zero crossing occurs at $\theta = 40°$, but none appears at $\theta = 20°$. The elevation angle of the cone of confusion for this configuration, with a modified receiver, is between 20° and 40°, which might be marginally acceptable in practice.

2. Two Ring 13X SVOR; inner ring radiating 30 and 90 hz., outer ring radiating remaining harmonics. All antennas at the same height.

The most severe changes in the factor Equation (91) as regards generation of a false zero crossing with increasing elevation angle are those for n = 1 and n = 3. Since a large diameter ring array is not necessary to radiate these low order spatial harmonics efficiently (Section IV-A), and since the change in Equation (91) with elevation is less rapid if KR is small, it appears that false zero crossings may be avoided if 30 and 90 hz. are radiated separately by a smaller ring array concentric with the ring array that radiates the remaining harmonics. If the radii of the small and large rings are designated U and S respectively, then a straightforward extension of Equation (35) gives the following for the variable phase radiation pattern P of this configuration

$$P = \sum_{n=0}^{1} \frac{1}{2n+1} \frac{J_{2n+1}(KU\cos\theta)}{J_{2n+1}(KU)} \operatorname{Sin}[(2n+1)(\omega t-\phi)] + \frac{7}{13} \frac{J_{13}(KS\cos\theta)}{J_{13}(KS)} \tag{92}$$

$$\operatorname{Sin}[13(\omega t-\phi)] + \sum_{n=2}^{5} \frac{1}{(2n+1)} \frac{J_{2n+1}(KS\cos\theta)}{J_{2n+1}(KS)} \operatorname{Sin}[(2n+1)(\omega t-\phi)]$$

Results of computation of P from Equation (92) for three combinations of U and S are shown in Figures 86-88. In each case no false zero crossings occur at any elevation angle, hence the two ring configuration is theoretically capable of eliminating the 13X SVOR cone of confusion. This configuration has the practical disadvantage, however, of requiring two separate drum modulators, plus more antennas and feeders than configuration 1, (four loop ring array). The feasibility of the following third configuration, which is a variation of configuration 1, was therefore tested by computation.

3. Radiation of 30 hz. from a concentric four loop array. Ring array antennas at a greater height than four loop array antennas.

If the ring array elements are placed above an ideal ground plane at a height h that exceeds 1/2 wavelength, then their elevation pattern, which has the form $\sin(Kh \sin\theta)$ from image theory, will reach a null at some elevation angle. At and near this angle the ring array pattern will become attenuated relative to the four loop pattern, particularly if the four loop antenna heights are reduced somewhat from their normal value of 1/2 wavelength. Since the factor Equation (91) diminishes at high elevation angles for all harmonic orders, it might be expected that a judicious increase in ring array antenna height would result in a ring array pattern that maintains design amplitudes near the horizon but diminishes rapidly at the higher elevations, thus avoiding false zero crossings while still maintaining the four loop bearing information.

If the ring antenna heights are designated h_2 and the four loop antennas heights h_1, then the variable phase pattern, which is Equation (35) modified to account for the four loop array by use of the term Equation (89), and further modified to include the different ring and four loop elevation patterns, is

$$P = \cos\theta \sin(\omega t-\phi) + \frac{h_1}{h_2} \frac{\sin(Kh_2\sin\theta)}{\sin(Kh_1\sin\theta)} \{ \frac{7}{13} \frac{J_{13}(KR\cos\theta)}{J_{13}(KR)} \sin[13(\omega t-\phi)]$$

$$+ \sum_{n=1}^{5} \frac{1}{2n+1} \frac{J_{2n+1}(KR\cos\theta)}{J_{2n+1}(KR)} \sin[(2n+1)(\omega t-\phi)]\} \qquad (93)$$

Graphs of Equation (93) are presented as Figures 89-91. In all three figures, $h_1 = (3\lambda/8)$ while h_2 increases successively from $3\lambda/4$ to $9\lambda/8$ in the three figures. Figure 89 shows a false zero crossing at 80° elevation, while the other figures show no false zero crossings, hence no theoretical cone of confusion.

Equation (93) is based on perfect imaging in the ground plane, so that the favorable results shown in Figures 89-91 will be most closely approximated if the entire array is ground mounted. If the array is mounted on an elevated counterpoise, nearly ideal imaging in the counterpoise may still be expected at the higher elevations (Ref. 19), and can be exploited to attenuate the ring pattern relative to the four loop pattern, in order to avoid false zero crossings.

XI FEASIBILITY OF VERY LARGE APERTURE SVOR

The obvious advantages of a very large aperture SVOR are:

a) Reduction in course scalloping in proportion to the aperture (Section II).

b) Reduction in statistical station error (Section V) roughly in proportion to aperture.

c) Smaller angular region in which little scalloping reduction is realized (Section II).

One operational disadvantage could be encroachment of the multiplexed SVOR harmonics on the band used for voice transmissions. The highest harmonic of a 50X SVOR would be 1500 hz., which is well into the voice band. Possible solutions of this difficulty are:

a) Turning off the SVOR harmonics during voice transmission, leaving only 30 hz. to provide guidance equivalent to a conventional VOR.

b) Transmission of variable phase on an AM subcarrier. If the variable phase was transmitted on a carrier frequency displaced from the reference carrier by approximately 7 khz, transmissions of a 50X SVOR would be single sideband AM, and would not encroach on either voice or reference channels. The disadvantage of this solution is increased complexity of the receiver modification for SVOR.

A large aperture SVOR must comprise at least 2N + 1 antennas, where N is the average scalloping reduction factor. Thus, the multiplicity of the antenna and feeder system will increase in proportion to aperture.

A drum modulator of practically reasonable size is probably not feasible for N>20 because of close spacing between the quarter wave rods around the drum periphery. However an electronic modulator is technically feasible (see Section XII).

Simultaneous radiation of all the required harmonics from a single ring would become increasingly difficult as N is increased, since a ring radius would have to be found which was sufficiently removed from the zeros of $J_n(KR)$, n = 1, -- N, so that all harmonics would be radiated without excessively large antenna currents. For this reason, it is probable that a very large aperture SVOR would consist of a four loop array and two concentric ring arrays, the smaller of which would probably be about the diameter of a 5X SVOR (14 feet, 14 antennas).

The techniques described in Section X for eliminating the cone of confusion of a 13X SVOR appear equally applicable to a very large aperture SVOR.

XII FEASIBILITY OF ELECTRONIC SVOR MODULATOR

The drum modulator has the great advantage that all antennas are driven from a single source through lossless passive elements, thus locking the phase of the antenna currents to the phase of the source and conserving the limited power output of the modulation eliminator. There appears to be no suitable electronic technique for achieving lossless, linear modulation of a number of outputs from a single high level source. A feasible alternative is use of a multiplicity of modulated power amplifiers, each equipped with a phase locked loop to clamp the output phase to the reference carrier phase. The component amplifiers and phase detectors of a phase locked loop are available today as integrated circuit packages, and the power requirements of each output are low (order of one watt), so that even a large number of such circuits would not require excessive space or power. One difficulty would be the provision of a multiplicity of modulation waveforms, all identical except for a progressive phase lag. However, by building up the modulation waveform in a large number of steps, with a built in program for selection and time progression of the steps, modern computer type circuitry should provide a means for realizing such phase stepped waveforms in a straightforward manner.

XIII ALTERNATIVE PROCESSING OF SVOR SIGNALS

The SVOR signal is clearly redundant from an information theory standpoint, since an N fold reduction in scalloping could be obtained by using only the Nth harmonic to obtain an ambiguous fine bearing. The ambiguity would be resolved by the conventional VOR signal in the manner of precision multilobe VOR. However, the redundancy of the SVOR signal serves a purpose in permitting very simple and unambiguous signal processing, namely zero crossing phase detection. Conventional phase detectors can readily be converted to zero crossing phase detection (Section VI-B), and digital phase detectors, which are probably technically inevitable, would automatically be zero crossing detectors if they took the form of counters which were started and stopped at zero crossings of the reference and variable waveforms. The possibility of processing SVOR signals in the same way as PVOR (multilobe) nevertheless exists and could be done at the option of the user. A precision reference phase could be generated within the receiver by harmonic multiplication of the normal reference.

XIV GENERAL CONCLUSIONS

1. Square Wave VOR is a means of reducing course scalloping and station error in a flexible, inexpensive manner that is particularly suited to digital phase measurement because no receiver modification would be required to benefit from SVOR if the digital receiver consisted of a reference pulse counter that was turned on and off at zero crossings of reference and variable phase signals. The combination of SVOR and digital receiver would reduce multipath and virtually eliminate receiver error.

2. Conventional receivers can be easily changed to zero crossing phase detectors. Theory and experimental results show that the modification has no measurable effect on receiver performance with conventional signals. The modification has the side benefit of making course width independent of percent modulation.

3. Simulation tests of 11 conventional receivers showed that the multiplexed SVOR harmonics caused a bias error whose standard deviation for ten receivers was 0.8°. The 11th receiver (DR 560), which showed a bias error of 3.5°, also had poor compatibility with SSB DVOR. Flight tests showed no increase in roughness or station error indicated by a conventional receiver when SVOR signals were added to the conventional VOR signal.

4. A 13X SVOR (thirteenfold scalloping reduction) comprising a 30 loop, 33 foot diameter ring array has been designed and appears entirely feasible.

5. Very large aperture SVOR appears feasible. The multiplicity of antennas and feeders will increase in proportion to aperture. Scalloping reduction will be in proportion to aperture. A receiver equipped with a zero crossing phase detector can correctly process and benefit from signals from an SVOR of any aperture.

REFERENCES

1. Analyses of Precision Omnirange Systems Final Report, FAA Contract ARDS-589, Adcom Corp., 1965. Pg. 63.

2. Redlich, R., "Sampling Synthesis of Ring Arrays", IEEE Transactions Antennas and Propagation, Vol. AP-18, No. 1, pp. 116-118, January 1970.

3. Ramo, S. and Whinnery, J., "Fields and Waves in Modern Radio", pg. 20, Wiley, 1959.

4. Sandretto, P.,"Electronic Avigation Engineering", pg. 422, International Telephone and Telegraph Corp., New York, 1958.

5. Anderson, S. and Flint, R., "The CAA Doppler Omnirange", Proc. I.R.E., May, 1959.

6. Skolnik, M. I.,"Introduction to Radar Systems", McGraw-Hill, 1962.

7. Weeks, W.L., "Antenna Engineering", McGraw-Hill, 1968.

8. McLachlan, N.W., "Bessel Functions for Engineers", Oxford University Press, 1961.

9. Cheng, D.K., "Analysis of Linear Systems", Addison-Wesley, 1959.

10. Jones, D.C., "A First Course in Statistics", G. Bell Ltd., London.

11. Hildebrand, F.B., "Advanced Calculus for Engineers", Prentice-Hall, 1949.

12. Anderson, S.R., "Why a Digital VOR", prepared for RTCA Special Committee, SC-121, 31 July 1970.

13. Willey, V.E.,"Development and Evaluation of a Double-Sideband DVOR System with High Level Reference Modulation". NAFEC Report #FAA-NA-71-36, June 1971.

14. Kraus, J.D., "Antennas", McGraw-Hill, 1950.

15. Harrington, R., "Time Harmonic Electromagnetic Fields", McGraw-Hill, 1961.

16. Redlich, R., "Radiation from Filamentary Circular Loops", Proc. IEEE, Vol. 52, No. 9, September 1964.

17. "Reference Data for Radio Engineers", I.T.T. Corporation, New York, 1956.

18. Collin, R.E., "Field Theory of Guided Waves", McGraw-Hill, 1960.

19. Redlich, R., "Image Radiation From a Finite Ground Plane in Two Dimensions", IEEE Trans. Ant. and Propag., Vol. AP-16, No. 3, May, 1968.

20. U.S. Patent 3,754,259. Omnirange Navigation Apparatus and Method, R.W. Redlich, Aug., 1973. The U.S. Government holds the rights to Claim 4 of this patent.

FIGURE 1. EFFECT OF INTERFERENCE ON VARIABLE PHASE OF IDEAL SQUARE WAVE VOR

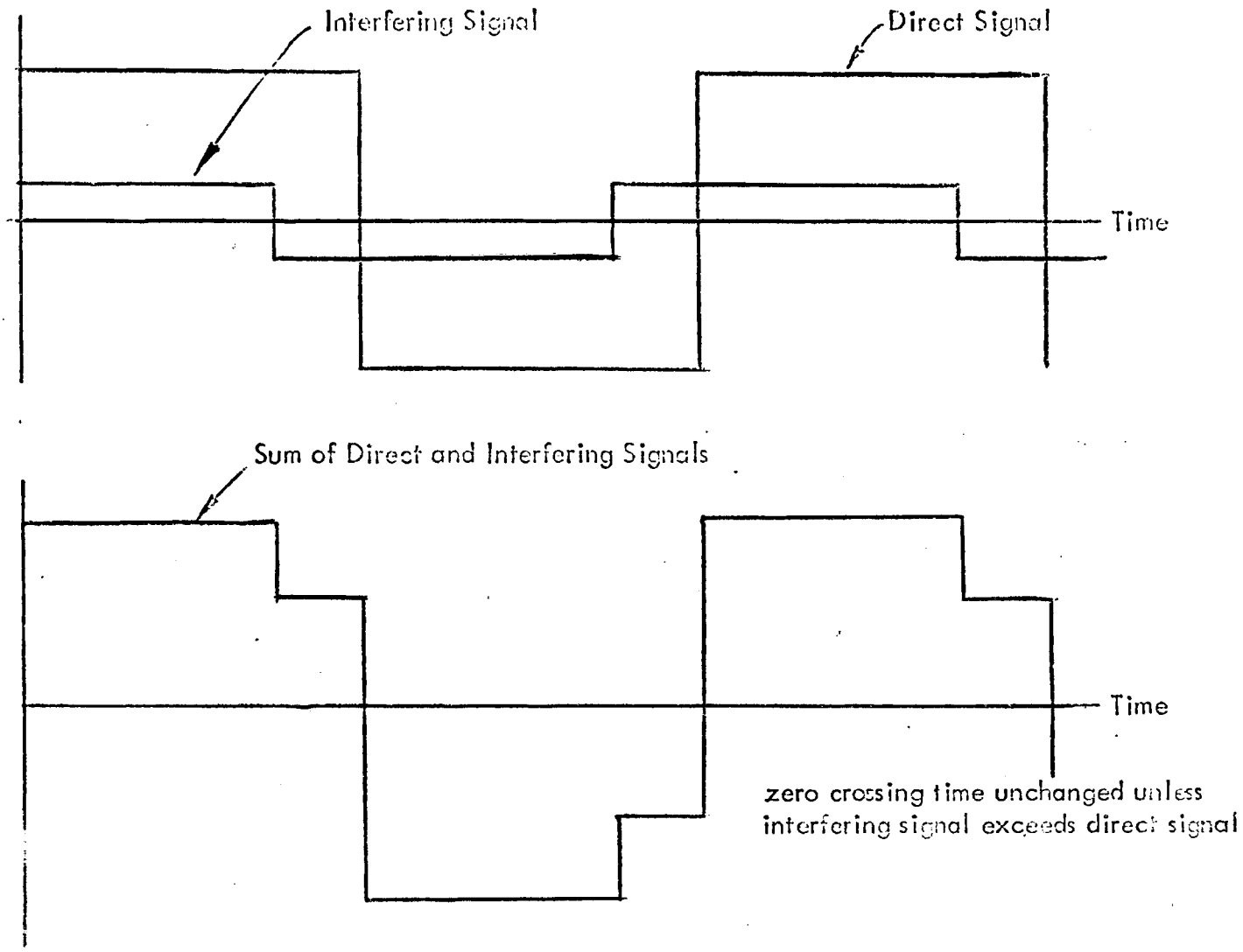

FIGURE 2. VARIABLE PHASE POLAR PATTERN OF IDEAL SQUARE WAVE VOR

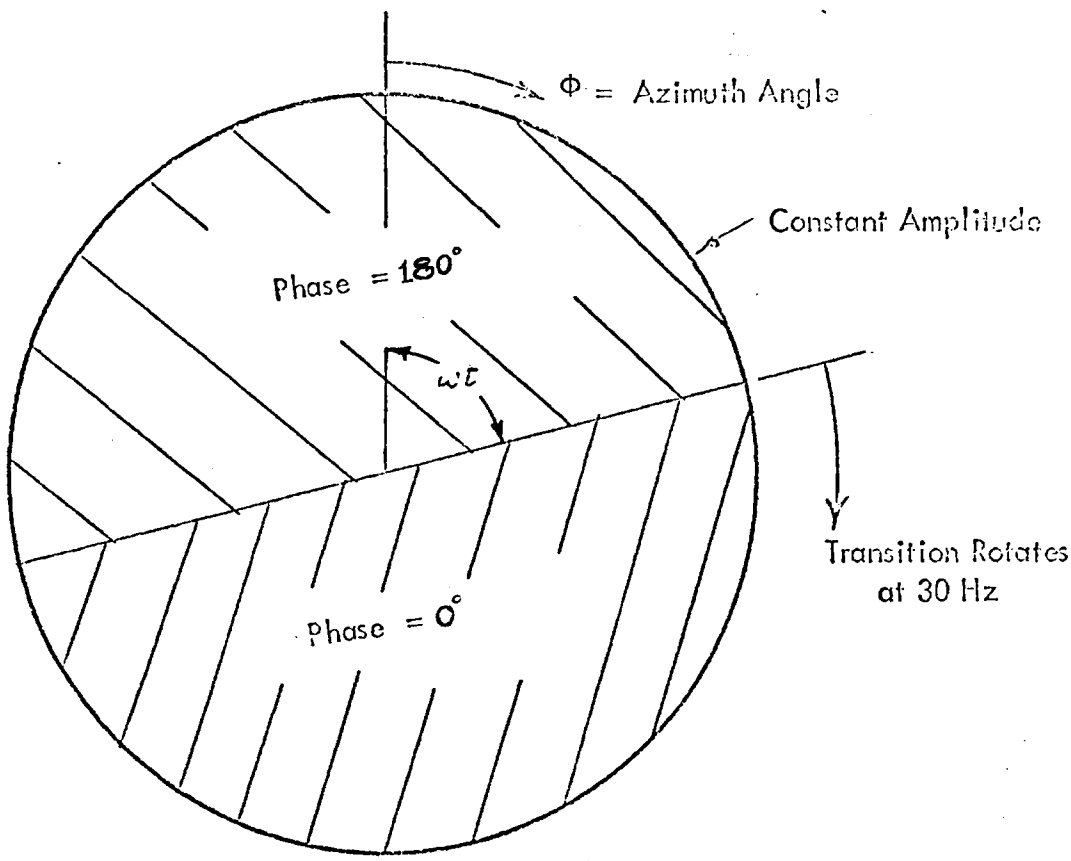

$$\text{pattern} = \sum_{n=0}^{\infty} (1/2n+1) \sin((2n+1)(\omega t - \phi))$$

FIG. 3

5X SVOR AND CONVENTIONAL
VARIABLE PHASE SIGNALS

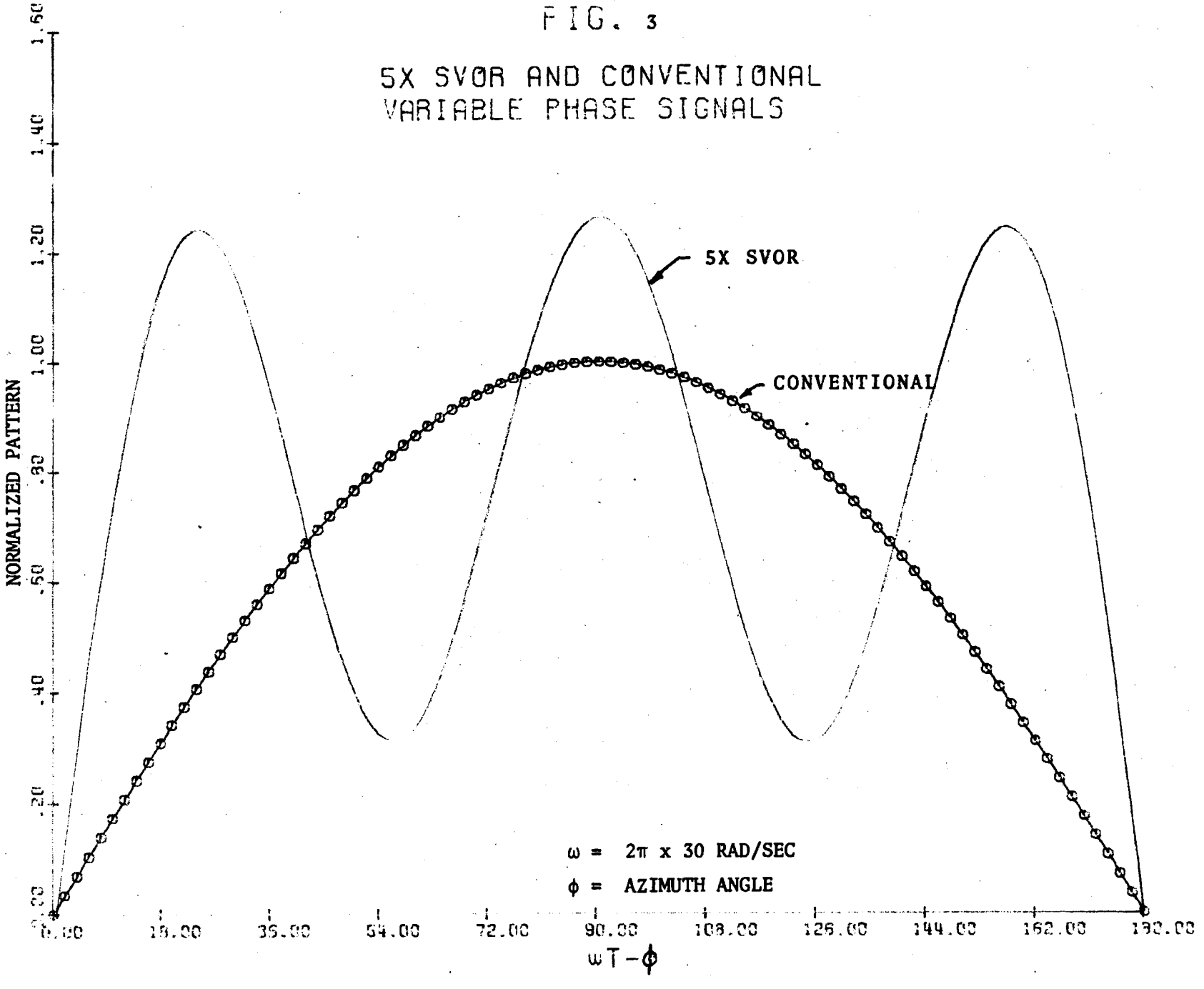

FIG. 4

POLAR PLOT OF CONVENTIONAL AND
5X SVOR VARIABLE PHASE SIGNALS

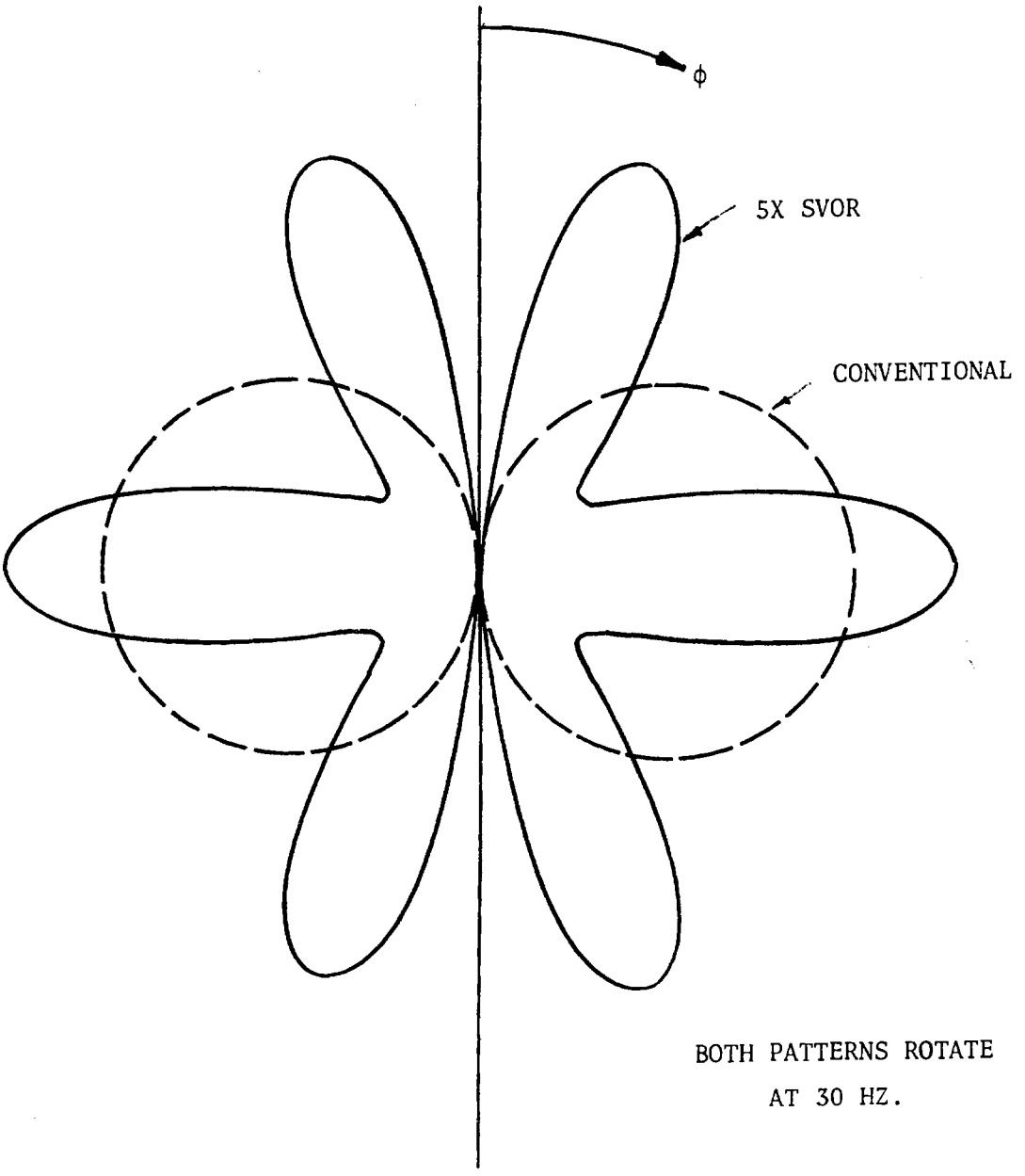

Figure 5. Radiation Patterns 5X Square Wave VOR

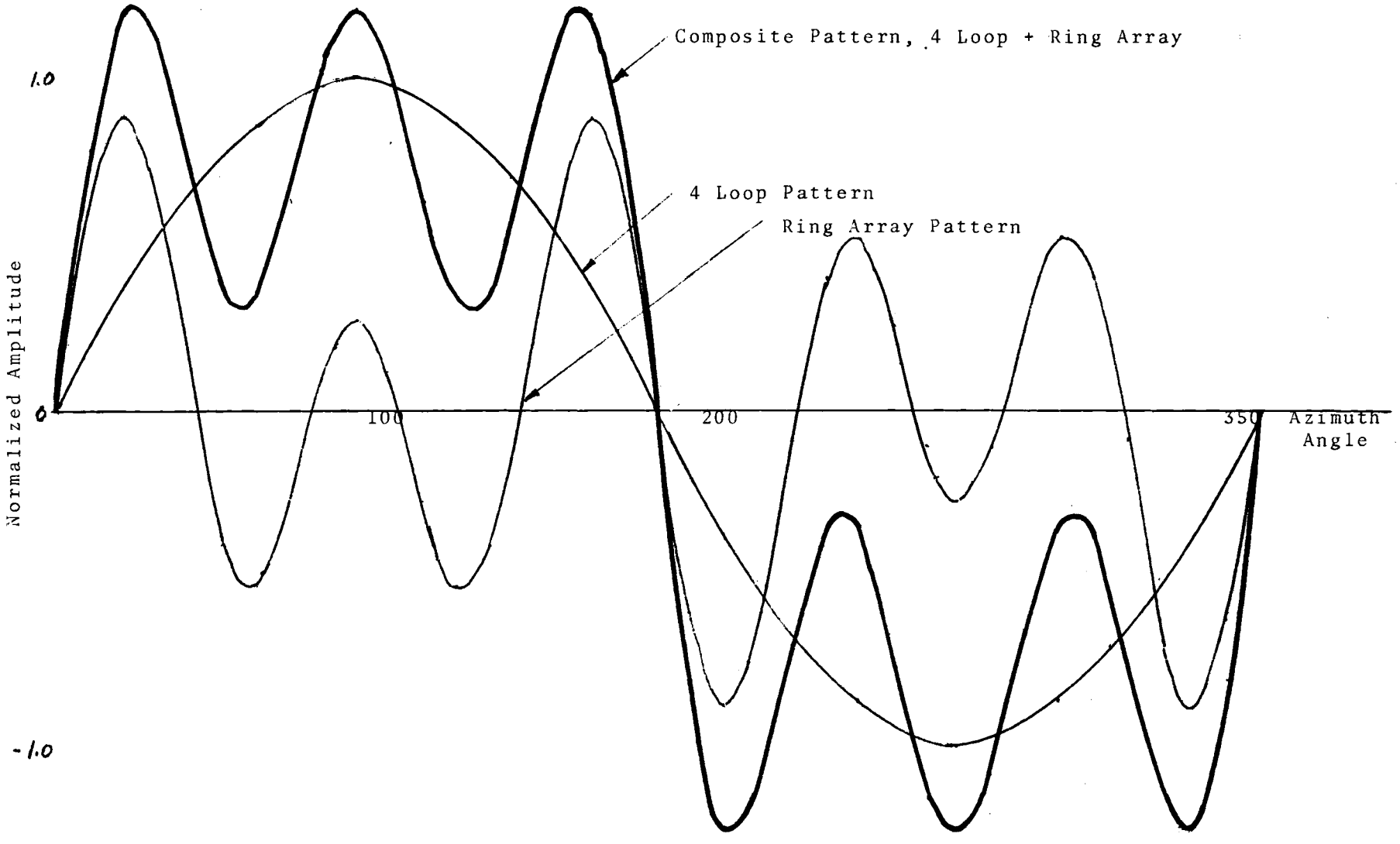

FIG. 6

MULTIPATH ERROR REDUCTION BY
5X & 13X SVOR

(COMPARED TO CONVENTIONAL VOR).

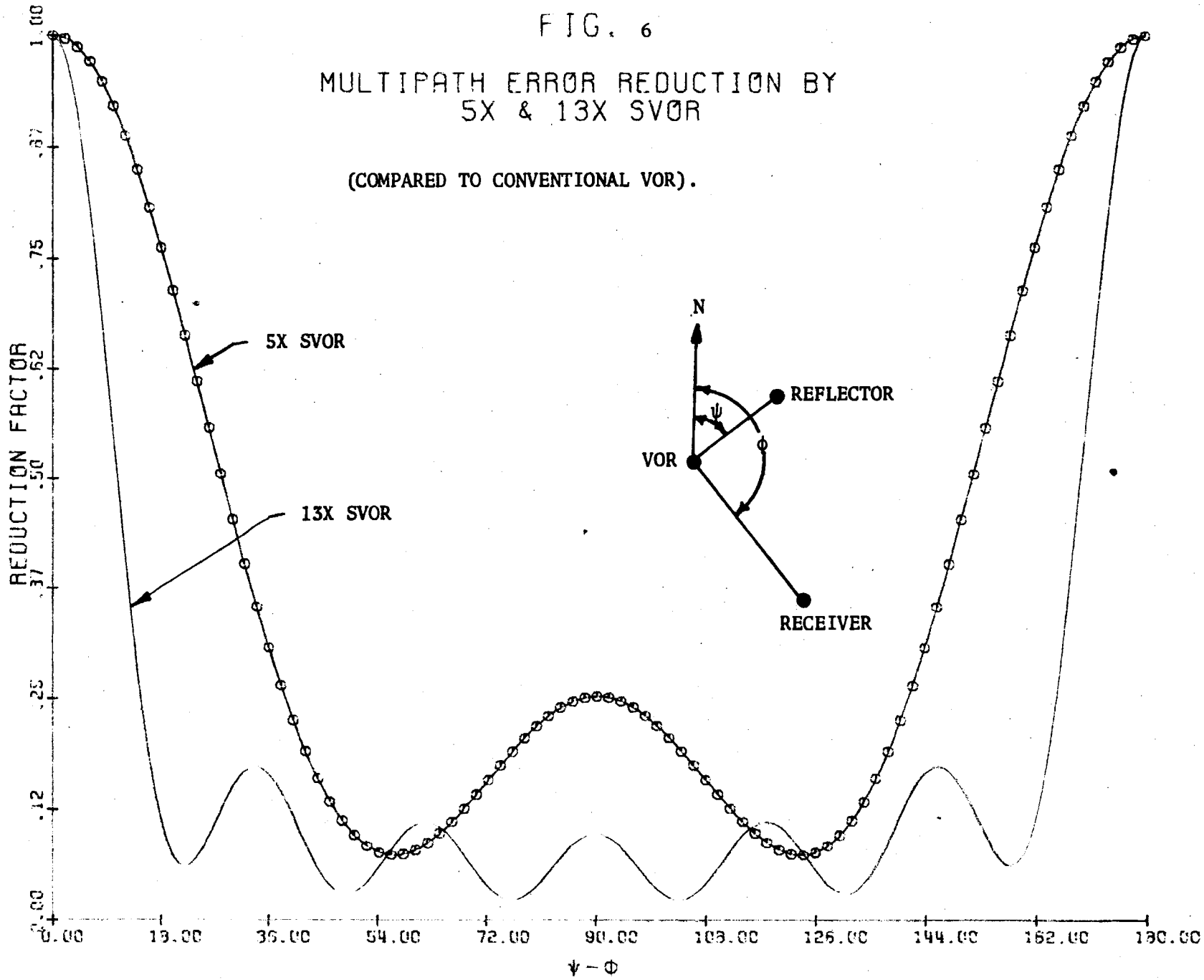

FIG. 7. STATIC MULTIPATH ERROR OF 5X SVOR, 13X SVOR, AND CONVENTIONAL VOR FOR THE SAME REFLECTOR.

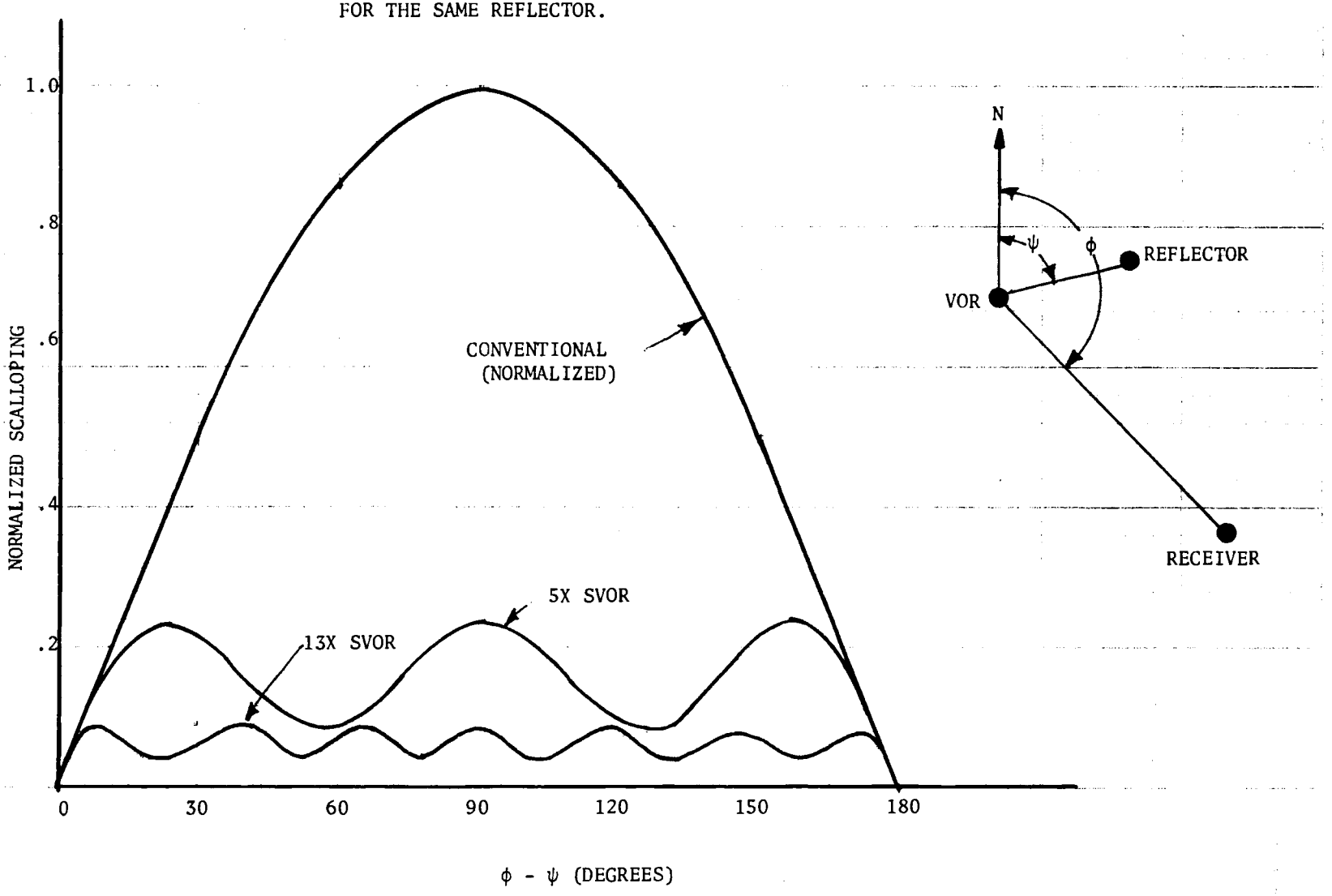

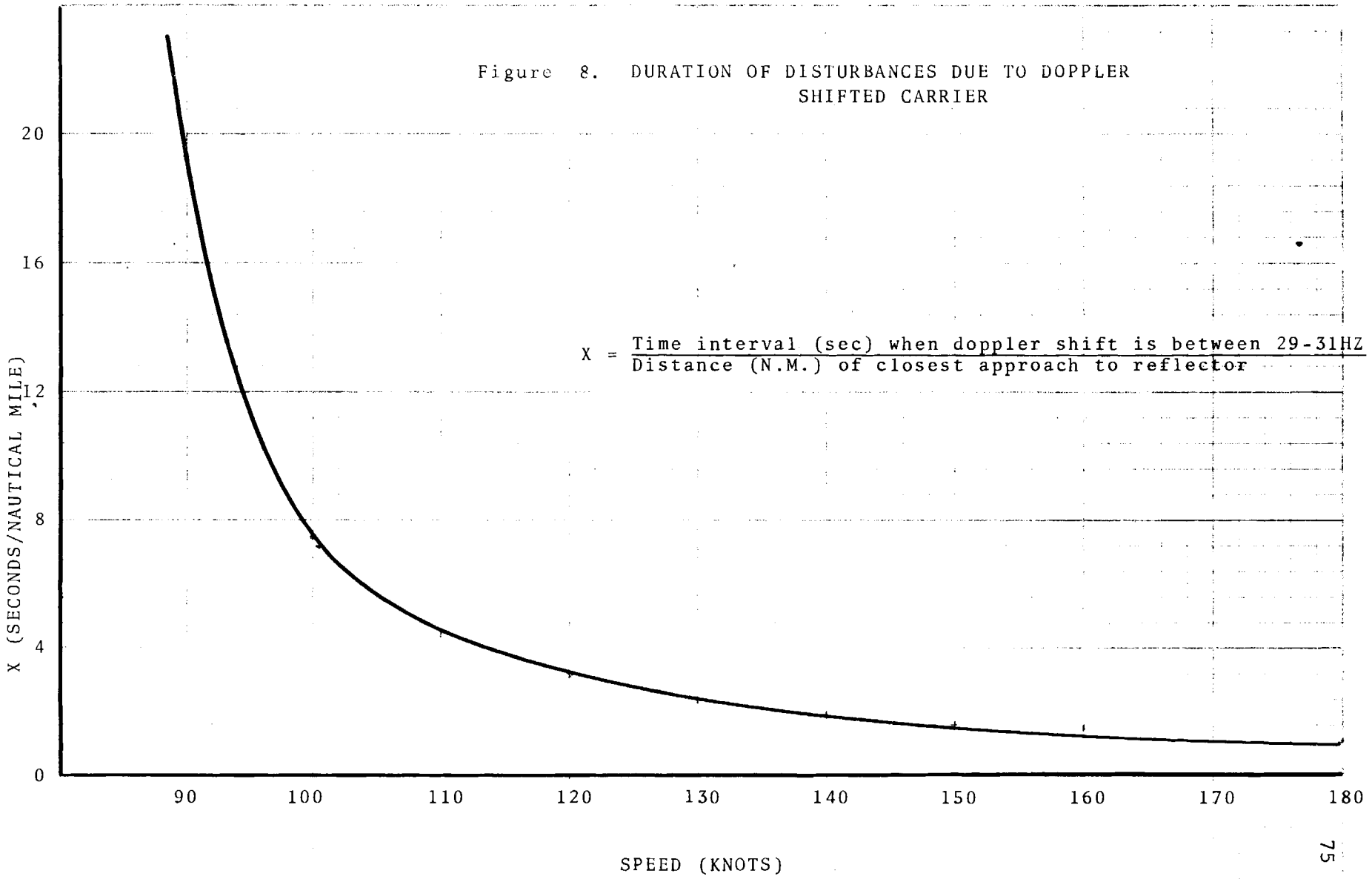

Figure 8. DURATION OF DISTURBANCES DUE TO DOPPLER SHIFTED CARRIER

FIG. 9. CDI DISTURBANCE DURING RADIAL FLIGHT BETWEEN A VOR AND A WATER TOWER, WITH ONLY REFERENCE PHASE BEING TRANSMITTED.

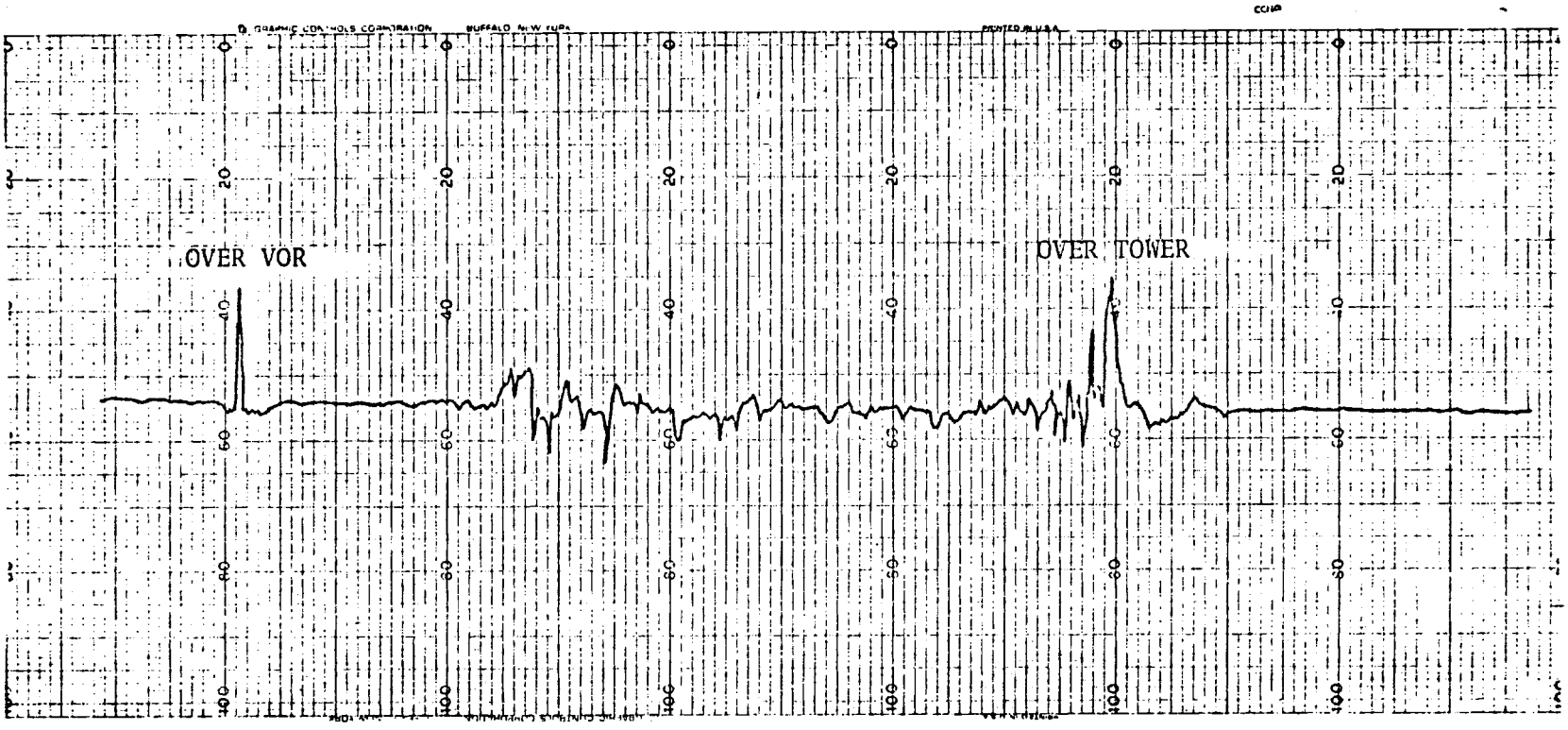

SPEED - 80 KNOTS
ALTITUDE - 150' ABOVE TERRAIN
CHART WIDTH = 20°
CHART SPEED = 10 SEC/INCH

FIG. 10. STATION ERROR REDUCTION BY 5X SVOR.
6 MI. ORBITAL DATA (NAFEC, 8/10/72).

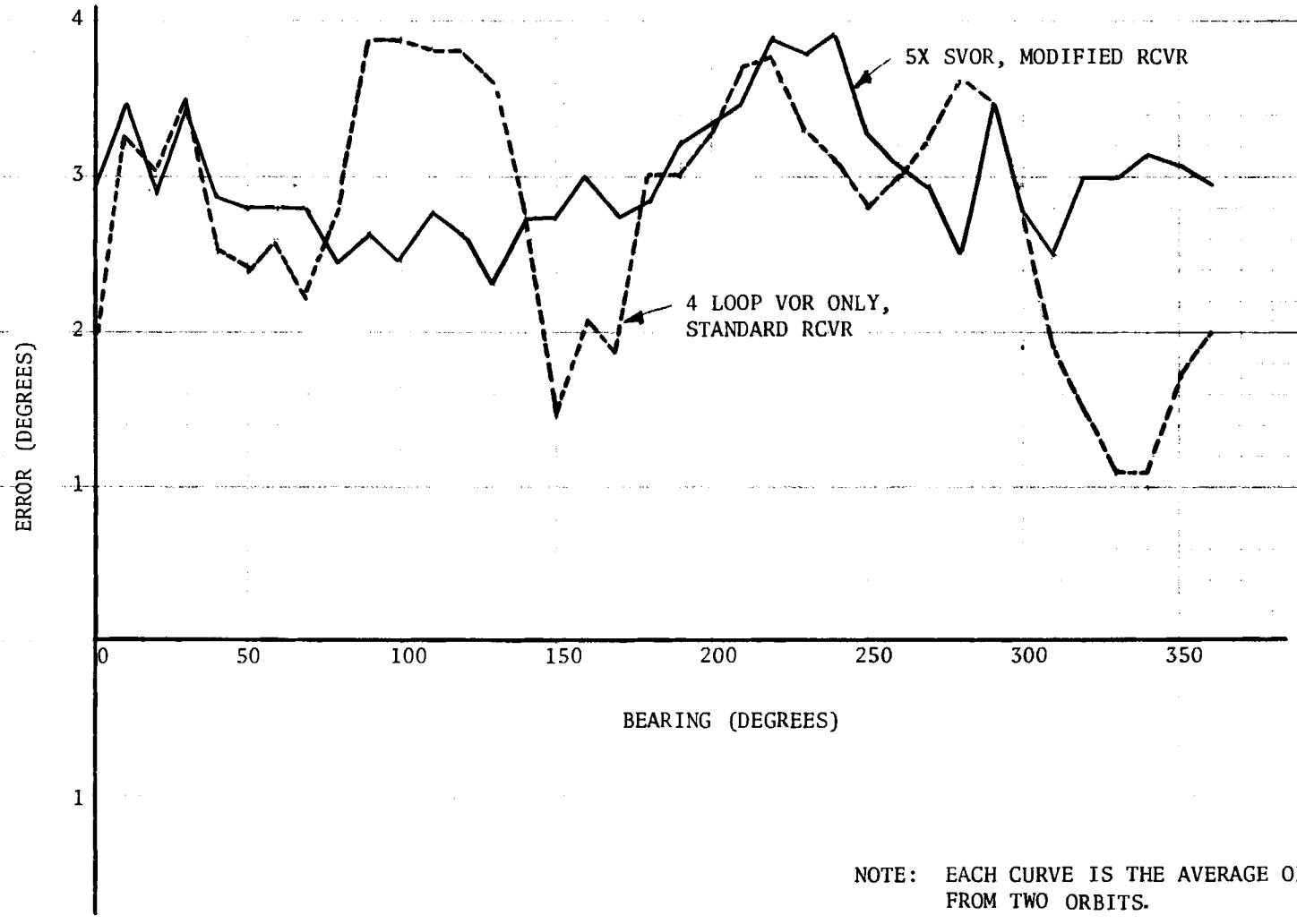

NOTE: EACH CURVE IS THE AVERAGE OF DATA FROM TWO ORBITS.

FIG. 11. STATION ERROR REDUCTION BY 5X SVOR.GROUND CHECK AT COUNTERPOISE EDGE (NAFEC, 2/10/72).

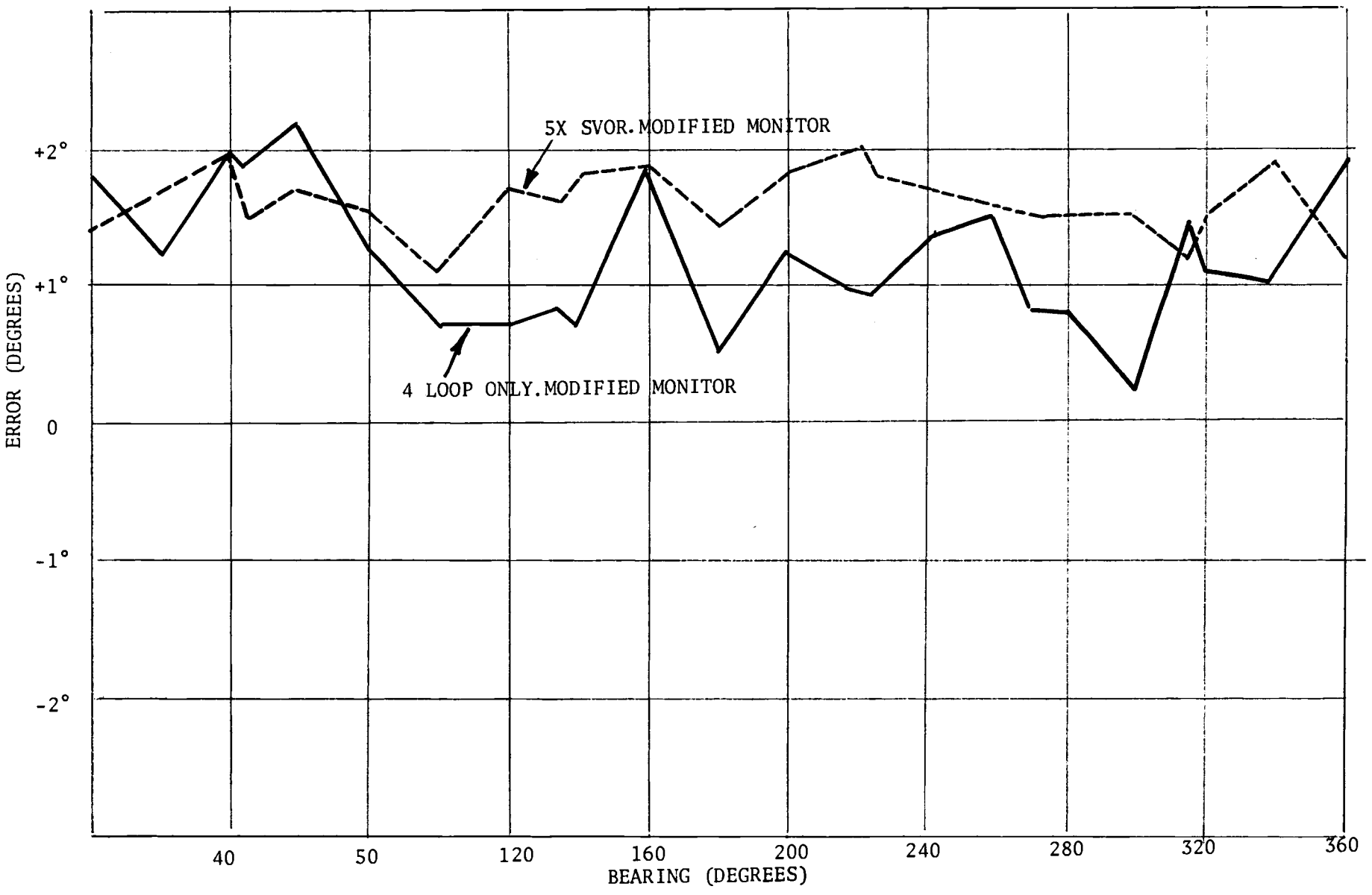

Figure 12

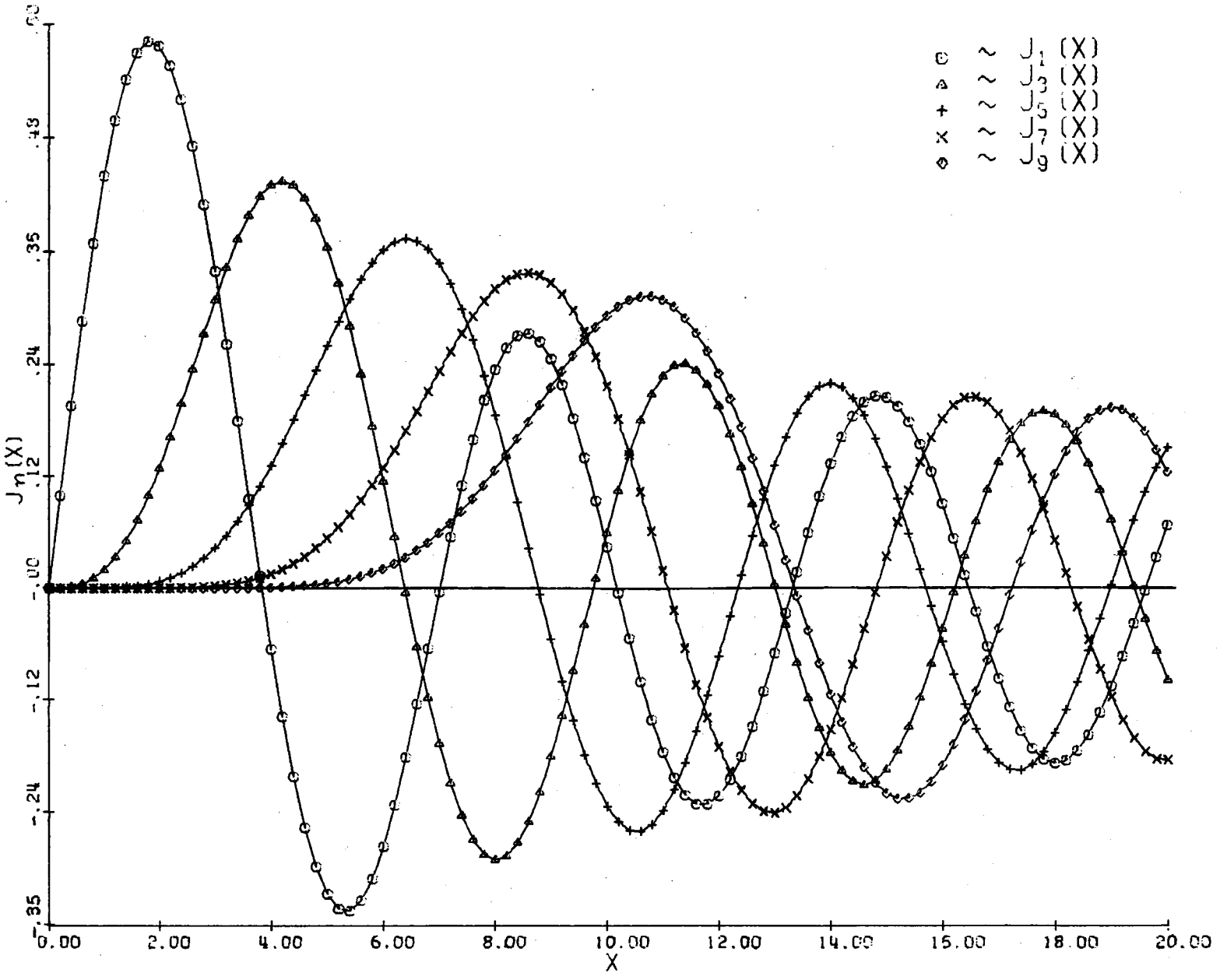
○ ~ $J_1(X)$
△ ~ $J_3(X)$
+ ~ $J_5(X)$
× ~ $J_7(X)$
◇ ~ $J_9(X)$
$J_n(X)$
.60
.48
.36
.24
.12
-.00
-.12
-.24
-.36
0.00
2.00
4.00
6.00
8.00
10.00
12.00
14.00
16.00
18.00
20.00
X

Figure 13

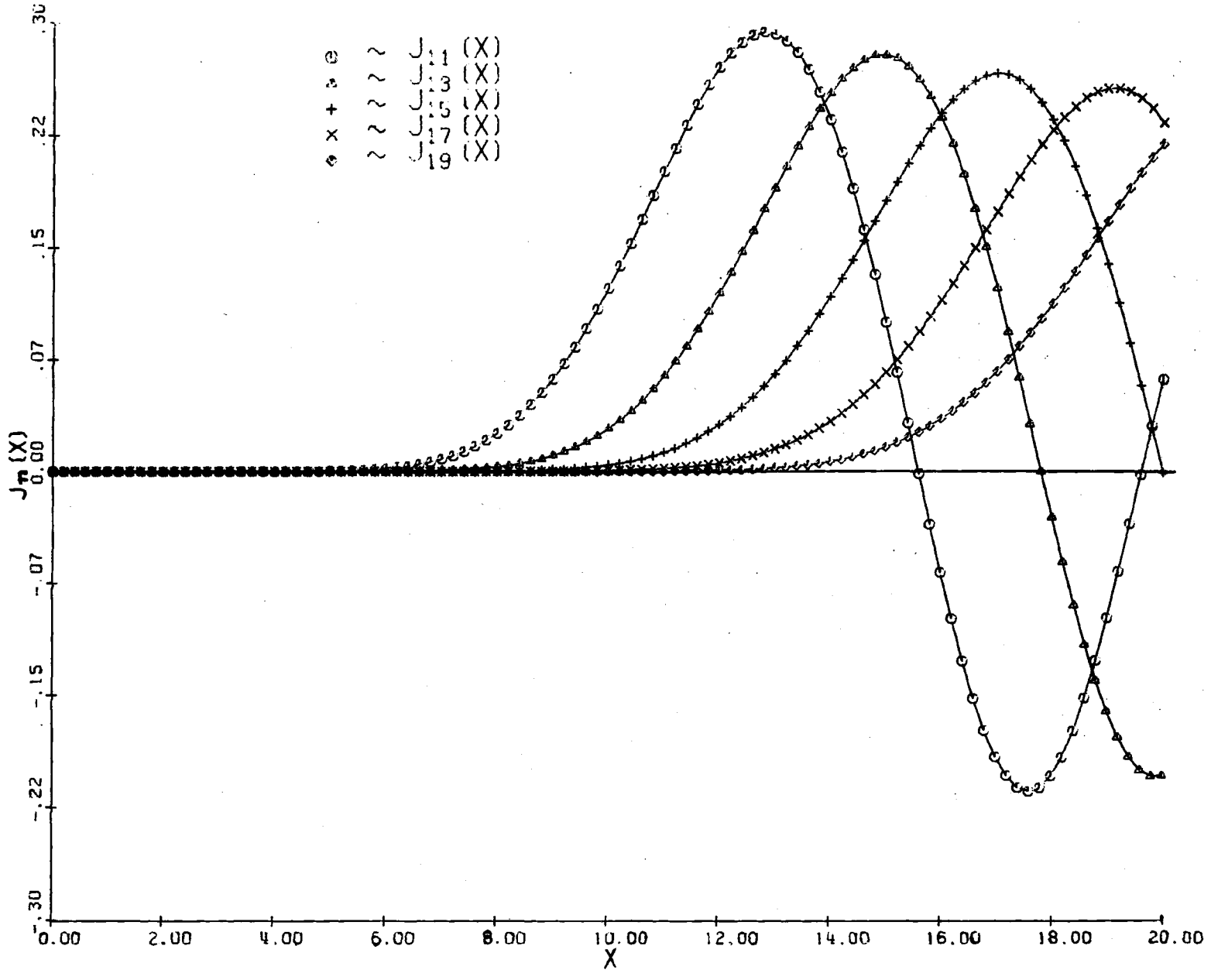
J11 (X)
J13 (X)
J15 (X)
J17 (X)
J19 (X)
Jn (X)
.30
.22
.15
.07
0.00
-.07
-.15
-.22
-.30
0.00
2.00
4.00
6.00
8.00
10.00
12.00
14.00
16.00
18.00
20.00
X

FIGURE 14
CONVERSION OF CONVENTIONAL RECEIVER TO ZERO CROSSING DETECTION

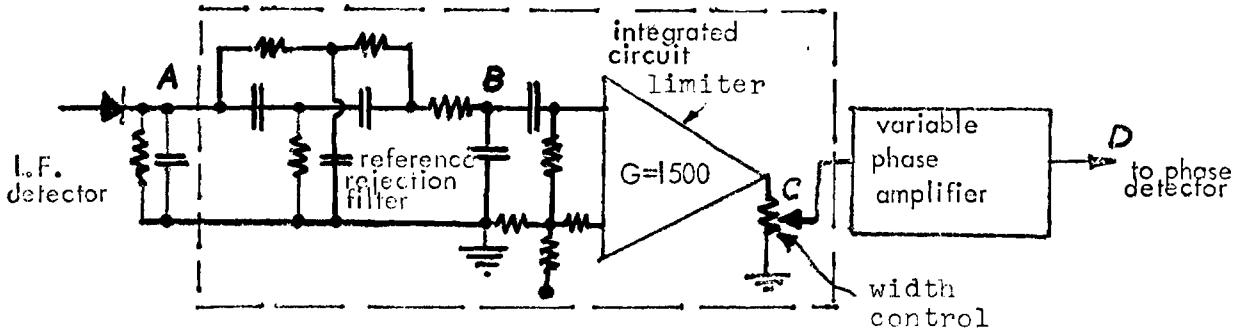

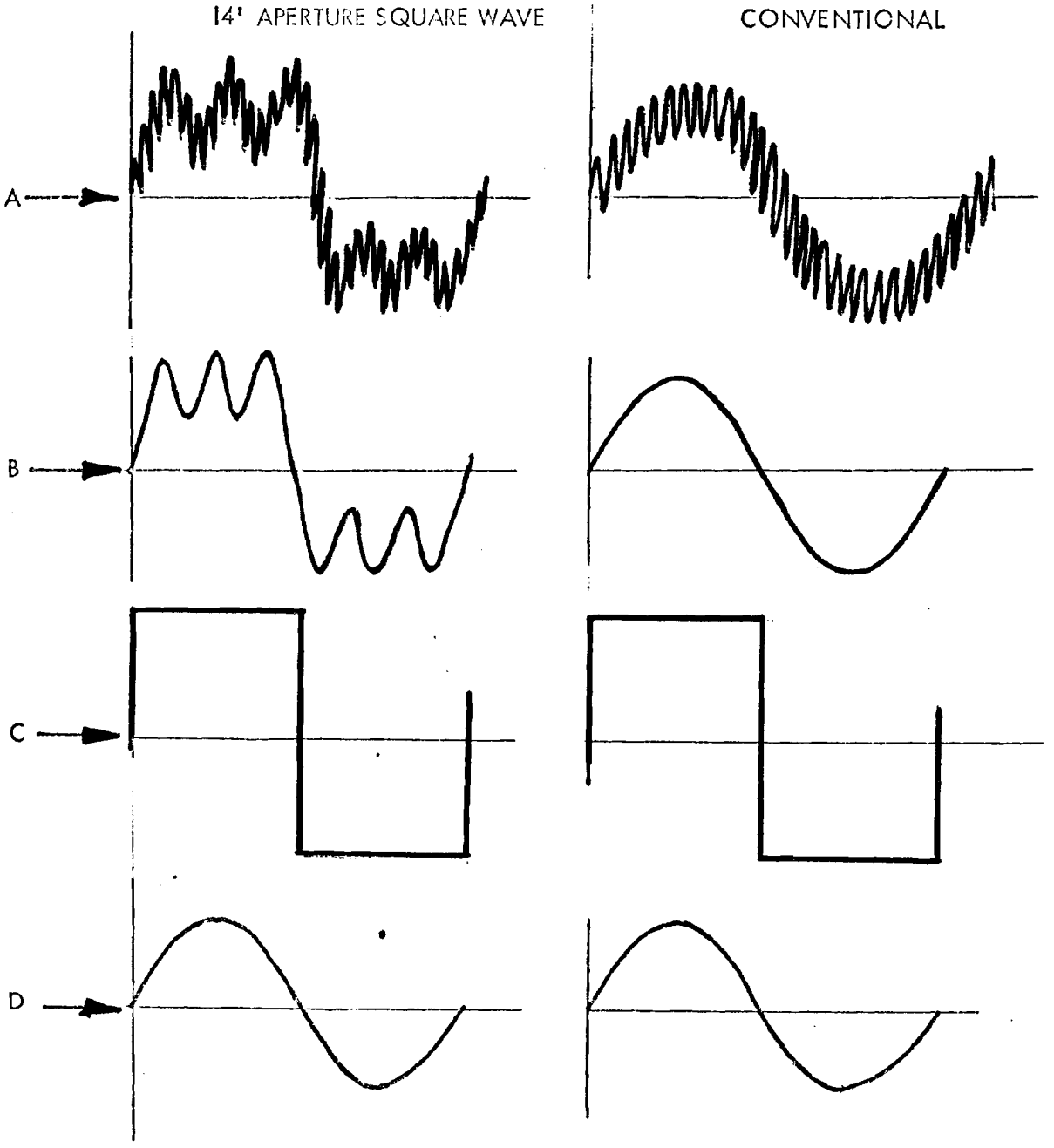

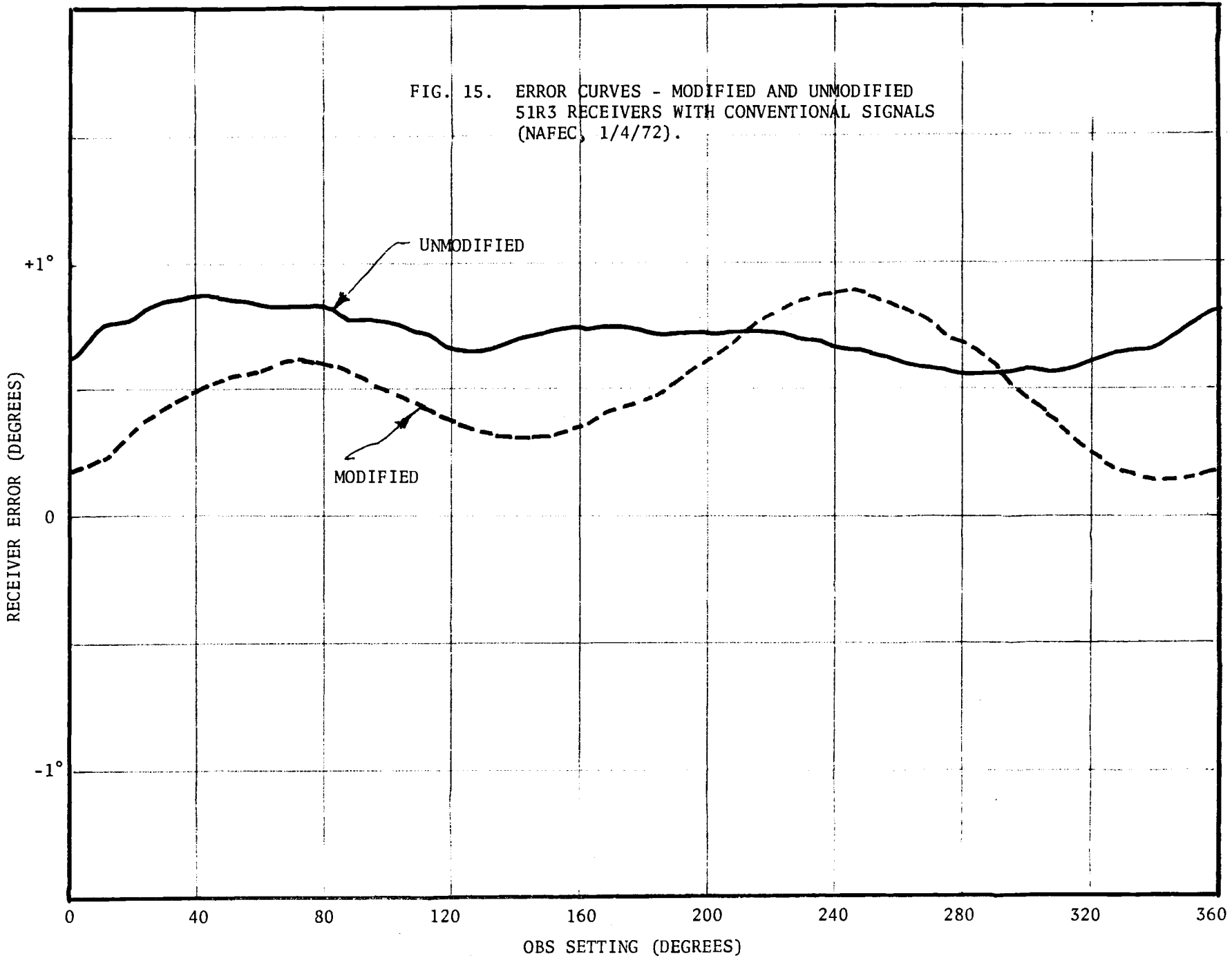

FIG. 15. ERROR CURVES - MODIFIED AND UNMODIFIED 51R3 RECEIVERS WITH CONVENTIONAL SIGNALS (NAFEC, 1/4/72).

FIG. 16. STATION ERROR - MODIFIED AND UNMODIFIED 51R3 RECEIVERS
6 NM ORBIT. 4 LOOP VOR (NAFEC, 1/24/72)

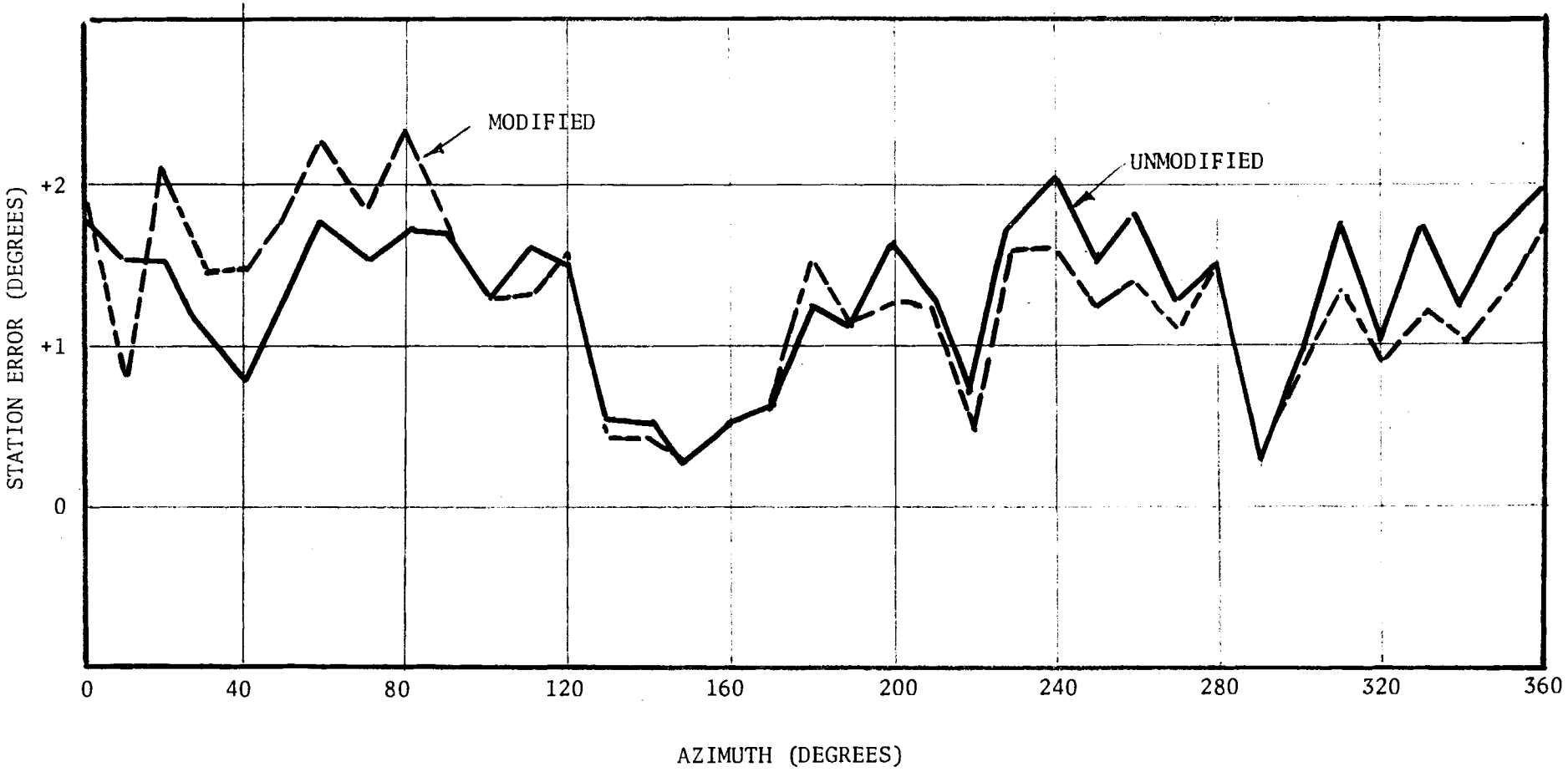

FIG. 17. ROUGHNESS AND SCALLOPING 4 LOOP VOR - 20 NM ORBIT MODIFIED AND UNMODIFIED 51R3 RECEIVERS (NAFEC, 1/21/72).

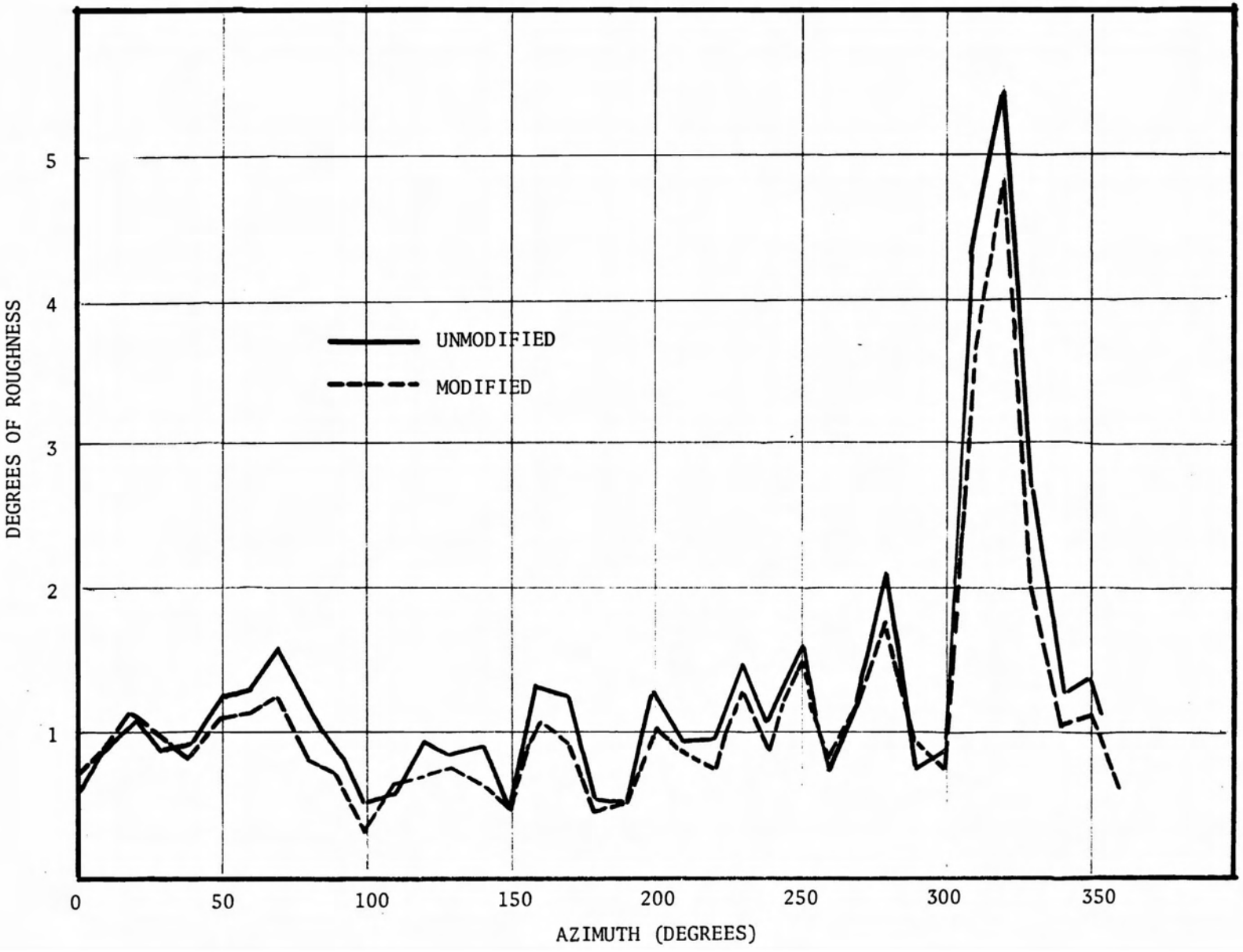

FIG. 18. POLARISCOPE RUN - 90° RADIAL 4 LOOP VOR - MODIFIED AND UNMODIFIED 51R3 RECEIVERS (NAFEC 1/17/72).

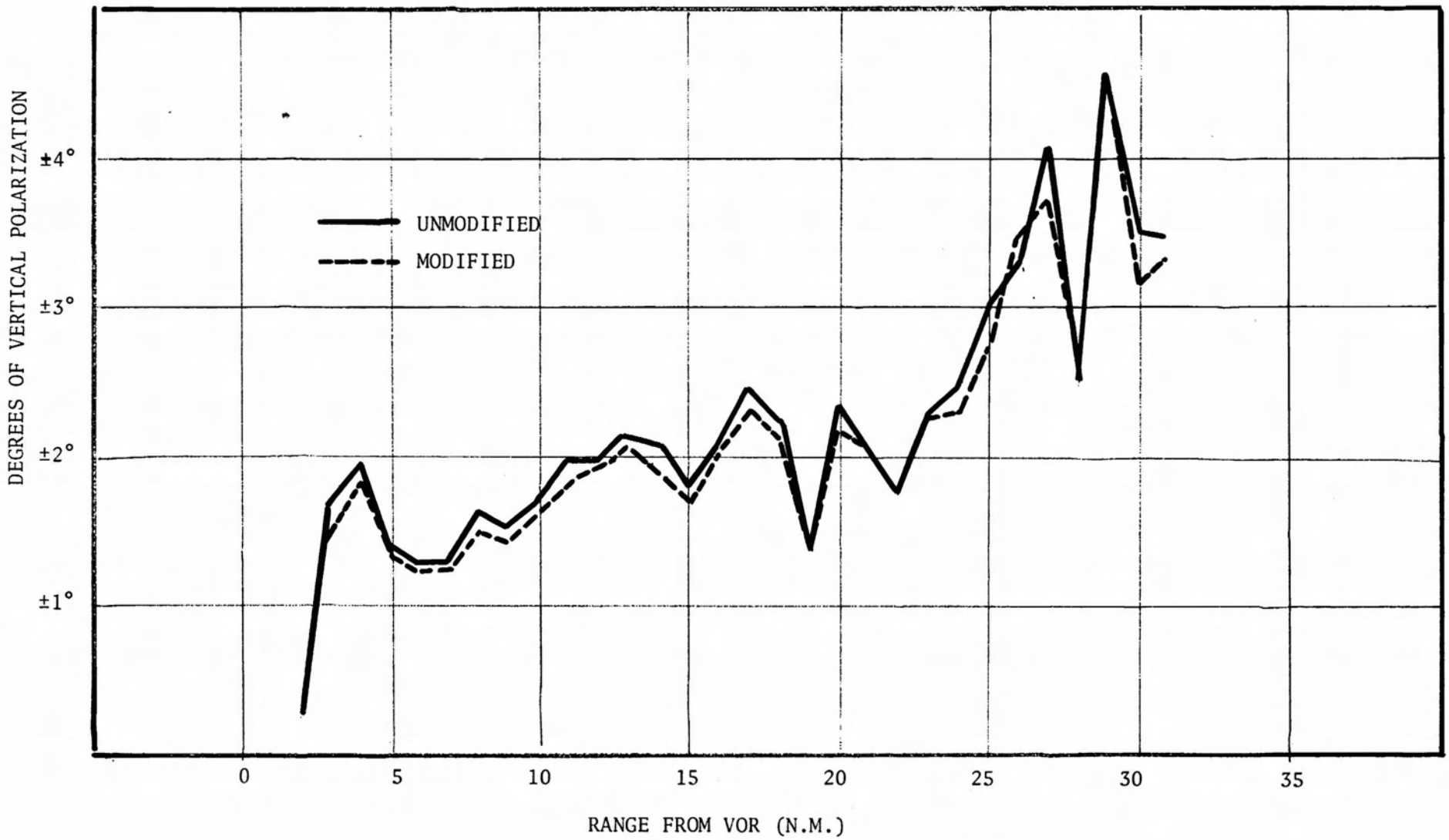

Figure 19. Eight Mile Orbit. Four Loop VOR Only (SVOR Ring Array Not Energized) (Ohio U. 10/71)

---------- Conventional 51R3

———————— 51R3 Modified for Zero Crossing Detection

Scale: 10° Chart Width

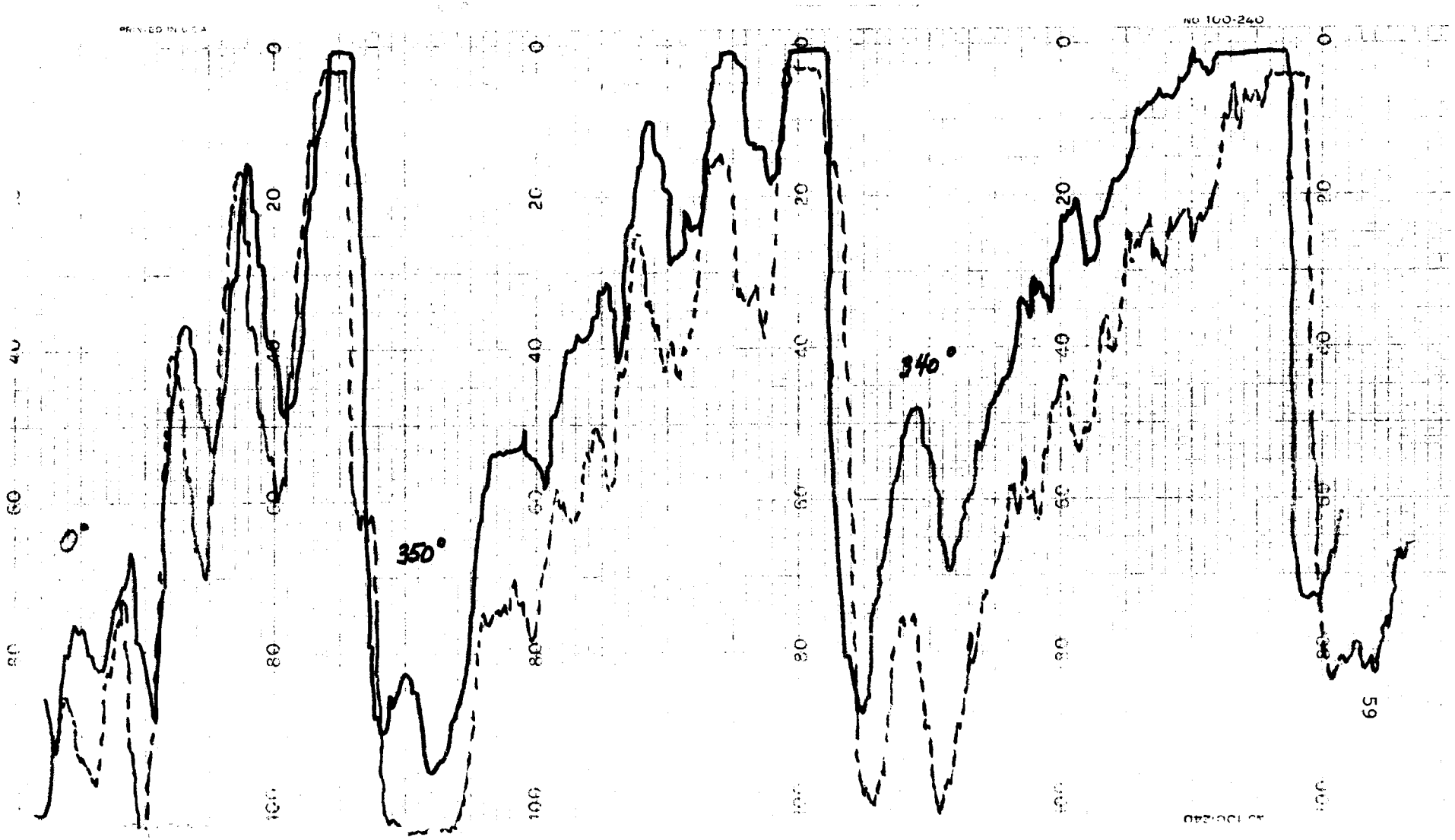

Figure 20. Eight Mile Orbit. Four Loop VOR Only (SVOR Ring Array Not Energized)(Ohio U. 10/71)

-------- Conventional 51R3

———— 51R3 Modified for Zero Crossing Detection

Scale: 10° Chart Width

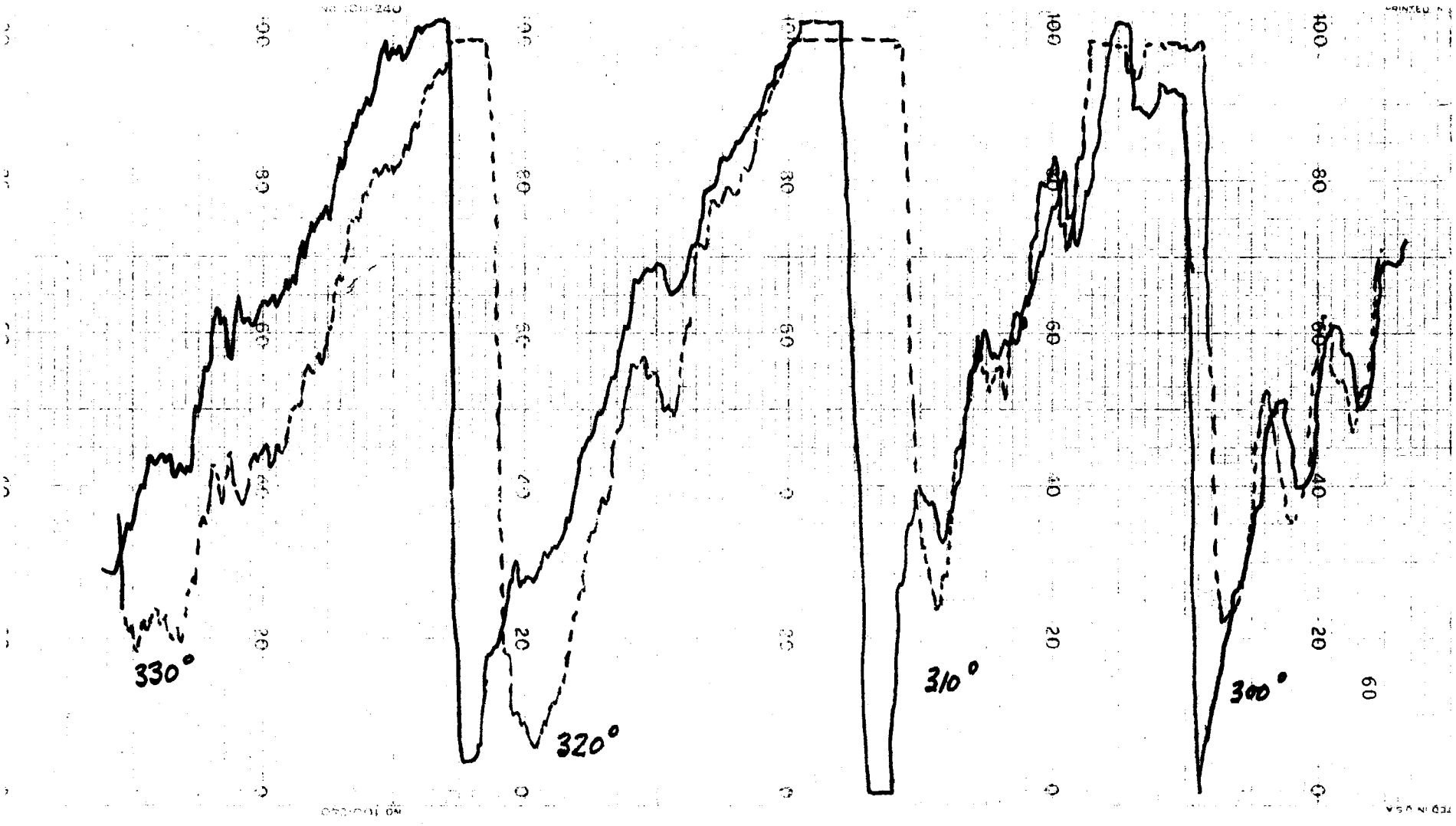

Figure 21. Eight Mile Orbit. Four Loop VOR Only (SVOR Ring Array Not Energized)(Ohio U. 10/71)

-------- Conventional 51R3

———— 51R3 Modified for Zero Crossing Detection

Scale: 10° Chart Width

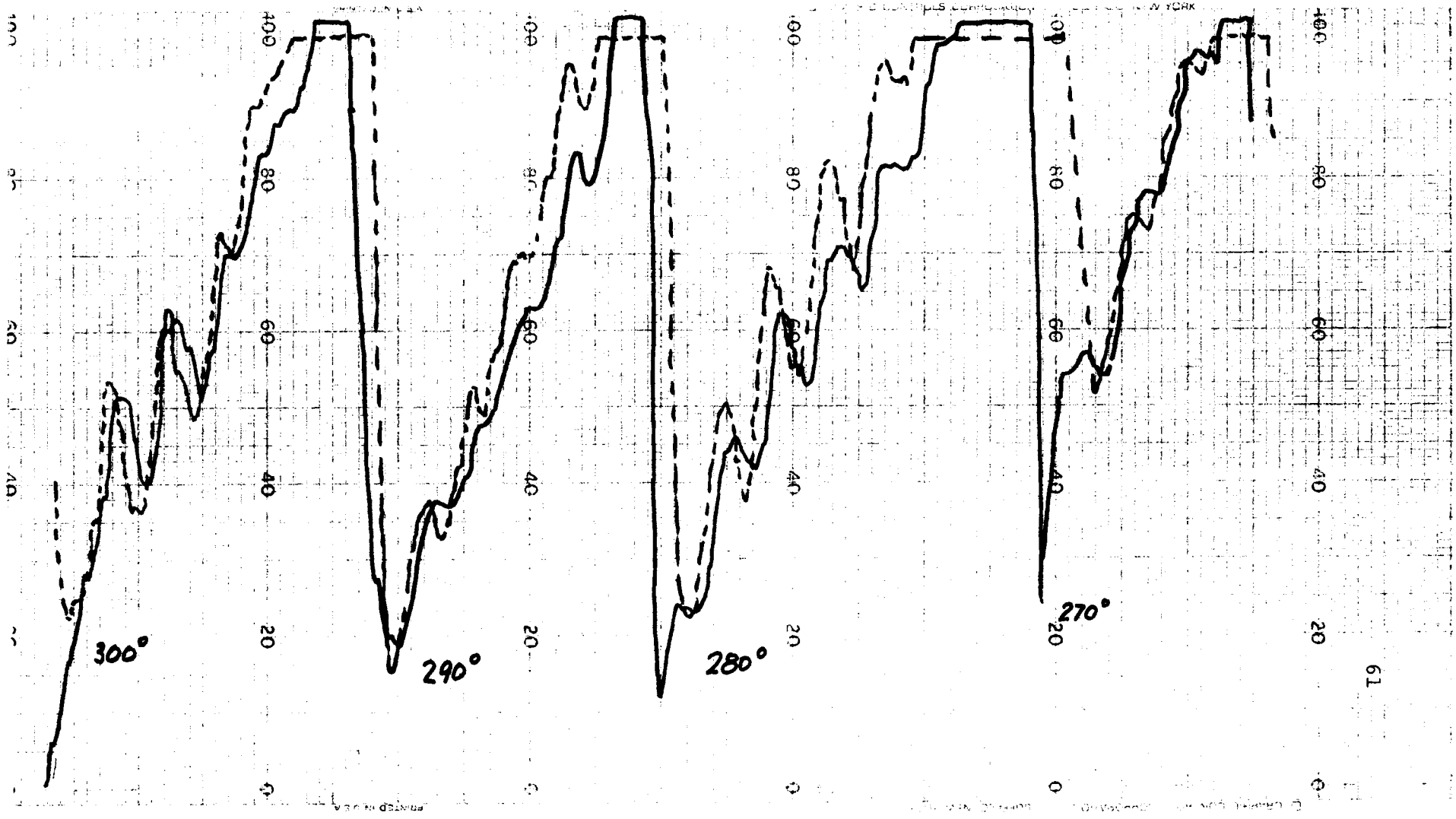

Figure 22. Eight Mile Orbit. Four Loop VOR Only (SVOR Ring Array Not Energized)(Ohio U. 10/71)

-------- Conventional 51R3

———— 51R3 Modified for Zero Crossing Detection

Scale: 10° Chart Width

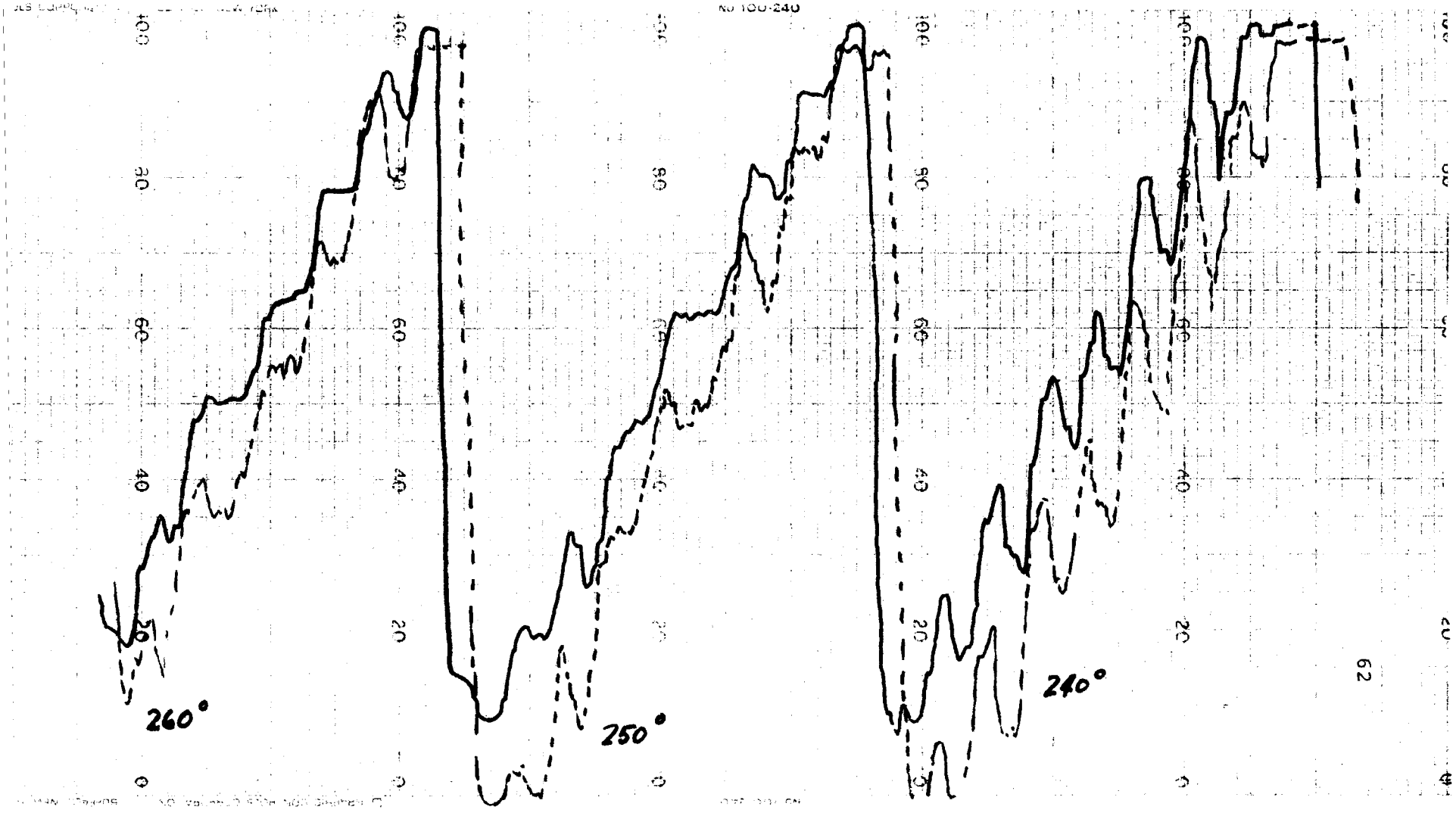

Figure 23. Eight Mile Orbit. Four Loop VOR Only (SVOR Ring Array Not Energized) (Ohio U. 10/71)

-------- Conventional 51R3

———— 51R3 Modified for Zero Crossing Detection

Scale: 10° Chart Width

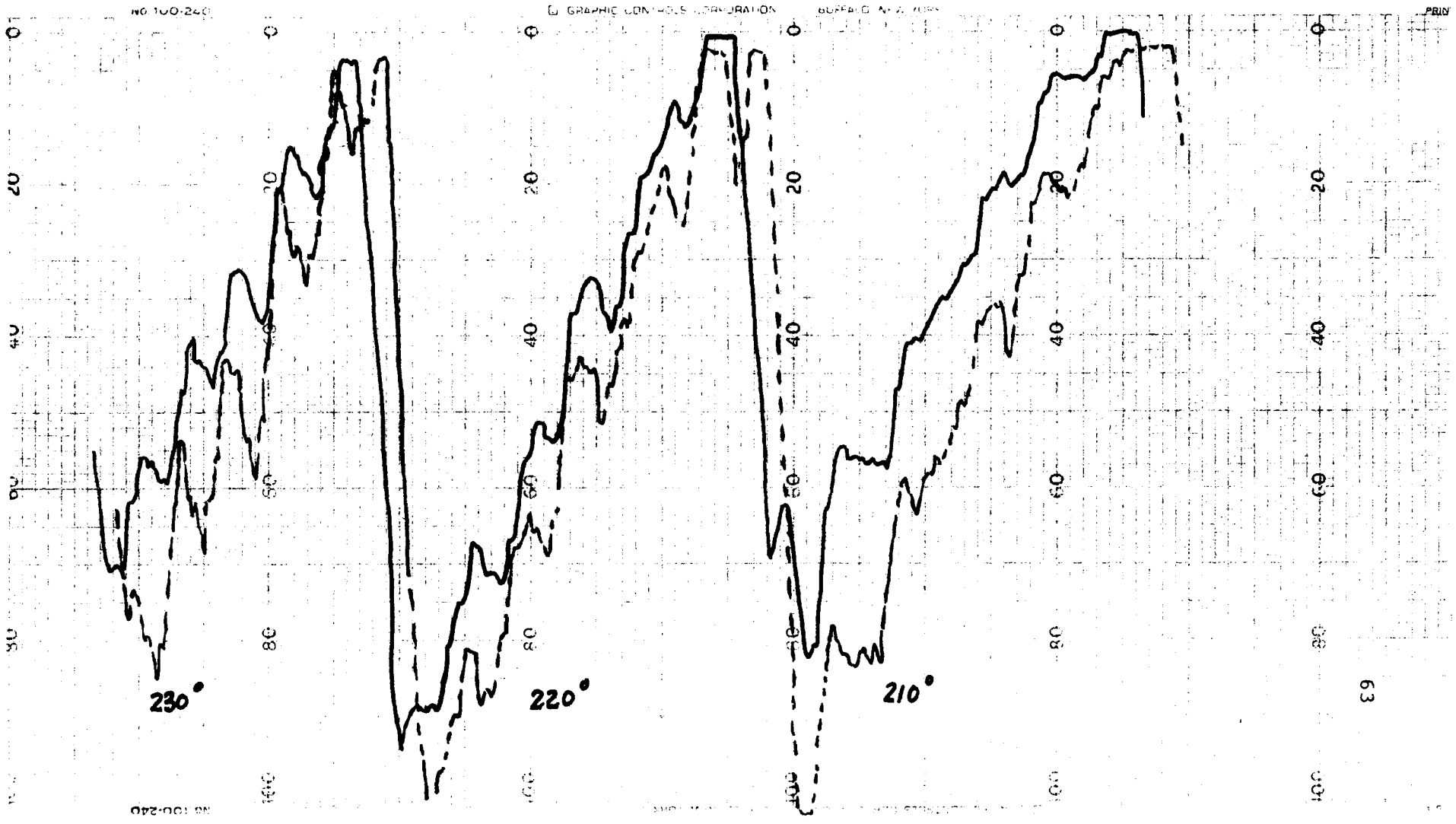

Figure 24. Eight Mile Orbit. Four Loop VOR Only (SVOR Ring Array Not Energized) (Ohio U. 10/71)

-------- Conventional 51R3

———— 51R3 Modified for Zero Crossing Detection

Scale: 10° Chart Width

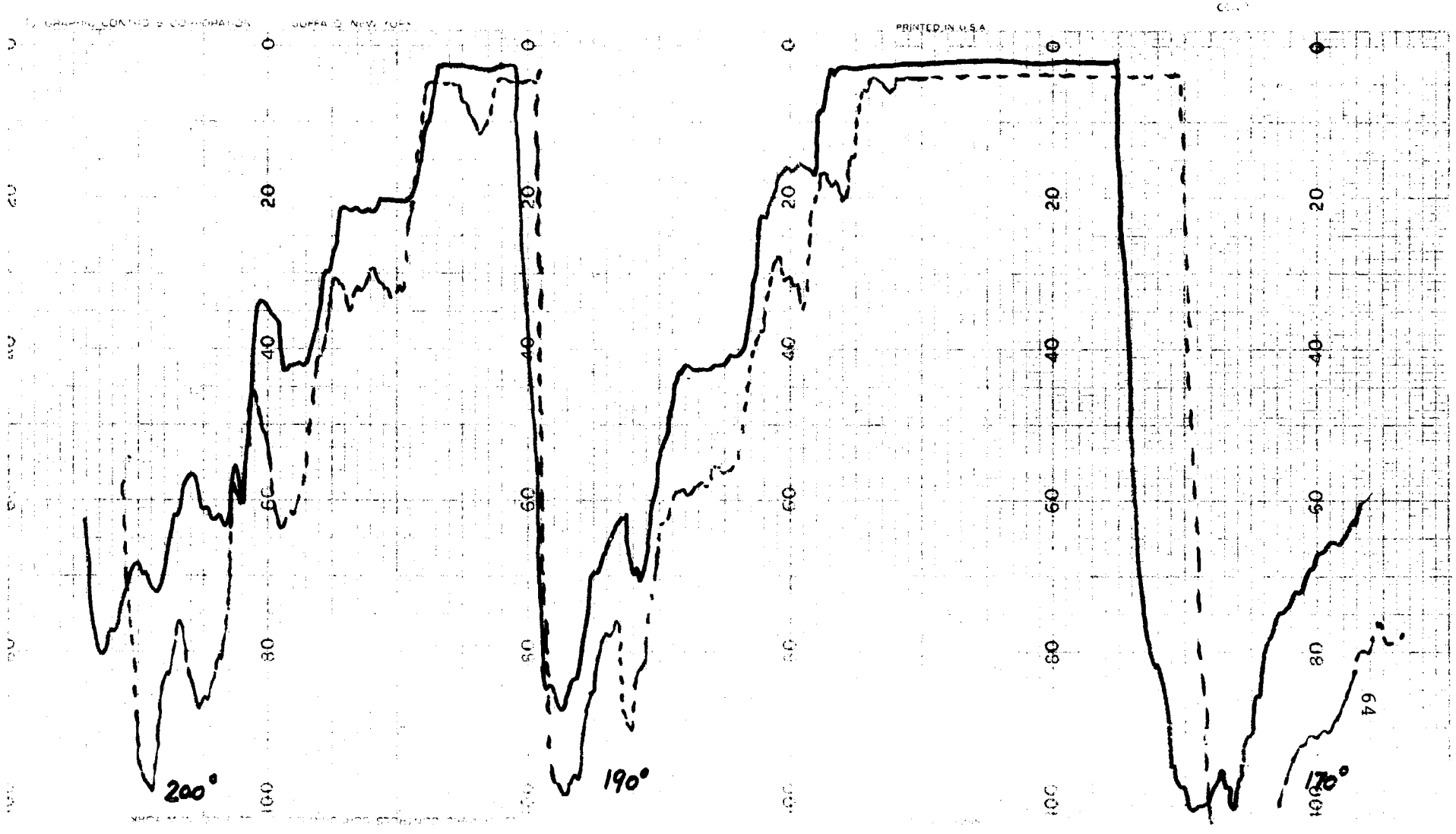

Figure 25. Eight Mile Orbit. Four Loop VOR Only (SVOR Ring Array Not Energized) (Ohio U. 10/71)

-------- Conventional 51R3

———— 51R3 Modified for Zero Crossing Detection

Scale: 10° Chart Width

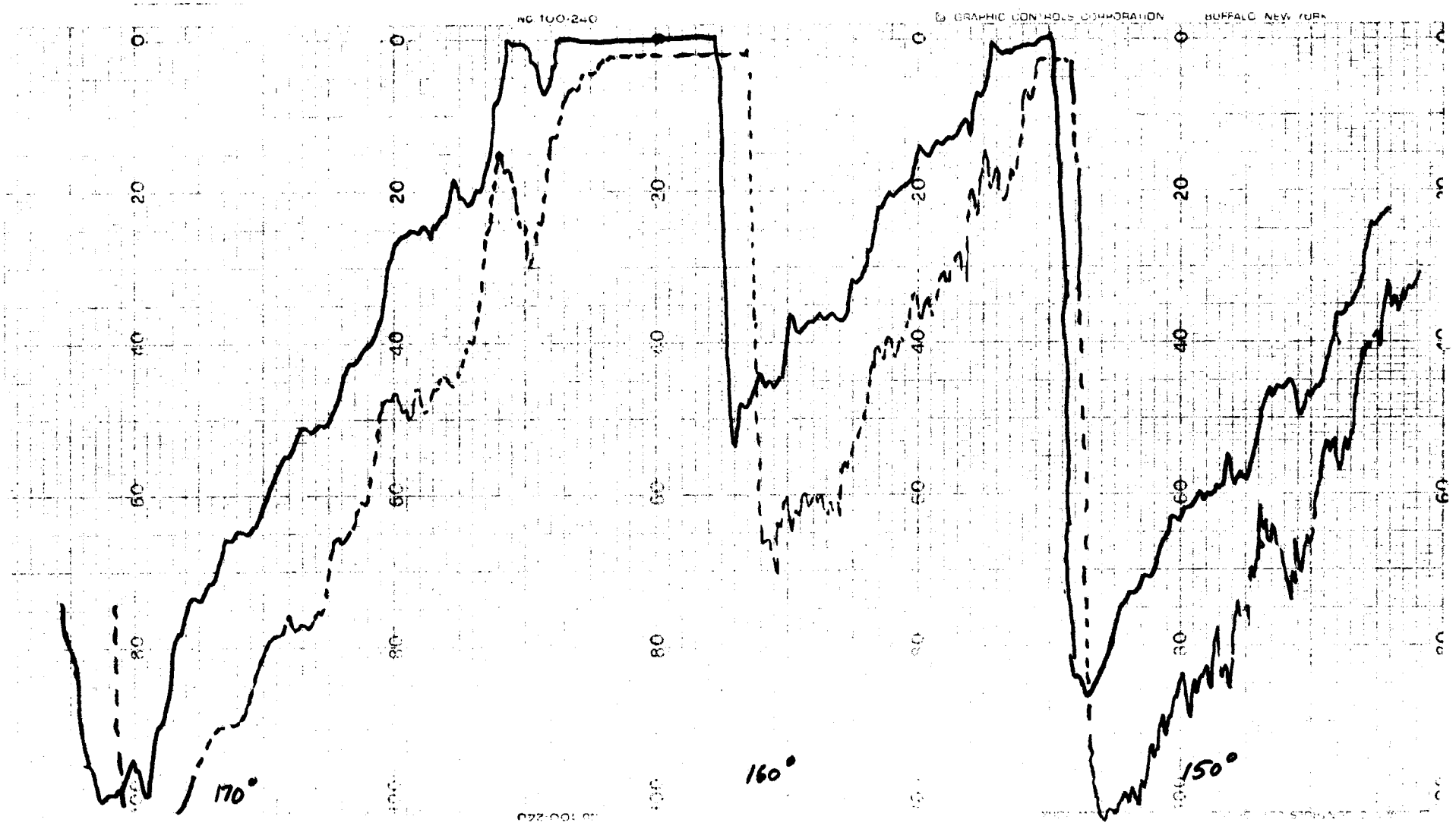

Figure 26. Eight Mile Orbit. Four Loop VOR Only (SVOR Ring Array Not Energized) (Ohio U. 10/71)

-------- Conventional 51R3

———— 51R3 Modified for Zero Crossing Detection

Scale: 10° Chart Width

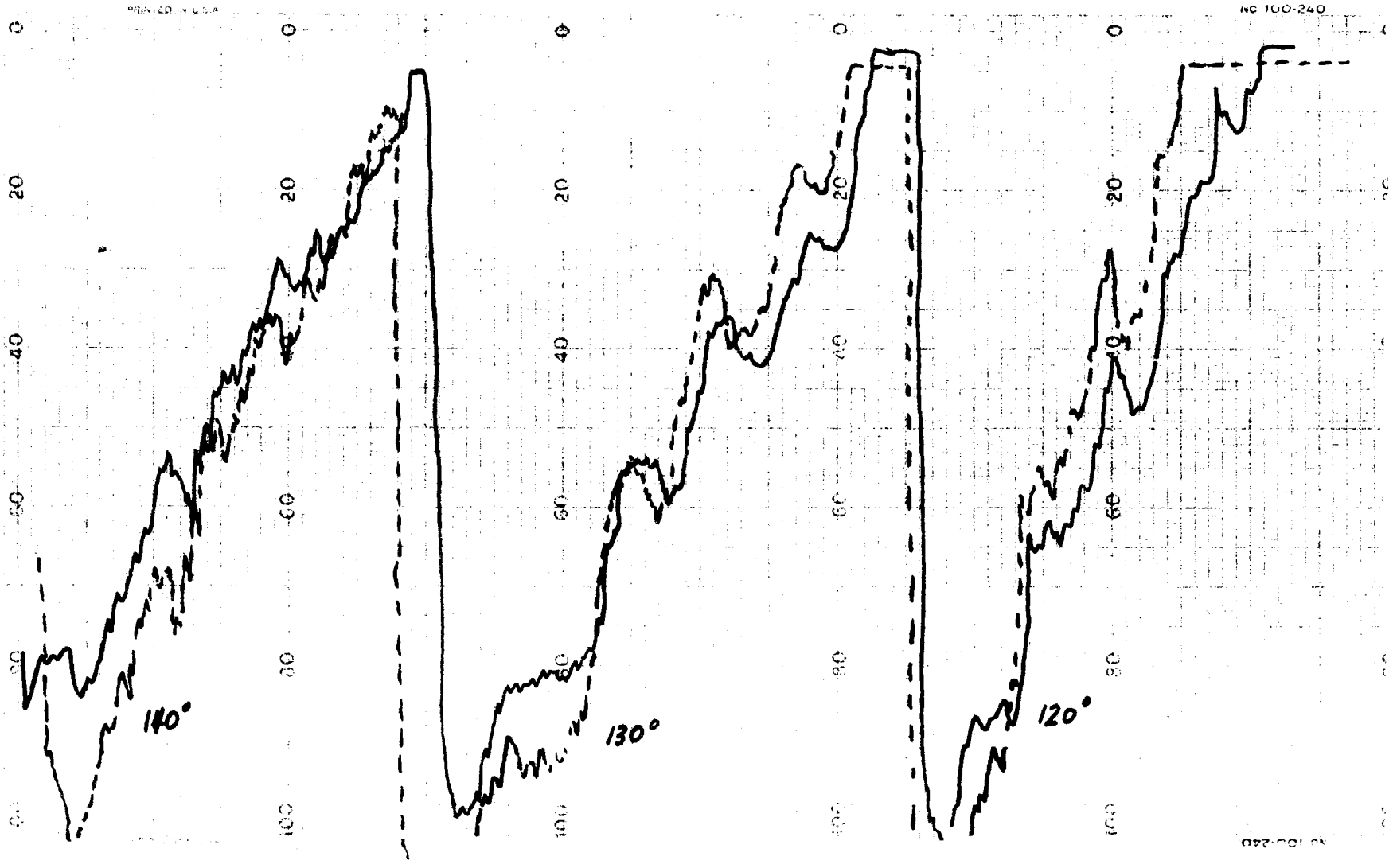

Figure 27. Eight Mile Orbit. Four Loop VOR Only (SVOR Ring Array Not Energized) (Ohio U. 10/71)

-------- Conventional 51R3

———— 51R3 Modified for Zero Crossing Detection

Scale: 10° Chart Width

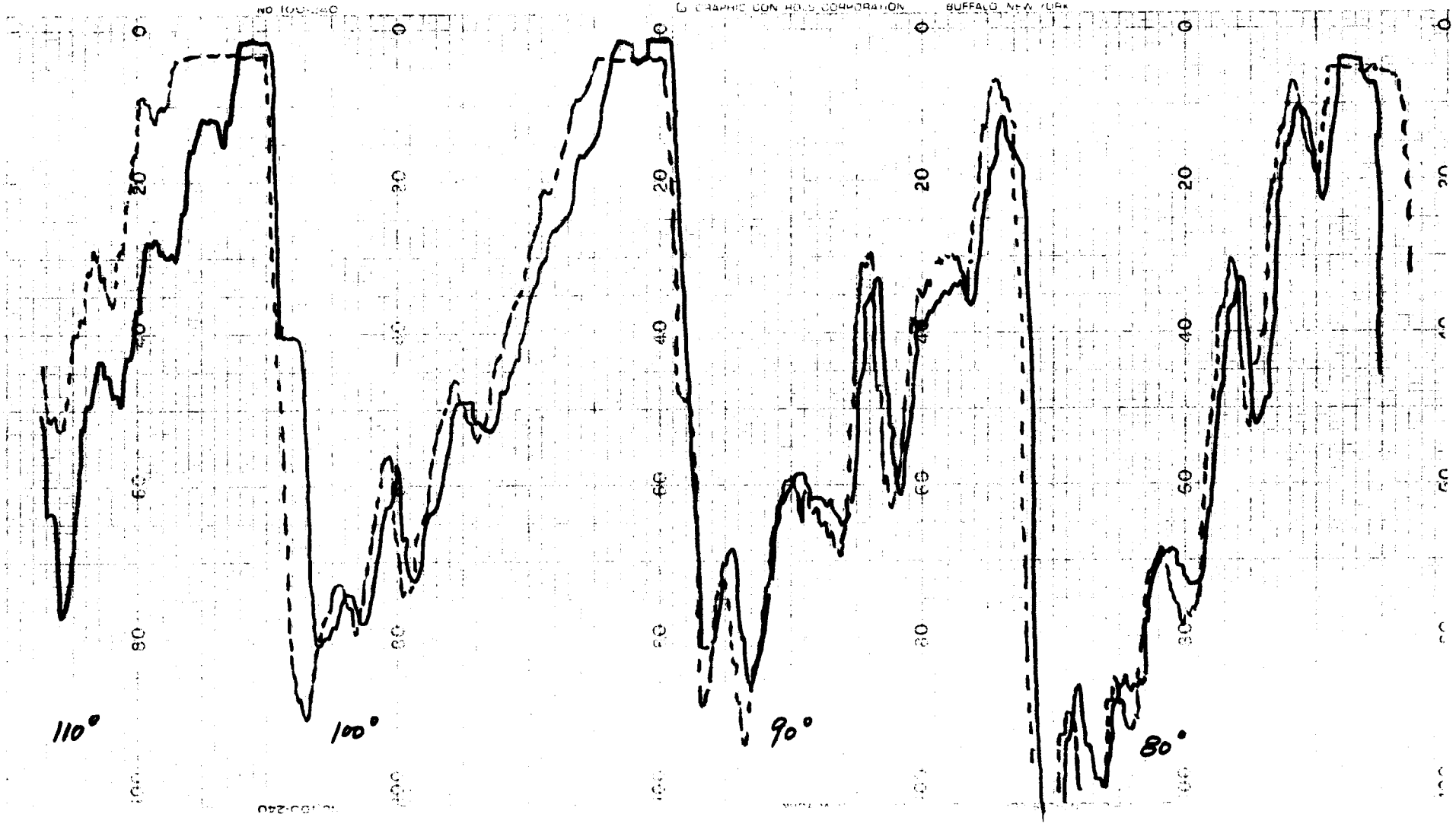

Figure 28. Eight Mile Orbit. Four Loop VOR Only (SVOR Ring Array Not Energized) (10/71)

-------- Conventional 51R3

———— 51R3 Modified for Zero Crossing Detection

Scale: 10° Chart Width

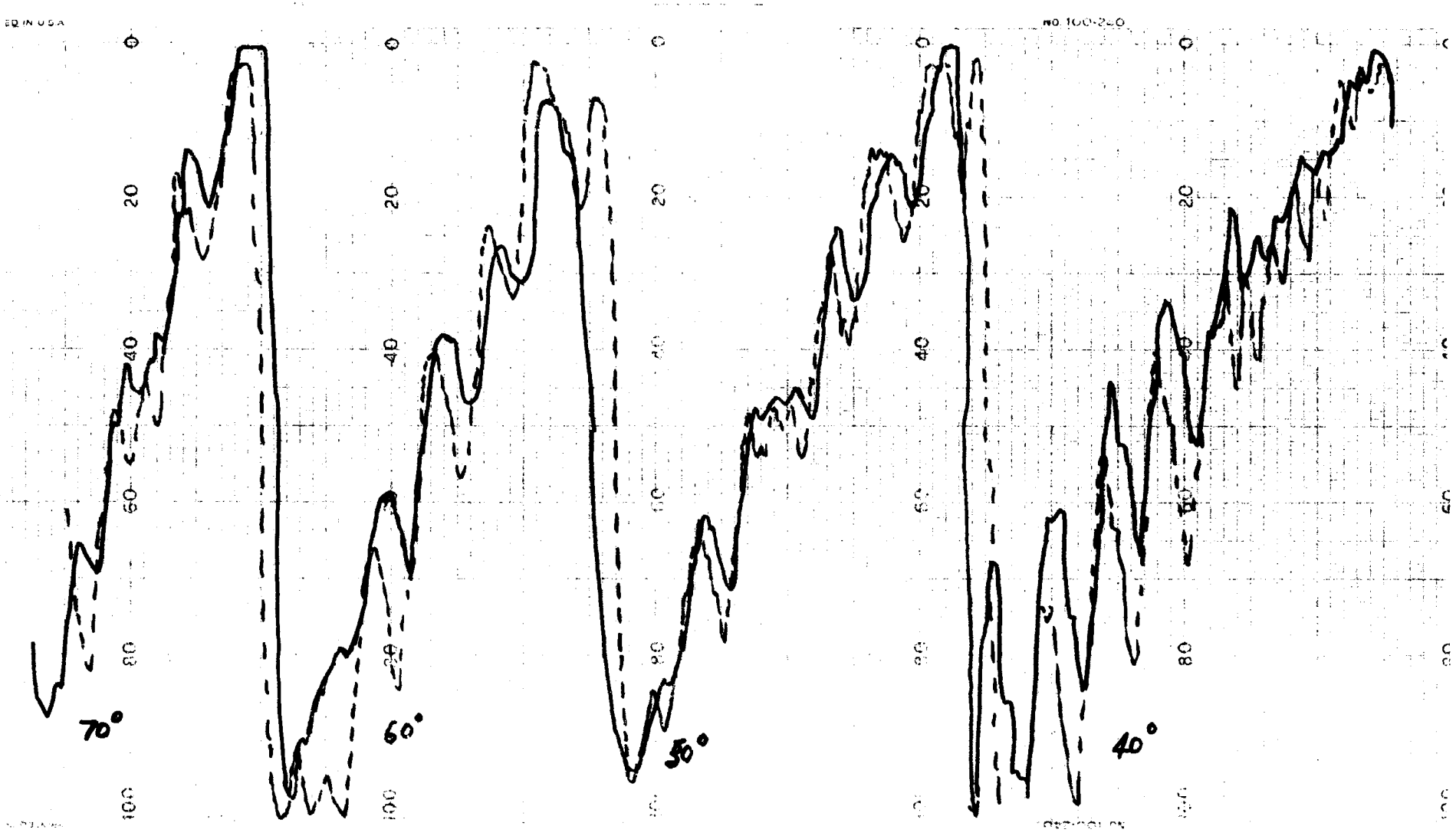

Figure 29. Eight Mile Orbit. Four Loop VOR Only (SVOR Ring Array Not Energized) (Ohio U. 10/71)

-------- Conventional 51R3

———— 51R3 Modified for Zero Crossing Detection

Scale: 10° Chart Width

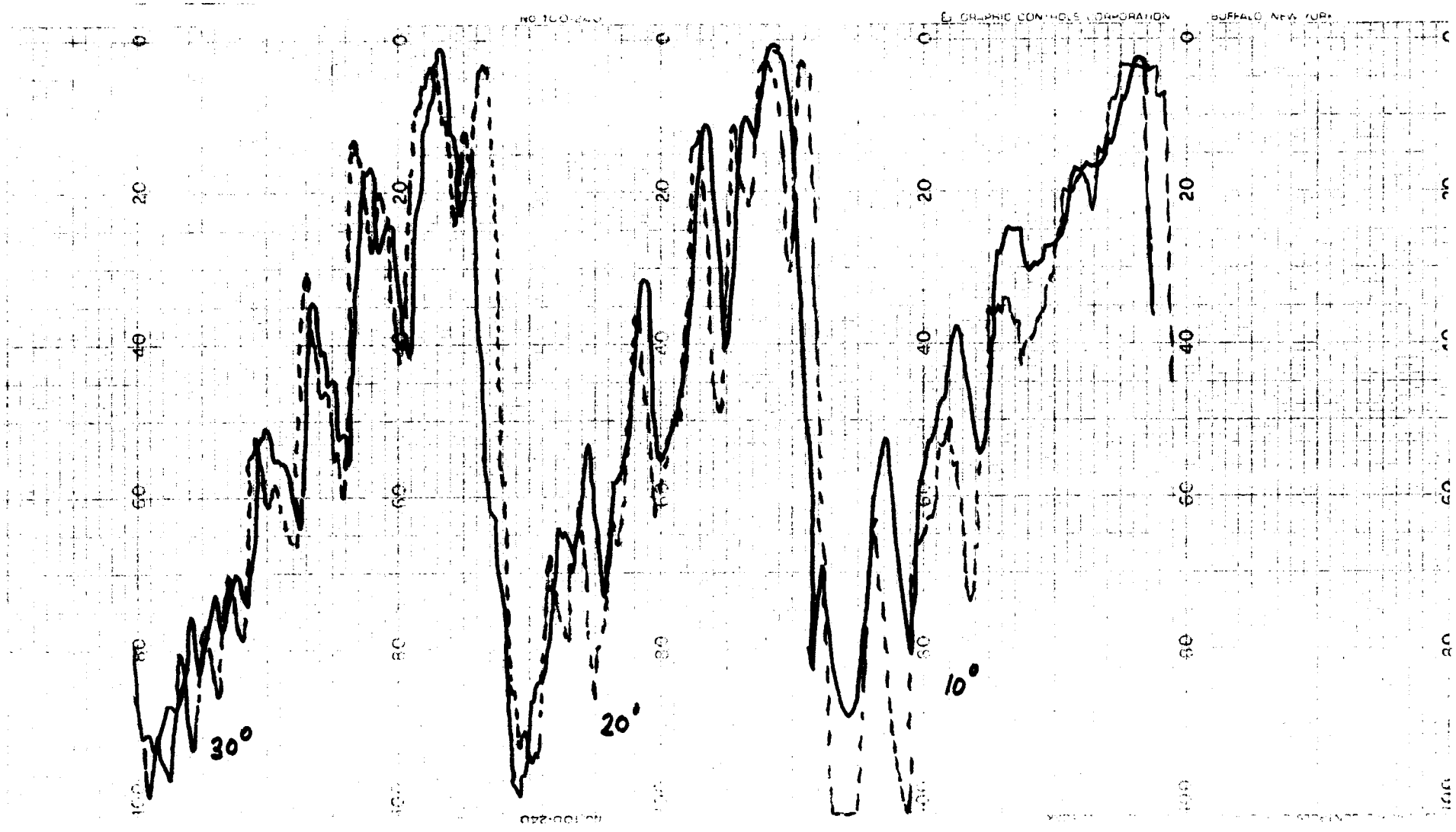

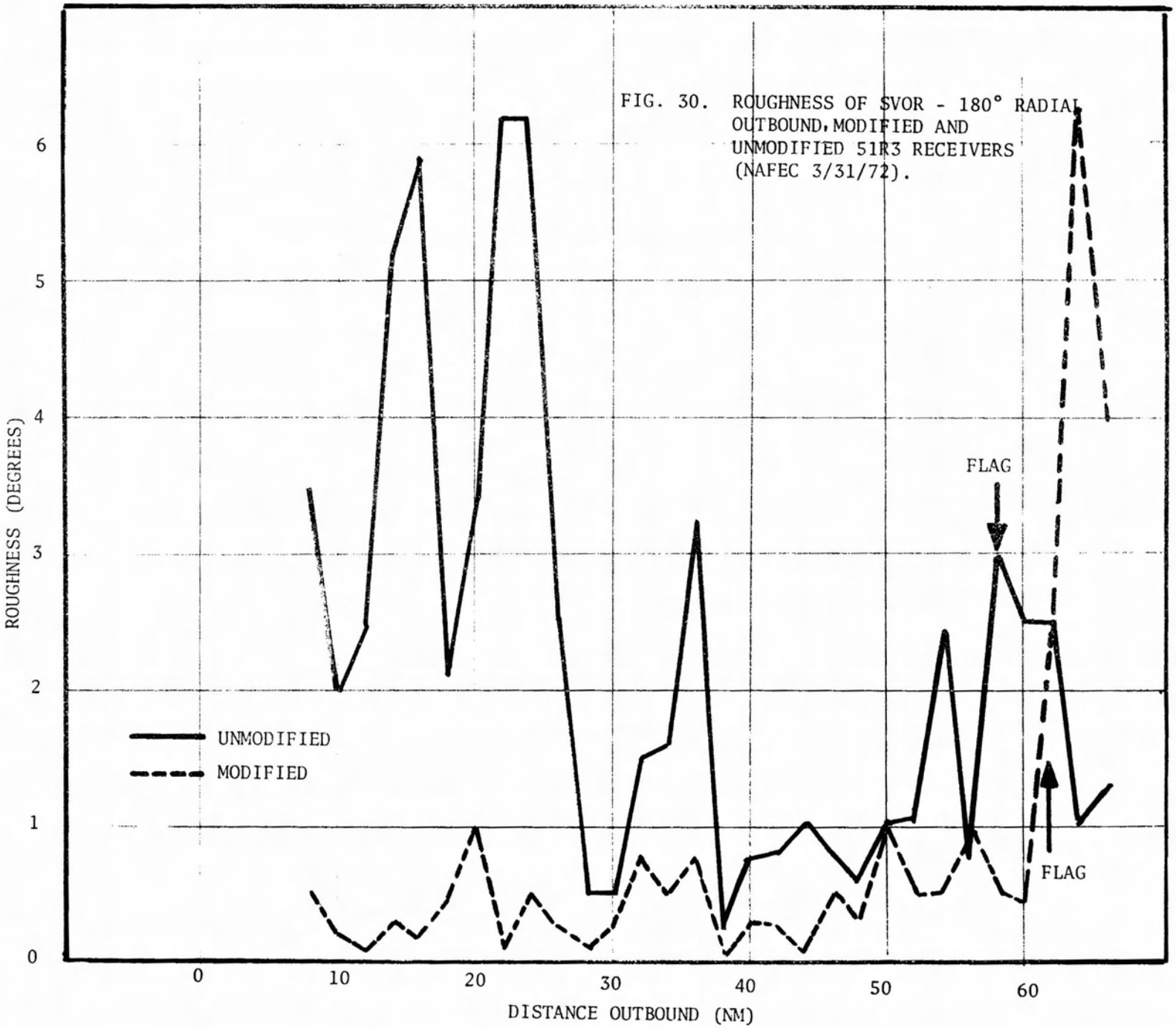

FIG. 30. ROUGHNESS OF SVOR - 180° RADIAL OUTBOUND, MODIFIED AND UNMODIFIED 51R3 RECEIVERS (NAFEC 3/31/72).

FIGURE 31.

Instrumentation for Testing Conventional VOR Receivers With Square Wave VOR Signals

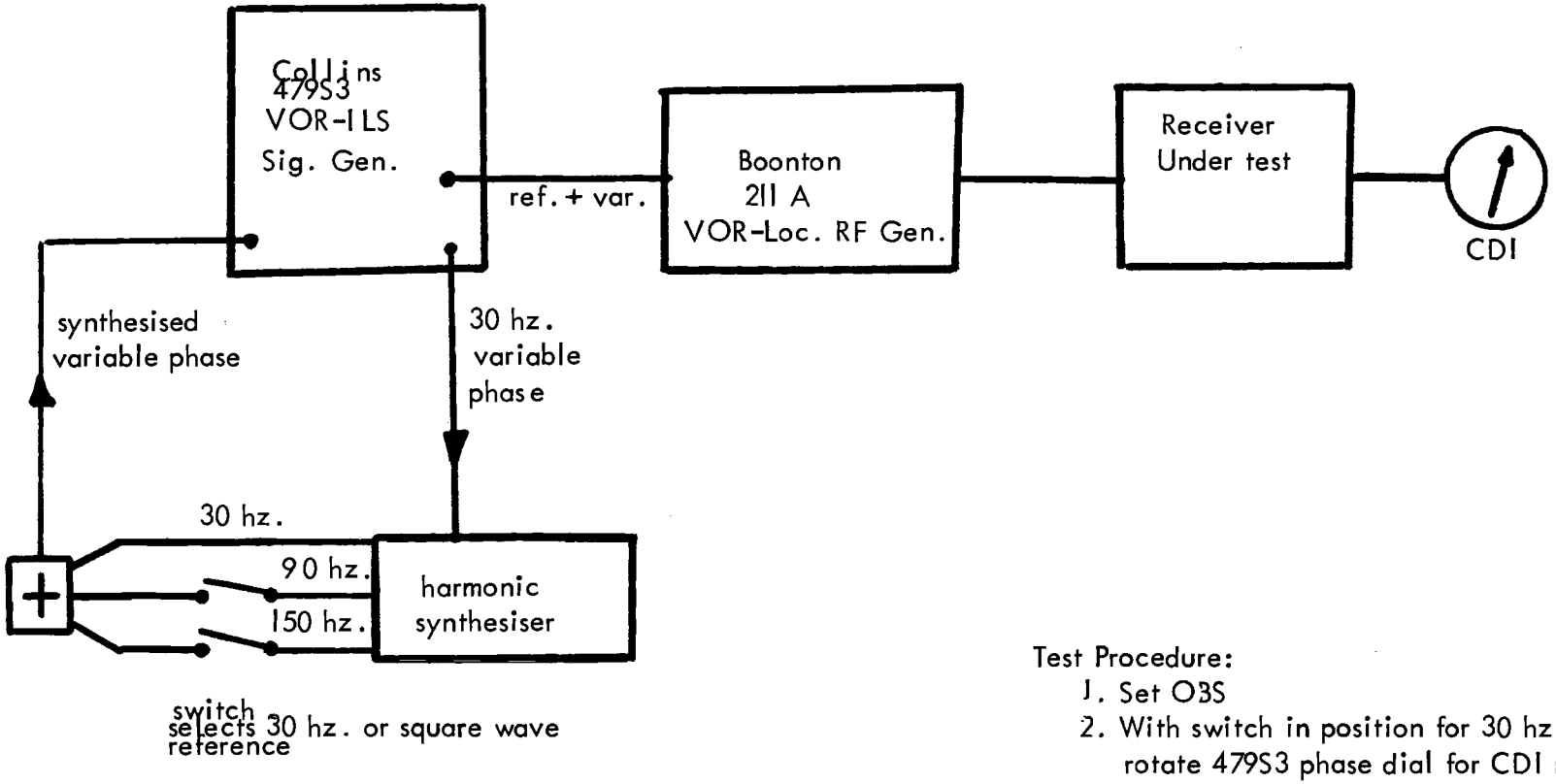

Test Procedure:

1. Set OBS
2. With switch in position for 30 hz. var., rotate 479S3 phase dial for CDI null and record reading
3. With switch in position for square wave variable, rotate 479S3 phase dial for CDI null and record reading.

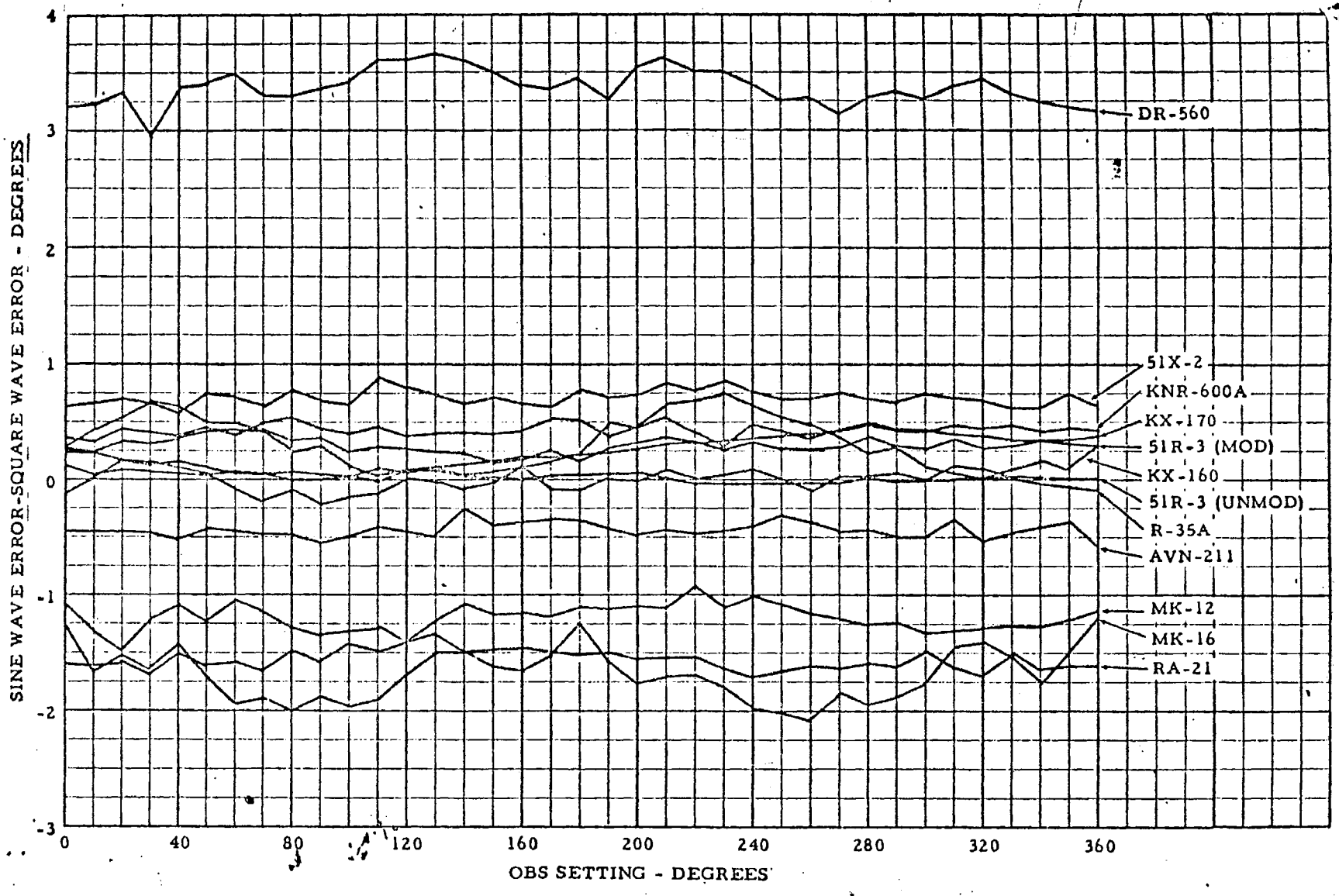

FIGURE 32.- RECEIVER SIGNAL DIFFERENCE, COMPOSITE OF 12 RECEIVERS.
SINE WAVE ERROR MINUS SQUARE WAVE ERROR
(NAFEC DATA)

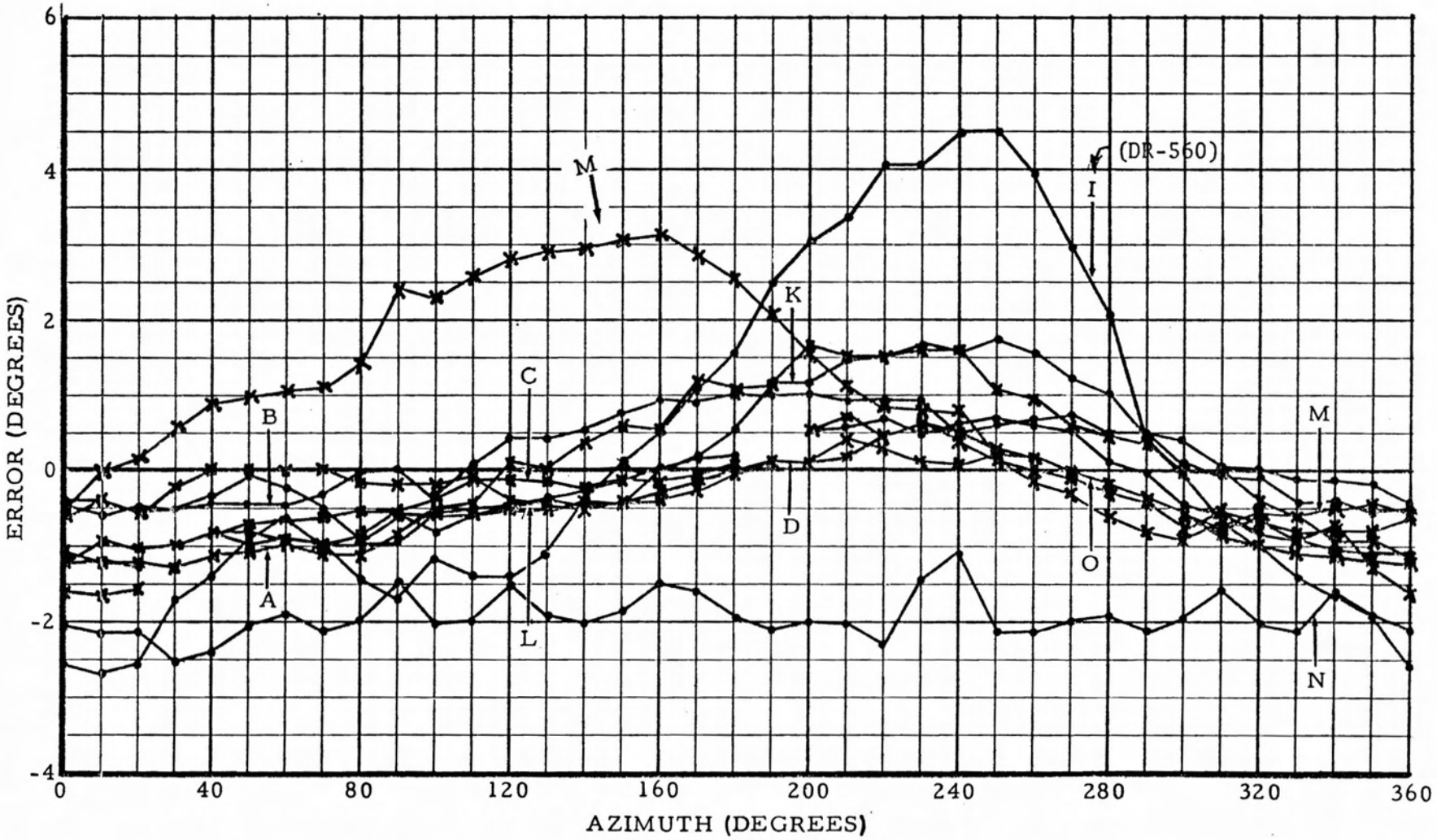

Figure 33. COMPOSITE INDICATED STATION ERROR FROM SSDVOR STATIC TESTS (TAKEN FROM REF. 13)

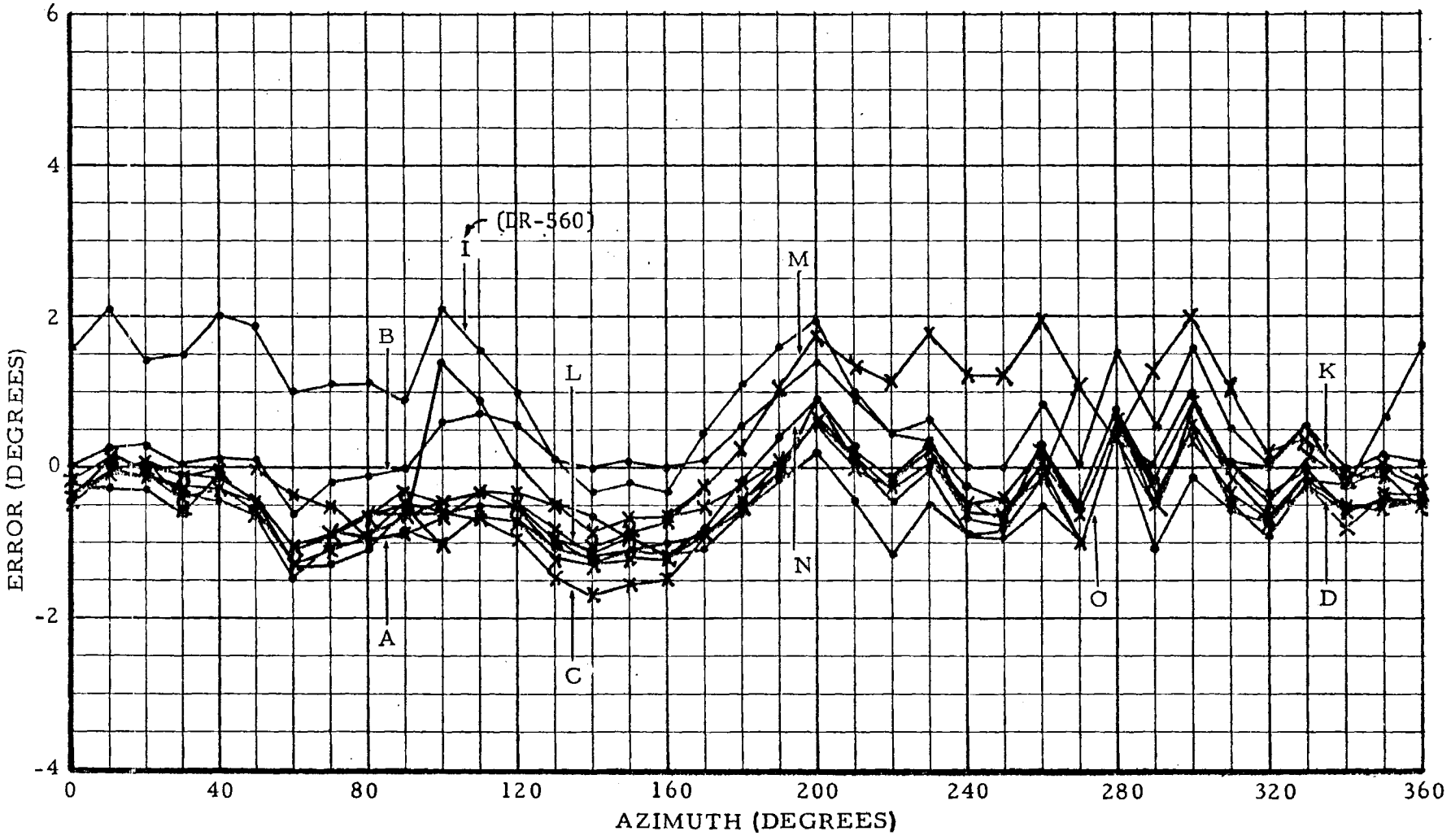

Figure 34. COMPOSITE INDICATED STATION ERROR FROM CONVENTIONAL VOR STATIC TESTS (TAKEN FROM REF. 13)

FIG. 35. STATION ERROR. 5X SVOR WITH AND WITHOUT RING ARRAY SIGNAL. 6 NM ORBIT. CONVENTIONAL RECEIVER (NAFEC 8/10/72).

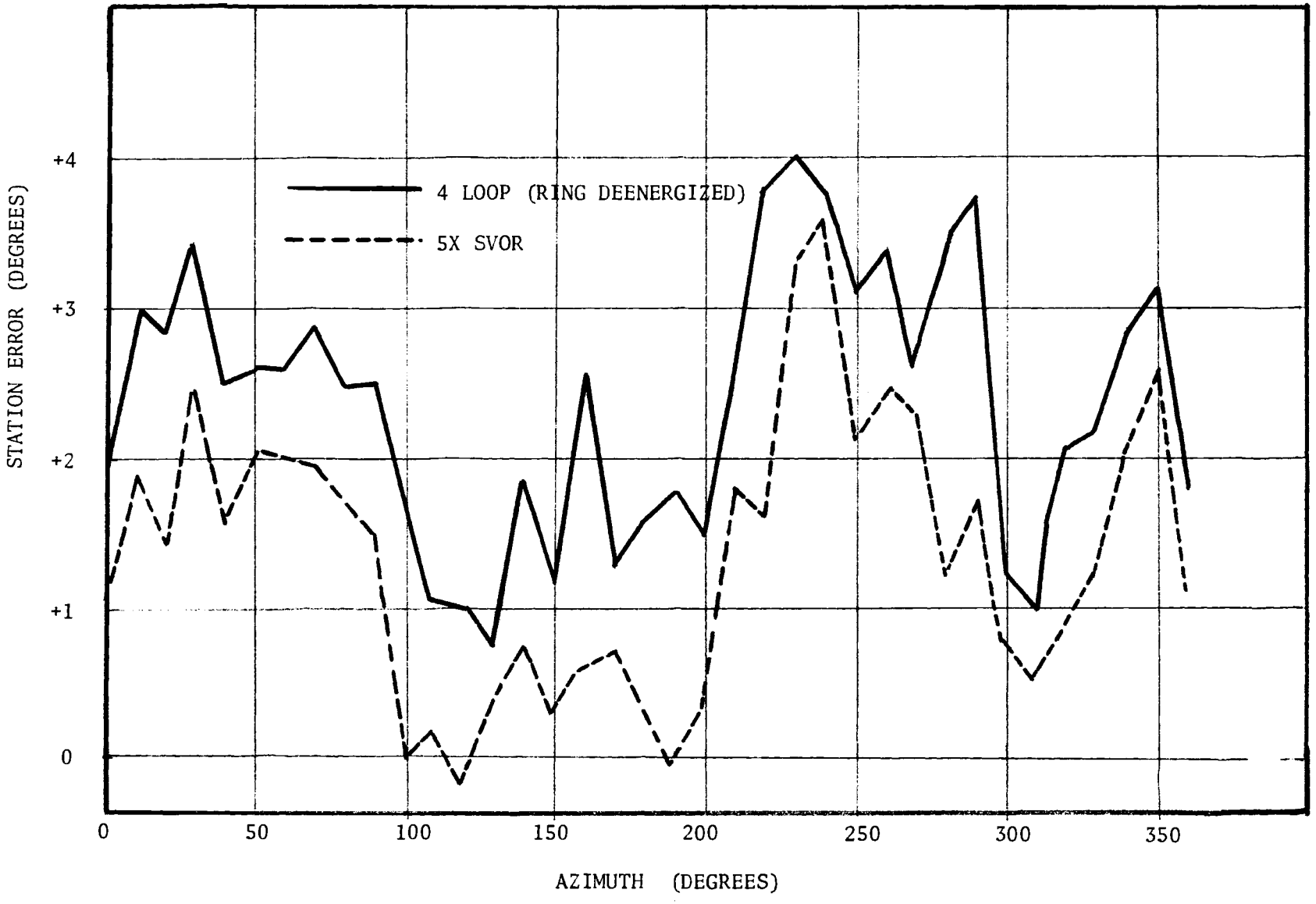

FIG. 36. STATION ERROR. 4 LOOP VOR WITH AND WITHOUT DEENERGIZED 5X SVOR RING ARRAY. 6 NM ORBITS. CONVENTIONAL RECEIVER (NAFEC 8/10/72).

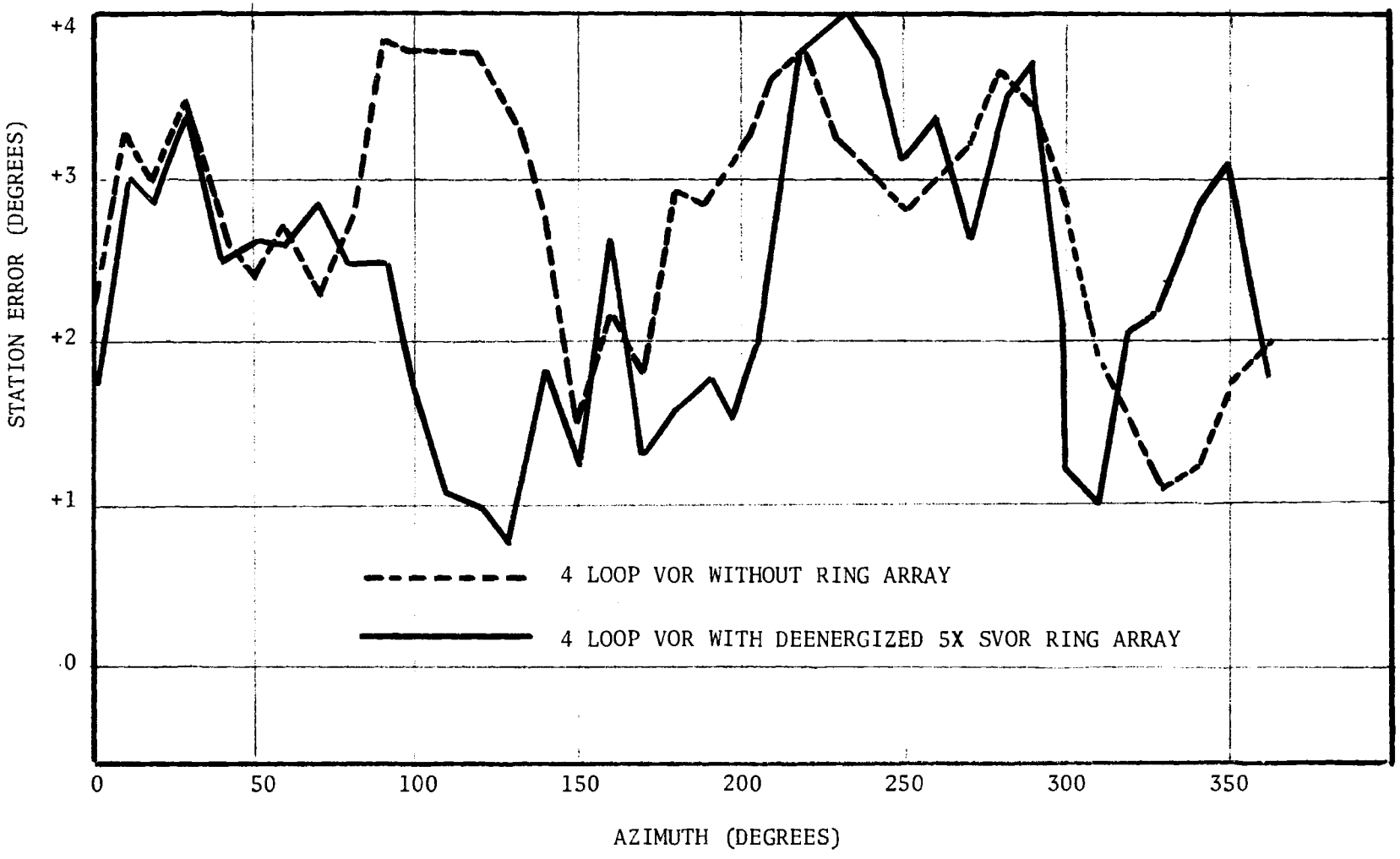

FIG. 37. POLARISCOPE RUNS. 4 LOOP VOR AND SVOR. MODIFIED AND UNMODIFIED RECEIVERS. 214° RADIAL (NAFEC 1/17/72, 3/29/72) TACAN ANTENNA NOT INSTALLED.

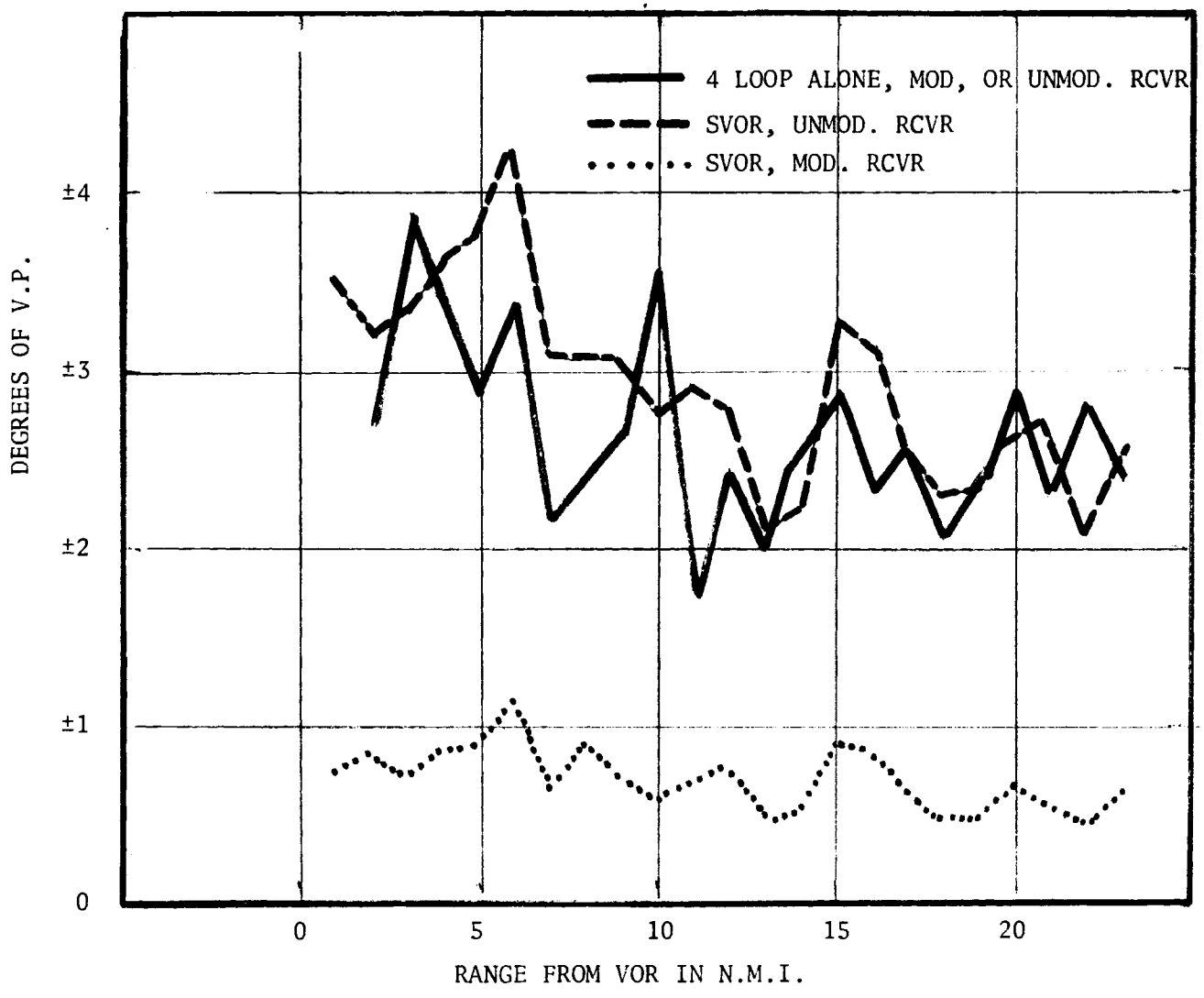

FIG. 38. POLARISCOPE RUNS. 5X SVOR.90° RADIAL, WITH AND WITHOUT TACAN ANTENNA, CONVENTIONAL RECEIVERS (NAFEC 3/29/72, 4/14/72).

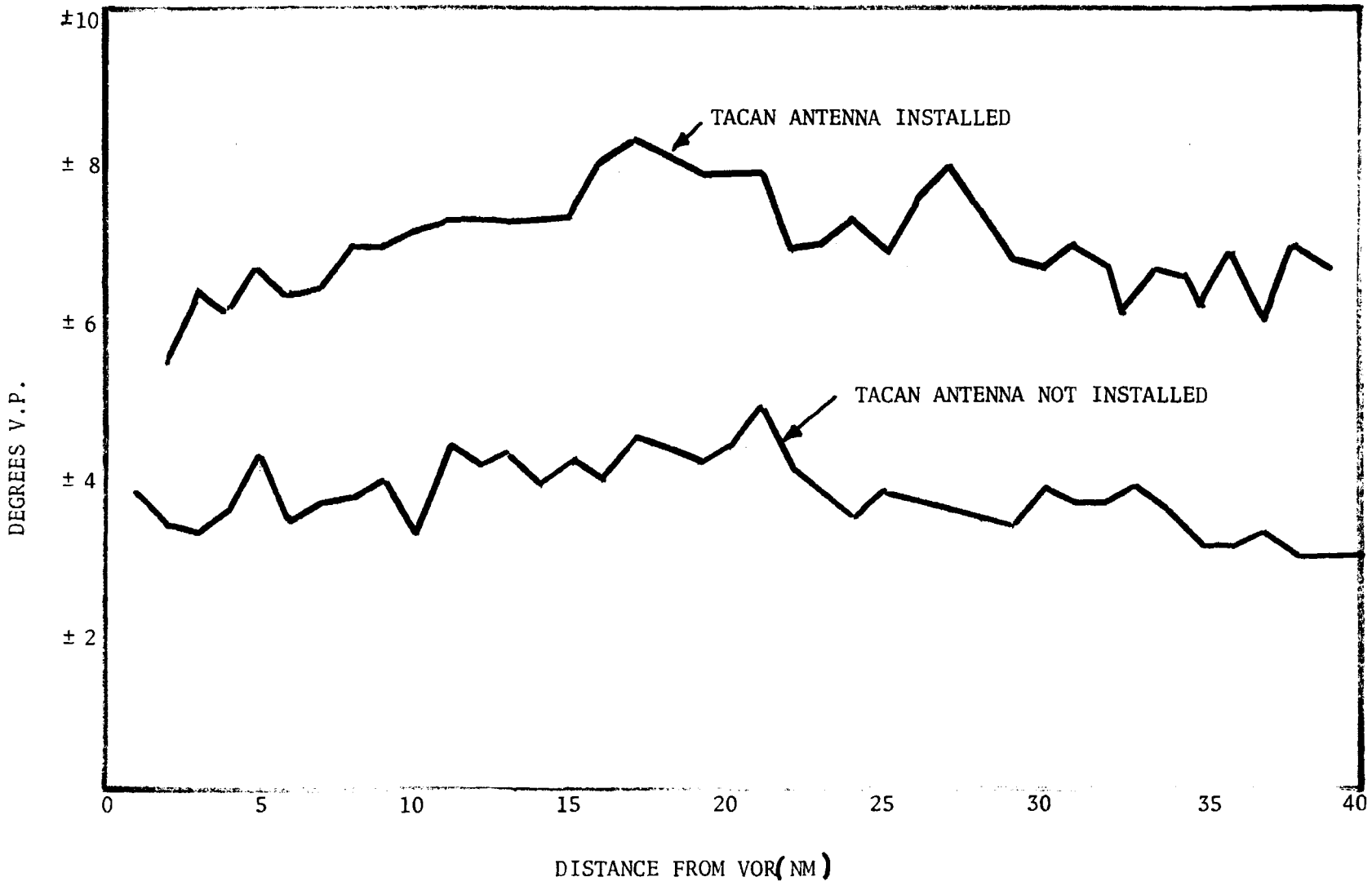

Figure 39. SVOR DRUM MODULATOR.

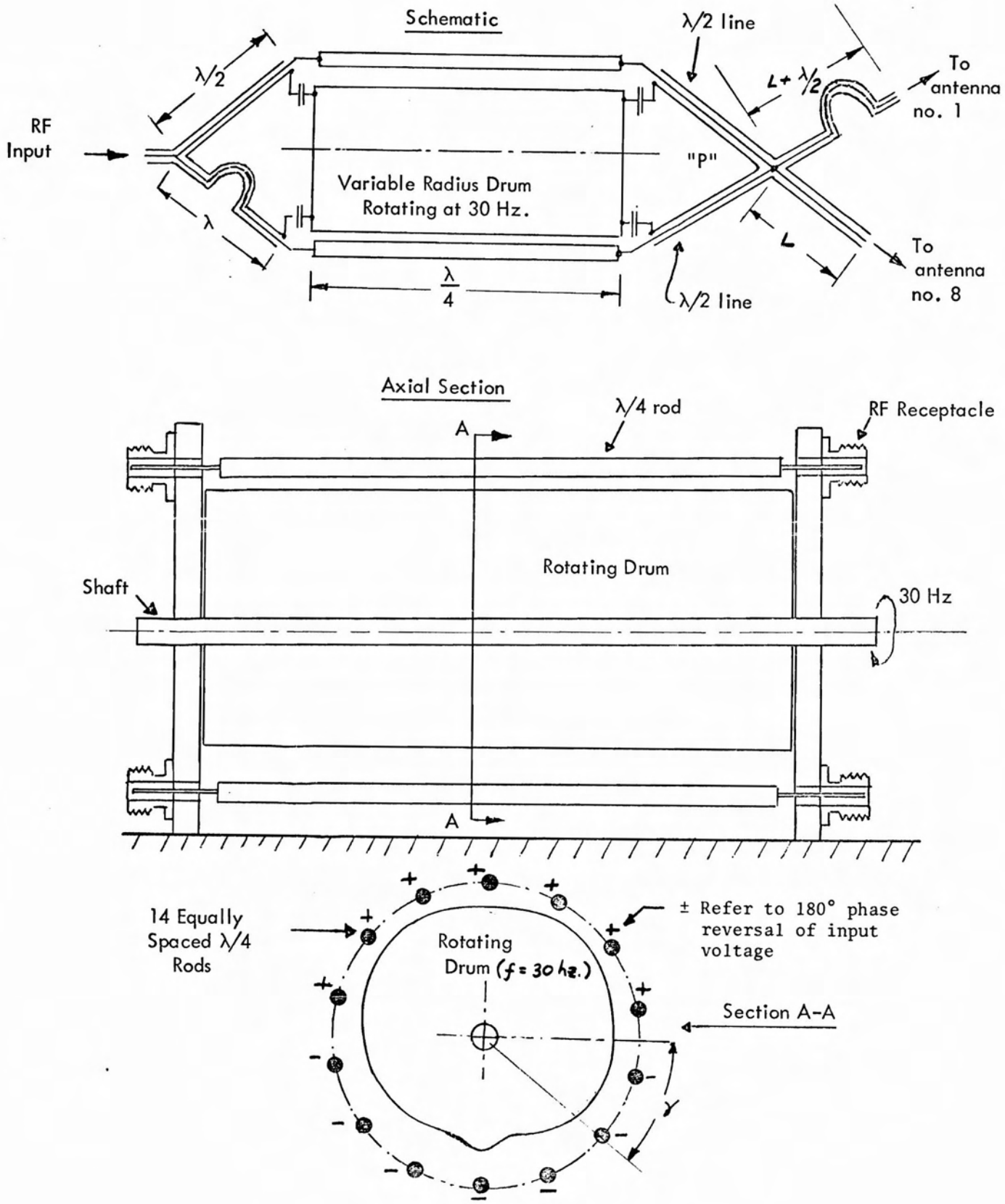

Figure 40.

ARRAY LAYOUT

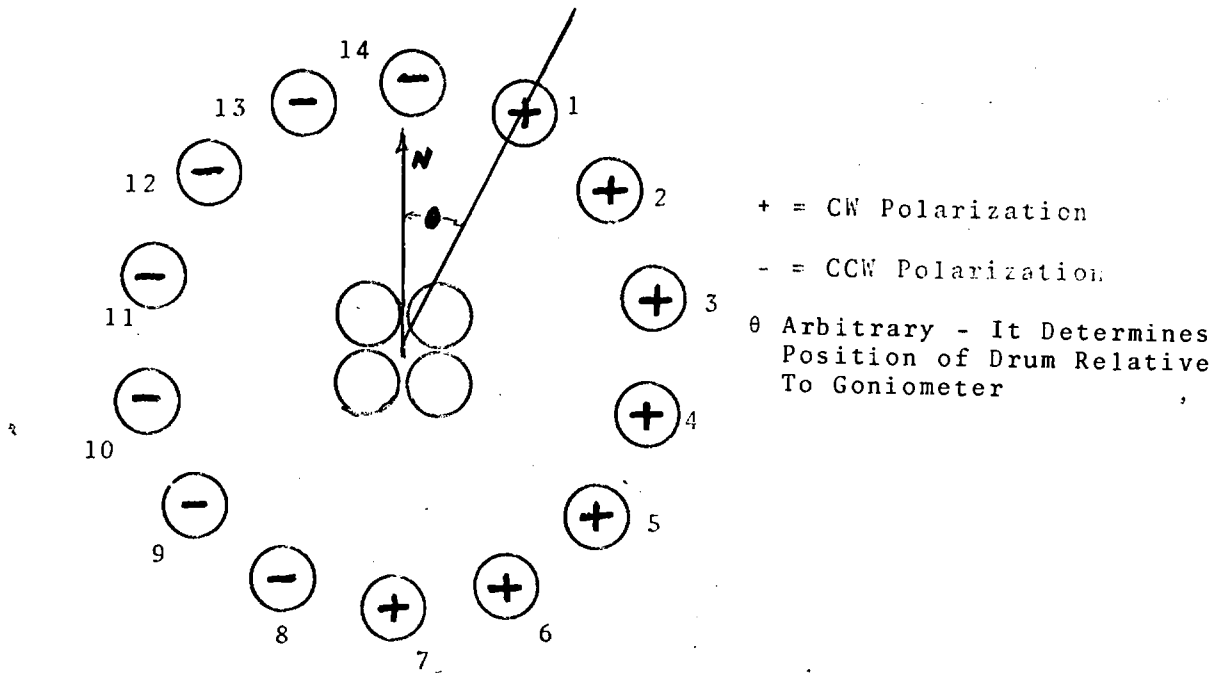

Modulator Schematic

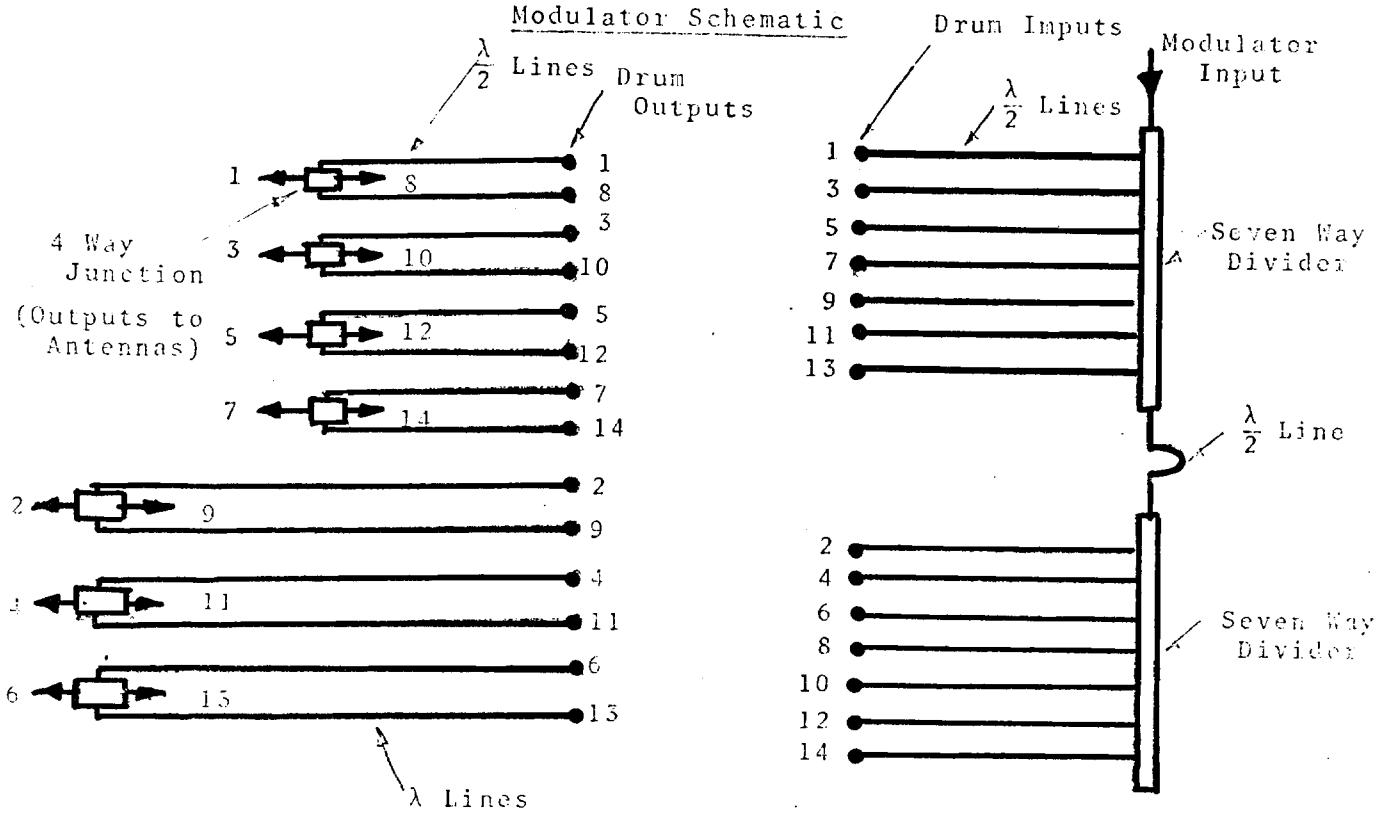

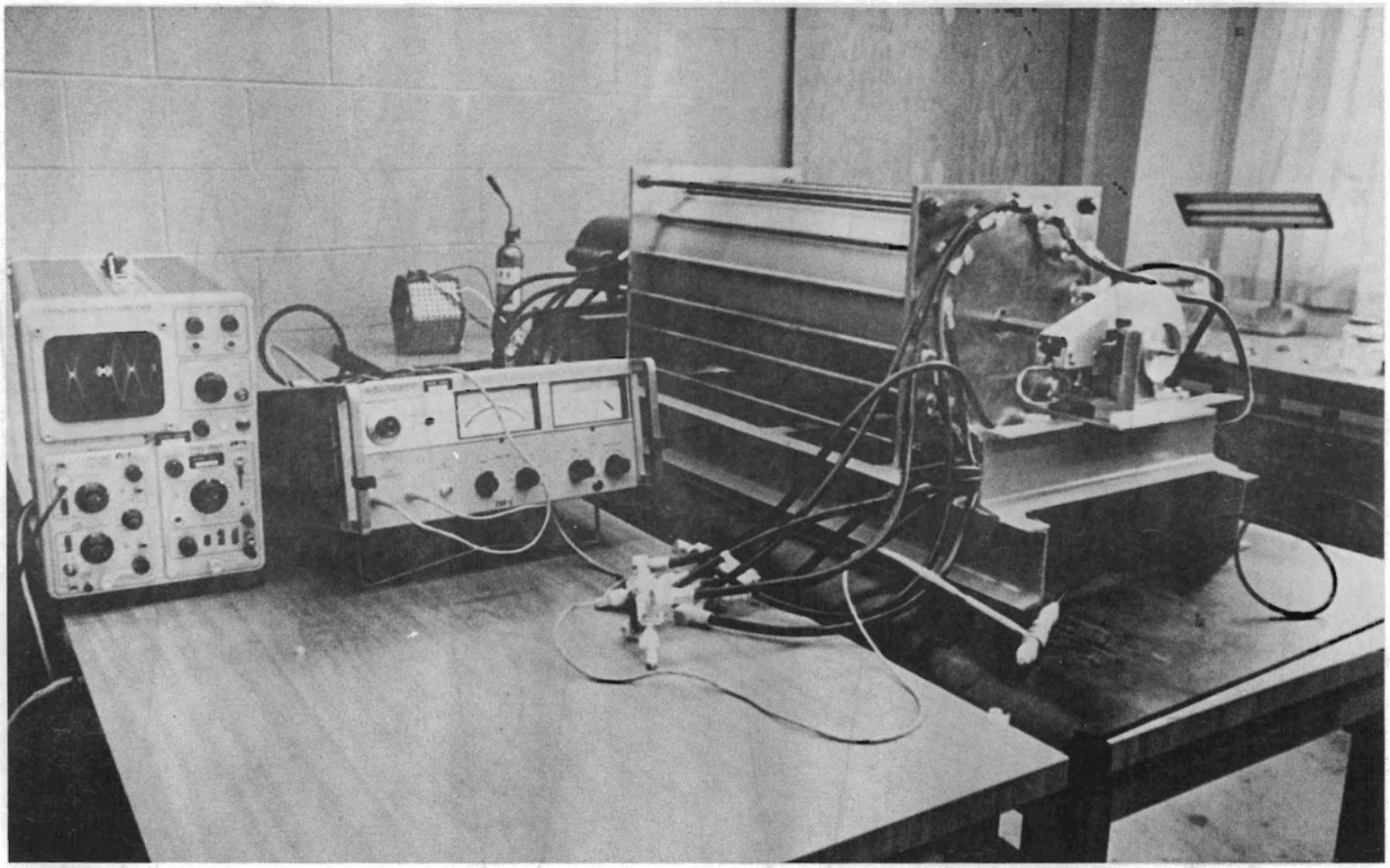

FIG. 41. SINGLE RING SVOR MUDULATOR BEING BENCH TESTED. MODULATED RF OUTPUT WAVEFORM IS VISIBLE ON THE OSCILLOSCOPE SCREEN.

FIG. 42. SINGLE RING 5X SVOR DRUM MODULATOR - OUTPUT OF ONE PAIR OF RODS VS. DRUM ROTATION.

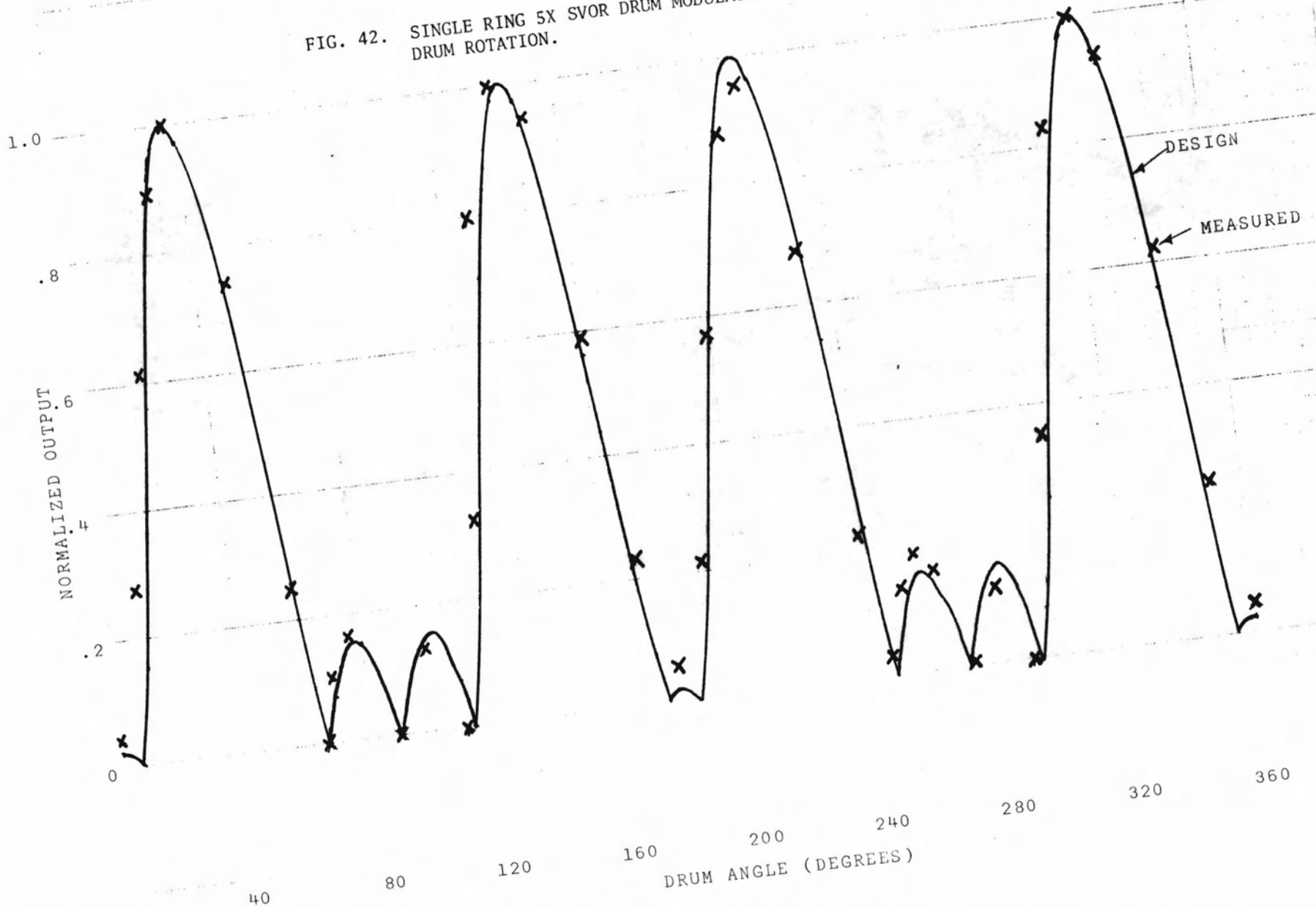

FIG. 43. SINGLE RING 5X SVOR DRUM MODULATOR - PHASE VS. DRUM ROTATION.

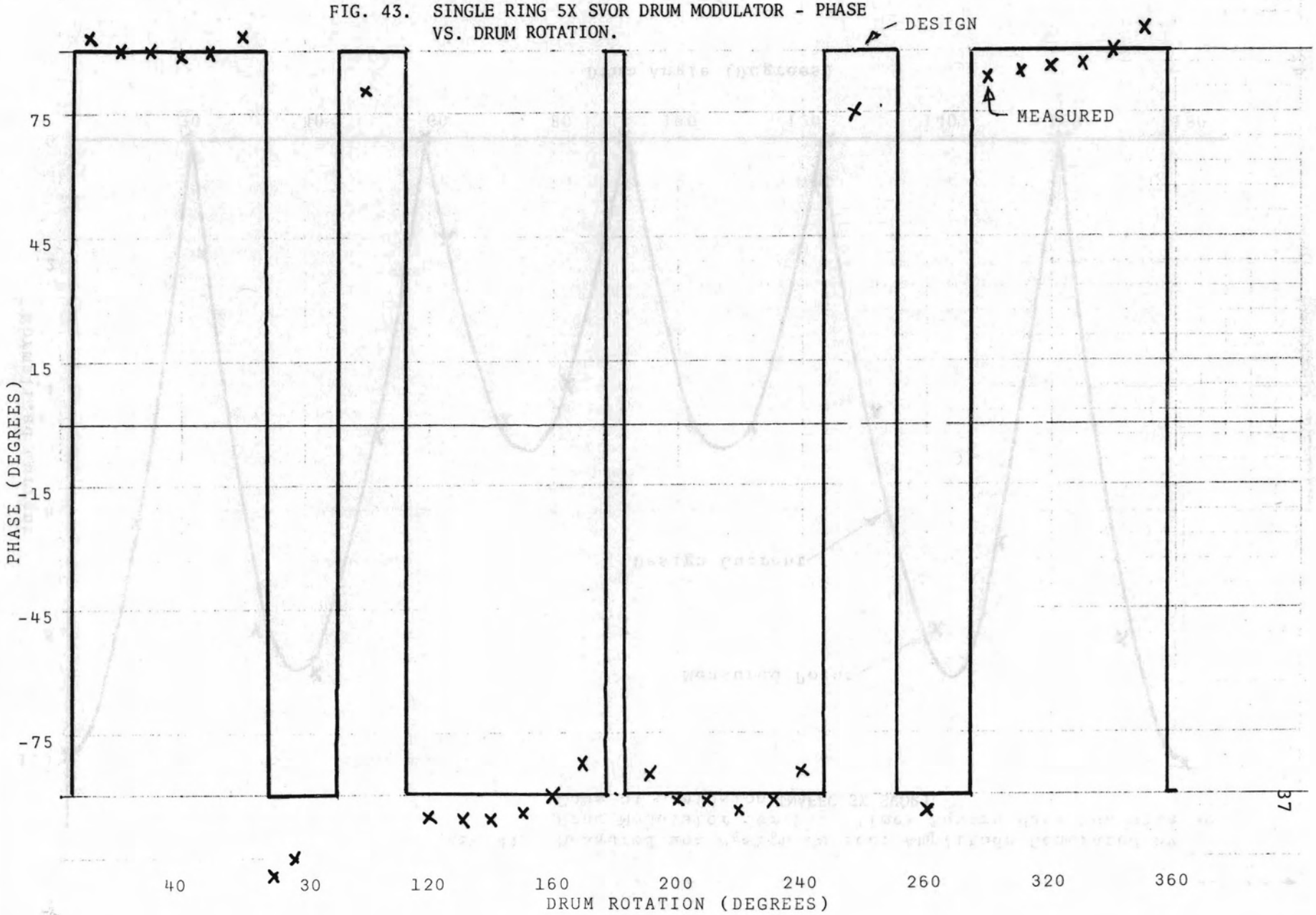

Figure 44. Measured and Design Current Amplitude Generated by Drum Modulator for Five Times Square Wave VOR with No Cone of Confusion (NAFEC 5X SVOR)

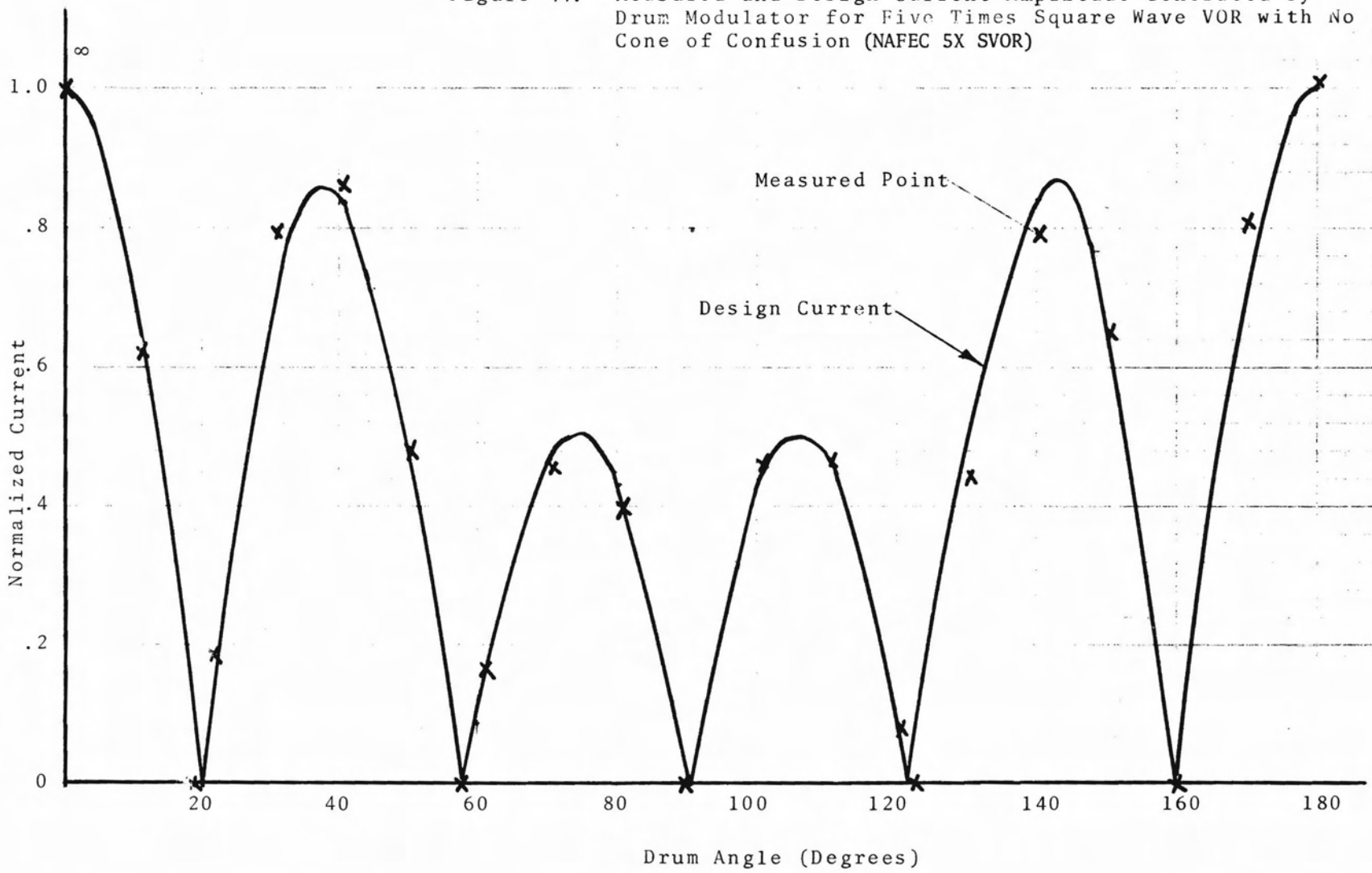

Figure 45. Measured and Design Current Phase Generated by Drum Modulator for 5 Times Square Wave VOR with No Cone of Confusion (NAFEC 5X SVOR)

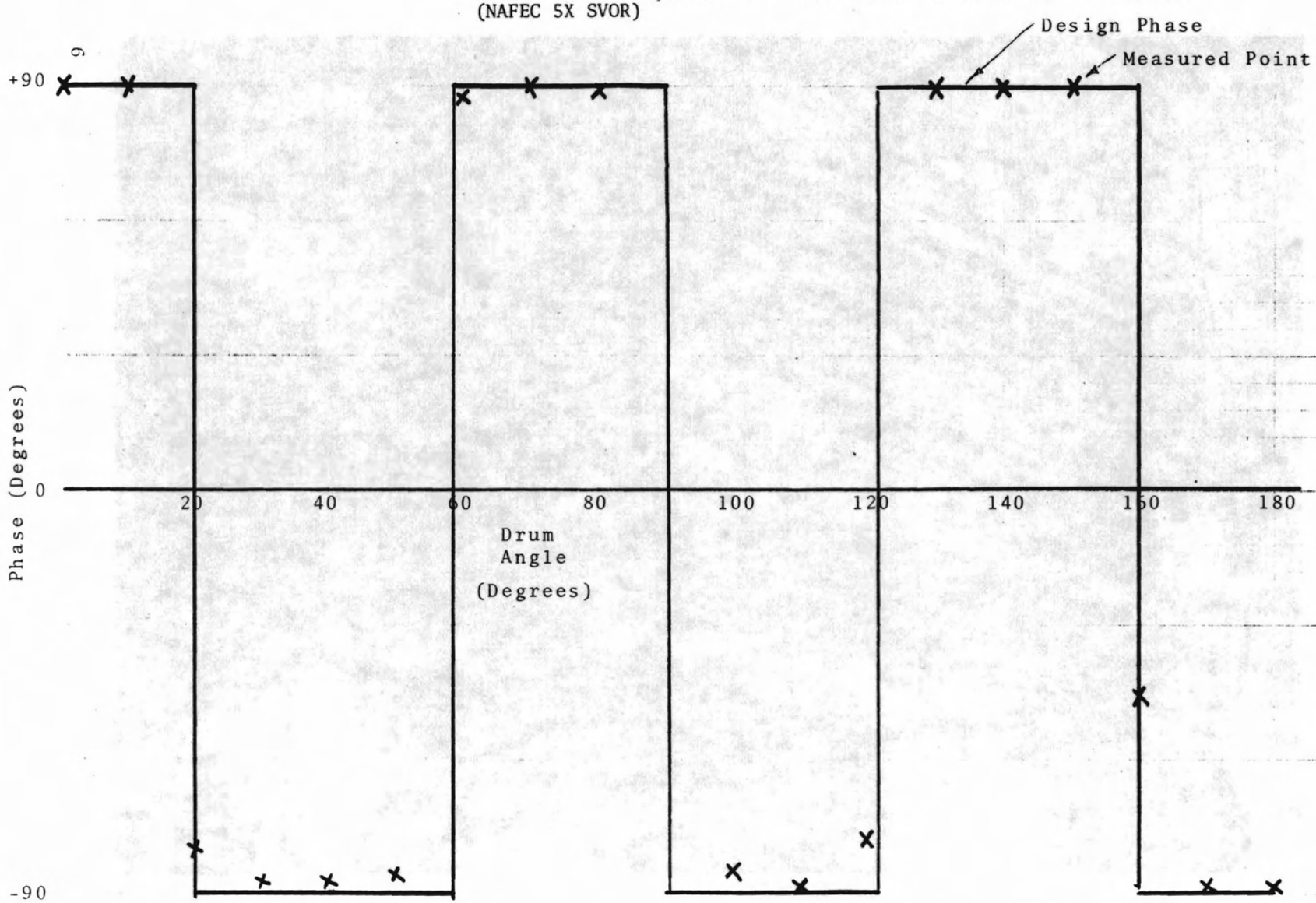

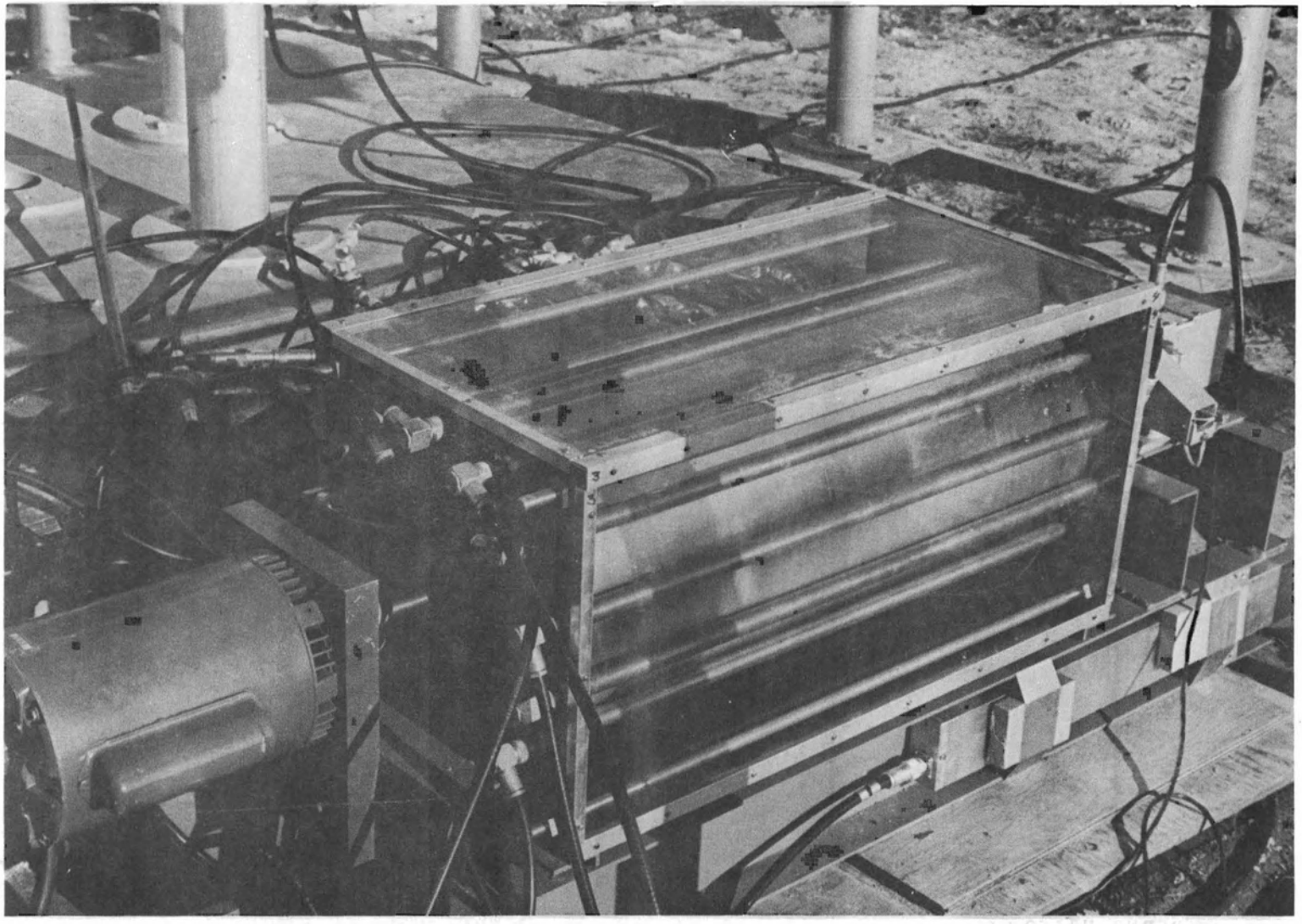

FIG. 46. DRUM MODULATOR FOR 5X SVOR TESTED AT NAFEC.

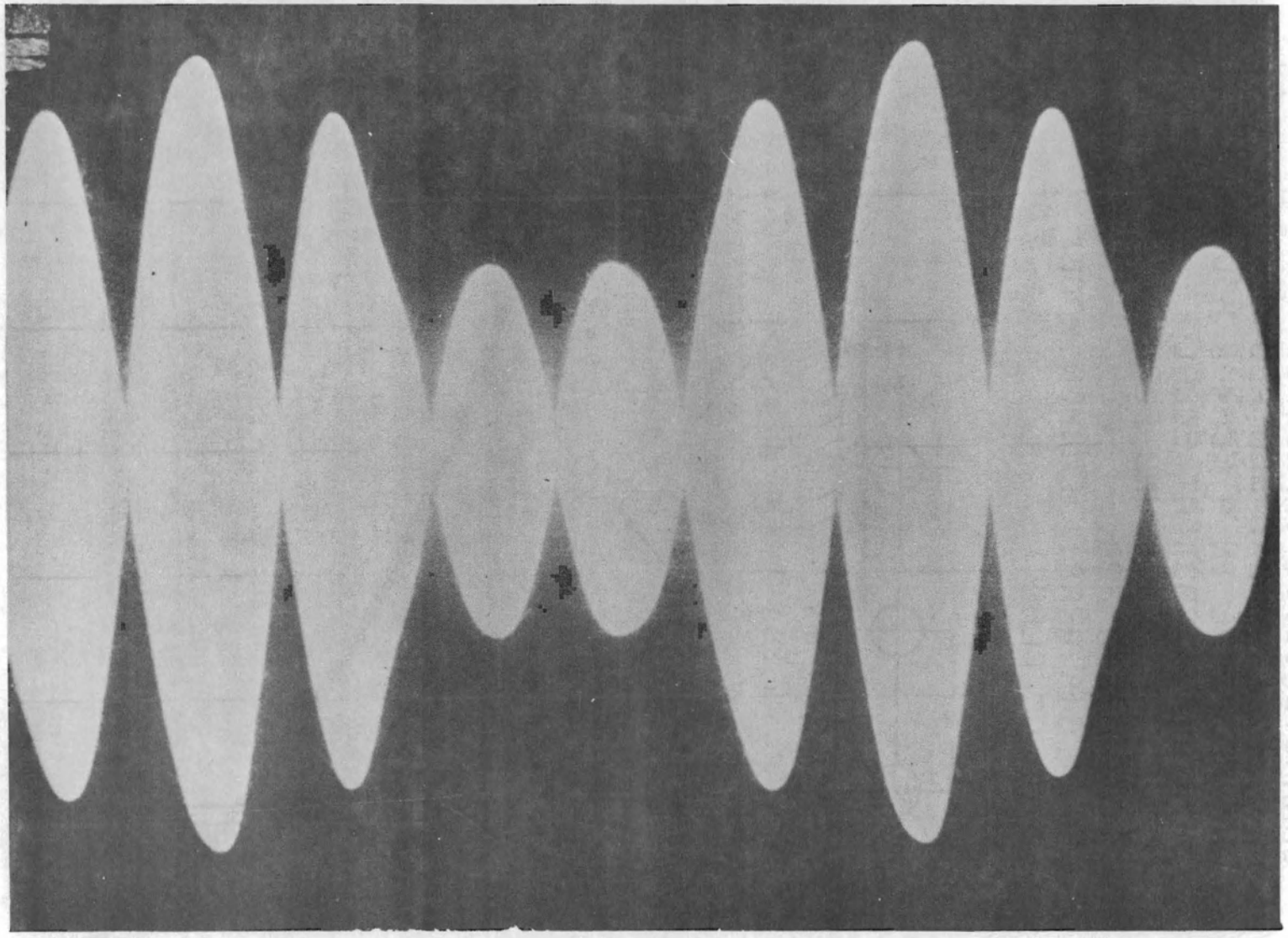

FIG. 47. OSCILLOSCOPE PHOTO-MODULATED RF OUTPUT OF DRUM MODULATOR FOR NAFEC 5X SVOR.

Figure 48.

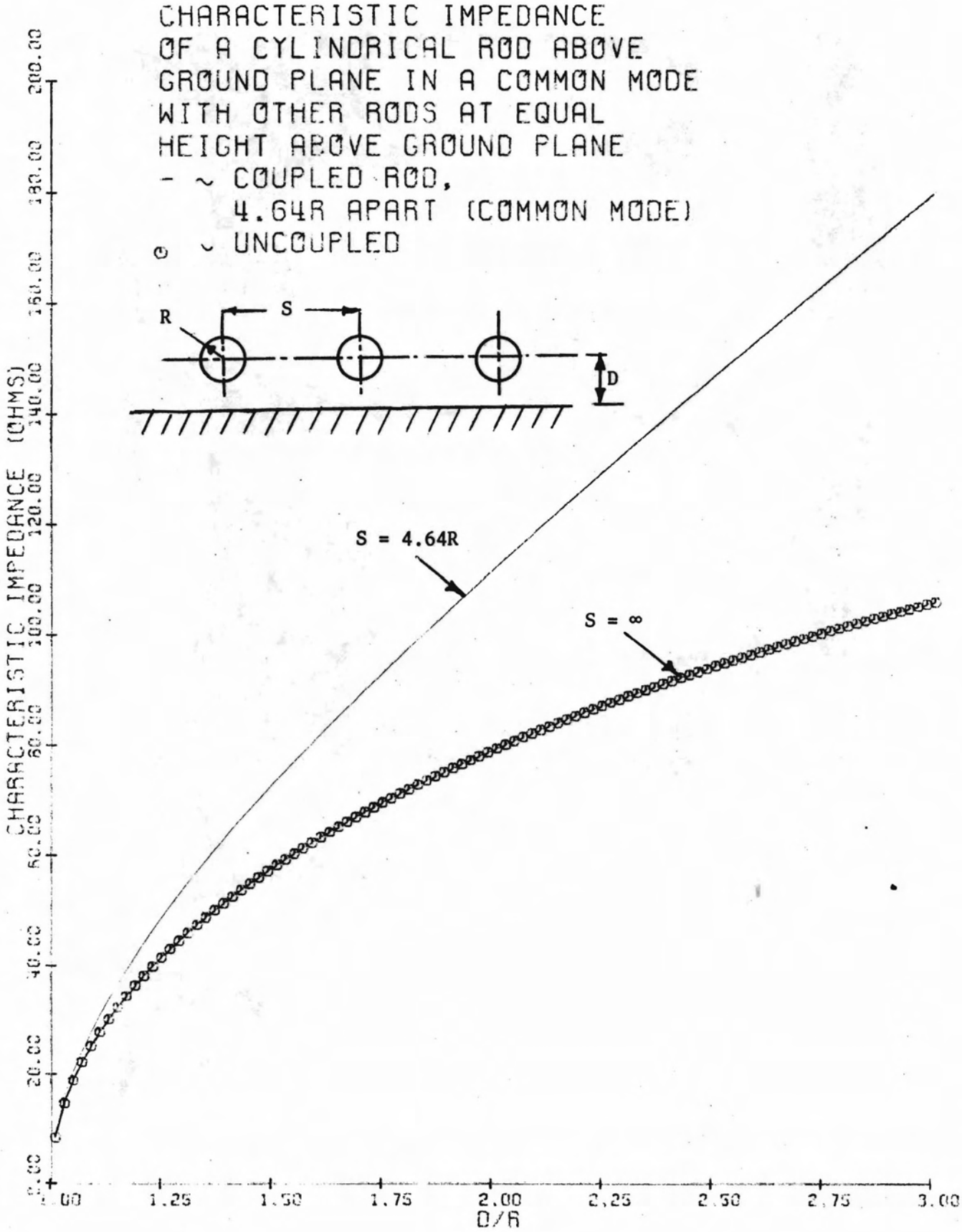
CHARACTERISTIC IMPEDANCE
OF A CYLINDRICAL ROD ABOVE
GROUND PLANE IN A COMMON MODE
WITH OTHER RODS AT EQUAL
HEIGHT ABOVE GROUND PLANE
- ~ COUPLED ROD,
4.64R APART (COMMON MODE)
o ~ UNCOUPLED
R
S
D
S = 4.64R
S = ∞
CHARACTERISTIC IMPEDANCE (OHMS)
200.00
180.00
160.00
140.00
120.00
100.00
80.00
60.00
40.00
20.00
0.00
1.00
1.25
1.50
1.75
2.00
2.25
2.50
2.75
3.00
D/R

FIG. 49. PROTOTYPE SINGLE RING 5X SVOR. (ALBANY, OHIO, 5/70).

FIG. 50. CALCULATED AZIMUTH PATTERNS OF SINGLE RING 5X SVOR FOR SEVERAL ELEVATIONS.

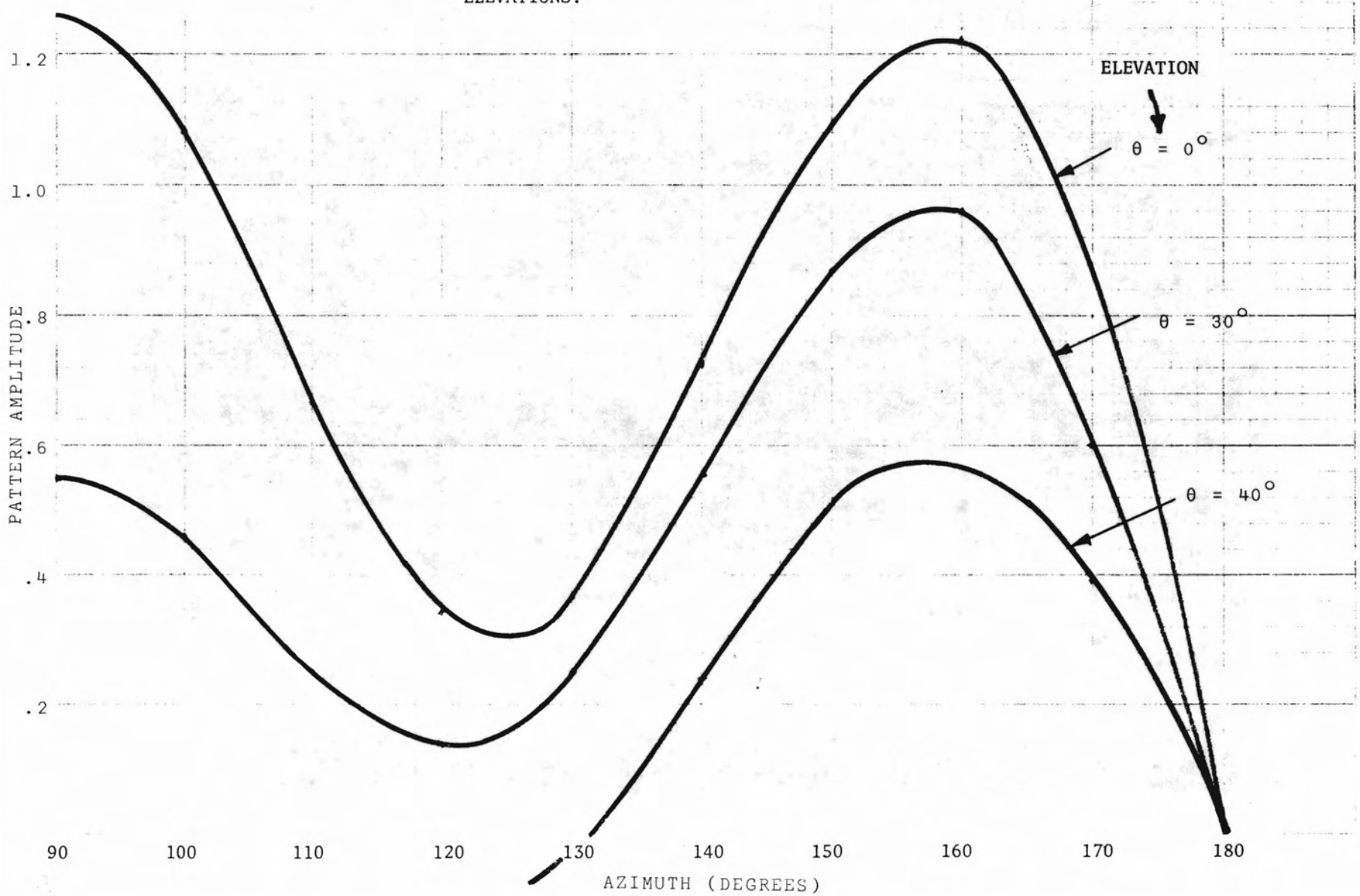

FIG. 51. MEASURED AND DESIGN CURRENTS IN LOOPS OF SINGLE RING 5X SVOR.

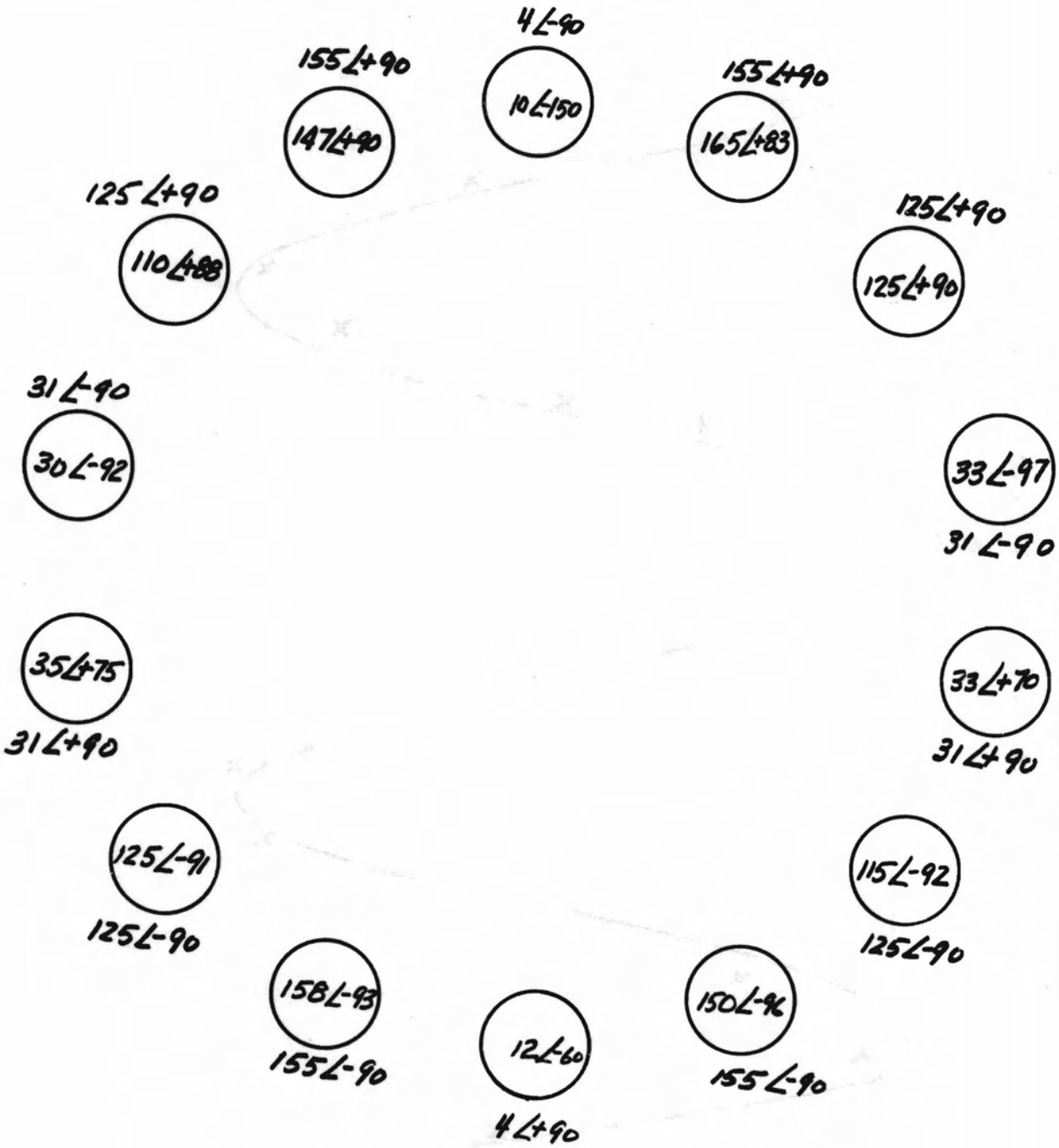

MEASURED VALUES INSIDE CIRCLES

FIG. 52. SINGLE RING 5X SVOR RADIATION PATTERN.

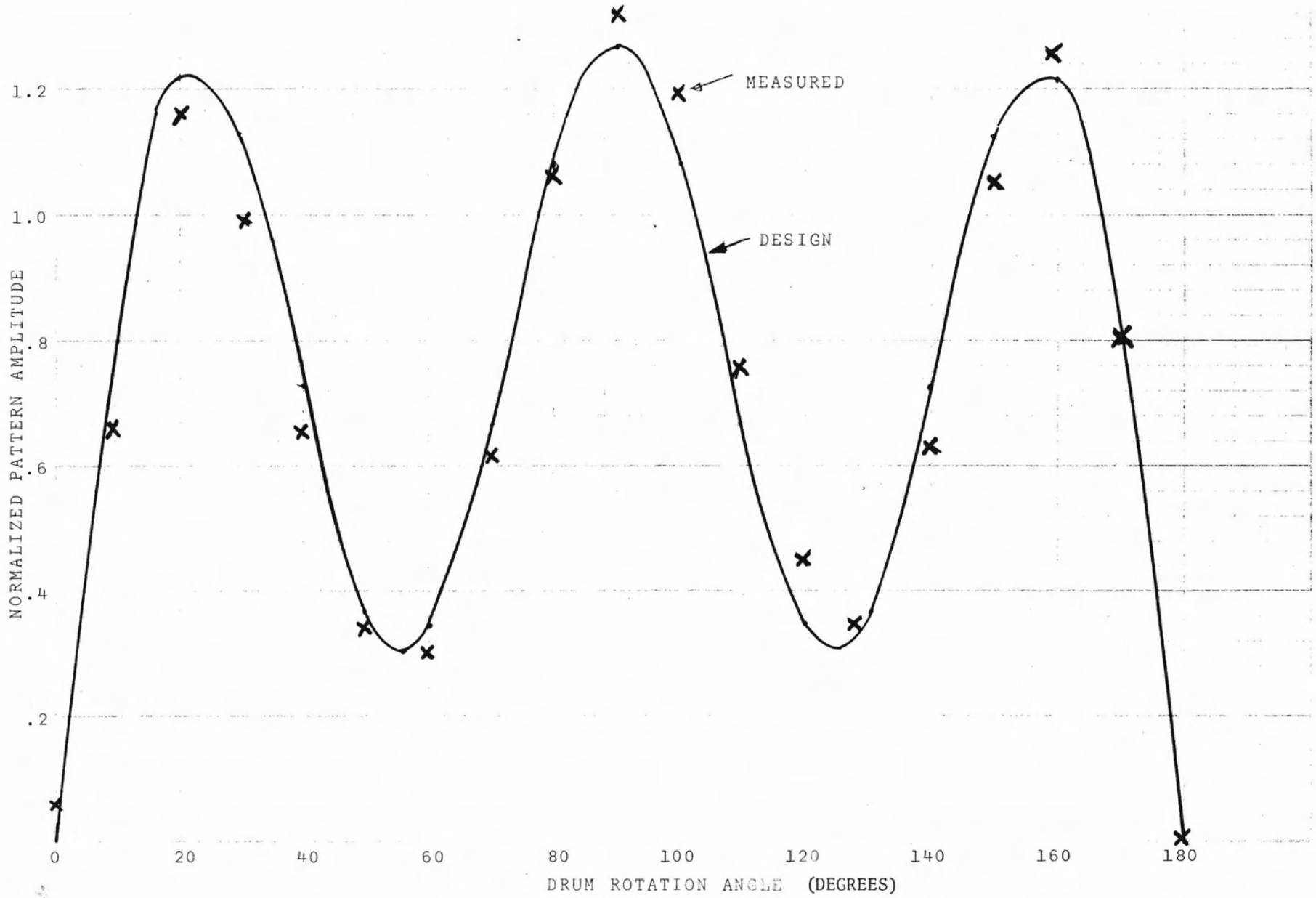

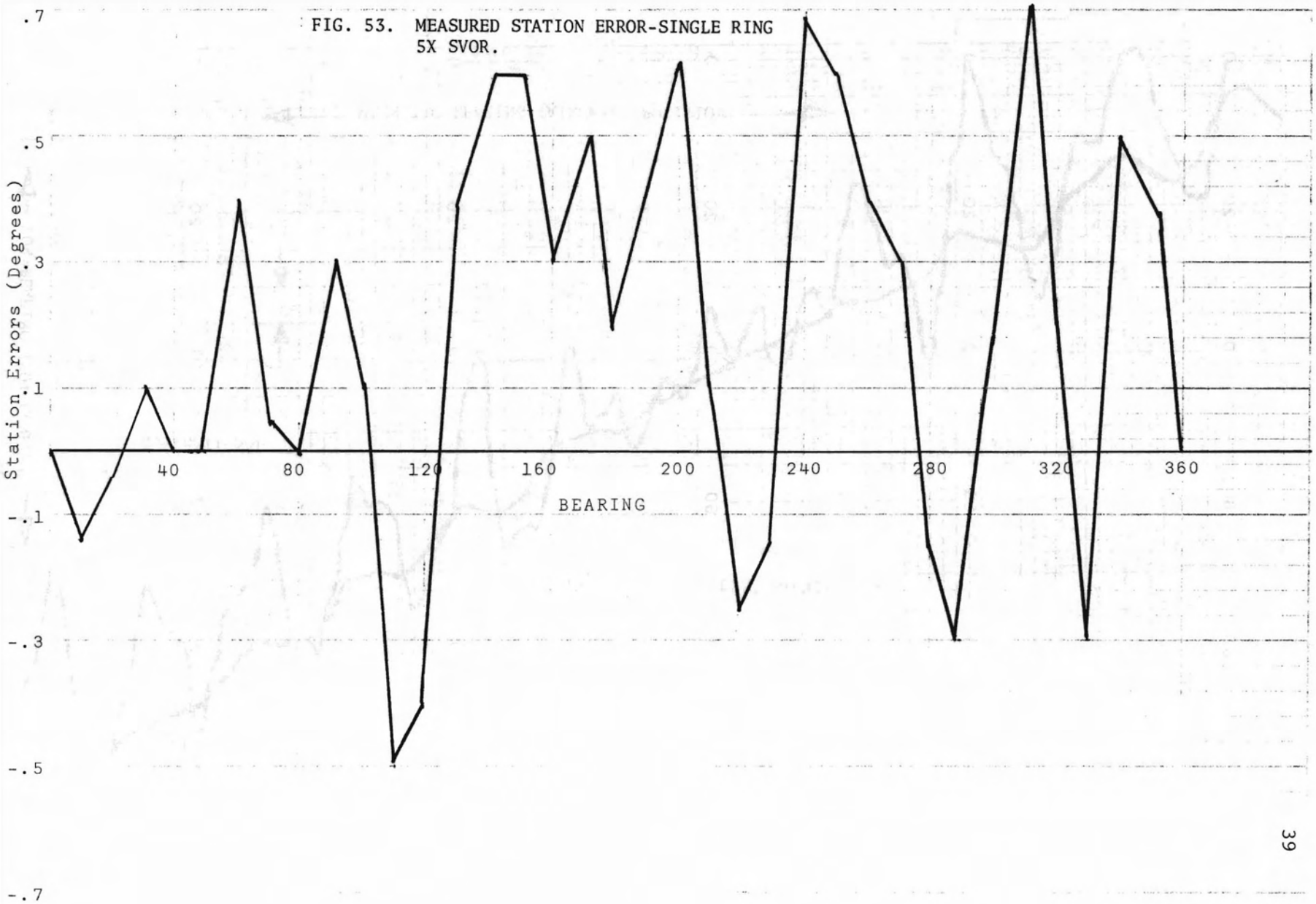

FIG. 53. MEASURED STATION ERROR-SINGLE RING 5X SVOR.

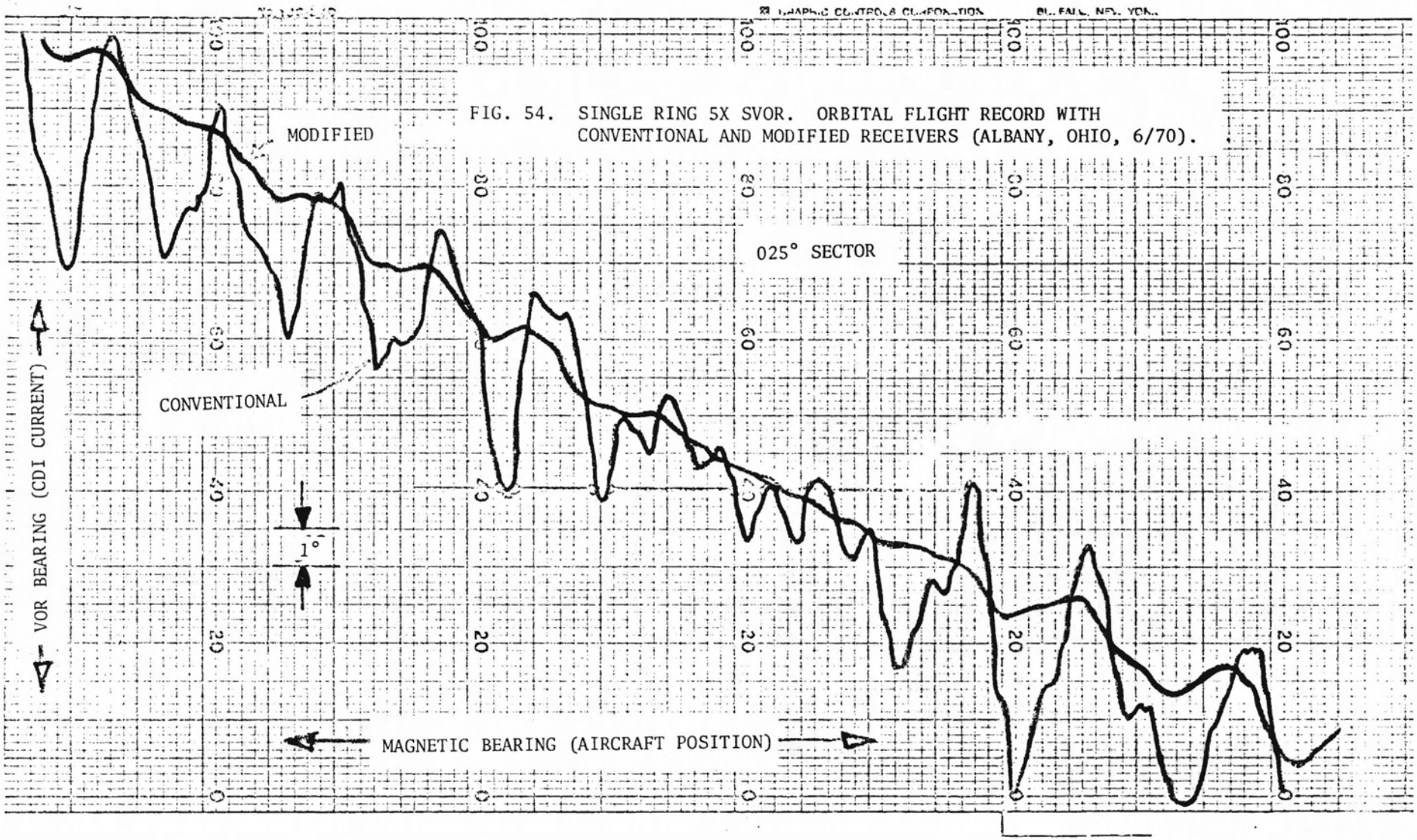

FIG. 54. SINGLE RING 5X SVOR. ORBITAL FLIGHT RECORD WITH CONVENTIONAL AND MODIFIED RECEIVERS (ALBANY, OHIO, 6/70).

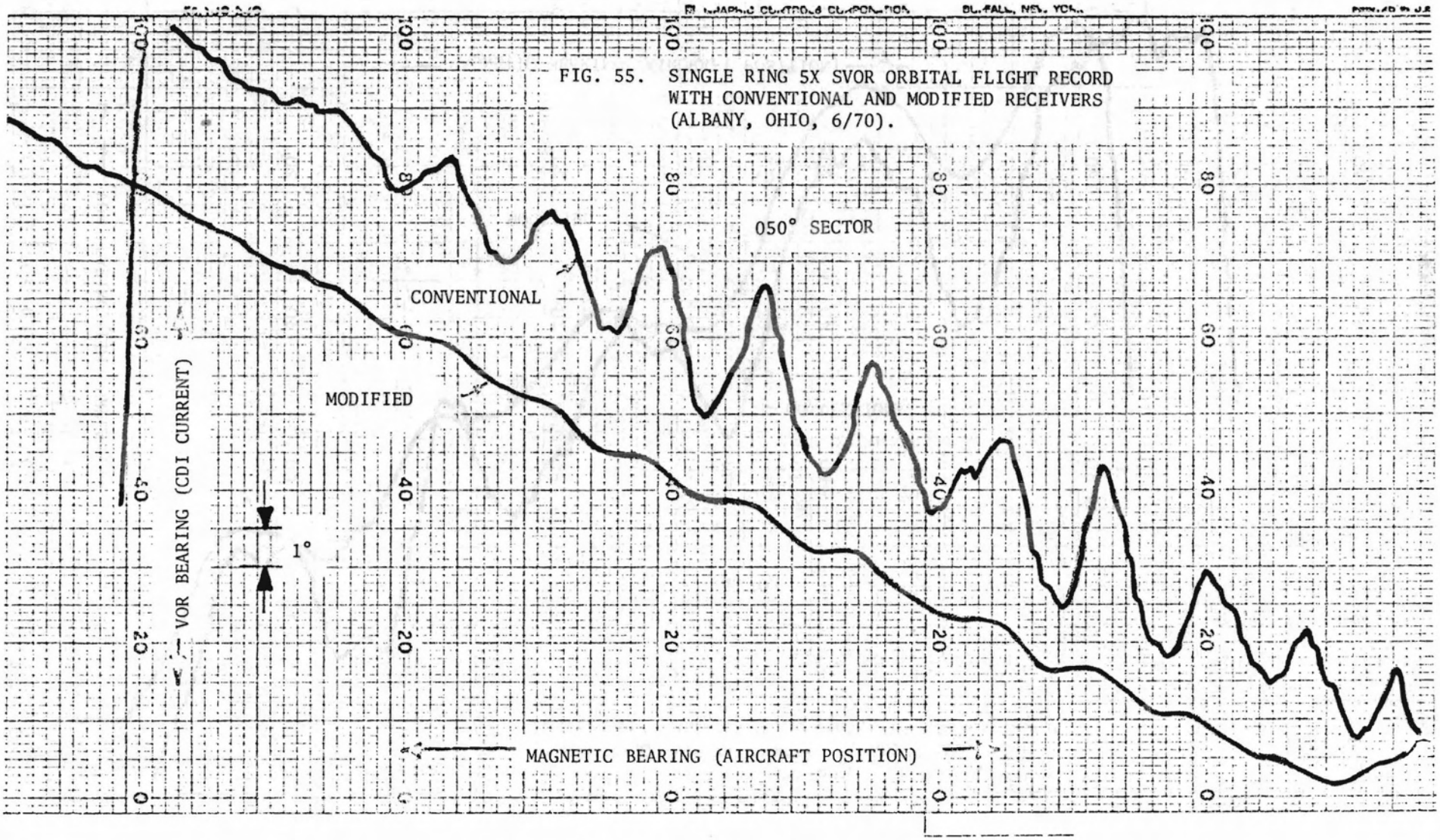

FIG. 55. SINGLE RING 5X SVOR ORBITAL FLIGHT RECORD WITH CONVENTIONAL AND MODIFIED RECEIVERS (ALBANY, OHIO, 6/70).

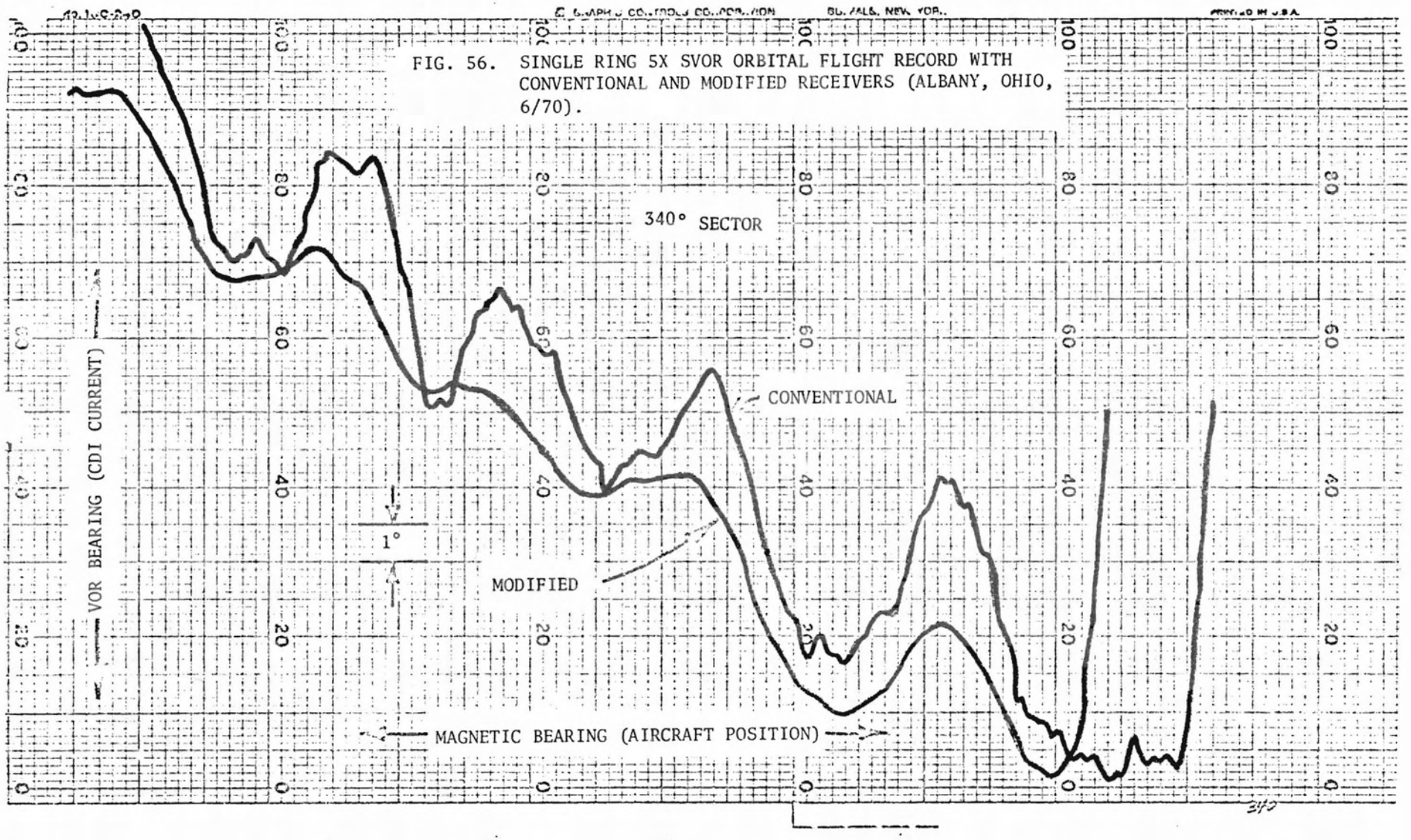

FIG. 56. SINGLE RING 5X SVOR ORBITAL FLIGHT RECORD WITH CONVENTIONAL AND MODIFIED RECEIVERS (ALBANY, OHIO, 6/70).

FIG. 57. SINGLE RING 5X SVOR. MEASURED SCALLOPING WITH CONVENTIONAL AND MODIFIED RECEIVERS (ALBANY, OHIO, 6/70).

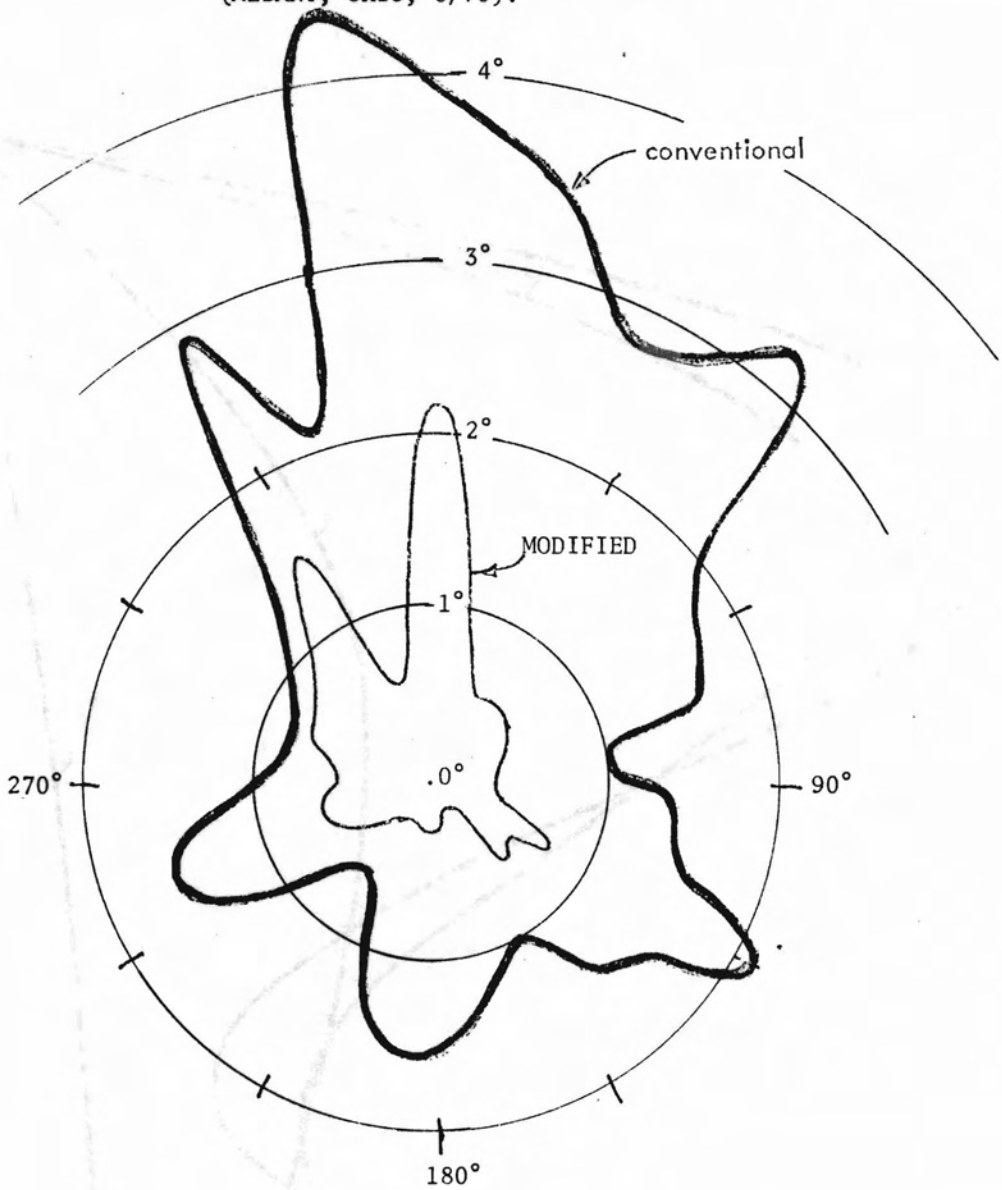

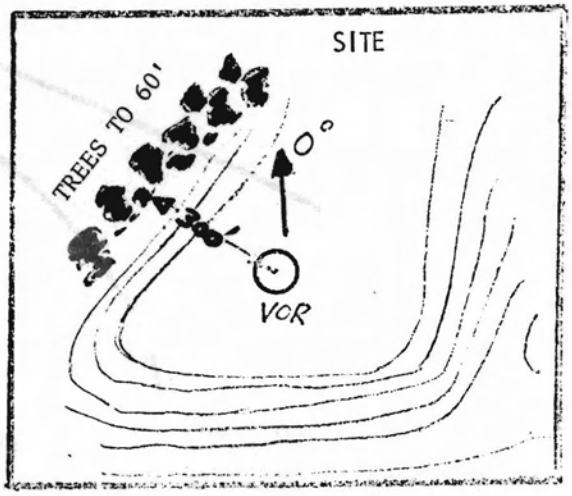

FIG. 58. 5X SVOR WITH NO CONE OF CONFUSION CALCULATED AZIMUTH PATTERNS FOR SEVERAL ELEVATIONS.

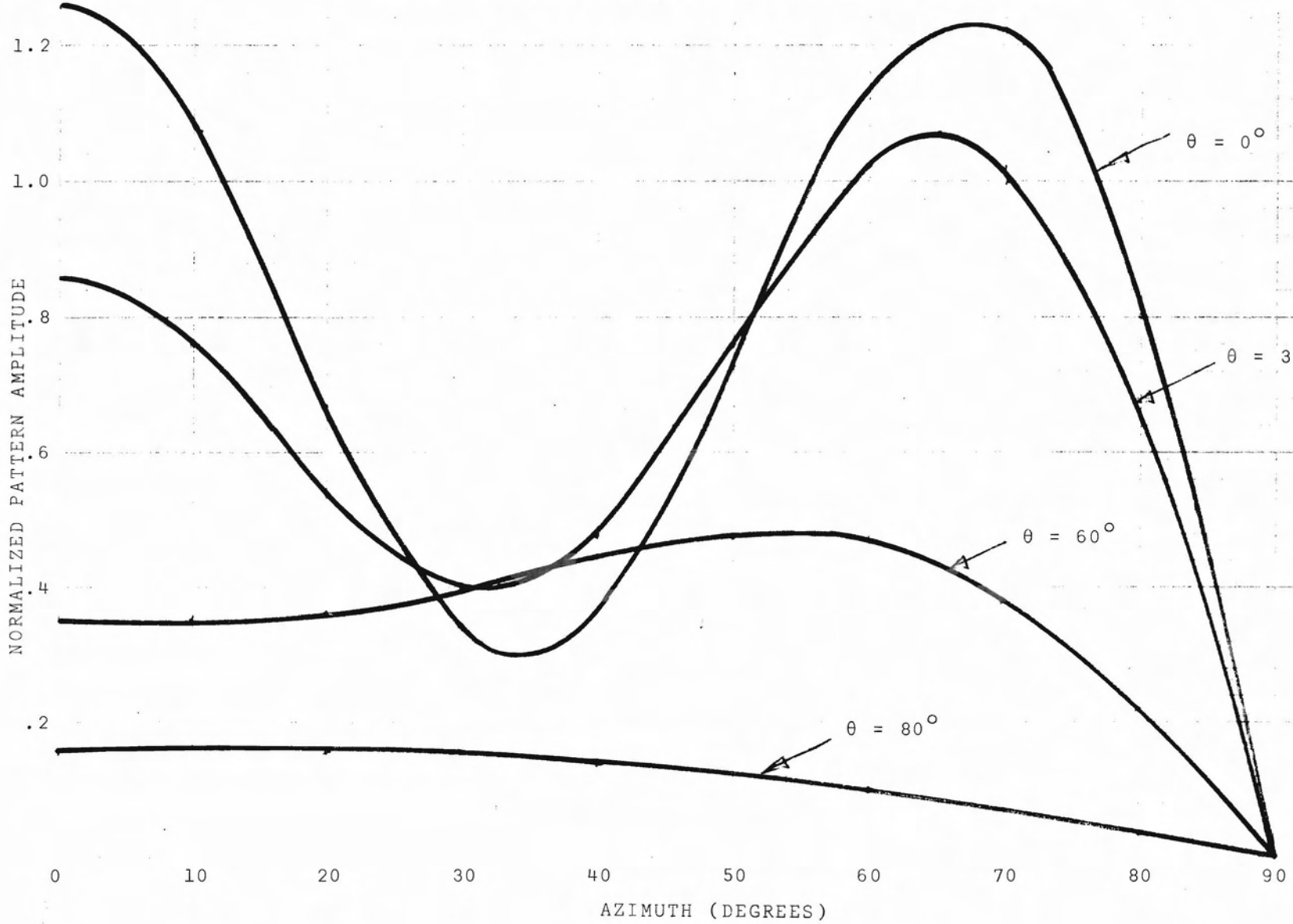

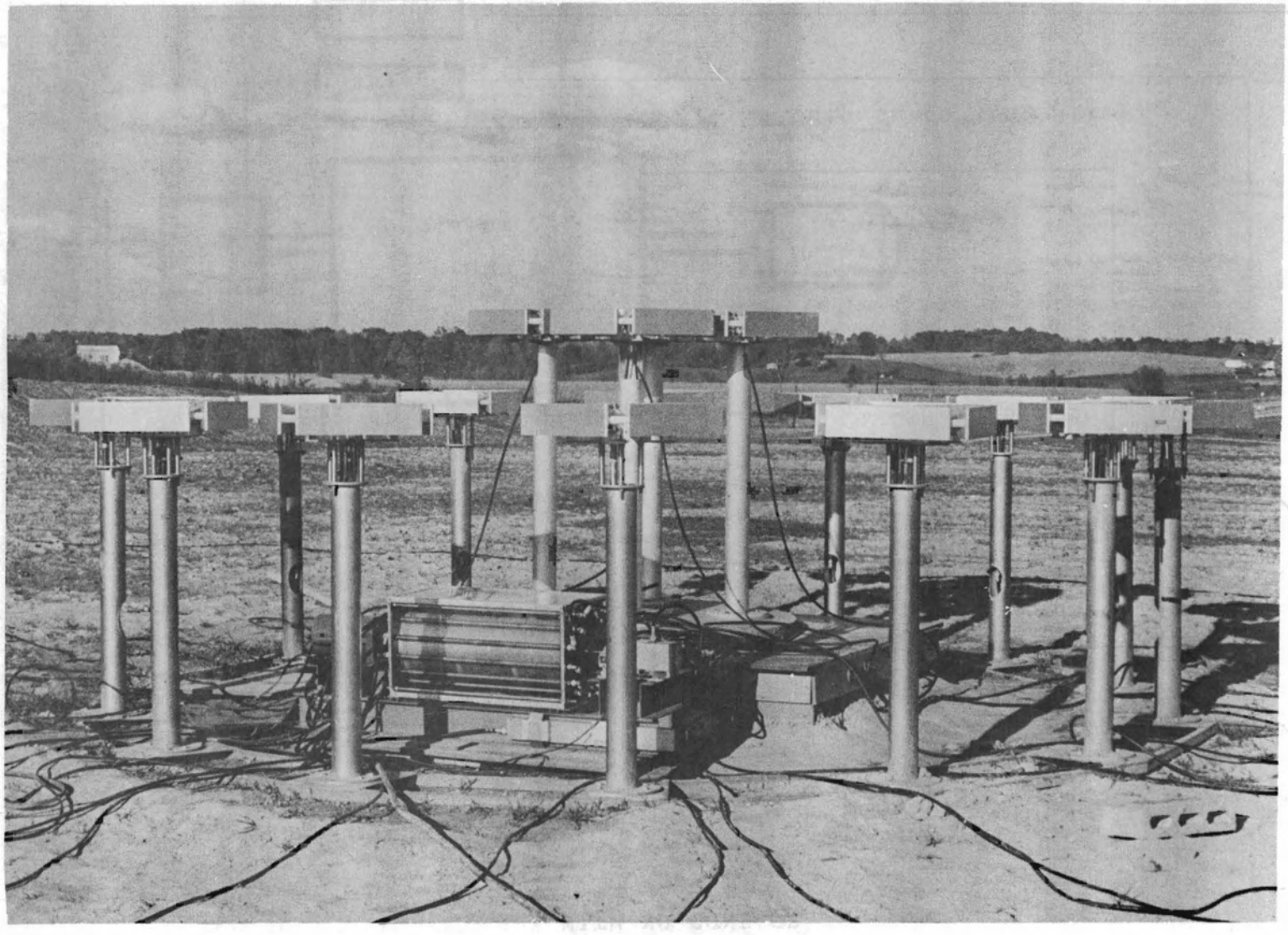

FIG. 59. 5X SVOR WITH SEPARATE 30 HZ. RADIATION (ALBANY, OHIO, 9/71).

Figure 60. OVERALL SCHEMATIC
5X SVOR
WITH NO CONE OF
CONFUSION

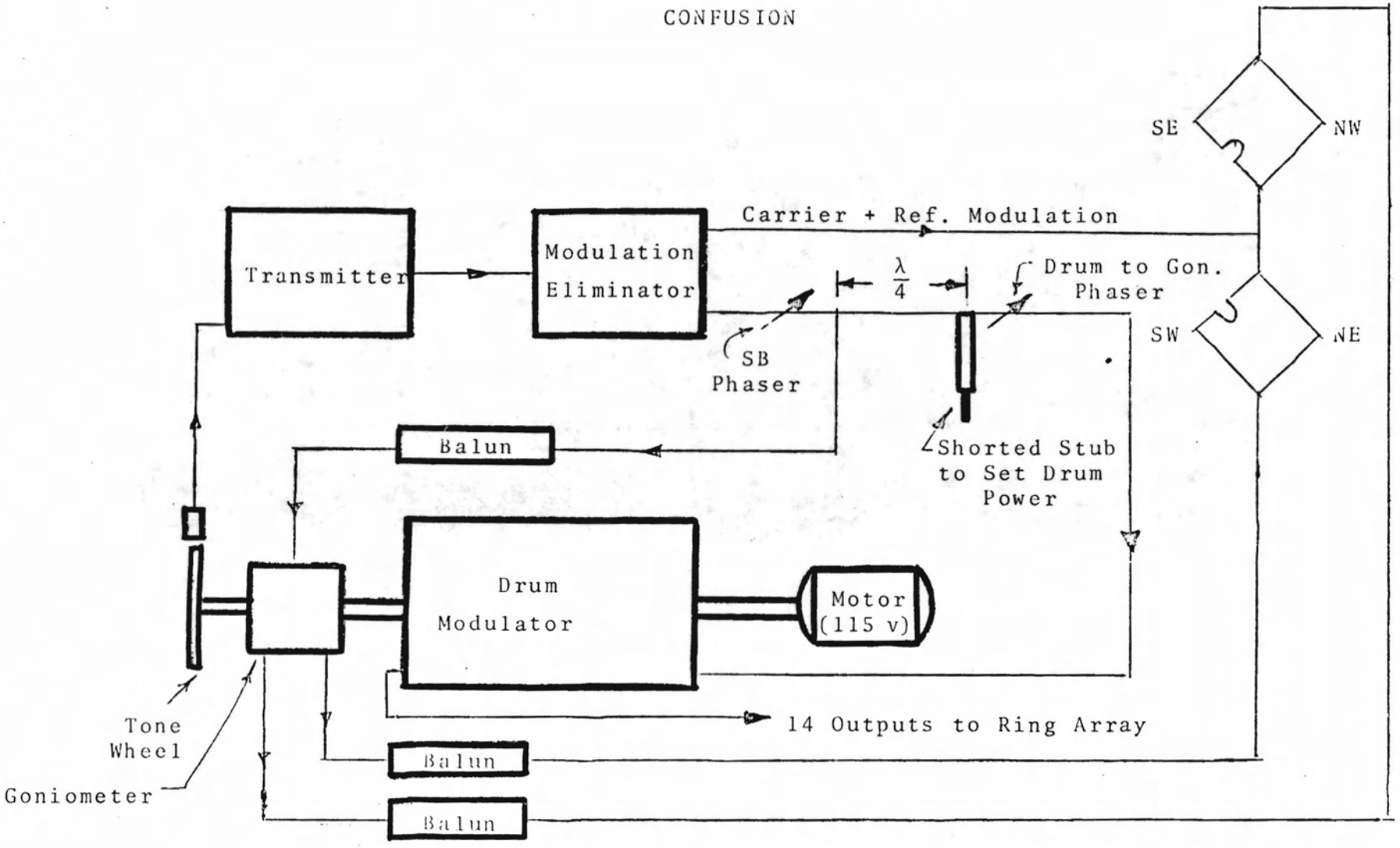

FIG. 61. RADIATION PATTERNS. 5X SVOR WITH NO CONE OF CONFUSION (COMPARE FIG. 5).

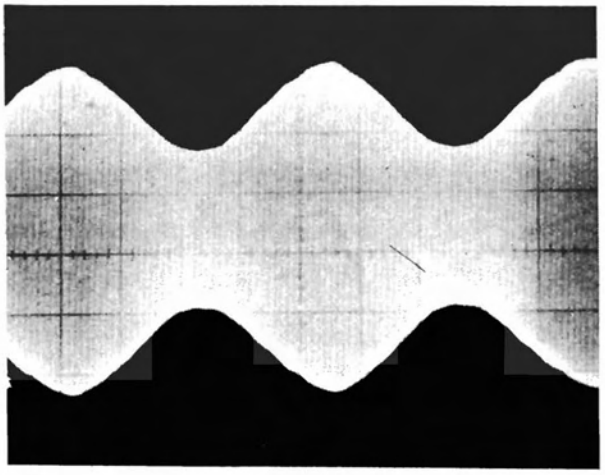

30 HZ FROM 4 LOOP ARRAY ALONE

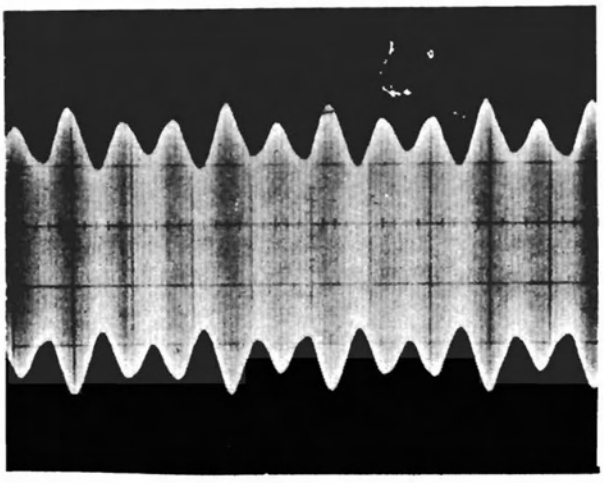

90 AND 150 HZ FROM RING ARRAY ALONE

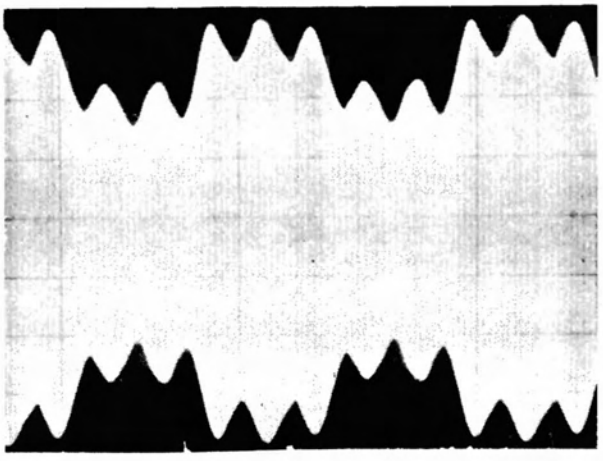

LOOP PLUS RING ARRAY SIGNALS

FIG. 62. STATION ERROR - FIVE TIMES SQUARE WAVE VOR WITH NO CONE OF CONFUSION (OHIO U. 9/72).

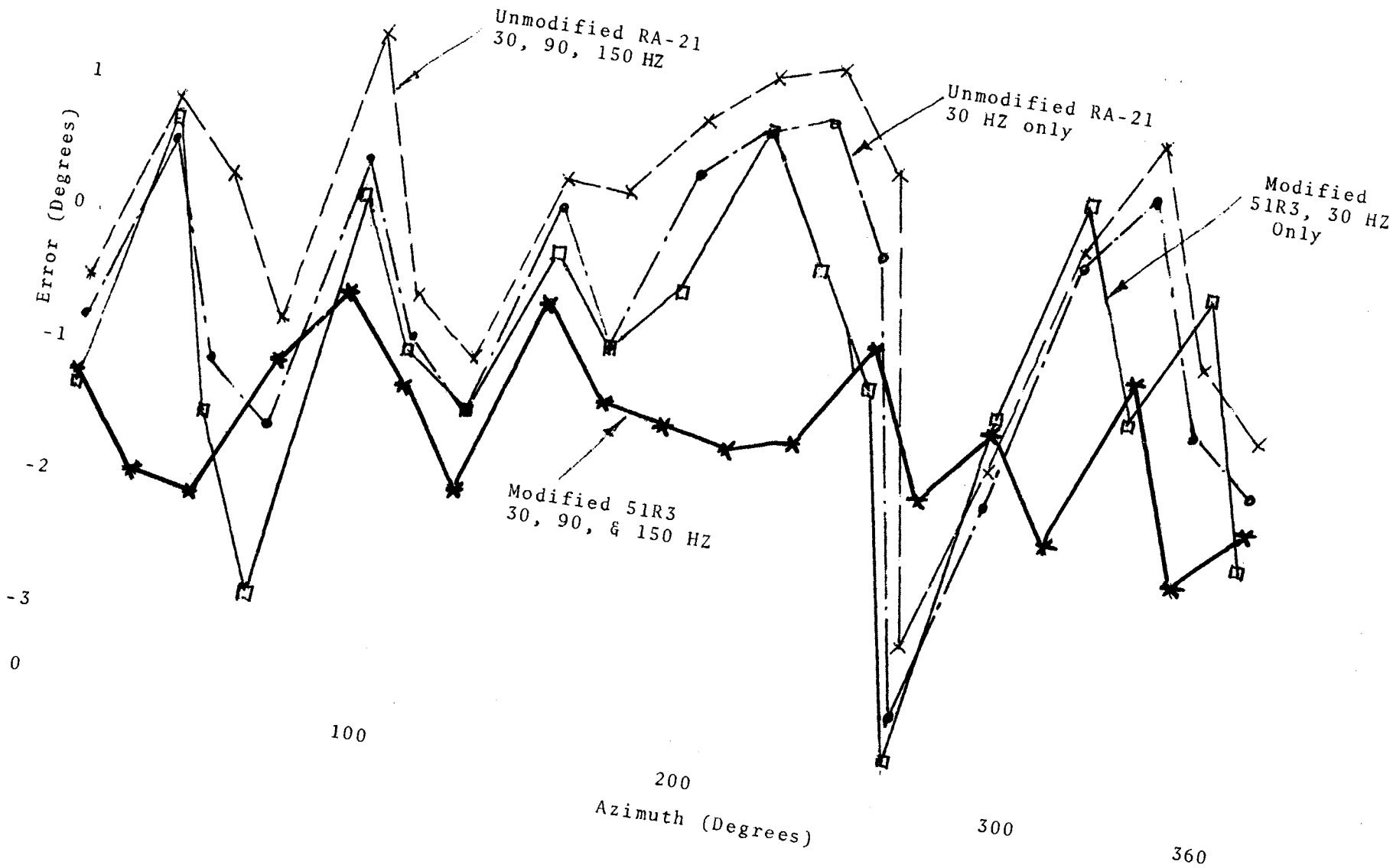

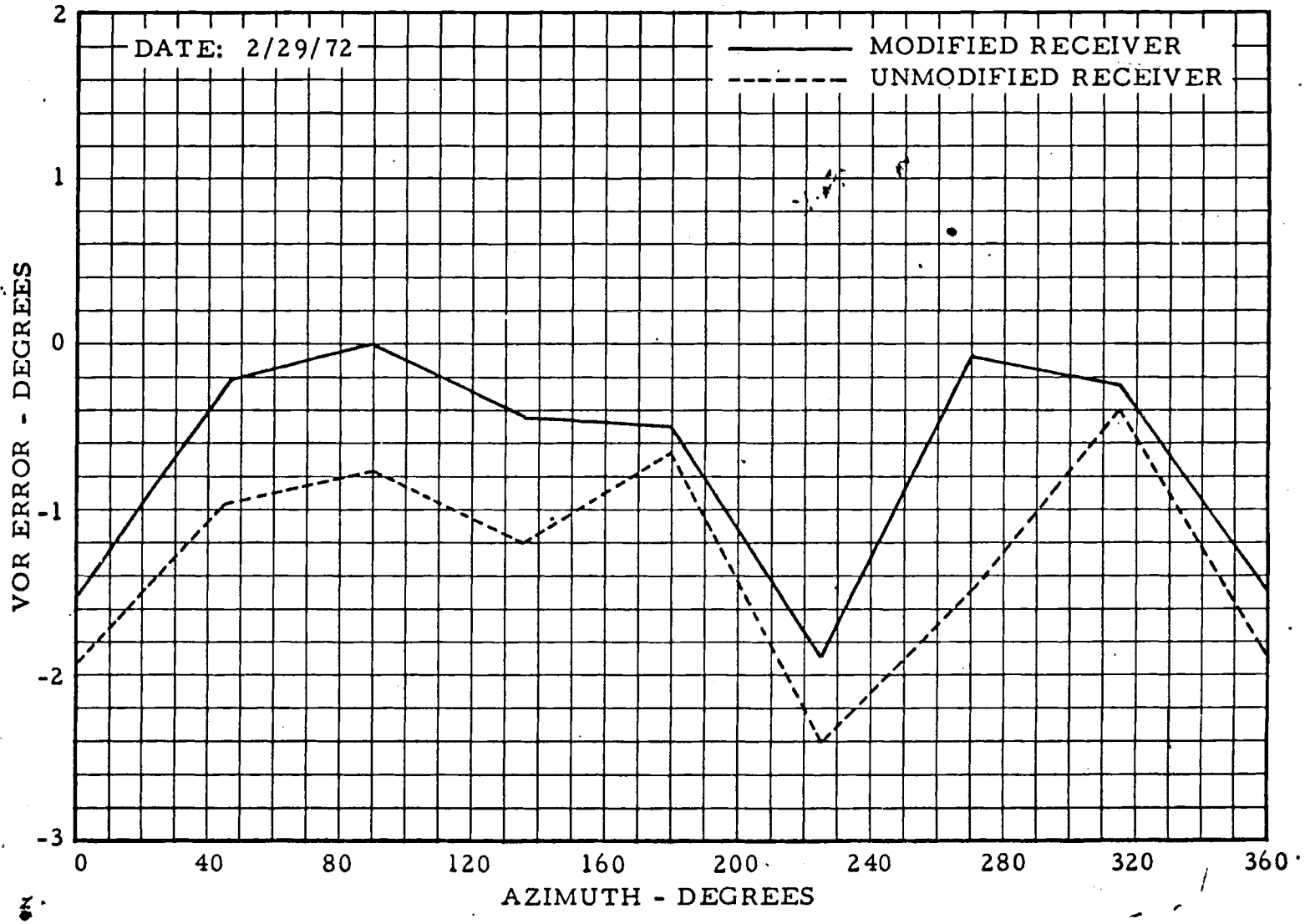

FIGURE 63. - FOUR-LOOP VOR, EIGHT POINT GROUND CHECK, 500 FOOT RADIUS
(NAFEC DATA)

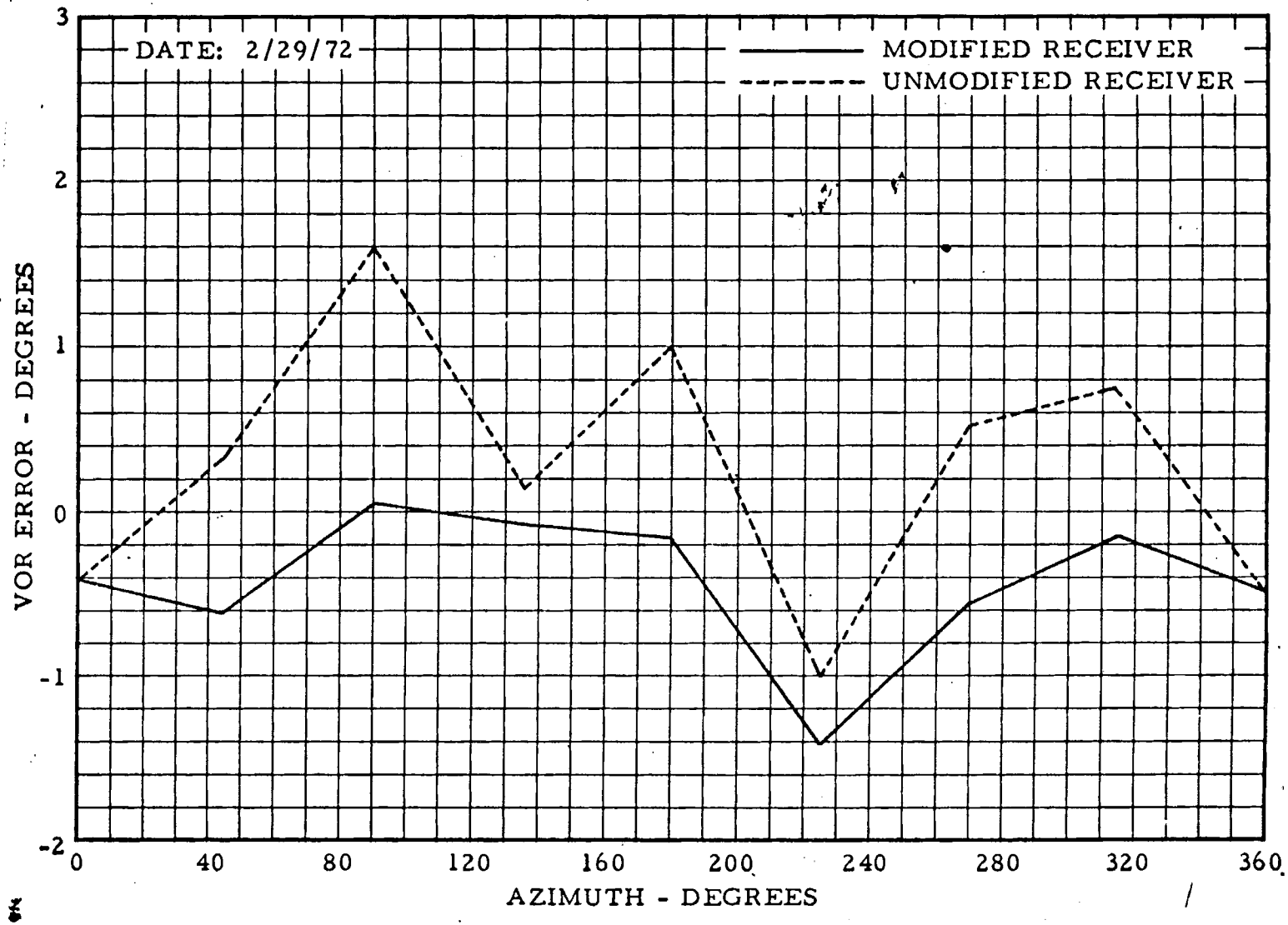

FIGURE 64.- SVOR, EIGHT POINT GROUND CHECK, 500 FOOT RADIUS
(NAFEC DATA)

Figure 65. Eight Mile Orbit. Five Times Square Wave VOR. (OHIO U. 10/71).

---------- Conventional 51R3 Receiver

———————— 51R3 Receiver Modified for Zero Crossing Detection

Scale: 10° Chart Width

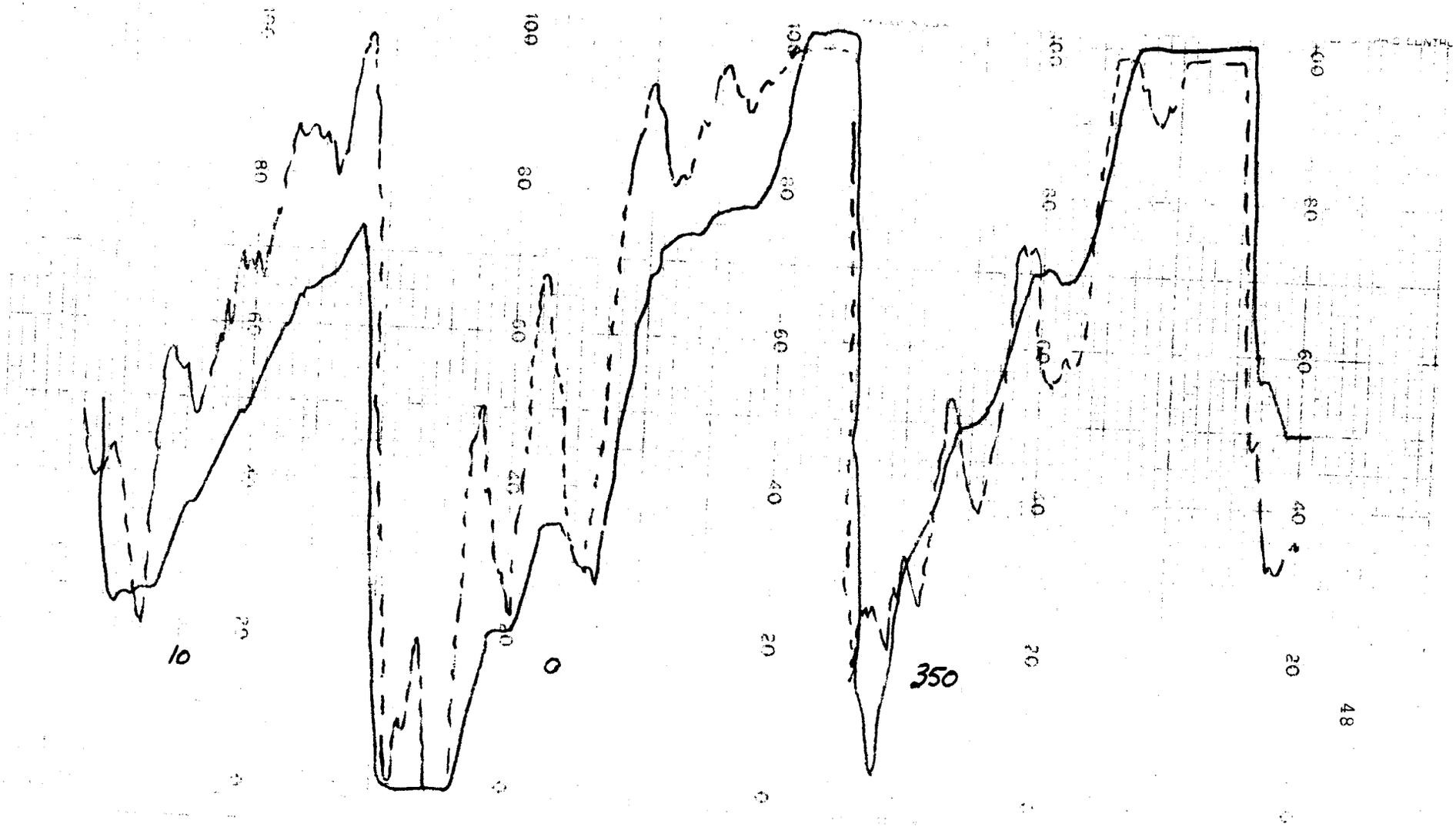

Figure 66. Eight Mile Orbit. Five Times Square Wave VOR. (OHIO U. 10/71).

---------- Conventional 51R3 Receiver

———————— 51R3 Receiver Modified for Zero Crossing Detection

Scale: 10° Chart Width

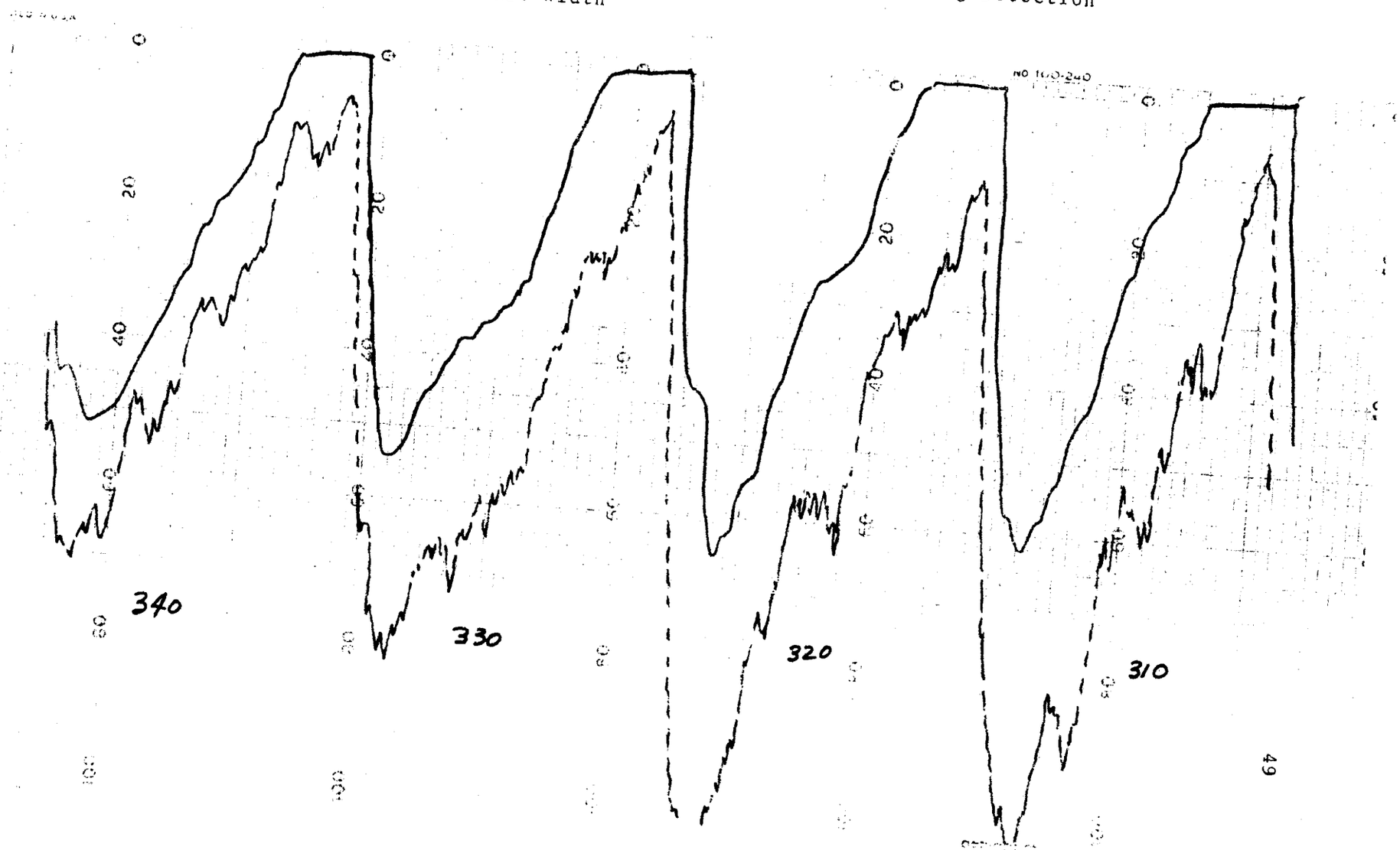

Figure 67. Eight Mile Orbit. Five Times Square Wave VOR. (OHIO U. 10/71).

---------- Conventional 51R3 Receiver

———————— 51R3 Receiver Modified for Zero Crossing Detection

Scale: 10° Chart Width

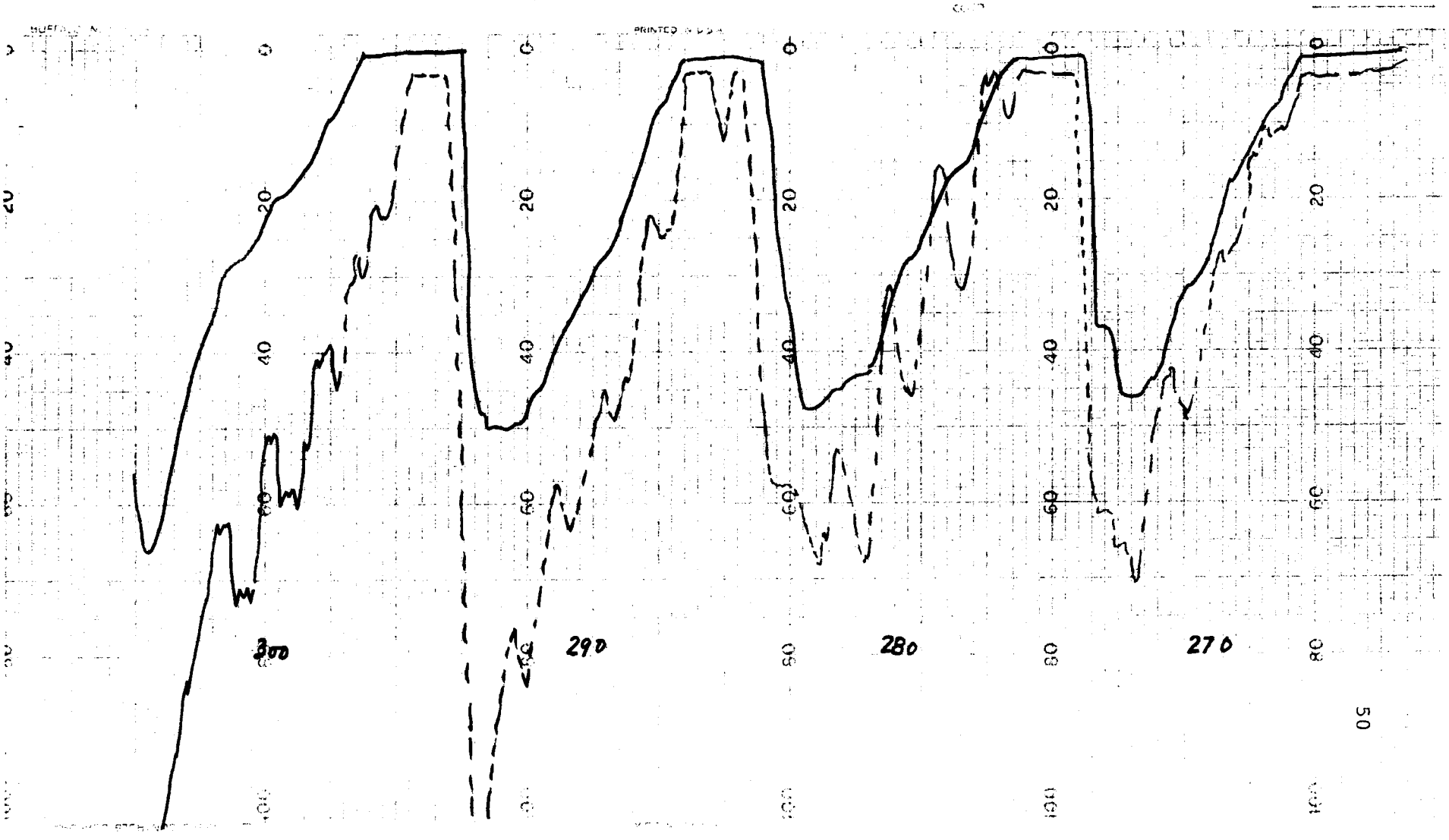

Figure 68. Eight Mile Orbit. Five Times Square Wave VOR. (OHIO U. 10/71).

---------- Conventional 51R3 Receiver

———————— 51R3 Receiver Modified for Zero Crossing Detection

Scale: 10° Chart Width

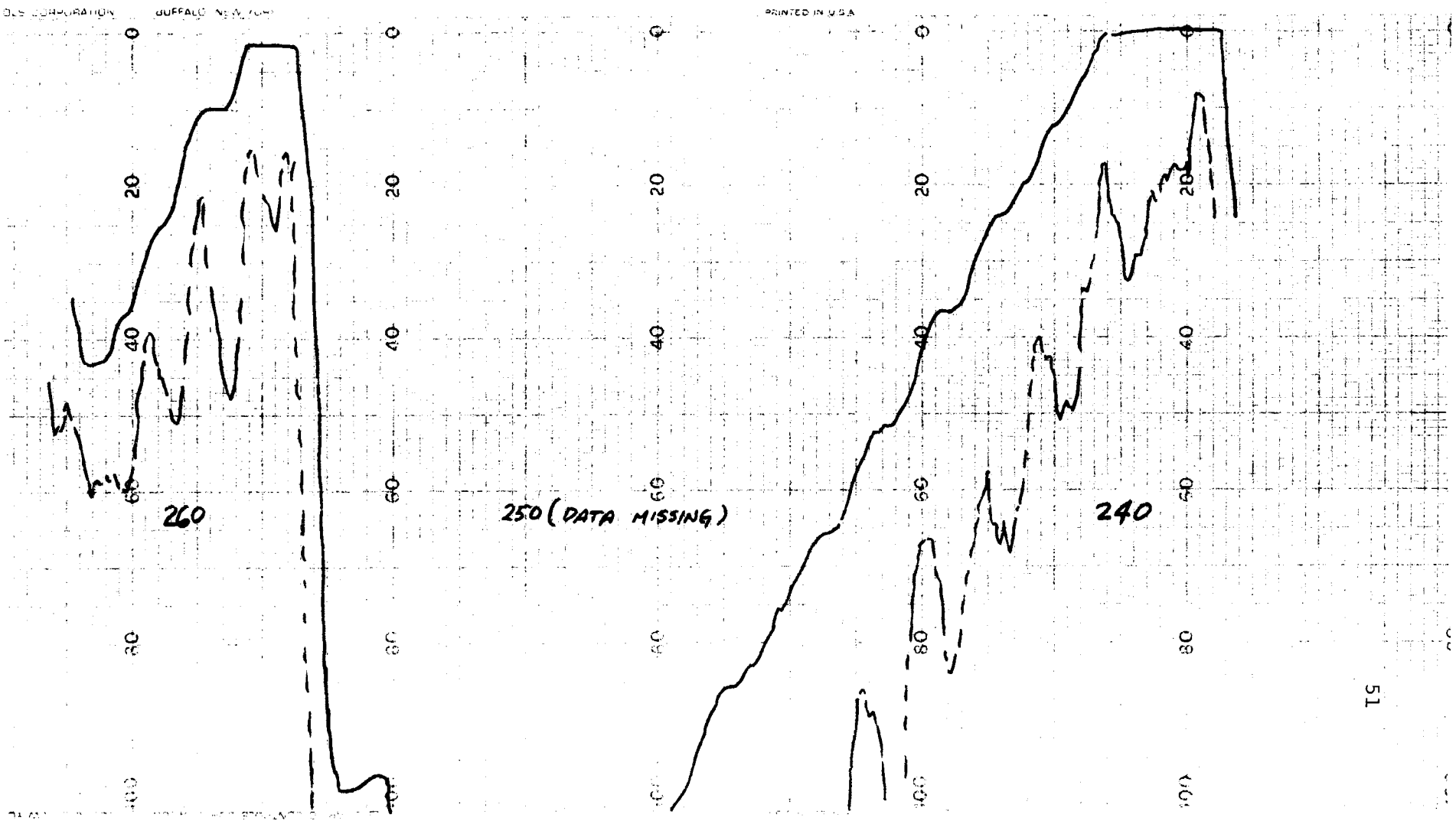

Figure 69. Eight Mile Orbit. Five Times Square Wave VOR. (OHIO U. 10/71).

---------- Conventional 51R3 Receiver

———————— 51R3 Receiver Modified for Zero Crossing Detection

Scale: 10° Chart Width

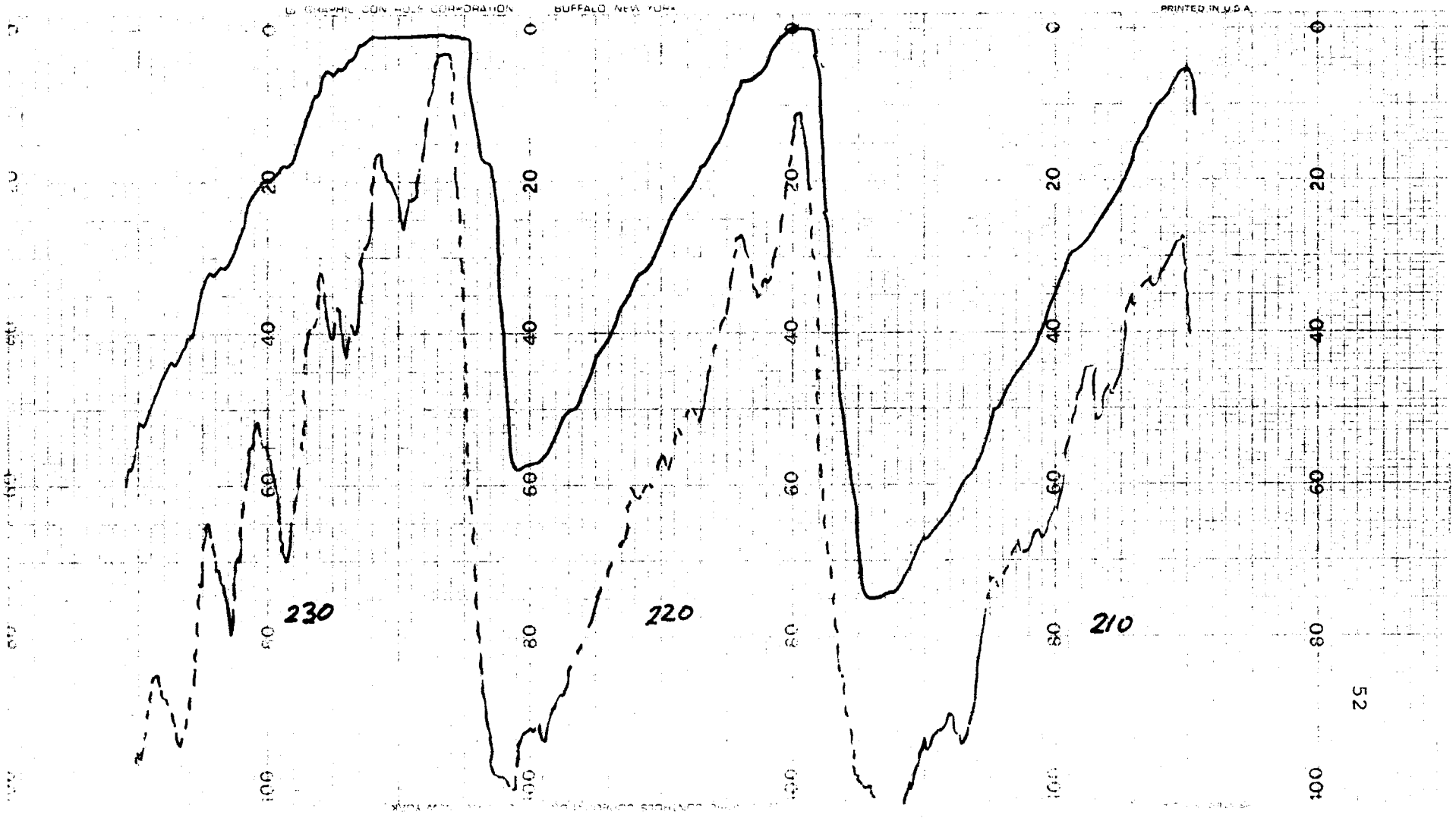

Figure 70. Eight Mile Orbit. Five Times Square Wave VOR. (OHIO U. 10/71).

---------- Conventional 51R3 Receiver

———————— 51R3 Receiver Modified for Zero Crossing Detection

Scale: 10° Chart Width

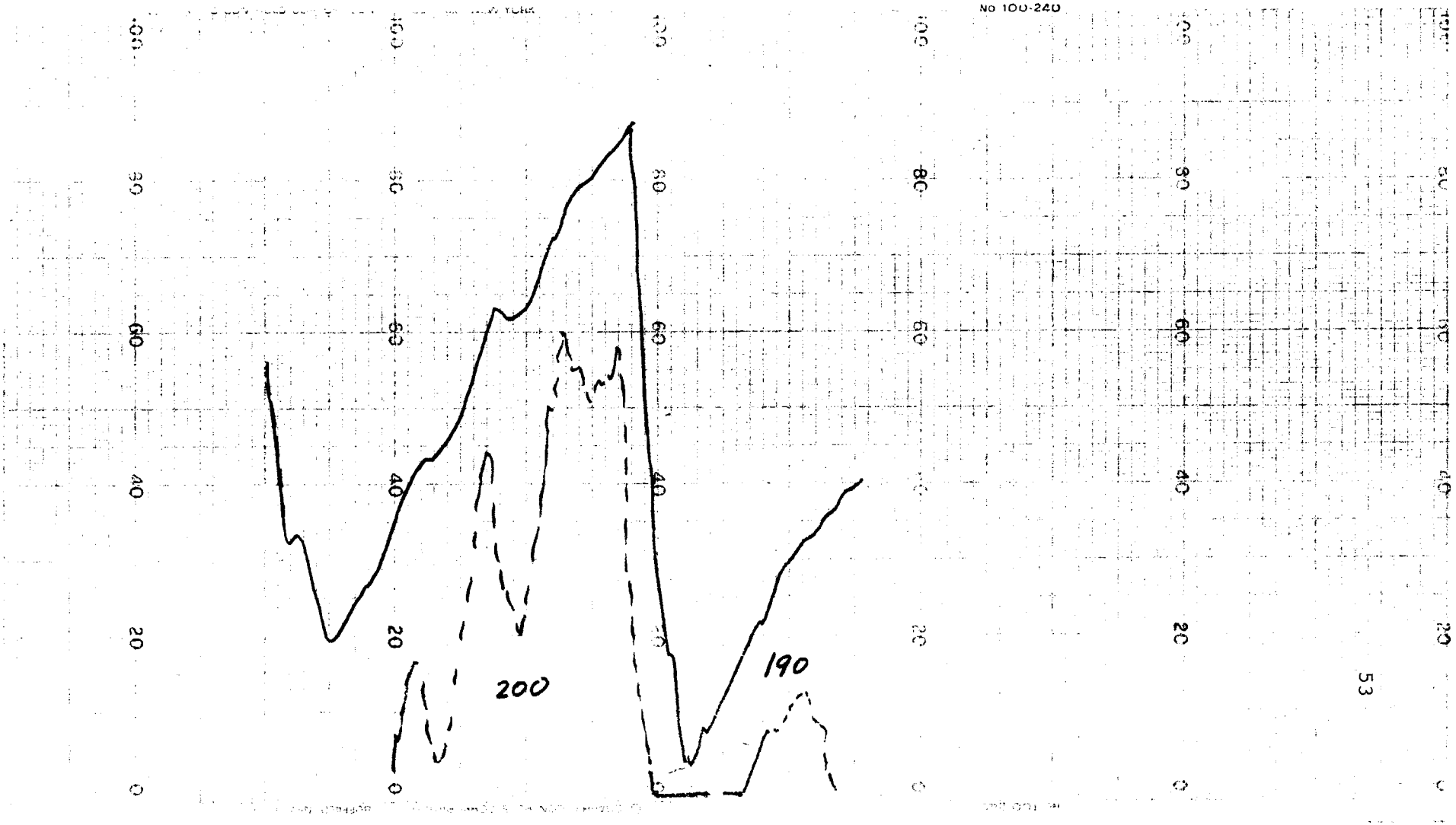

Figure 71. Eight Mile Orbit. Five Times Square Wave VOR. (OHIO U. 10/71).

---------- Conventional 51R3 Receiver

———————— 51R3 Receiver Modified for Zero Crossing Detection

Scale: 10° Chart Width

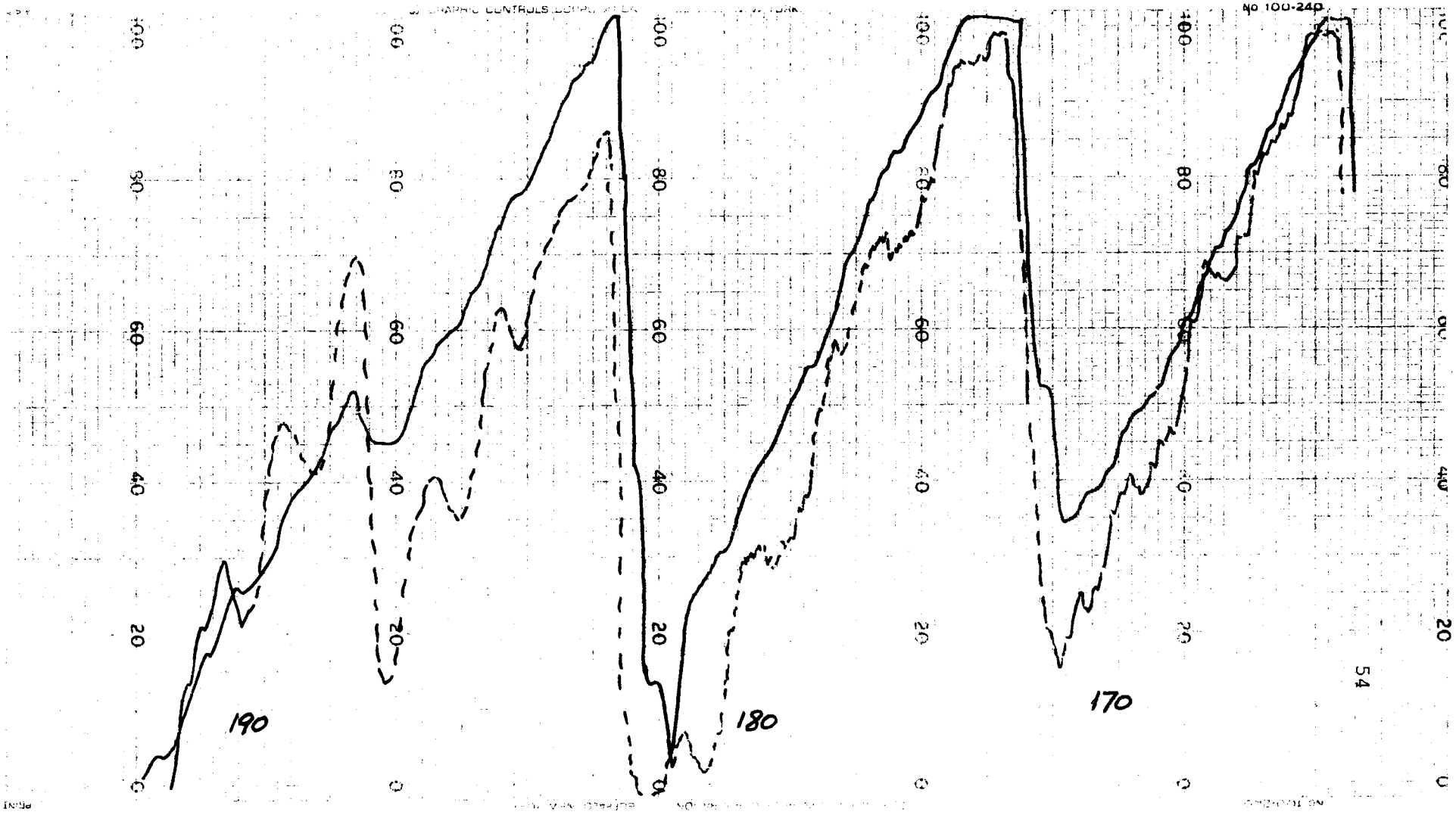

Figure 72. Eight Mile Orbit. Five Times Square Wave VOR. (OHIO U. 10/71).

---------- Conventional 51R3 Receiver

———————— 51R3 Receiver Modified for Zero Crossing Detection

Scale: 10° Chart Width

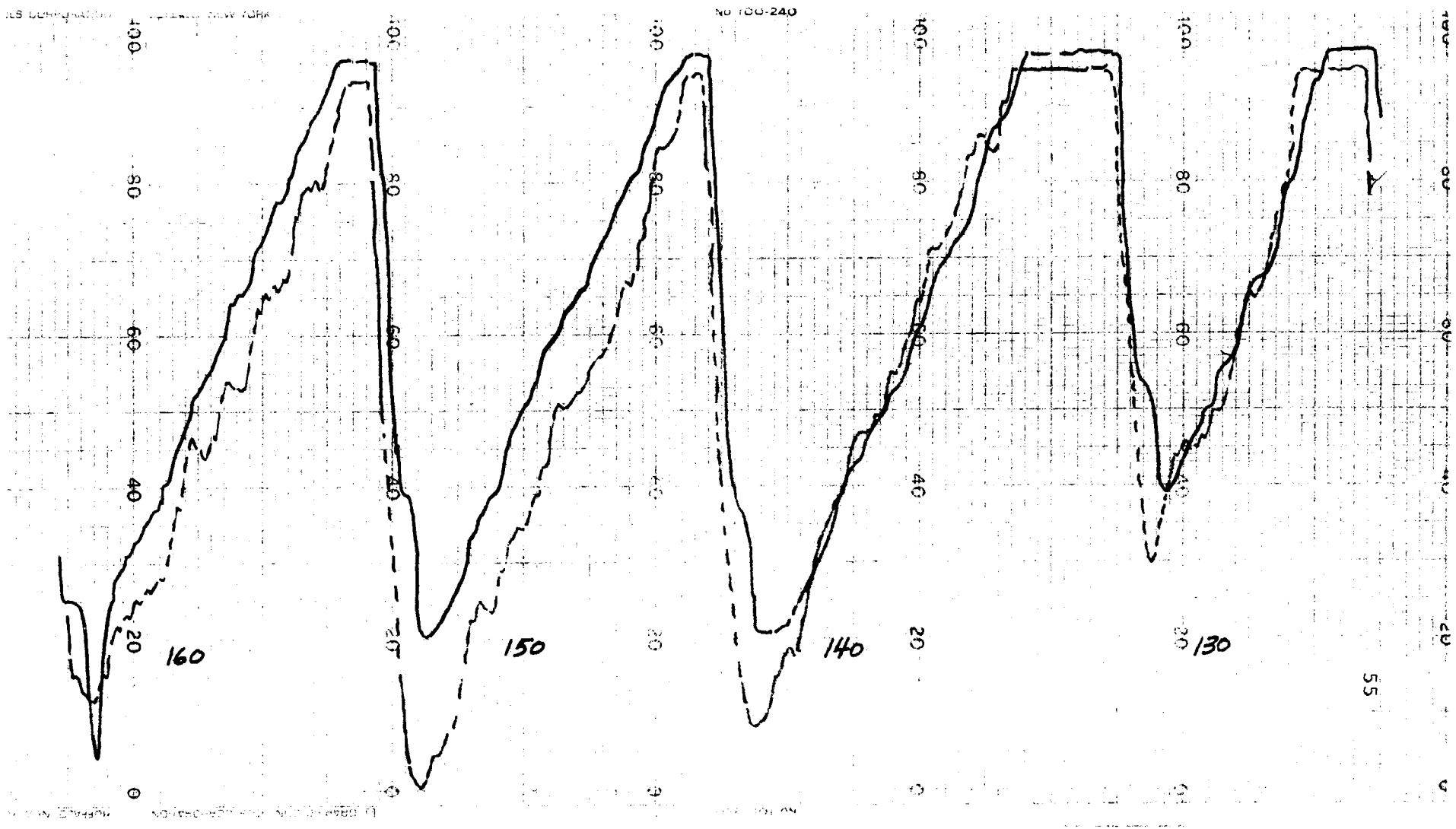

Figure 73. Eight Mile Orbit. Five Times Square Wave VOR. (OHIO U. 10/71).

---------- Conventional 51R3 Receiver

———————— 51R3 Receiver Modified for Zero Crossing Detection

Scale: 10° Chart Width

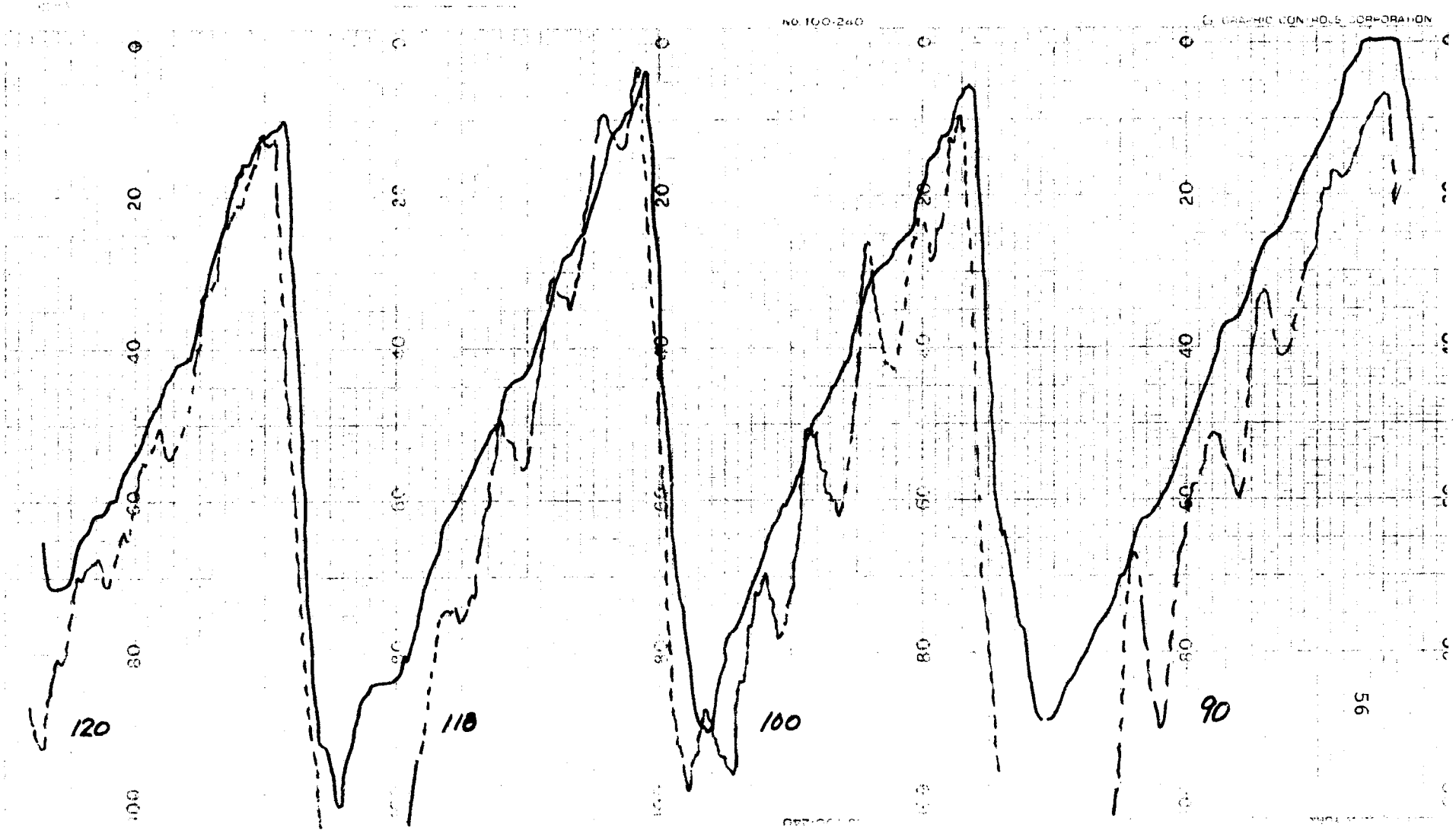

Figure 74. Eight Mile Orbit. Five Times Square Wave VOR. (OHIO U. 10/71).

---------- Conventional 51R3 Receiver

———————— 51R3 Receiver Modified for Zero Crossing Detection

Scale: 10° Chart Width

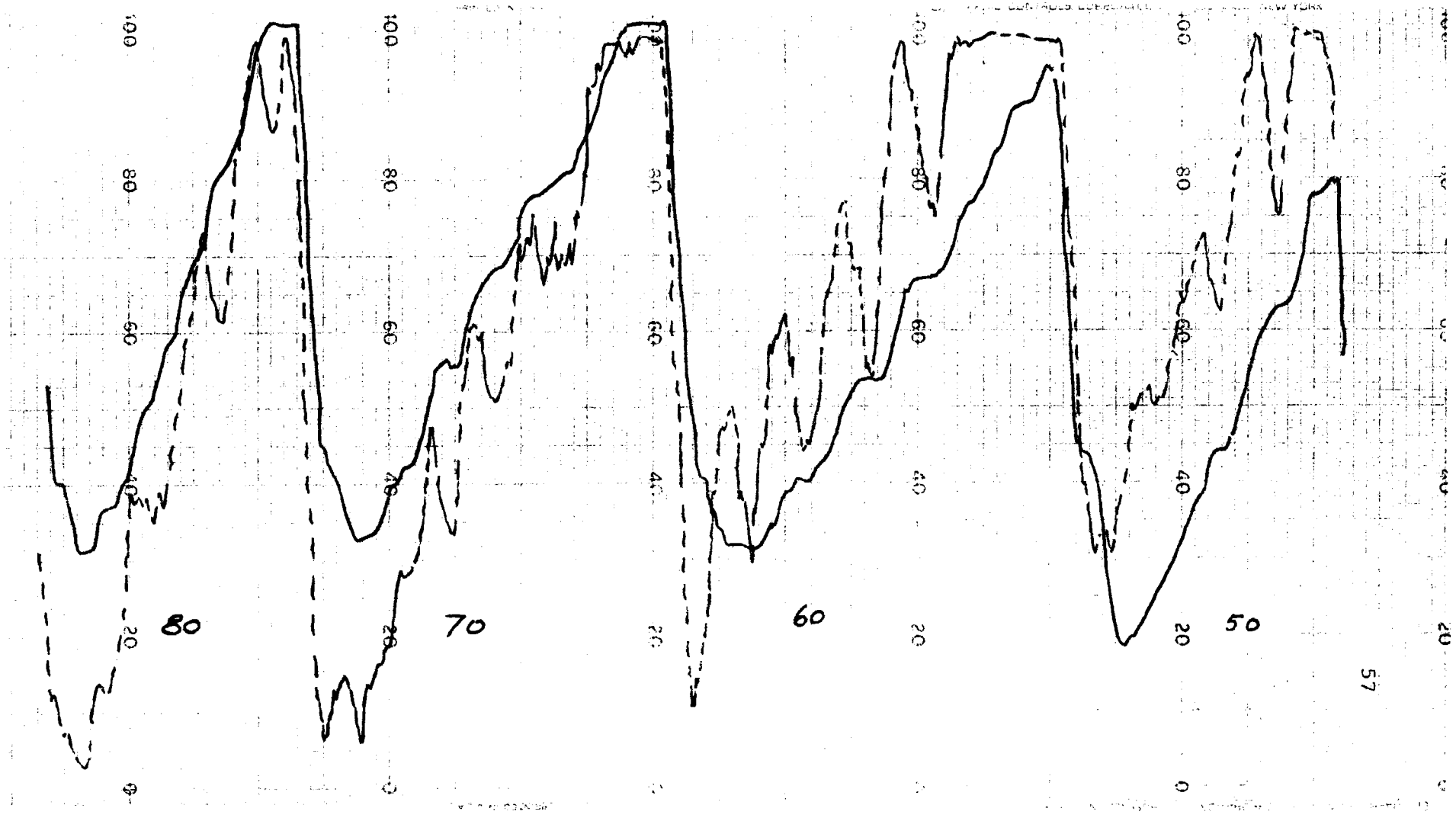

Figure 75. Eight Mile Orbit. Five Times Square Wave VOR. (OHIO U. 10/71).

---------- Conventional 51R3 Receiver

———————— 51R3 Receiver Modified for Zero Crossing Detection

Scale: 10° Chart Width

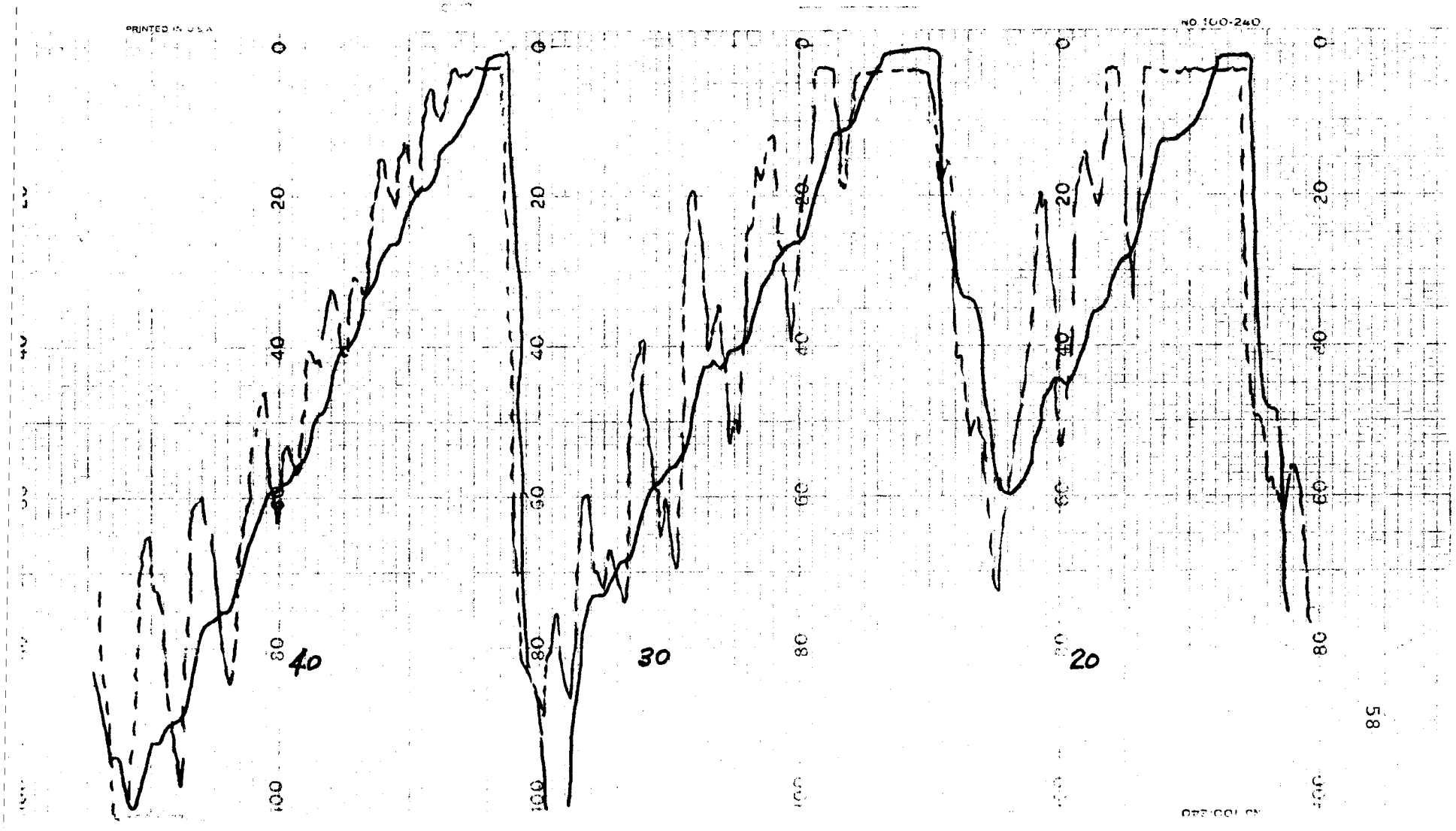

Figure 76. CDI Current-Radial Flight Outbound on 090° (Ohio University 10/72)
Altitude: 1500' above terrain
Scale: Chart Width = 10°, Chart Length, 5 S.M.
Receiver: 51R3 Modified for Zero Crossing Detection

Note: The two records shown were not made simultaneously. They were traced on to this figure to contrast flyability of four loop and Square Wave VOR's.

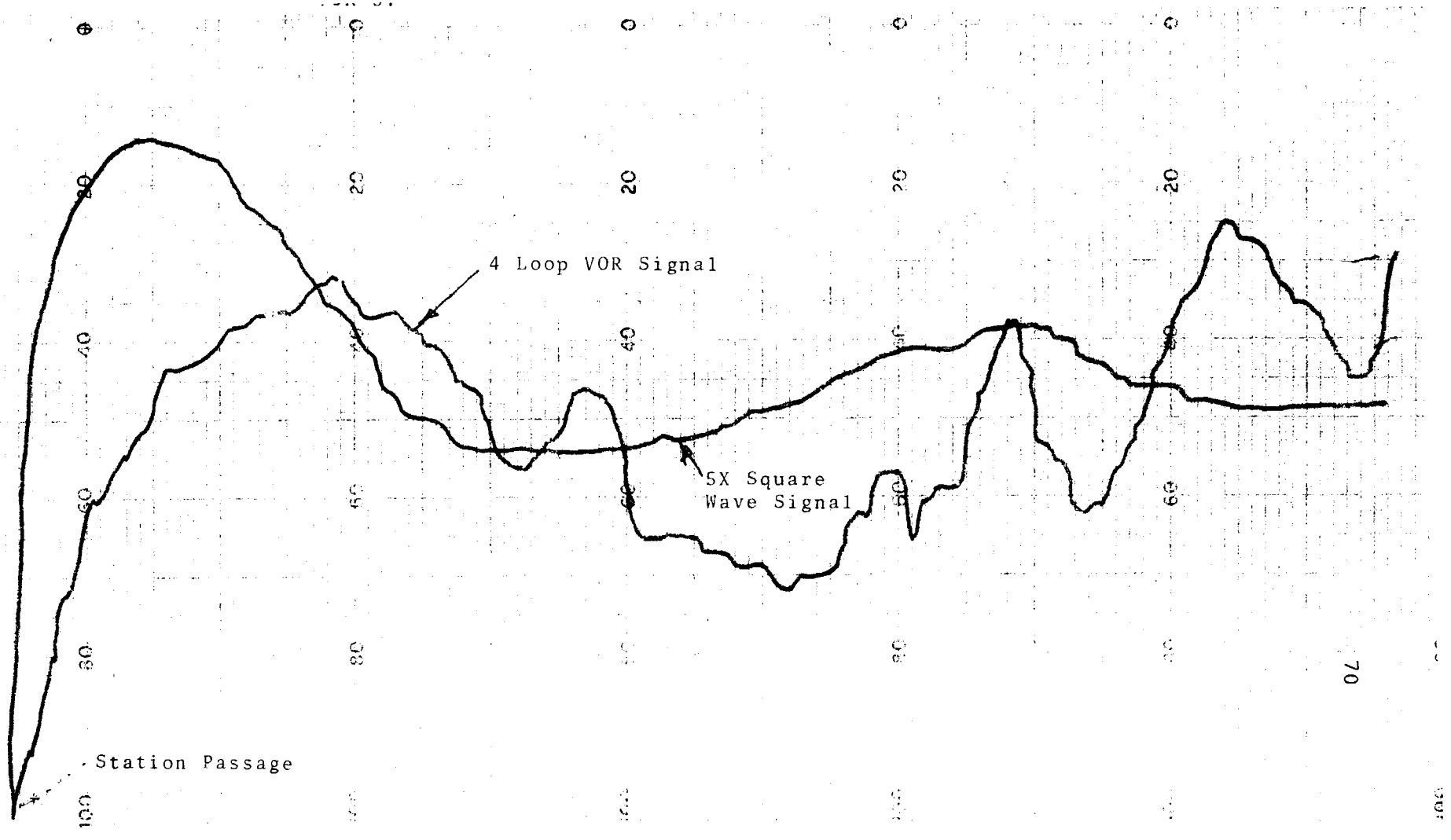

Figure 77. CDI Current - Radial Flight Outbound on 225° (Ohio University 10/72)
Altitude: 1500' above Terrain
Scale: Chart Width = 10°, Chart Length = 5 S.M.
Receiver: 51R3 Modified for Zero Crossing Detection
Note: The two records shown were not made simultaneously. They were traced on to this figure to contrast flyability of the four loop and Square Wave VOR's

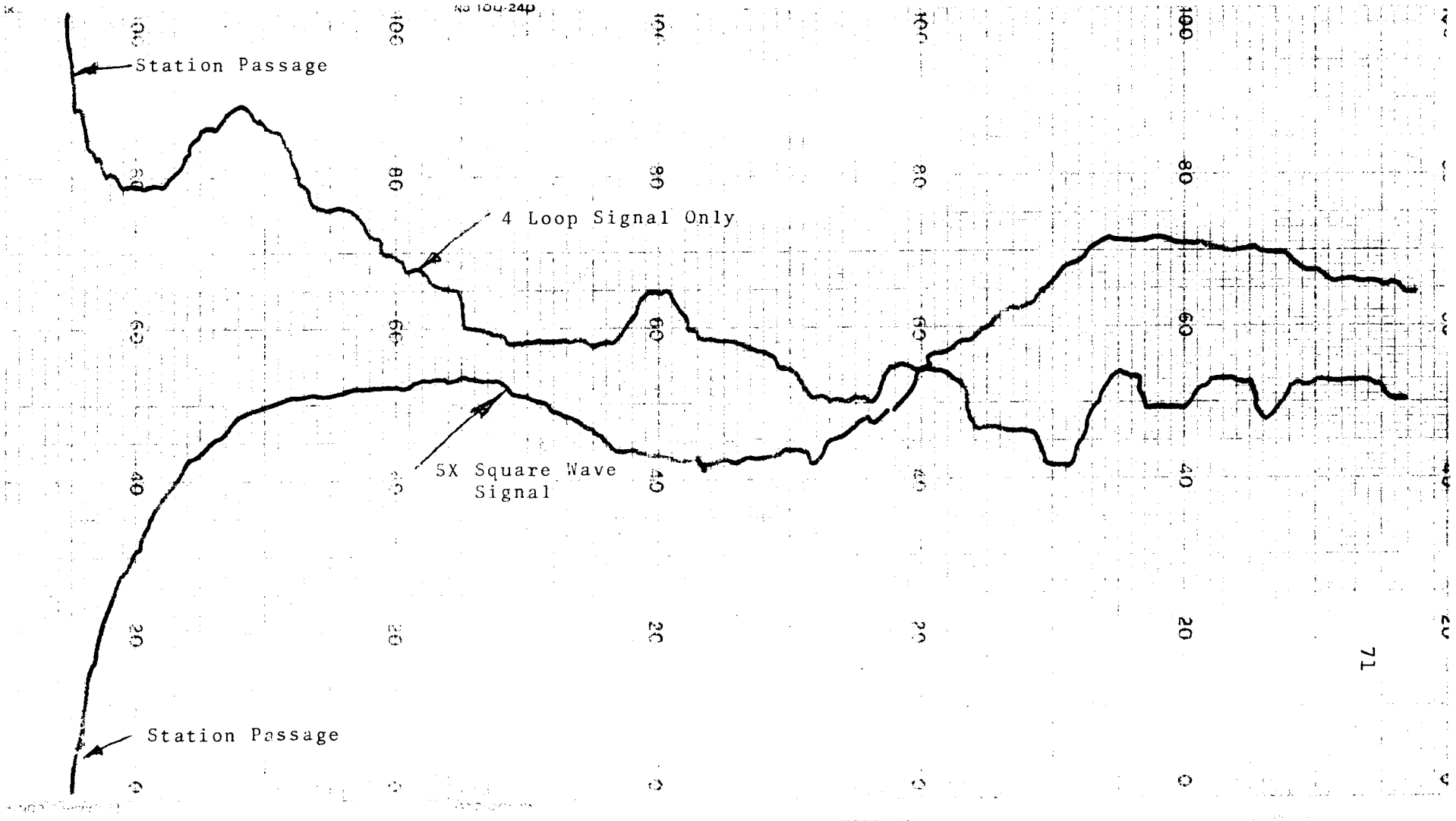

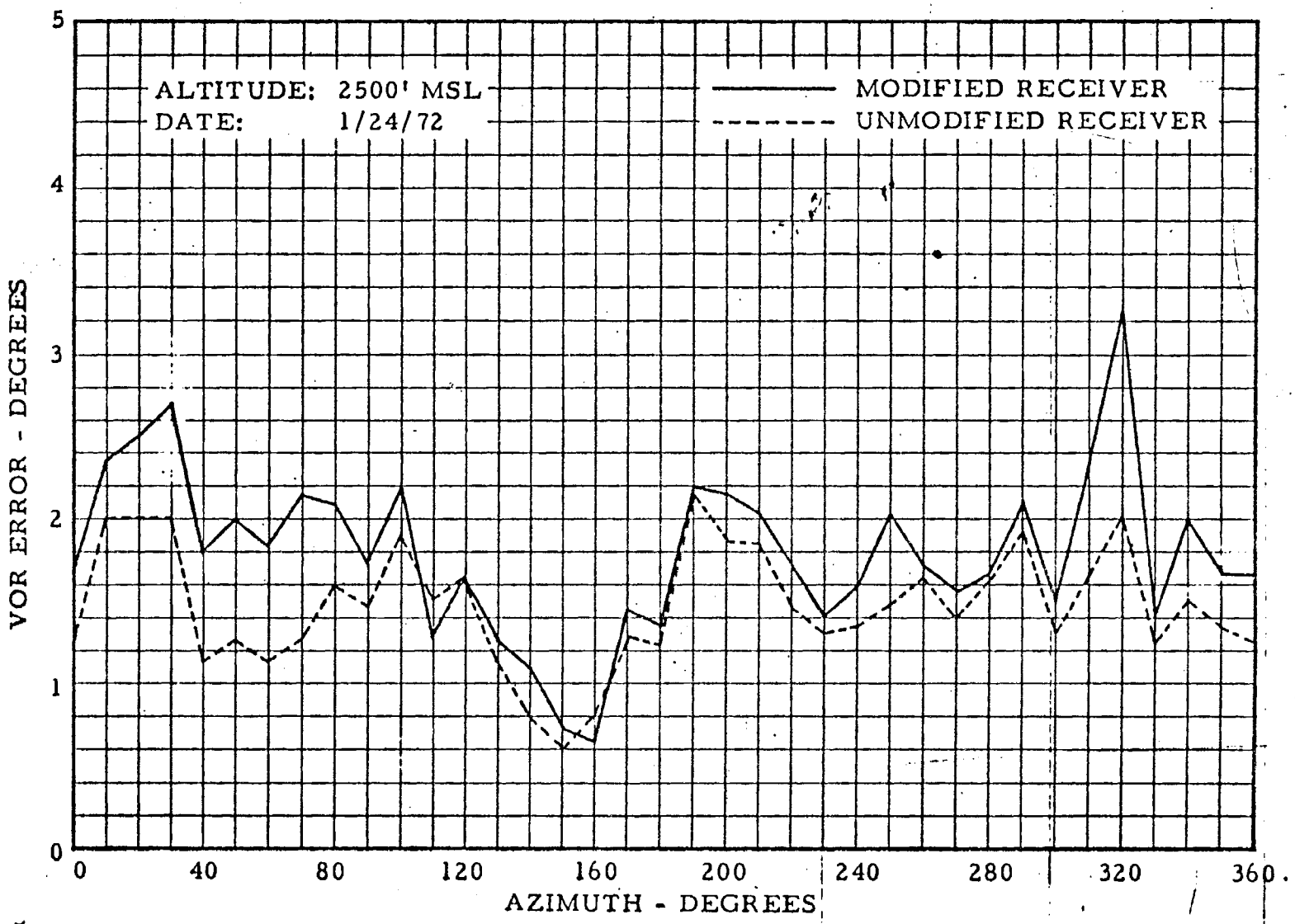

FIGURE 78. - FOUR-LOOP VOR STATION ERROR, 20 NMI ORBIT NO. 2, ONE RECEIVER MODIFIED
(NAFEC DATA)

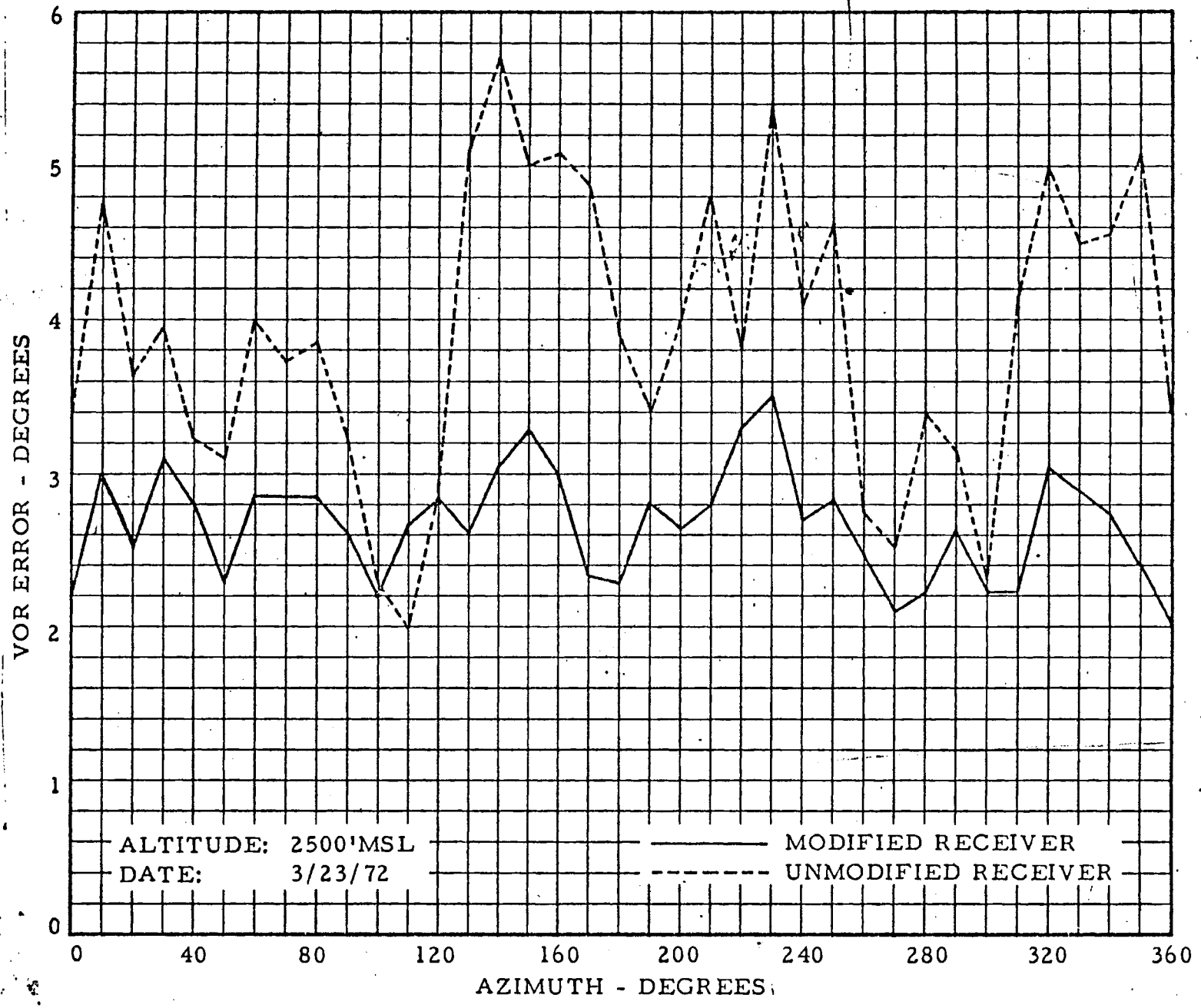

FIGURE 79 - SVOR STATION ERROR, 20 NMI ORBIT NO. 3
(NAFEC DATA)

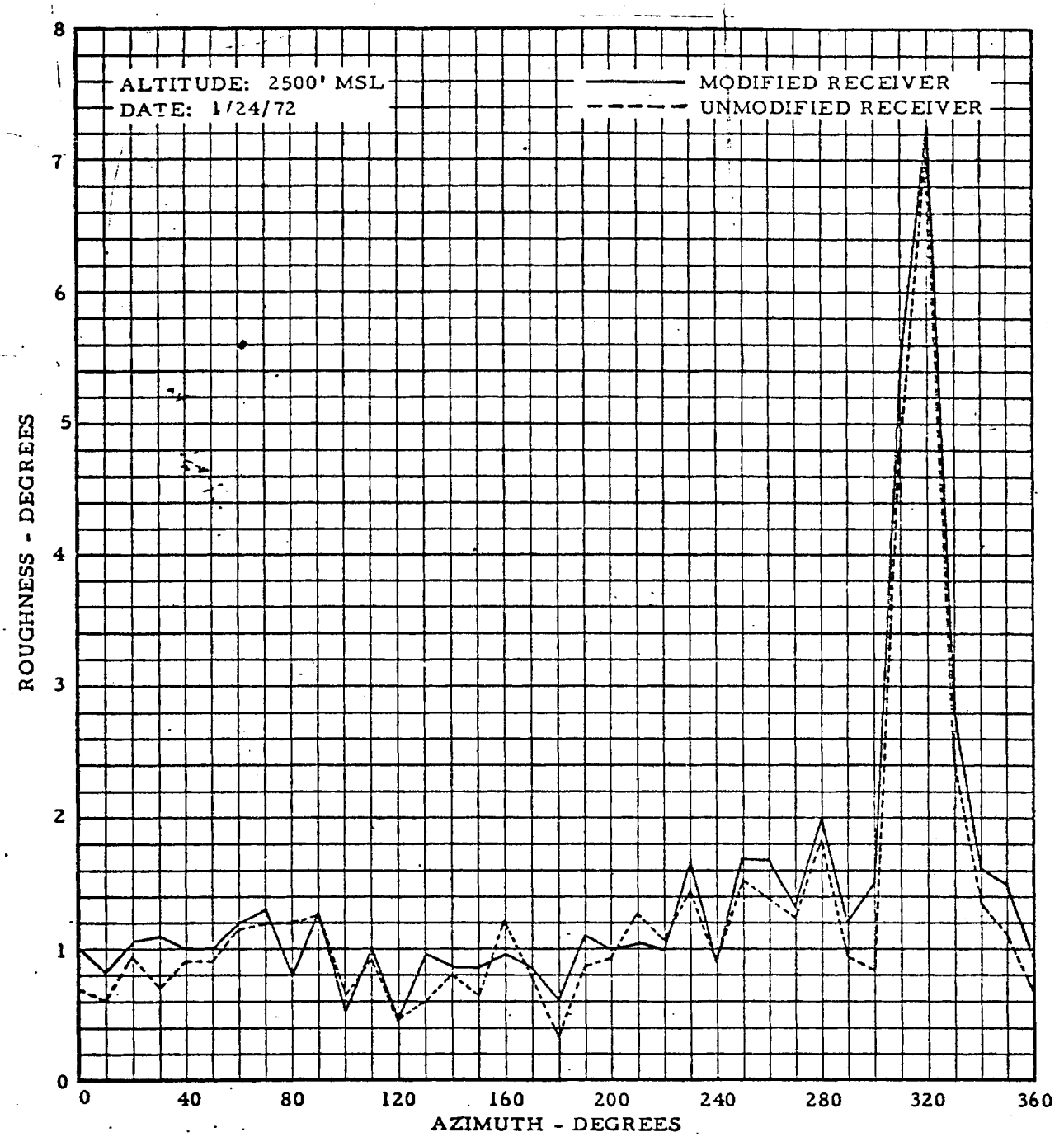

FIGURE 80.- FOUR-LOOP VOR ROUGHNESS AND SCALLOPING, 20 NMI ORBIT NO. 2, ONE RECEIVER MODIFIED

(NAFEC DATA)

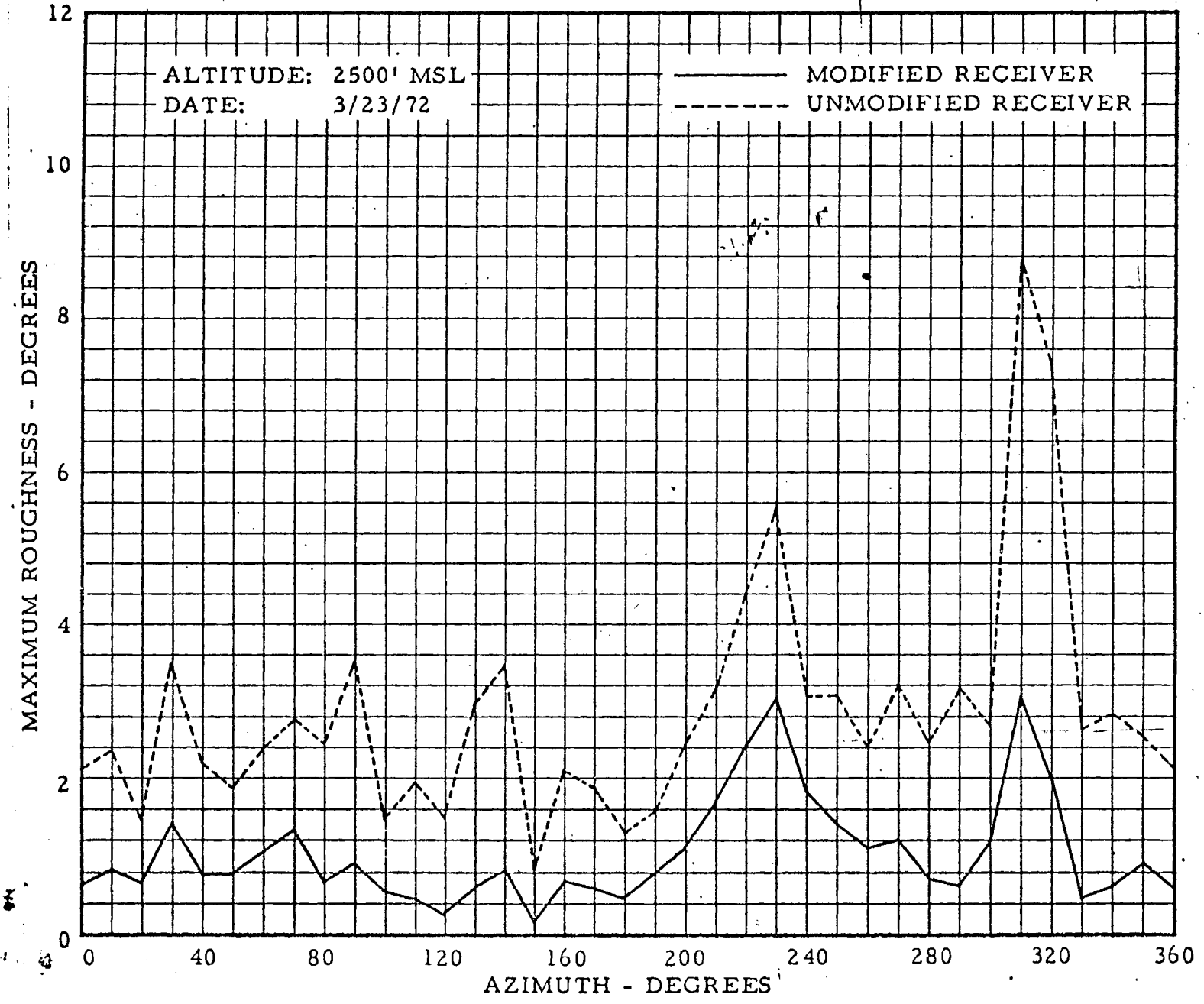

FIGURE 81 - SVOR ROUGHNESS AND SCALLOPING, 20 NMI ORBIT NO. 1
(NAFEC DATA)

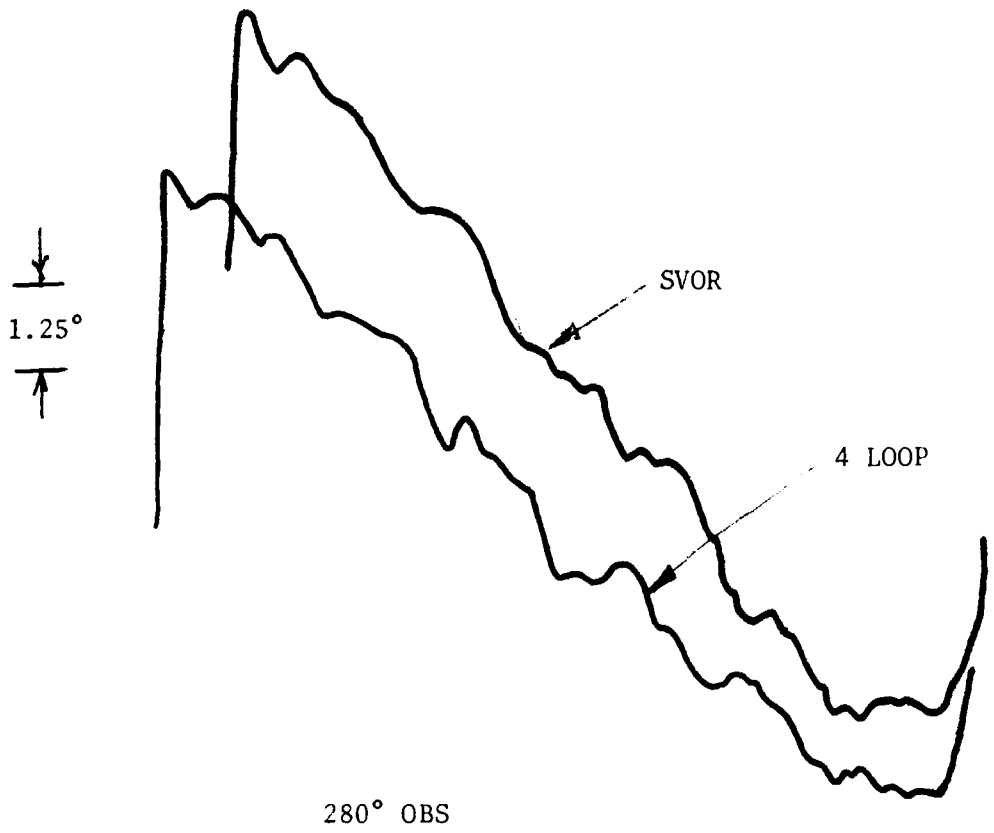

FIG. 82. 6 NM ORBITS. CONVENTIONAL RECEIVER. ONE ORBIT WITH FULL 5X SVOR. ONE ORBIT WITH 4 LOOP ARRAY ONLY. (NAFEC, Aug. 10, 1972).

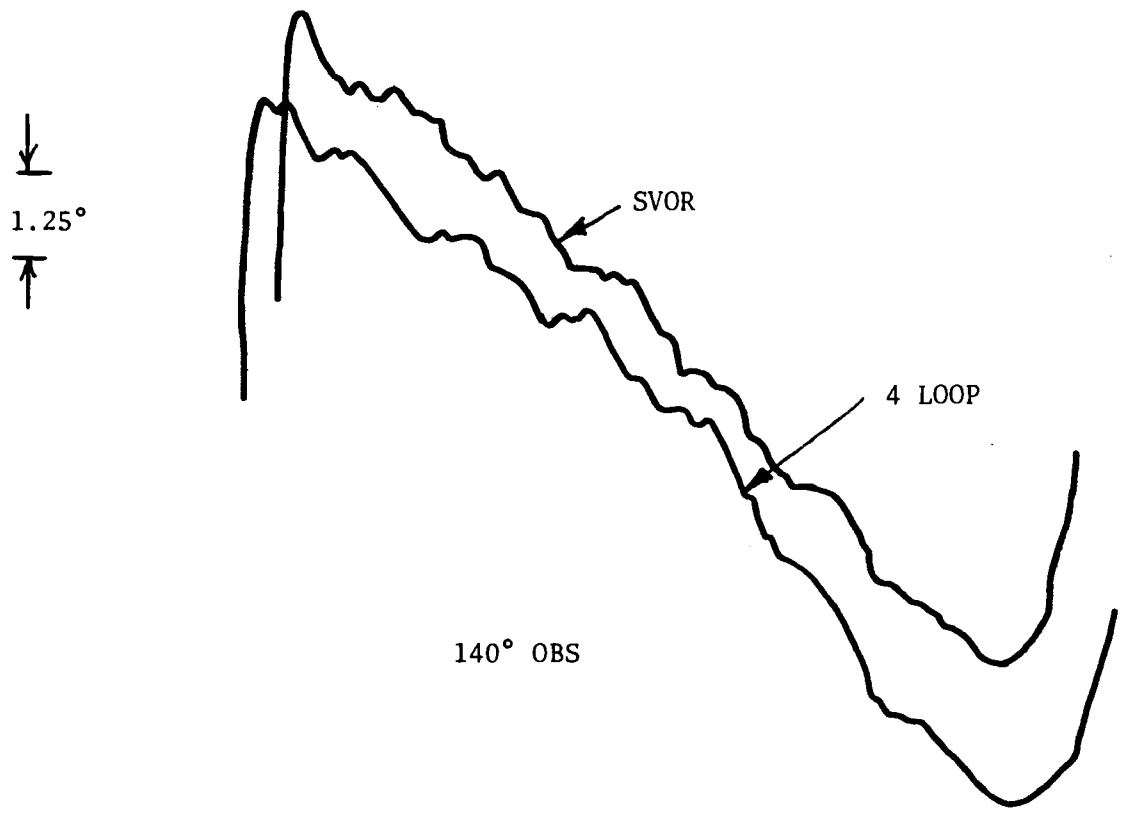

FIG. 83. 6 NM ORBITS. UNMODIFIED RECEIVER. ONE ORBIT WITH FULL 5X SVOR. ONE ORBIT WITH 4 LOOP ARRAY ONLY. (NAFEC, Aug. 10, 1972).

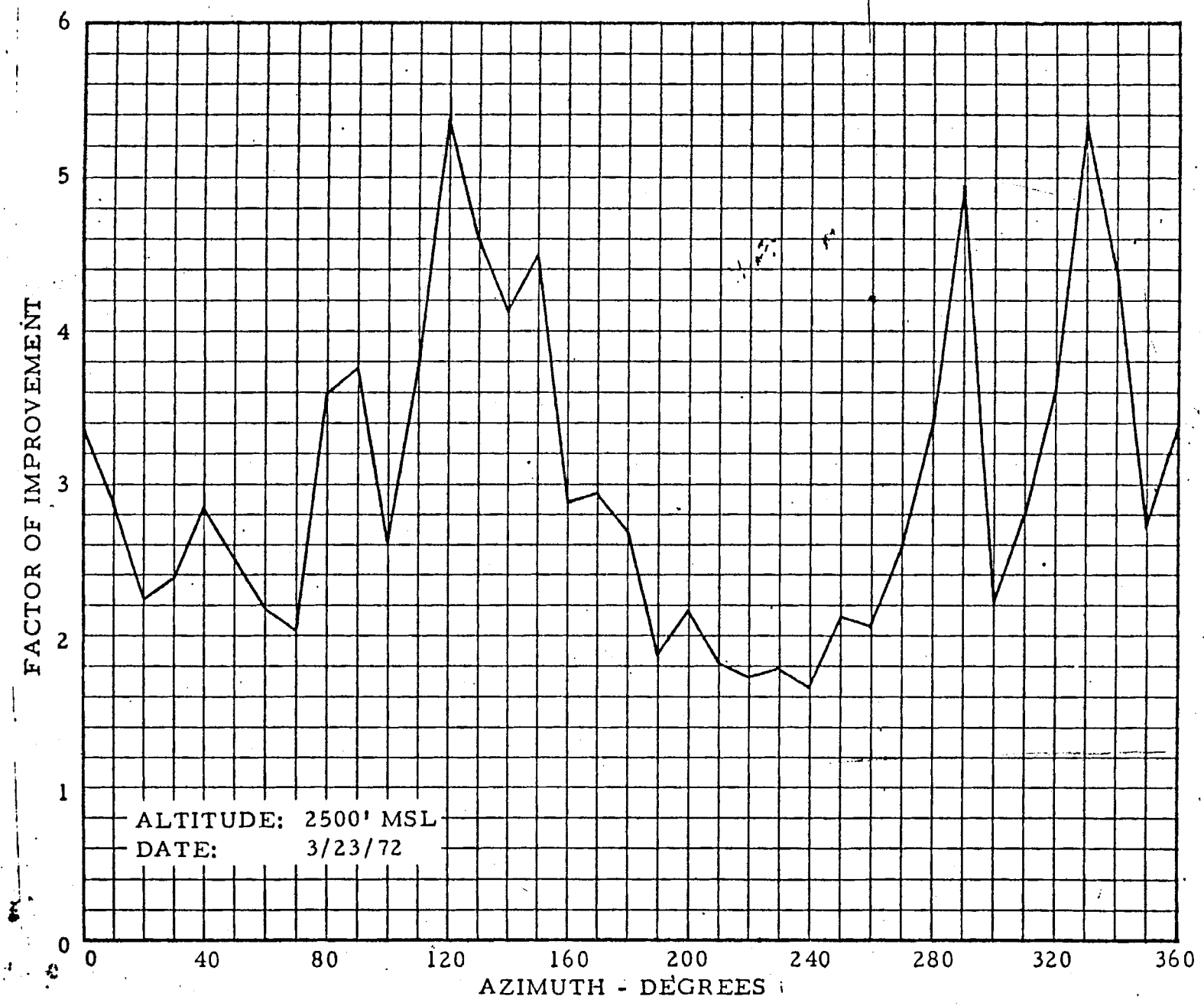

FIGURE 84 - SVOR IMPROVEMENT FACTOR, 20 NMI ORBIT NO. 1

Figure 85. 13X SVOR - VARIABLE PHASE PATTERN VS. AZIMUTH AT SEVERAL ELEVATIONS. (ARRAY CONSISTS OF A 4 LOOP VOR CONCENTRIC WITH A RING ARRAY).

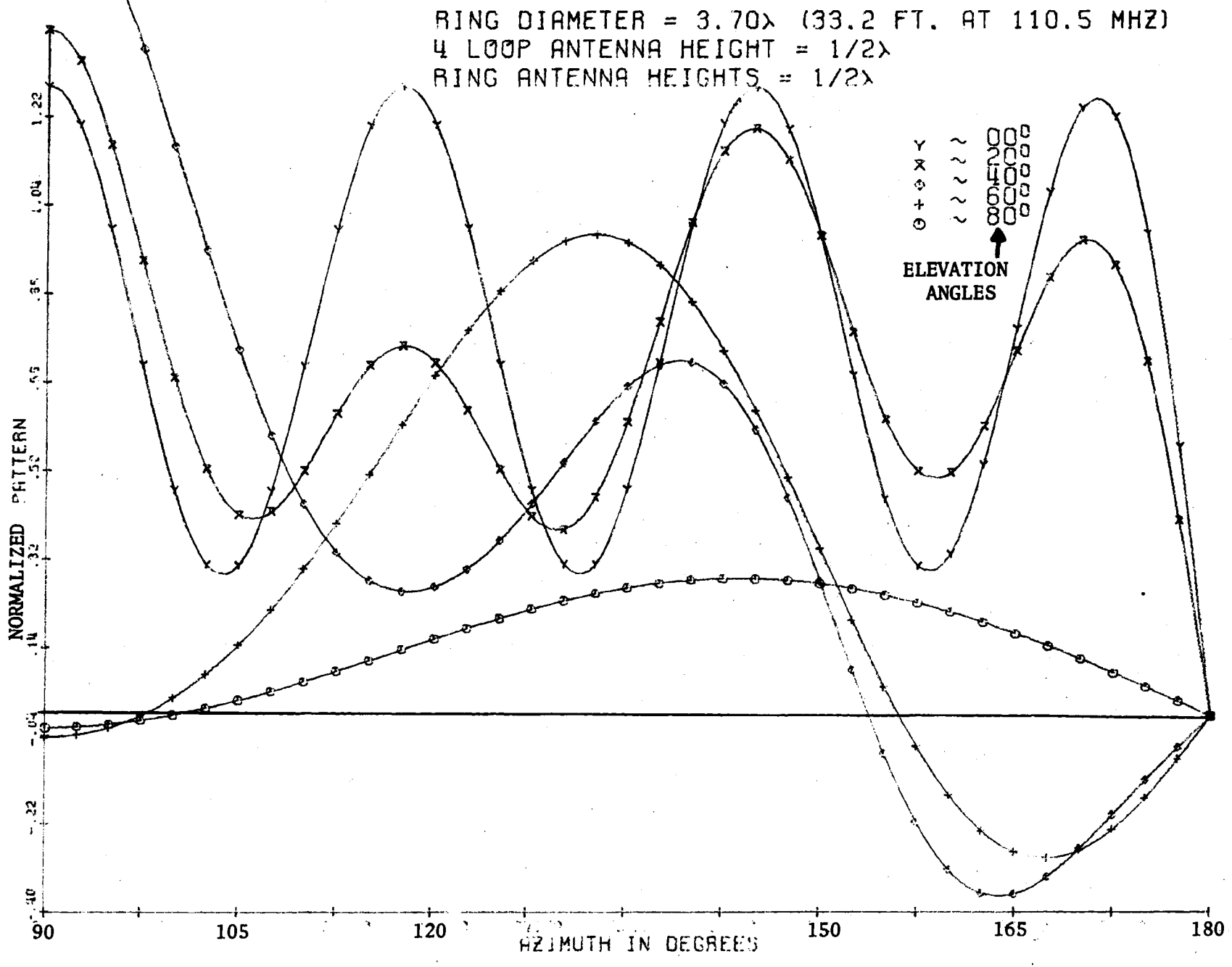

FIG. 86. TWO RING 13X SVOR - VARIABLE PHASE PATTERN VS. AZIMUTH FOR SEVERAL ELEVATIONS.

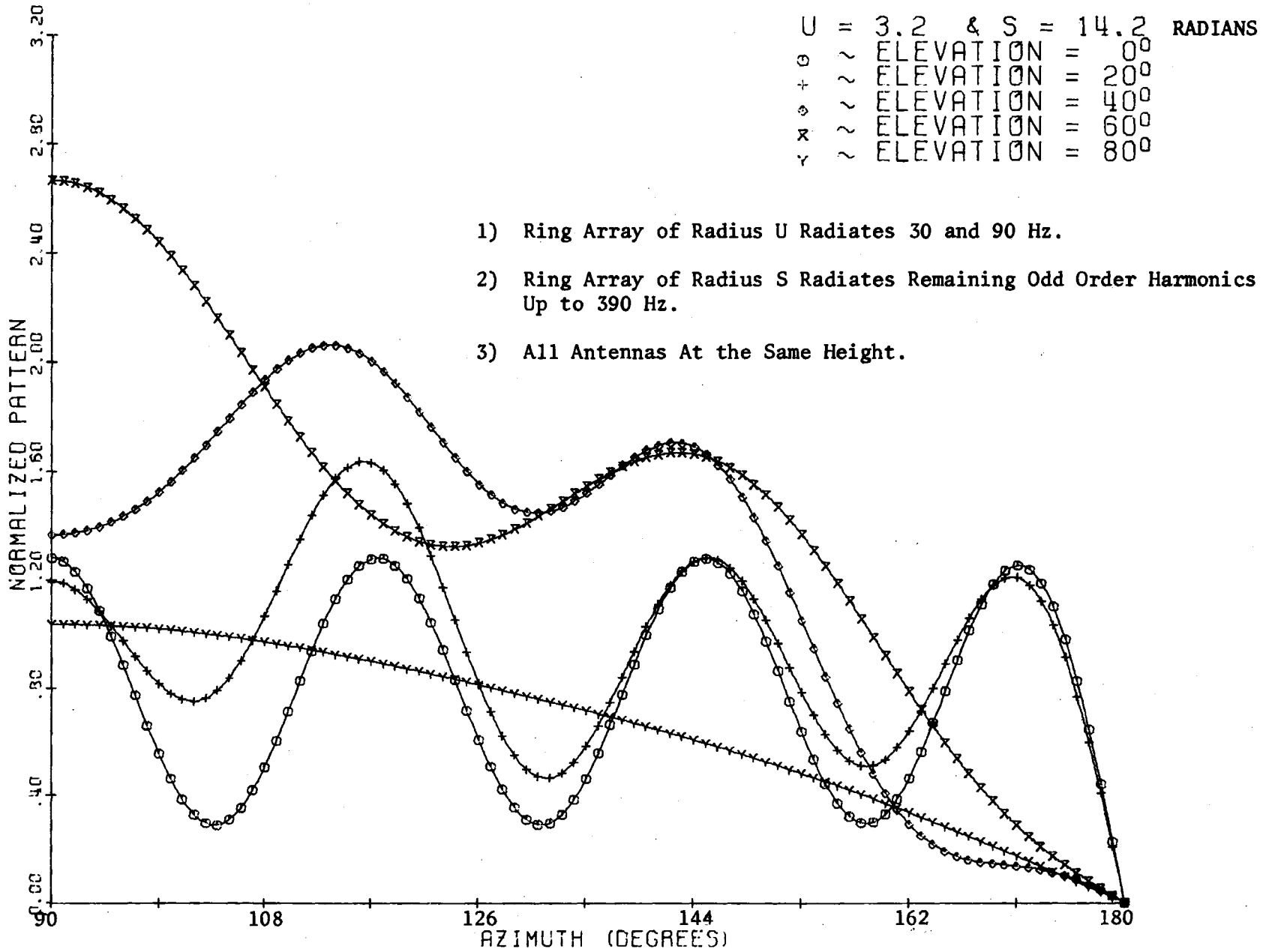

FIG. 87. TWO RING 13X SVOR - VARIABLE PHASE PATTERN VS. AZIMUTH FOR SEVERAL ELEVATIONS.

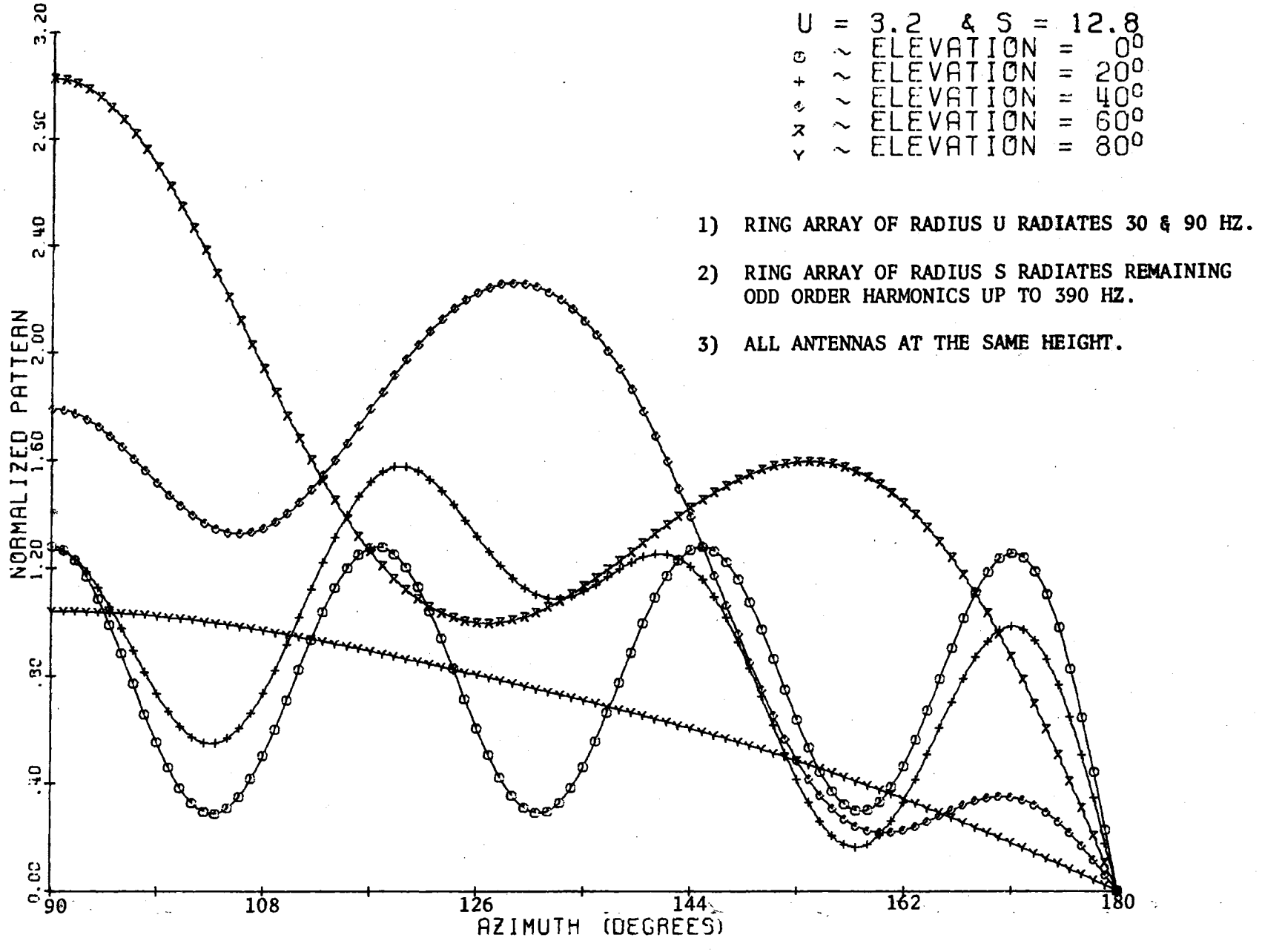

1) RING ARRAY OF RADIUS U RADIATES 30 & 90 HZ.

2) RING ARRAY OF RADIUS S RADIATES REMAINING ODD ORDER HARMONICS UP TO 390 HZ.

3) ALL ANTENNAS AT THE SAME HEIGHT.

FIG. 88. TWO RING 13X SVOR - VARIABLE PHASE PATTERN VS. AZIMUTH FOR SEVERAL ELEVATIONS.

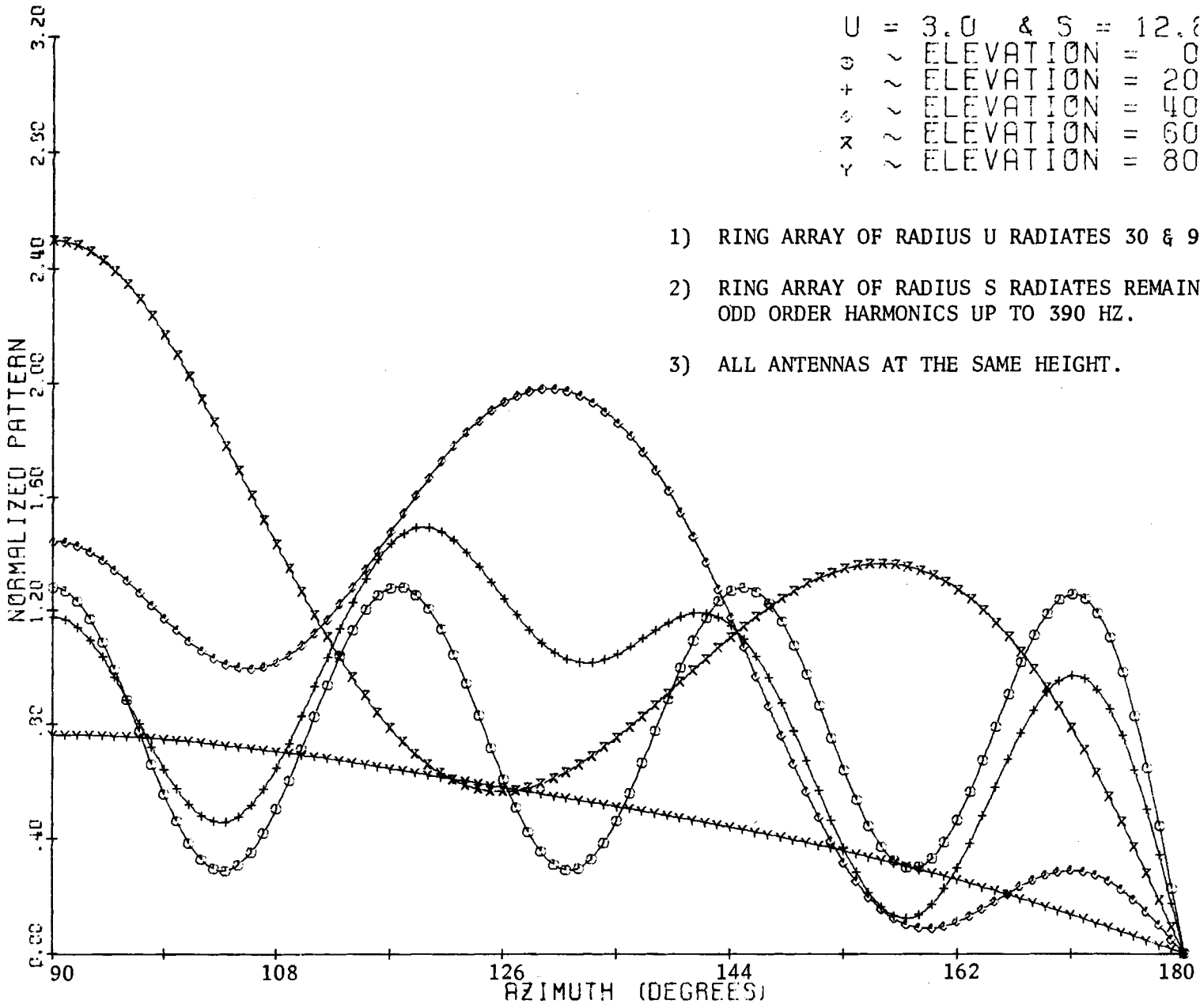

FIG. 89. 4 LOOP PLUS RING 13X SVOR - VARIABLE PHASE PATTERN VS. AZIMUTH FOR SEVERAL ELEVATIONS.

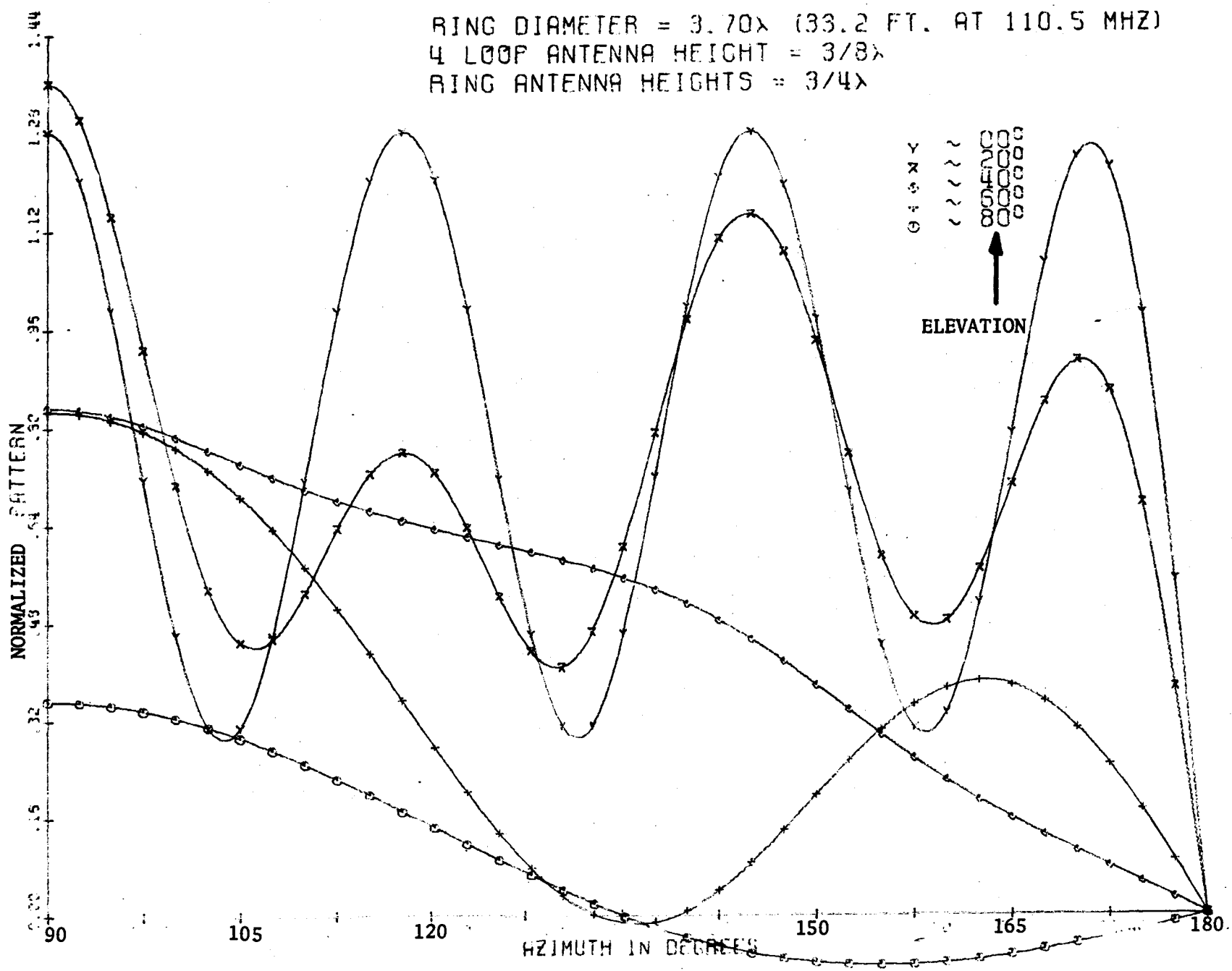

FIG. 90. 4 LOOP PLUS RING 13X SVOR - VARIABLE PHASE PATTERN VS. AZIMUTH FOR SEVERAL ELEVATIONS.

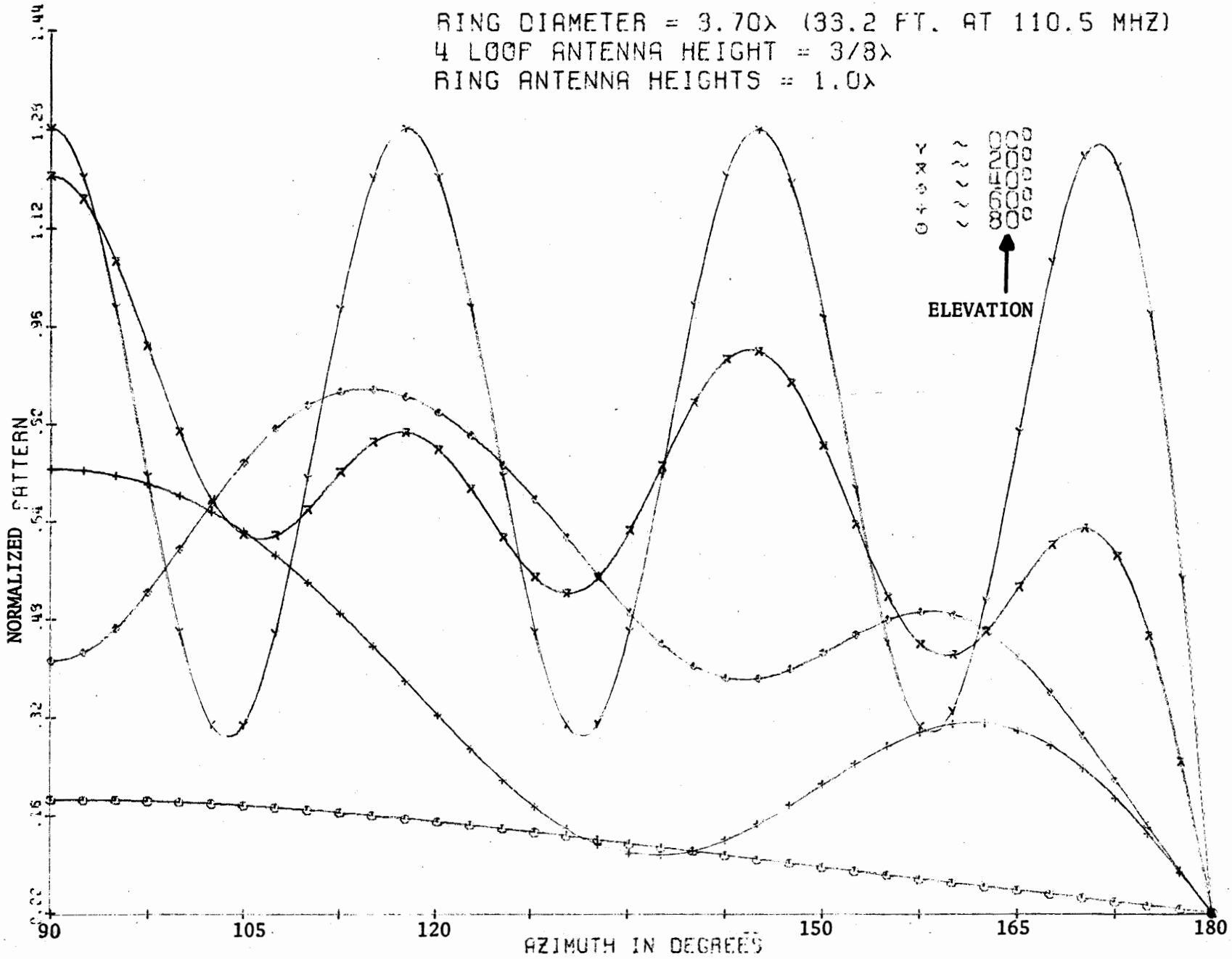
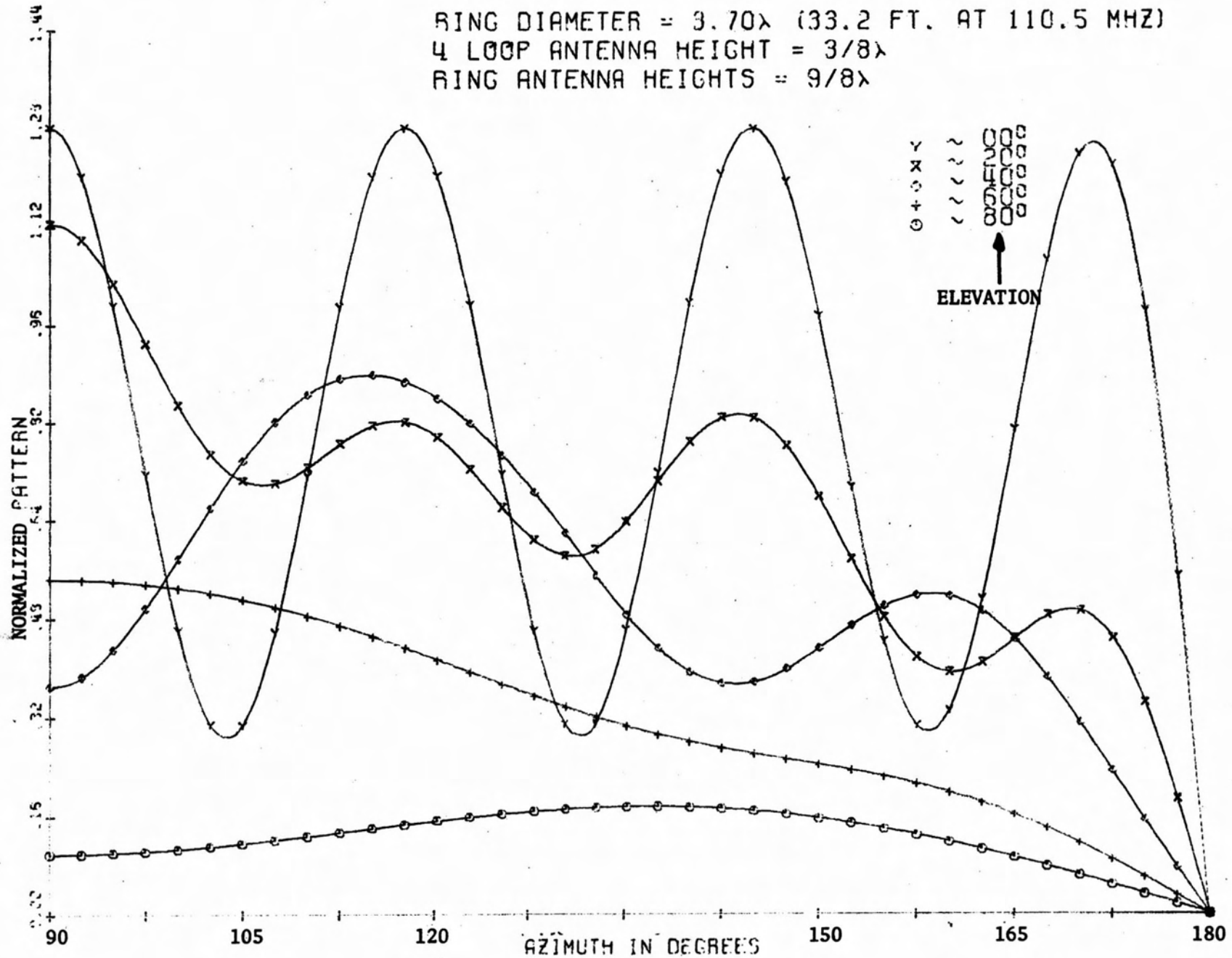
FIG. 91. 4 LOOP PLUS RING 13X SVOR - VARIABLE PHASE PATTERN VS. AZIMUTH FOR SEVERAL ELEVATIONS.